Chemical Recycling and Upcycling of Poly(ethylene) Terephthalate

by

Matthew J. Price



A thesis submitted to the University of Birmingham for the degree of Doctor of Philosophy

School of Chemistry

College of Engineering and Physical Sciences

University of Birmingham

June 2023

UNIVERSITY OF
BIRMINGHAM

University of Birmingham Research Archive

e-theses repository

This unpublished thesis/dissertation is copyright of the author and/or third parties. The intellectual property rights of the author or third parties in respect of this work are as defined by The Copyright Designs and Patents Act 1988 or as modified by any successor legislation.

Any use made of information contained in this thesis/dissertation must be in accordance with that legislation and must be properly acknowledged. Further distribution or reproduction in any format is prohibited without the permission of the copyright holder.

Abstract

Poly(ethylene)terephthalate (PET) is the most commonly used plastic in the world, yet it is almost always (*ca.* 98%) discarded after use. The millions of tonnes of PET thrown away every day represent a valuable untapped chemical and material resource. In this work the chemical recycling and upcycling by glycolysis and alcoholysis will be explored as routes towards greater utilisation of plastic waste at the end of its lifespan. As a direct result of this study, the particle size is shown to have a significant effect on

Chapter 1 is a literature review of the state of the art of polymer Chemical Recycling to Monomer (CRM), PET chemical recycling and upcycling and additive manufacturing of chemically degraded polymer.

Chapter 2 is a publication-ready article on the development of a low-temperature alcoholysis process for PET upcycling to functional monomers, and the subsequent crosslinking of these monomers into novel, 3D-printable materials. PET is shown to be upcyclable by alcoholysis using perillyl alcohol and prenol at 120 °C. Upcycled, 3D-printed materials can be derived from the perillyl monomer by formulating it with a three-armed thiol, dye and diluent.

Chapter 3 is a moderate-scale screen of Lewis acid and base combination dual catalysts for PET glycolysis, using metal acetates and amine bases. Moreover, the activity was measured by two different degradation models and these were compared and contrasted. Several catalyst combinations, such as $Mg(OAc)_2$/MTBD and $Zn(OAc)_2$/Im, were shown to have high pseudo-first order rate constants. A well-correlated (R^2 = 0.941) model was developed using the M^2E^3D program for $Zn(OAc)_2$/base catalyst rate constants.

Chapter 4 reports a Density Functional Theory study into the mechanism of PET glycolysis by a selection of bases with zinc acetate. The specific mechanistic pathways were described in detail and structure-property-activity relationships were developed. It was found that the

mechanism proceeds *via* a transition state in which the acetate ligand acts as a base towards the nucleophile, yet remains bound to the metal.

Chapter 5 expands upon the literature's scope of glycolysis of PET which includes impurities such as dyes, fabrics and flame retardants. The activities of common highly active catalysts were compared and contrasted. The industrial catalyst $Zn(OAc)_2$ / urea (1:4) was found to be most active towards mixed fabric blends. Dyestuffs were found to have at most 15% effect on the rate constant, and flame retardant less than 5%.

Chapter 6 presents a summary of the above chapters' experimental results, any future work that can be accomplished in the area, and an overview of the problem and solutions presented herein.

Acknowledgements

First and foremost I would like to thank Andrew Dove, my supervisor, for his steadfast support, guidance and understanding throughout the past four years. Through the ups and downs he has lent his experience and knowledge, helping shape me into a more thoughtful, organised and well-rounded scientist. I would also like to thank Antoine Buchard for additional collaboration and support with the computational side of my research. Additionally I want to thank Chiara, Josh and Arianna for general mentorship in their roles as Dove Group Leaders.

I must next thank every single member of the Dove and O'Reilly Groups for the years I was present, for their outstanding moral, intellectual and technical support throughout the years. In particular I want to thank Kayla for mentoring me when I was but a first year. Siobhan, Shannon, Sètuhn, Connor, Anissa, Alisha, Jake, Beth, Jess, Louisa, Emma, Rachel, Sam, Steve, and many others must be recognised for always being up for a chat or to help me out with something.

Adam Spicer and Ben Tunley should also be thanked for putting up with my idea of leadership, and allowing me to grow alongside them. Ben especially must be thanked for the hard work he put into our collaboration.

I would be extremely remiss if I were to not mention a certain Edward Maynard. Throughout our time in the Dove Group, he has stood by me, always ready to lend an ear or just sit with me. I would not have made it through this degree without him; thank you, Ed.

There are several outside the department whom I would like to thank also, for the moral support required to pursue this PhD. Sophie made my first year manageable. Amy never failed to brighten up my day with our phone calls. Jack, Kate, Harry and Tom kept me grounded. Nathan, Helen, Connor, Em, Dan, Charlie, Ben, Rachel, Andrey, Bron and more; you have never failed to make me smile even in the darkest of times.

Of course I must thank my family, mum & dad, Zoe and Hattie, for keeping me sane during lockdown and beyond and for always encouraging me to pursue my dreams. I have endless gratitude for your support, and also that of my grandparents – especially for Grandma and Grandad, who sadly could not be here to see me finish this.

Finally I must thank the University of Birmingham for the Global Challenges Scholarship.

Table of Contents

ABSTRACT ..... **II**

GLOSSARY ..... **XVIII**

AUTHOR DECLARATION ..... **XXII**

1 GLOSSARY ..... ERROR! BOOKMARK NOT DEFINED.

1 INTRODUCTION **23**

1.1 A Plastics Problem? 23

1.2 Recycling: Primary to Quaternary 25

1.3 Poly(ethylene) Terephthalate (PET) – Catalysis of Chemical Recycling 29

1.4 PET CRM 30

1.4.1 Hydrolysis of PET *31*

1.4.2 Alcoholysis of PET *33*

1.4.3 PET CRM Methods Energy Usage *42*

1.5 Use of Density Functional Theory in PET Depolymerisation Mechanistic Studies 44

1.6 PET Upcycling 45

1.7 Additive Manufacturing In Upcycling 49

1.8 Summary and Outlook 50

1.9 References 50

2 LOW-TEMPERATURE UPCYCLING OF PET: NOVEL MATERIALS DERIVED FROM FUNCTIONAL AND RENEWABLY SOURCED ALCOHOLS **60**

2.1 Introduction 60

2.2 Results & Discussion 63

2.3 Conclusions 71

2.4 References 72

2.5 INSTRUMENTATION 74
2.6 MATERIALS 77
2.7 SYNTHETIC METHODS 77
2.7.1 General Procedure for the Glycolysis of PET 77
2.7.2 Generic Depolymerisation of PET by alcoholysis (10 mol% catalyst loading) 82
2.7.3 Synthesis of Crosslinked Networks 93
2.7.4 Synthesis of Blended Crosslinked Networks 93
2.7.5 Formulation of resin for 3D Printing 94
2.7.6 Depolymerisation of Crosslinked Networks 94
2.8 ADDITIONAL DATA 95
2.8.1 Conversion Plots 95
2.8.2 Arrhenius Plot 96
2.8.3 TGA Plots 97
2.8.4 DSC Plots 99
2.8.5 Tensile Testing Plots 101
2.8.6 DMA Plots 103
2.8.7 Mechanical Properties Summary 105
2.8.8 Photorheology Plots 106
2.8.9 UV/Vis Plots 107
2.8.10 UV Cure Working Cure Plots 108
2.9 REFERENCES 109
3. DUAL CATALYSIS OF PET GLYCOLYSIS 110
3.1. INTRODUCTION 110
3.2. RESULTS AND DISCUSSION 112
3.2.1. Depolymerisation of PET by Dual Catalysis – Methodology 112
3.2.2. $Zn(OAc)_2$ / Base-Catalysed Glycolysis 115

3.2.3. Metal Acetate Standalone Catalysis 123

3.2.4. Base Standalone Catalysis 129

3.2.5. Metal Acetate / Base Dual Catalyst Kinetics 131

3.2.6. Metal Acetate / TBD and MTBD Combinations 138

3.3. Conclusions 139

3.4. Supporting Information 141

3.4.1. Generic PET Dual-Catalysed Glycolysis Reaction 141

3.5. References 145

4. DENSITY FUNCTIONAL THEORY 147

4.1. Introduction 147

4.2. Results and Discussion 154

4.2.1. Catalyst Binding 154

4.2.2. Model Compounds 157

4.2.3. Mechanistic Deductions 164

4.3. Conclusions 165

4.4. Supporting Information 167

4.4.1. DFT Derivation Equations 167

4.4.2. Typical Gaussian Input Commands 168

4.4.3. Cartesian Coordinates of Optimised Structures 169

4.4.4. Energies of Optimised Structures 191

4.4.5. Imaginary Frequencies of Transition States 191

4.5. References 192

5. EFFECT OF IMPURITIES IN PET GLYCOLYSIS 193

5.1. Introduction 193

5.2. Results and Discussion 194

5.2.1. Undyed PCB Glycolysis 194

5.2.2. Dyed PCB Glycolysis *197*

5.2.3. Flame Retardant-Included PET Glycolysis *199*

5.3. CONCLUSIONS 203

5.4. SUPPORTING INFORMATION 205

5.4.1. PCB Depolymerisation Procedure *205*

5.4.2. Dyed PCB Purification Procedure *206*

- *References* *207*

6 CONCLUSIONS & PERSPECTIVES 209

Table of Figures

Figure 1.1. Production, Fate and Use of plastics, reproduced with permission from Geyer et al.[2] under Creative Commons Attribution Non-Commercial License..... 24

Figure 1.2. Scopus data for number of articles which include 'polymer' and 'recycling' in the title between 2000 and 2021. 25

Figure 1.3. The possible life cycles of a piece of consumer plastic. 27

Figure 1.4. Shrinking-core model of PET hydrolysis..... 33

Figure 1.5. Bases used in combination with $Zn(OAc)_2$, in decreasing pK_{aH} order. 41

Figure 1.6. Aminolytic upcyclic of PLA to produce 3D-printable resins. Reproduced with permission from Shao *et al.*.[2]..... 49

Figure 2.1. a) Scheme for commonly employed conditions for PET glycolysis. b) PET depolymerisation at 180 °C by glycolysis of 3 mm PET pellets, 1 mm PET pellets, and 0.3 mm PET powder. Catalyst loading = 1 mol%. c) First-order rate plots for PET

depolymerisation by glycolysis at 180-160 °C. Catalyst loading = 1-10 mol%. d) First-order rate plots for PET depolymerisation by glycolysis at 140-120 °C. Catalyst loading = 1-10 mol%. 64

Figure 2.2. a) PET depolymerisation at 120 °C by alcoholysis. Catalyst loading = 10 mol%. b) functionalised monomers, their respective conversions at 4 and 20 h measured by FTIR spectroscopy, and their final product yields (if isolated). 65

Figure 2.3. a) The upcycling of PET depolymerisation product into a crosslinked network. Radical thiol-ene reaction between prenol- and perillyl-based monomer and trimethylolpropane tris(3-mercaptopropionate) (TMPMP) (1:1 thiol:alkene stoichiometry) at 22 °C, 10 min. b) The upcycling of PET depolymerisation product into crosslinked networks: Uniaxial tensile testing at 21 ± 1 °C, 10 mm min^{-1} strain rate c) DSC thermogram for 1st heating cycle from −100 to 200 °C, 10 °C min^{-1}. d) Images of dogbone samples before and after tensile testing to show elastic recovery. 67

Figure S2.4. ^{1}H NMR spectrum of bis(2-hydroxyethyl)terephthalate (400 MHz, DMSO-d_6, 298 K). * = H_2O..... 79

Figure S2.5. ^{13}C NMR spectrum of bis(2-hydroxyethyl)terephthalate (100 MHz, DMSO-d_6, 298 K)..... 80

Figure S2.6. Example ^{1}H NMR spectrum of glycolysis reaction mixture aliquot (400 MHz, DMSO-d_6, 298 K)..... 81

Figure S2.7 ^{1}H NMR spectrum of bis(prenyl)terephthalate (400 MHz, $CDCl_3$, 298 K). * = H_2O..... 85

Figure S2.8 ^{13}C NMR spectrum of bis(prenyl)terephthalate (100 MHz, $CDCl_3$, 298 K)..... 86

Figure S2.9 ^{1}H NMR spectrum of bis(geranyl)terephthalate (400 MHz, $CDCl_3$, 298 K). ... 87

Figure S2.10 ^{13}C NMR spectrum of bis(geranyl)terephthalate (100 MHz, $CDCl_3$, 298 K). 88

Figure S2.11 ^{1}H NMR spectrum of bis(perillyl)terephthalate (400 MHz, $CDCl_3$, 298 K). * = H_2O..... 89

Figure S2.12 ^{13}C NMR spectrum of bis(perillyl)terephthalate (100 MHz, $CDCl_3$, 298 K)... 90

Figure S2.13 ^{1}H NMR spectrum of bis(nopyl)terephthalate (400 MHz, $CDCl_3$, 298 K). * = H_2O..... 91

Figure S2.14 ^{1}H NMR spectrum of bis(nopyl)terephthalate (100 MHz, $CDCl_3$, 298 K)..... 92

Figure S2.15 PET depolymerisation by glycolysis using Zn/DMAP catalyst at various loading, at a) 180 °C, b) 160 °C, c) 140 °C, d) 120 °C..... 95

Figure S2.16 Arrhenius Plots of PET powder depolymerisation using Zn/DMAP catalyst at 1 mol% and 10 mol%. 1 mol% E_a = 107 11 kJ mol^{-1}; 10 mol% E_a = 102 ±2 kJ mol^{-1}. 96

Figure S2.17 TGA thermograms of alcohols, from 25 to 600 °C, 10 °C min^{-1}. 97

Figure S2.18 TGA thermograms of networks annealed at 22 °C and 120 °C, from 25 to 600 °C, 10 °C min^{-1}. 98

Figure S2.19 DSC thermograms of network 1 (BPrT) annealed at 22 °C and at 120 °C from -25 to 150 °C, 10 °C min^{-1}. Position of T_g is indicated with vertical hashmark. 99

Figure S2.20 DSC thermograms of network 2 (BPeT) annealed at 22 °C and at 120 °C from -25 to 150 °C, 10 °C min^{-1}. Position of T_g is indicated with vertical hashmark. 100

Figure S2.21 Stress vs strain curves of network **1** samples (BPrT) annealed at 22 °C tested

at 10 mm min^{-1} strain rate (n = 5). Summary of results are shown in Table S3 101

Figure S2.22 Stress vs strain curves of network **2** (BPrT) samples annealed at 120 °C tested at 10 mm min^{-1} strain rate (n = 5). Summary of results are shown in Table S3 102

Figure S2.23 DMA temperature sweep of network **1** (BPrT) sample annealed at 22 °C from 50 to 150 °C, 5 °C min^{-1}..... 103

Figure S2.24 DMA temperature sweep of network **1** (BPrT) sample annealed at 120 °C from 50 to 150 °C, 5 °C min^{-1}. 104

Figure S2.25 Photorheology of 3D printing formulation showing storage/loss modulus crossover point at *ca.* 88 s..... 106

Figure S2.26 UV/Vis spectra of 3D printing resin formulation, alongside its UV-active components (BPeT monomer, TPO-L radical initiator, Sudan II dye). 107

Figure S2.27 UV curing time of 3D printing resin formulation with respect to thickness cured, at 900% intensity. 108

Figure 3.1**.** Exemplar ^{1}H NMR (400 MHz, DMSO-d_6, 298 K) spectrum of glycolysis reaction mixture aliquot. * = DMSO; ** = EG 112

Figure 3.2. Conversion-time (black) and initial rate constant (red) plots of $Zn(OAc)_2$ / DMA-catalysed PET glycolysis as described by Model 1 (left) and Model 2 (right). 117

Figure 3.3. Values of *k*' and *k*'' for each $Zn(OAc)_2$ / base combination catalysed PET glycolysis. 118

Figure 3.4. Plot of predictive equation for *k*' for $Zn(OAc)_2$ / base. $Zn(OAc)_2$ / MTBD given in red. 121

Figure 3.5. Contour plots of Equations 3.4a and 3.4b, and the positions of the data points on the curves. $Zn(OAc)_2$ / MTBD marked as a red triangle..... 122

Figure 3.6. a) Scatter plot of shown physicochemical properties with respect to the first-order rate constant *k*' of the metal acetate-catalysed glycolysis reaction (from left to right: La, Zn, Mg, Mn). 125

Figure 3.7. b) Scatter plot of shown physicochemical properties with respect to the first-order rate constant *k*'' of the metal acetate-catalysed glycolysis reaction (from left to right: Zn, La, Mg, Mn). 126

Figure 3.8. Comparison of Equations 5 for the 4-metal ($Zn(OAc)_2$, $Mn(OAc)_2$, $Mg(OAc)_2$, $La(OAc)_2$) initial data and the 8-metal (+ $Sc(OAc)_3$, $In(OAc)_3$, NaOAc, LiOAc) total data sets. 127

Figure 3.9. Improved predictive equation for metal acetate catalysed PET glycolysis activity. YAc given as the red triangle. 128

Figure 3.10. Pseudo-first-order rate constants (*k*' and *k*'') of standalone base-catalysed PET glycolysis *versus* pK_{aH}. 130

Figure 3.11. Pseudo-first-order rate constants (*k*' and *k*'') of catalyst combinations for $La(OAc)_3$. 132

Figure 3.12. Pseudo-first-order rate constants (*k*' and *k*'') of catalyst combinations for $Mg(OAc)_2$. 133

Figure 3.13. Pseudo-first-order rate constants (*k*' and *k*'') of catalyst combinations for $Mn(OAc)_2$. 134

Figure 3.14. 'Weak base' peak combinations measured against proxy Lewis acidity

variables. 136

Figure 3.15. ‘Weak base’ peak basicity plotted against Pauling electronegativity, with the $Sc(OAc)_3$ peak highlighted as a red triangle. 137

Figure 3.16. Conversion-time graphs for a) ‘strong bases’ alone, and in combination with b) $Zn(OAc)_2$ or c) $Mg(OAc)_2$. 138

Supplementary Figure S3.17. Gutmann-Beckett Acceptor Number *versus* *k*’ and *k*’’ values for $La(OAc)_3$, $Zn(OAc)_2$, and $Mg(OAc)_2$. 142

Supplementary Figure S3.18. $Mg(OAc)_2$ / base activity prediction curve. 143

Supplementary Figure S3.19. $La(OAc)_3$ / base activity (*k*’ and *k*’’) prediction curve. 144

Figure 4.1**.** Wavefunction and Radial Density Function AOs (pink) approximated by 3G GTOs (purple). 147

Figure 4.2. left: TBD:MSA glycolysis proposed TS; right: DFT calculations for the glycolysis of BPA-PC (yellow) and PET (green) using the Minnesota MN12SX functional in conjunction with the Pople 6-311+G(d,p) triple-zeta basis set. Reproduced with permission from Jehanno *et al.* 151

Figure 4.3. $Zn(OAc)_2$-base binding free energy ($\Delta G_{binding}$) *versus* basicity of the base, alongside geometries; grey = C, white = H, blue = N, red = O. 155

Figure 4.4. $Mg(OAc)_2$-base binding free energy ($\Delta G_{binding}$) *versus* basicity of the base, alongside geometries. 156

Figure 4.5. Minimum energy pathways for a) $Zn(OAc)_2$ / ABCO; b) $Zn(OAc)_2$ / Im. 158

Figure 4.6. Minimum energy pathway for c) $Zn(OAc)_2$ / DMA. 159

Figure 4.7. Three-dimensional structure and simplified scheme of the $Zn(OAc)_2$ / Im catalysed reaction's lowest-energy TS, showing the direction of the alcohol by the acetate ligand; white = H, grey = C, blue = N, red = O. 161

Figure 4.8. Comparison of activity with: Zn-O(Ac) distance (blue); (Ac)O-H(OR) distance (hydrogen bond) (red) 162

Figure 4.9. a) & b) Comparisons of activity *versus* Bürgi-Dunitz Angle; c) diagram of back-bonding of metal d-electrons; d) diagram of ideal intramolecular Bürgi-Dunitz Angle..... 163

Supporting Figure S4.10. The Schrödinger picture of interacting electrons, and the Kohn-Sham picture of non-interacting electrons in a constant potential (pink)..... 168

Figure 5.1. BHET yields of $Zn(OAc)_2$-catalysed glycolysis for various PET sources. Adapted with permission from Aguado *et al.*[6, 7] 193

Figure 5.2. Depolymerisation kinetics of undyed PCB with various catalysts (10 mol% loading); a) conversion-time plot; b) Model 1 semi-log plot; c) Model 2 plot. 195

Figure 5.3. Comparison of the three best catalysts from the undyed study using black dyed PCB. 197

Figure 5.4. Comparison of depolymerisation kinetics of undyed, black and red PCB using 10 mol% $Zn(OAc)_2$ / DMAP as the catalyst.**Figure 5.3.** Comparison of the three best catalysts from the undyed study using black dyed PCB. 197

Figure 5.4. Comparison of depolymerisation kinetics of undyed, black and red PCB using 10 mol% $Zn(OAc)_2$ / DMAP as the catalyst..... 198

Figure 5.5. BHET from dyed PCB after 0 (left), 1 (middle), and 2 (right) purification steps..... 199

Figure 5.6. Kinetic plot of glycolysis of PET catalysed by $Zn(OAc)_2$ / Im (10 mol%) with and without TDCPP.**Figure 5.5.** BHET from dyed PCB after 0 (left), 1 (middle), and 2 (right) purification steps. 199

Figure 5.6. Kinetic plot of glycolysis of PET catalysed by $Zn(OAc)_2$ / Im (10 mol%) with and without TDCPP. 200

Figure 5.7. Calculation of first-order rate constants using a) Model 1 and b) Model 2. ... 202

Supplementary Figure S5.8. ^{1}H NMR Spectrum (400 MHz, 298K, DMSO-d_6) of purified BHET. * = H_2O; X = potential dye 206

Figure 6.1. The routes explored in this work for PET upcycling and recycling. 209

Figure 6.2. Magazine covers representing the prevailing opinion on plastics then and now. 212

Table of Schemes

Scheme 1.1. Various methods of PET chemical recycling: a) hydrolysis; b) alcoholysis, specifically methanolysis; c) aminolysis, specifically methylaminolysis; d) glycolysis, specifically ethylene glycolysis. 30

Scheme 1.2. Trapping of EG by DMC in the PET methanolysis reaction, including regeneration of MeOH. 34

Scheme 1.3. Simplified shrinking-core model with fast initial steps and equilibrium final steps. 35

Scheme 1.4. A typical dual-catalysed PET alcoholysis/glycolysis reaction mechanism. 39

Scheme 1.5. Examples of ‘acyl’ pathway *versus* ‘Hydrogen-bonding’ pathway of TBD-catalysed PET alcoholysis. 45

Scheme 1.6. Proposed mechanism of acidolytic upcycling of PET. Reproduced with permission from Hoang *et al.*[1] under Creative Commons Non-Commercial Attribution License. 47

Scheme S2.1. Scheme of PET glycolysis reaction using $Zn(OAc)_2$ / DMAP at various temperatures. 77

Scheme 3.1. $Zn(OAc)_2$ / tropine mechanism proposed by Deng *et al.* 110

Scheme 3.2. Range of bases used in the study, and their pK_{aH} in water. 116

Scheme S3.3. Generic scheme of PET glycolysis by organometallic dual catalysis. 141

Scheme 4.1. Two possible mechanisms of TBD-catalysed transesterification: a) acyl-transfer; b) Hydrogen-bond stabilisation. 148

Scheme 4.2. Catalytic cycle choline acetate-catalysed PET glycolysis, as proposed by Liu *et al.* 150

Scheme 4.3. Generic Lewis acid/base-catalysed PET glycolysis catalytic cycle, wherein the Lewis acid and Base act in a ‘separate but in tandem’ fashion. 153

Scheme 4.4. Model reaction used to simplify polymer substrate. 157

Scheme 4.5. Proposed catalytic cycle of the $Zn(OAc)_2$ / Im-catalysed PET glycolysis reaction. 164

Scheme 5.1. Possible phosphine oxide poisoning of the catalyst. 200

Table of Tables

Table 1.1. Comparison of the most efficient hydrolysis, methanolysis and glycolysis conditions. [a]tetrabutylammonium iodide; [b]choline chloride; [c]1,3-dimethylurea 42

Table S2.1 Yields of functionalised monomers derived from crosslinked network alcoholysis. 94

Table S2.2. Summary of thermomechanical properties for crosslinked networks. [a]Glass transition temperature determined from inflection point in DSC thermogram from -100 to 150 °C, 10 °C min^{-1}. [b]Strain at break and stress at break determined from uniaxial tensile testing at 21 ±1 °C, 10 mm min^{-1} strain rate. All uncertainties are reported as 1 S.D. 105

Table 3.1. Range of bases used in the study, and their *k*' and *k*'' values. 117

Table 3.2. Parameters used in M^2E^3D analysis of $Zn(OAc)_2$ / base property-activity relationships. 119

Table 3.3. Parameters used in M^2E^3D analysis of $Zn(OAc)_2$ / MTD property-activity relationship. 123

Table 3.4. Metal acetate-only catalysed glycolysis first order rate constants *k*' and *k*''. .. 124

Table 3.5. Base-only catalysed glycolysis first order rate constants *k*' and *k*''. 129

Supporting Table S4.1. Double-Zeta and Triple-Zeta Energies for calculated structures..... 191

Supporting Table S4.2. Double-Zeta and Triple-Zeta Frequencies for calculated TSs.. 191

Table 5.1. Undyed PCB glycolysis catalyst activities (*k*' and *k*'') using Model 1 and Model 2. 196

Glossary

Abbreviation	**Long Name**
ABCO	quinuclidine *or* 1-azabicyclo[2.2.2]octane
ABS	Acrylonitrile butadiene styrene
BHET	bis(2-hydroxyethyl)terephthalate
BPA-PC	Bisphenol-A polycarbonate
CO_2	Carbon dioxide
CRM	Chemical recycling to monomer
DABCO	1,4-diazabicyclo[2.2.2]octane
DBU	1,8-diazabicyclo[5.4.0]undec-7-ene
DEG	Diethylene glycol
DES	Deep eutectic solvent

DMA	*N,N*-dimethylaniline
DMAP	*N,N*-dimethylaminopyridine
DMT	Dimethyl terephthalate
DMU	1,3-dimethylurea
DNA	Deoxyribonucleic acid
EEI	Environmental Energy Impact
EG	Ethylene glycol
IL	Ionic liquid
Im	Imidazole
LCA	Life cycle analysis
MeOH	Methanol
MHET	Mono(2-hydroxyethyl)terephthalate
MTBD	7-methyl-1,5,7-triazabicyclo-[4.4.0]-dec-5-ene
NaOH	Sodium hydroxide
NMI	*N*-methylimidazole

NO_x	Nitrogen oxides
p-TSA	*p*-toluene sulphonic acid
PCB	Polyester cotton blend
PE	polyethylene
PET	poly(ethylene) terephthalate
PIL	Poly(ionic liquid)
PLA	Poly(lactic acid)
PHB	Poly(hydroxy) butyrate
PP	polypropylene
ROCOP	Ring-opening copolymerisation
ROP	Ring-opening polymerization
SO_x	sulphur oxides
TA	Terephthalic acid
TBD	1,5,7-triazabicyclo-[4.4.0]-dec-5-ene
TS	Transition state

$Zn(OAc)_2$	Zinc acetate

Author Declaration

This thesis is submitted to the University of Birmingham in support of my application for a Doctor of Philosophy award. This work has not been submitted for any degree or award previously.

Parts of the thesis are displayed in pre-publication format suitable for publication as outlined in the University of Birmingham alternative thesis format guidelines.

Experiments, materials characterisation, data collection and analysis, writing and figure design was performed by myself, except for co-author contributions which are outlined below and before each chapter.

Chapter 2 – Manuscript Prepared: Matthew J. Price, Benjamin F. Tunley, J. C. Worch, A. P. Dove, Low-temperature Upcycling of PET: Novel Materials Derived from Functional and Renewably Sourced Alcohols, *Manuscript Prepared*.
Dr Josh Worch (University of Birmingham) provided technical advice and editing advice.
Benjamin Tunley (University of Birmingham) collected kinetic and characterisation data for several of the bioderived alcohols screened.

Chapter 3 – Dr Arianna Brandolese (University of Birmingham) provided guidance and editing of the chapter.

Chapter 4 – Prof. Antoine Buchard (University of Bath) provided guidance and editing of the chapter.

Chapter 5 – Dr Arianna Brandolese (University of Birmingham) provided guidance and editing of the chapter.

Thesis - Prof. Andrew P. Dove (University of Birmingham) supervised in addition to providing guidance and editing the thesis.

Introduction

1.1 A Plastics Problem?

If the world is powered by oil, it is built with plastic. Plastic is in almost everything we buy, use, and throw away; this culture of disposability is becoming an ever-greater threat to our environment. Yet plastic is a veritable wonder material; it has unparalleled gas- and liquid-impermeability, transparency, low weight, strength, flexibility and many other important properties.[3] Therefore, ways of living with plastic must be found, as well as ways of reducing its effect on the environment.

Plastic is a material made up of a single (or blend of) polymer(s), a material made up of single-molecule chains from hundreds to millions of repeat units in length. There are many naturally-occurring polymers, including DNA, but the first fully synthetic polymer was created in 1907 by Leo Baekeland, who coined the term ‘plastic’.[4] Since then, over 10 billion tonnes of plastic have been created[5, 6]– most of which ends up back in the environment, to degrade ever so slowly over the course of millennia.[7] This has a detrimental impact on the environment, as these mostly undegradable particles persist and cause problem from the macroscopic, where they may interfere with and kill land and sea animals, to the microscopic, where they can be taken up by plant roots when present in soil[8] and transported by wind and rain.[2] Moreover, plastic has even been found in human blood.[9]

Although nobody knows the true extent of the health and environmental issues surrounding plastic waste, it would be reasonable to say that it is a burgeoning crisis. It could be said, however, that a large portion of the so-called ‘plastics problem’ is more of a ‘plastic waste problem’, as it is when these plastics enter the environment from landfill or improper waste collection that they pose significant environmental challenge (although the ‘plastic crisis’ does involve the use of non-renewable resources, such as oil, and so is not limited solely to the

plastic waste problem). There are many angles from which to attack such a problem, but one significant angle is recycling.[10, 11] Recycling is defined as the reprocessing of material to be used in new products.

As of 2017, approximately 9% of global plastic produced has been recycled once, and only *ca*. 1% has been recycled more than once, while 12% was incinerated for energy, and the remaining 79% went directly to landfill or into the environment (Figure 1.1).[12] Based on this statistical analysis and other similar studies[13] it is clear there is scope for greater recycling for end-of-life plastics, rather than sending to landfill.

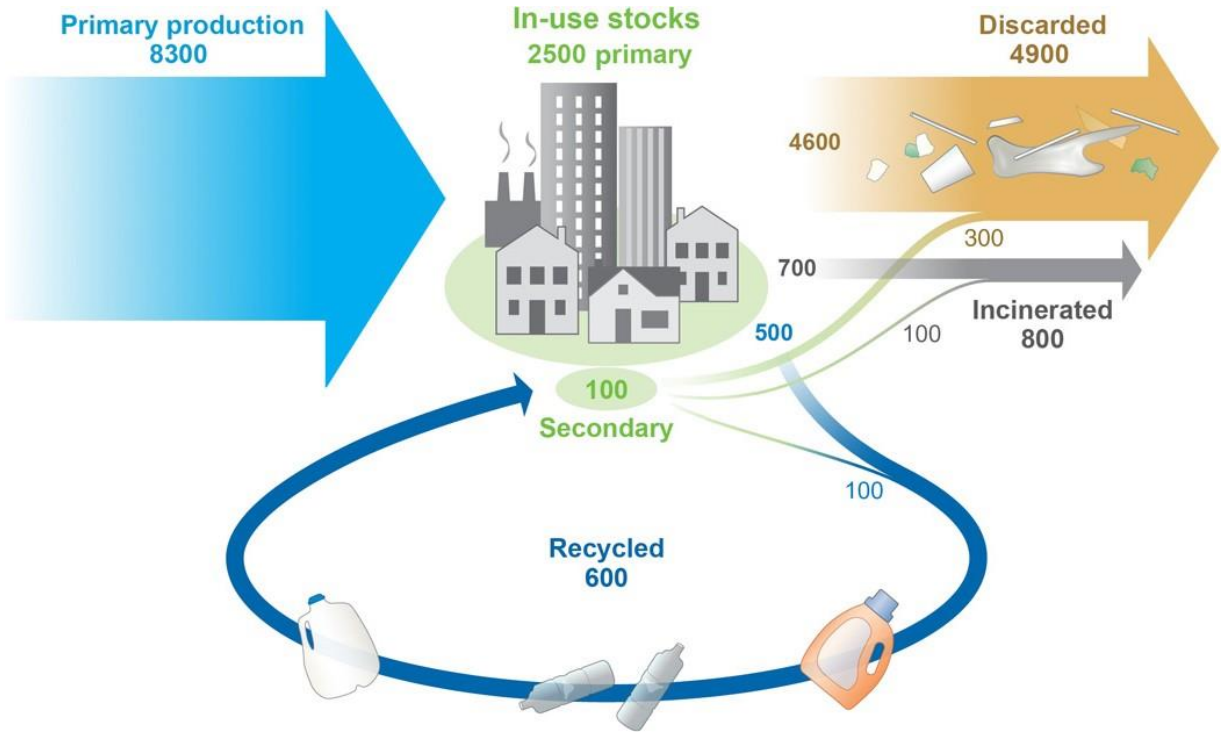


Figure 1.1. Production, Fate and Use of plastics, reproduced with permission from Geyer et al.[2] under Creative Commons Attribution Non-Commercial License.

Advocates for plastics recycling have existed since the 1970s,[14] but public concern for environmental presence of plastic was piqued with the entry of Blue Planet II (2017) into the cultural zeitgeist (although it does not appear to have translated into a permanent effect on public lifestyle).[15] Since then, research interest in polymer recycling has more than doubled (Figure 1.2), although, of course, it cannot be implied there is necessarily causation in this correlation.

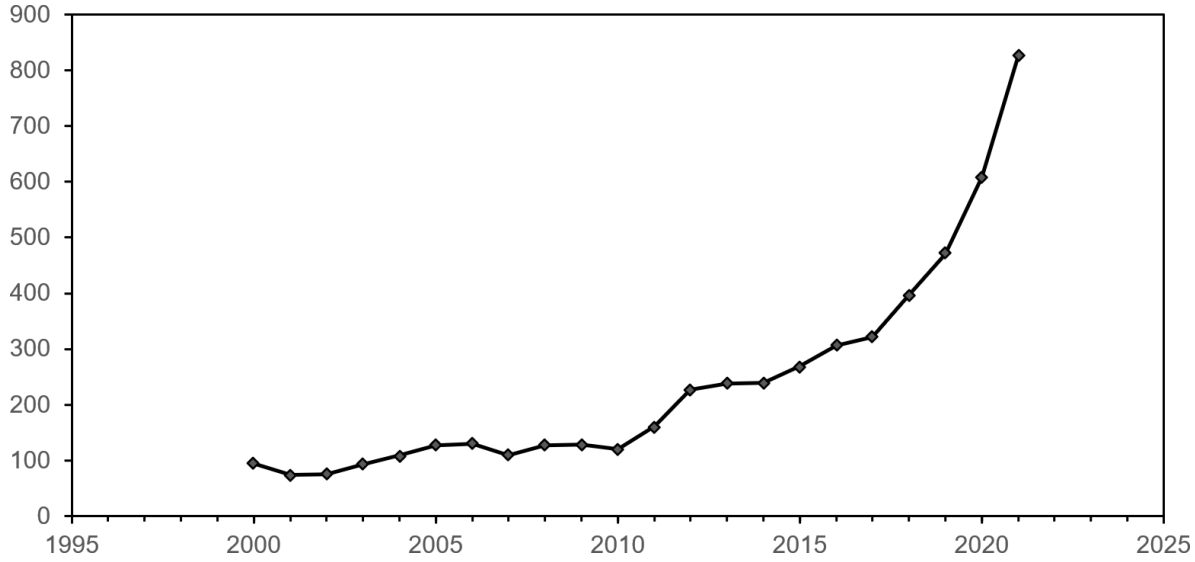


Figure 1.2. Scopus data for number of articles which include 'polymer' and 'recycling' in the title between 2000 and 2021.

1.2 Recycling: Primary to Quaternary

Plastic recycling can be divided into four broad categories, from primary to quaternary (Figure 1.3). Primary recycling, also known as re-extrusion, is an in-plant, pre-consumer process of re-extruding waste scraps of plastic.[16] Since this is not a post-consumer method, it will not be covered here.

The predominant method of plastic recycling, secondary, is achieved by a process known as mechanical recycling, wherein polymers are shredded and melted to be physically reprocessed into new shapes.[17] However, there are several disadvantages to this approach, principally that

the polymer chains degrade as a result of chain scission, and impurities such as alternate polymers, dyes, plasticisers, flame retardants, food and dirt are incorporated into the new material. This can lead to a process known as 'downcycling',[18, 19] in which the quality and therefore value of the polymer decreases with each cycle, eventually reaching the point where the only viable option is to release the plastic to landfill[19] – although mechanical recycling is not always downcycling, when performed effectively. For example, poly(ethylene) terephthalate (PET) bottles may be downcycled into carpet, then again into road filler, then finally landfilled.[20] Thus, sorting and cleaning are important aspects of mechanical recycling, preventing these impurities from entering the waste stream in the first place, consequently increasing the purity and the value of the recyclate.

Another method of recycling plastics is energy reclamation, known as quaternary recycling,[21] wherein polymers are incinerated and the energy recovered from their incineration is used to power turbines and recover electricity. This has a significant benefit as it can reclaim value out of near-valueless polymers at the end of their lives, especially highly unreactive polyolefins. In fact, polyolefins such as polyethylene (PE) and polypropylene (PP) have calorific values comparable with fuel oils such as kerosene.[22] Quaternary recycling's major downside, however, is that it produces large amounts of carbon dioxide (CO_2), a major greenhouse gas. The impurities in the plastics can cause large amounts of nitrate (NO_x) and sulphate (SO_x) gases to be evolved also, which are both highly dangerous to humans and destructive to ozone in the atmosphere, as well as being greenhouse gases themselves.[23]

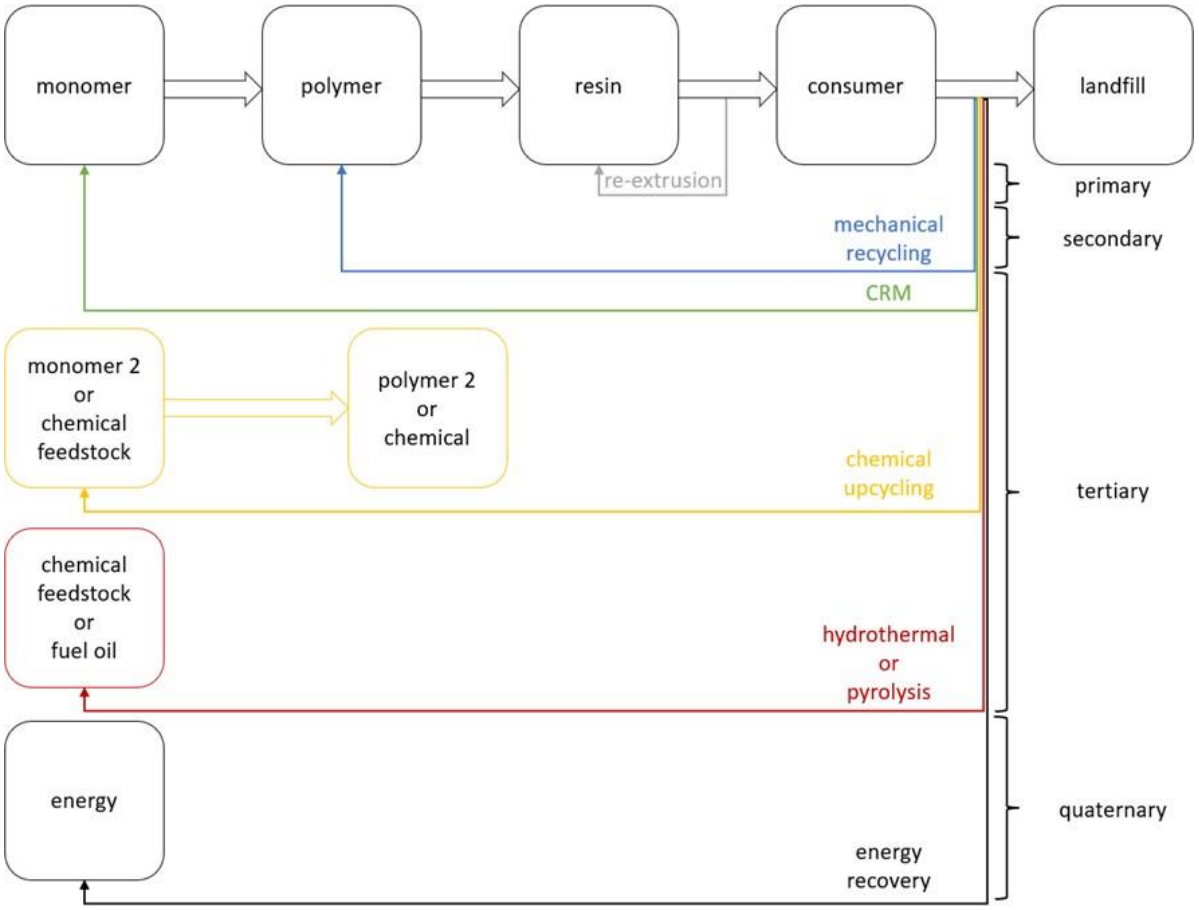


Figure 1.3. The possible life cycles of a piece of consumer plastic.

In contrast to these approaches is chemical recycling, or tertiary recycling. Unlike the other approaches, chemical recycling aims to break down the polymer chain chemically to its component parts (also known as 'chemolysis'), then use chemical sorting and purification techniques to obtain these in pure form. Chemical recycling can itself be divided into four methods: Chemical Recycling to Monomer (CRM), chemical upcycling, hydrothermal depolymerisation, and pyrolysis. CRM involves returning a polymer to its constituent monomer, which can then be used to produce new, 'virgin-like' plastic.[24] Chemical upcycling (henceforth referred to merely as 'upcycling') involves turning polymer into more valuable fine chemicals or materials,[25, 26] such as solvents.[27] Pyrolysis allow polymer to be degraded into raw hydrocarbons for use as chemical feedstocks or fuel oil.[24, 28] Hydrothermal cracking degrades polymer chains into small molecules such as phenols and esters.[26]

Pyrolysis can be applied to nearly all commodity polymers, including the polyolefins which are usually too chemically stable to be degraded by CRM, such as PE, PP and acrylonitrile butadiene styrene (ABS). It is also useful for valorising mixed plastic streams which cannot be easily sorted.[29] However, utilising temperatures of up to 1000 K (*ca.* 700 °C) and high pressures,[30, 31] the high energy costs, and low-value yield make pyrolysis a 'last resort' method of waste valorisation.

Hydrothermal cracking is similar in concept to pyrolysis; however, it uses supercritical water (i.e., above water's critical point: T_c = 647 K (374 °C) and P_c = 22.1 MPa) to both crack recyclate and capture products. In the same way as pyrolysis, hydrothermal cracking is also applicable to a wide variety of polymers, including polyolefins which are not currently recyclable by CRM.[32] On the other hand, this method suffers from major drawbacks including the use of elevated temperatures and pressures besides the scalability issues from lab scale to commercialization.

CRM has been demonstrated extensively with polyesters such as PET and poly(ethylene) phthalate, poly(lactic acid) (PLA) (although this usually goes *via* lactic acid as an isolated intermediate, rather than *via* lactate, the traditional monomer of PLA),[33] and polyhydroxyalkanoates (including, but not limited to, polylactones and polyhydroxybutyrate (PHB)),[34] as well as polycarbonates such as bisphenol-A polycarbonate (BPA-PC)[20] and ROCOP-derived polycarbonates, polythioesters,[21] and polyethers.[23, 35] It forms the basis of the 'circular economy' model of polymer sustainability, with theoretically infinite cycles of polymer to monomer and back to polymer being possible.[29] In practice, there are often degrees of degradation involved in the depolymerisation step, preventing a complete 100% circular economy. For example, catalysed ring-opening polymerisation (ROP) of trimethylene carbonate (TMC) to poly(trimethylene carbonate) is a relatively facile reaction; however, the depolymerisation to monomer only occurs at temperatures above 543 K (270 °C) and is not very selective – decarboxylation and oligomer presence prevent CRM from reaching its ideal state.

Upcycling involves use of functional molecules to degrade polymers or post-functionalise monomers (or polymers, though this will not be covered here).[36] One such example is glycolytic upcycling of BPA-PC into various compounds such as the solvent ethylene carbonate (EC) or the functionalised monomer 2-allyloxymethyl-2-ethyltrimethylene carbonate (AOMEC).[37, 38] PLA also has been shown to be upcycled primarily by alcoholysis,[2] although aminolysis is another possible route for PLA upcycling.[39] Polyethylene, often a difficult polymer to chemically recycle, has been shown to be able to be upcycled by hydrogenolysis to form high purity liquid oil fractions,[39] or by acid-catalysed hydrolysis to form functional diacids.[40]

1.3 Poly(ethylene) Terephthalate (PET) – Catalysis of Chemical Recycling

PET is a commodity polymer which comprises *ca.* 10% of global plastic resin production and *ca.* 70% of synthetic fibre production,[41] making it one of the most important commodity polymers worldwide. It is an aromatic polyester, meaning it has at least one ester group in its backbone per repeat unit, as well as an aromatic group. This ester group is a useful synthetic handle which allows PET to be degraded, by one of several different mechanisms (Scheme 1.1 includes some examples of the PET chemical recycling methods mentioned below):

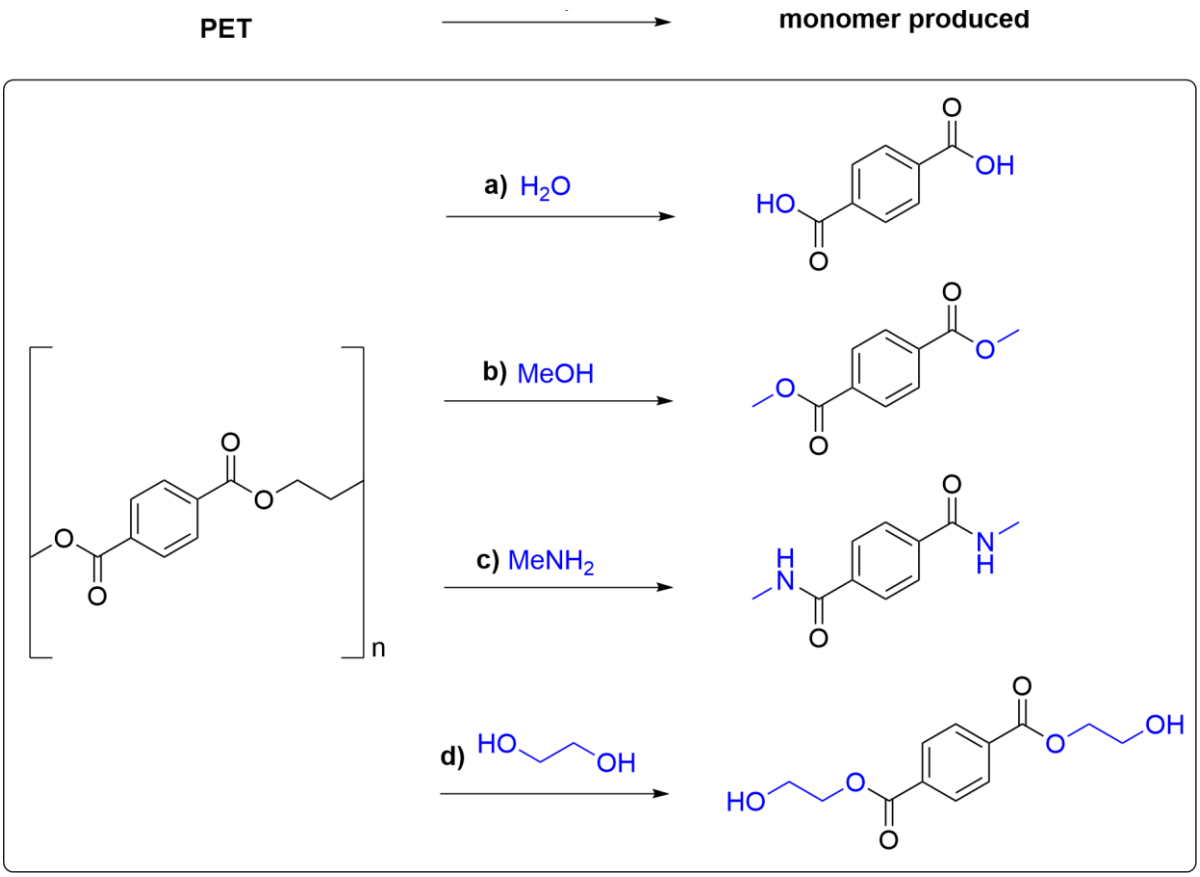
1. hydrolysis (breaking of the ester bond by water, forming a carboxylic acid and an alcohol);
2. alcoholysis (breaking of the ester bond by an alcohol, forming a new ester and alcohol);
3. glycolysis (breaking of the ester bond by a diol, forming two new alcohols, one with an ester bond in);
4. acidolysis (breaking of the ester bond by a carboxylic acid, forming a new ester and an alcohol);

5. ammonolysis (breaking of the ester bond by ammonia, forming a primary amide and an alcohol)

6. aminolysis (breaking of the ester bond by an amine, forming a secondary or tertiary amide and an alcohol).

7. hydrogenolysis (breaking of the ester bond by reduction with hydrogen, forming either two alcohols or an acid and a hydrocarbon)

Scheme 1.1. Various methods of PET chemical recycling: a) hydrolysis; b) alcoholysis, specifically methanolysis; c) aminolysis, specifically methylaminolysis; d) glycolysis, specifically ethylene glycolysis.



1.4 PET CRM

CRM of PET involves reformation of one of a limited pool of terephthalate-based monomers. Hydrolysis produces terephthalic acid and methanolysis produces dimethyl terephthalate, both of which can be repolymerised *via* condensation polymerisation using ethylene glycol (EG) into PET. Glycolysis is somewhat different, in that its depolymerisation product, bis(2-hydroxyethyl)terephthalate (BHET), can be directly repolymerised into PET, making it a strong (or, by the strictest definition, the only) candidate for CRM.

Acidolysis, ammonolysis, aminolysis and hydrogenolysis all create products that are not easily repolymerisable back into PET. These therefore fall under upcycling methods, rather than CRM methods, and their products are therefore used for purposes other than PET formation. It is possible to use alcoholysis and glycolysis as upcycling methods as well, although it is theoretically possible to repolymerise alcoholysis monomers back to PET under the right conditions.

1.4.1 Hydrolysis of PET

Hydrolysis of PET has several benefits, including low temperatures and pressures, and the utilisation of simple and safe catalysts, but it also has long reaction times compared with other methods of PET chemical recycling. This leads to increased total energy use. PET hydrolysis was first indicated in patents in the late 1950s and early 1960s,[42] using either alkaline or neutral solutions. These reaction conditions were often relatively high temperatures and pressures, above 373 K (100 °C) and 1 MPa. Uncatalysed neutral hydrolysis was the subject of several patents in the 1980s and 90s; catalysed neutral hydrolysis was introduced alongside, in Kozlov *et al.*'s 1984 paper introducing alkali metal acetates as catalysts.[43] Alkaline hydrolysis has mostly been employed using sodium or potassium hydroxide, which are variably considered as catalysts or not in the literature.[39, 44, 45] Catalysts such as quaternary ammonium salts have also been employed as phase transfer agents alongside the alkalis.[46]

A method for acid hydrolysis was patented by Brown and O'Brien in 1976,[47] and introduced ambient conditions to hydrolysis by utilising strong mineral acids such as phosphoric and nitric acids, although sulfuric acid is borne out as most popular in the literature.[48] Later additions to the literature report acidic catalysts such as *p*-toluenesulfonic acid (*p*-TSA), which enabled degradation of PET to 100% conversion in 1.5 h at 423 K (150 °C) (*cf.* concentrated sulfuric acid which takes 5 h under the same conditions).[49]

Hydrolysis is the method by which PET hydrolase enzymes such as *Is*PETase[50] degrade PET into mono(2-hydroxyethyl)terephthalate (MHET), or terephthalic acid (TA) and EG. These enzymes are bacterial or fungal in origin,[51] and cutinases have been shown to be the most efficient of these enzymes.[52, 53] Enzymes are very effective catalysts for their specific function and can function extremely efficiently at much lower temperatures than most chemical catalysts, but are generally more difficult to fine-tune for specific properties than chemical catalysts. For example, small changes in the binding site of *Is*PETase have been shown to have significant effects on its efficiency.[54] Nonetheless, this burgeoning field shows a great deal of promise. Recent developments include the use of machine learning to engineer novel PET hydrolases.[55] The most effective PET hydrolase to date is the compost-derived LCC^{ICCG} enzyme, which reaches a depolymerisation conversion of *ca.* 90% in 10 hours at *ca.* 70 ^{o}C.[56, 57]

Microwave heating alongside co-alcoholysis using a variety of organometallics (the most efficient of which was sodium methoxide) has also been shown to increase the depolymerisation speed, fully converting PET from polymer to TA in 5 minutes at 343 K (70 °C).[58]

Hydrolysis of PET has been shown to be a surface-mediated process,[41] likely a result of the relatively high crystallinity of PET preventing significant swelling over depolymerisation timescales. In fact, reduction of the crystallinity of PET by melt-extrusion with EG has been shown to significantly increase the depolymerisation speed.[42] The kinetics of PET hydrolysis are modelled using the shrinking-core model, first proposed by Yoshioka *et al.* in 1998.[59] This work

used Scanning Electron Microscopy imaging and kinetic plots of nitric acid-catalysed (and later work sulfuric acid-catalysed)[60] hydrolysis to determine the model (as illustrated in Figure 1.4). They found the apparent rate constant could be calculated according to Equation 1 below, where *C* is conversion (or 'degree of degradation').

$$(1 - C) - \frac{2}{3} - 1 = Kt \qquad 1$$

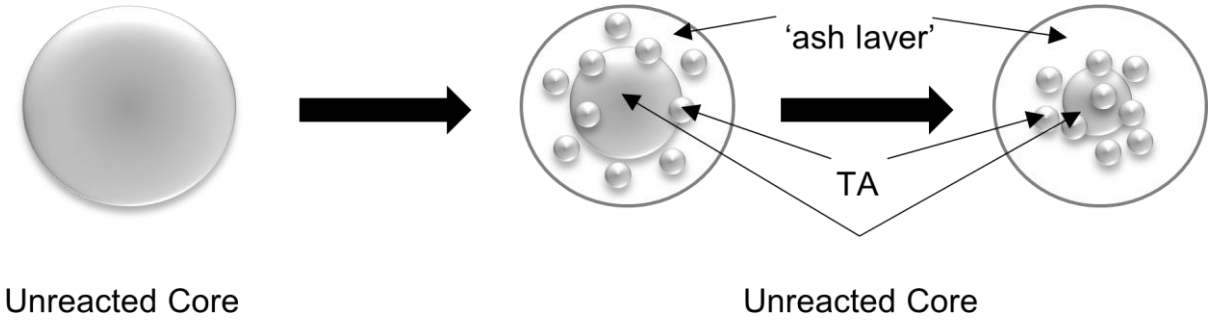


Figure 1.4. Shrinking-core model of PET hydrolysis.

Later studies added cracking and fragmentation to the possible steps required.[12, 61] It is possible variations in the crystallinity of the PET samples used in these studies was responsible for the variation in presence of a cracking step.

1.4.2 Alcoholysis of PET

Alcoholysis, primarily methanolysis, has many of the benefits of hydrolysis but is often performed at higher pressures, leading to faster reaction times at the cost of higher energy expenses. Methanolysis can be achieved by subcritical methods: pressures greater than 2-8 MPa and temperatures from 453 – 553 K (180 – 280 °C),[59, 62] or supercritical methods: temperatures and pressures exceeding 513 K (240 °C) and 8.22 MPa.[63]

Most early (pre-millennium) methanolysis methods are described in patents rather than scientific literature. The reaction can be catalysed by typical transesterification catalysts, with the most common being the aforementioned $Zn(OAc)_2$;[59, 64] also by organometallics such

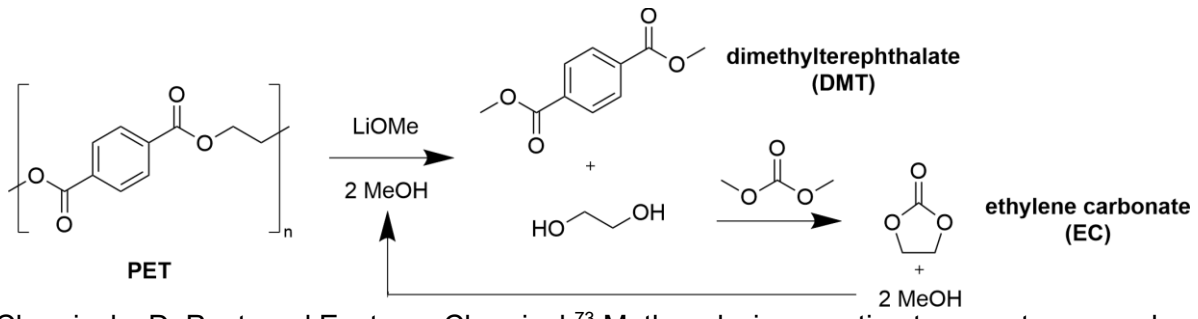
as aluminium triisopropoxide or zinc oxide,[65, 66] and by organocatalysts such as arylsulfonic acids.[67] Ionic liquids like choline acetate,[68] and polyionic liquids (PILs) containing Zn^{2+} and other metal ions are reported later as well.[69]

Supercritical methanolysis often foregoes the catalyst and increases the rapidity, at the cost of high temperature and pressure requiring higher energy costs.[70, 71] Complete depolymerisation into DMT and EG was possible in under 5 minutes in all cases, which drastically reduces the time component of energy consumption in comparison with glycolysis or hydrolysis, although the temperature component was of course significantly higher.

One publication of note is Tanaka *et al.*'s 2021 paper which describes the use of dimethyl carbonate (DMC) to 'capture' EG during PET methanolysis, forcing the equilibrium towards the products and allowing the temperature to be dropped to nearly room temperature at ambient pressure (as illustrated in Scheme 1.2).[72] This represents a significant improvement in PET depolymerisation by reduction in energy usage by application of very low active temperatures.

Industrial methanolysis plants are owned by several large corporations such as Hoechst, Dow

Scheme 1.2. Trapping of EG by DMC in the PET methanolysis reaction, including regeneration of MeOH.

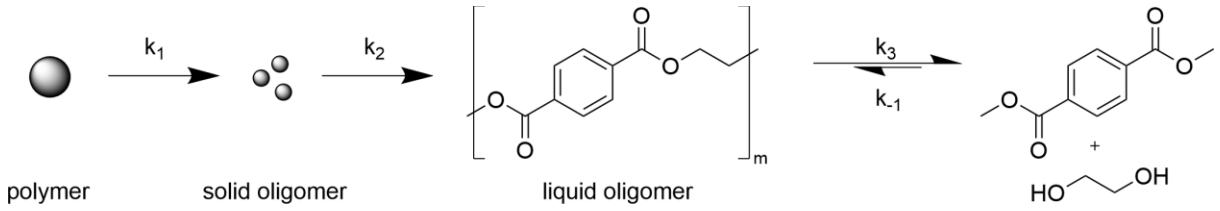


Chemicals, DuPont, and Eastman Chemical.[73] Methanolysis operating temperature can also be reduced to ambient conditions in the presence of dichloromethane (DCM) as cosolvent,[74, 75] although this of course reduces the sustainability of the reaction conditions.

Other methods of alcoholysis also exist, such as degradation of PET using butanol, octanol, and others.[65, 67, 73, 76, 77] These are sometimes posited as forms of upcycling, however, particularly in the case of alcoholysis using isooctanol, as dioctyl terephthalate can be used as a plasticiser.[78]

The kinetics of PET alcoholysis has been studied mostly in the context of methanolysis. The main model is still that of a modified shrinking-core model, however because of the fact that several monomers and oligomers can form before DMT is produced, the kinetics of methanolysis can become quite mathematically complex.[79] A simplified model assumes the depolymerisation of PET into solid oligomers is very fast and into liquid oligomers is fast, and both are irreversible steps, and so the equilibrium between liquid oligomer and DMT + EG is the key step (Scheme 1.3).[80]

Scheme 1.3. Simplified shrinking-core model with fast initial steps and equilibrium final steps.



This allows the mathematics to be simplified into the following equations, wherein *C* is PET conversion:

$$\frac{\mathrm{d[PET]}}{\mathrm{dt}} = -k'[PET] \qquad 2$$

$$k't = \ln\left(\frac{1}{1-C}\right) \qquad 3$$

This allows PET methanolysis to be approximated as a pseudo-first-order reaction, assuming the nucleophilic solvent (MeOH) is in excess. This is confirmed in literature examples.[2]

1.4.3 Glycolysis of PET

Single Catalysis

Glycolysis is another specific method of alcoholysis, usually involving EG as the nucleophile (although other glycols such as propylene glycol or diethylene glycol (DEG) are also viable),[81-83] which produces BHET as its major product. BHET can be directly repolymerised back into PET at temperatures above 543 K (270 °C) and low pressure,[84] making it – and by extension glycolysis as a whole – an attractive target for depolymerisation.

Glycolysis of PET was reported initially by Vaidya and Nadkarni in 1987 *via* propylene glycol,[85, 86] then by the same *via* EG a year later, using $Zn(OAc)_2$ as the catalyst.[87] Soon after, Baliga and Wong extended the EG glycolysis process to other metal acetate catalysts (lead, cobalt and manganese), finding that $Zn(OAc)_2$ was nonetheless superior at a reaction temperature of 463 K (190 °C).[88] Additionally, the presence of green pigment was found to have no effect on depolymerisation kinetics. $Zn(OAc)_2$ has since proven itself the staple and benchmark PET glycolysis catalyst,[89-96] although a later study showed manganese acetate surpassed $Zn(OAc)_2$ at a wider variety of temperatures.[97] Despite $Zn(OAc)_2$'s cementation as the default glycolysis catalyst, other metal-containing catalysts have been developed, such as alkali metal salts,[98-100] titanium phosphate,[96] metal chlorides and acetates such as $ZnCl_2$ and $MgCl_2$,[101-103] sulfated oxides such as ZnO/SO_4,[104, 105] single and mixed metal oxides such as ZnO and $ZnMn_2O_4$,[91, 106-108] titanate nanotubes,[109] heteropolyacids such as Zn^{2+}-loaded phosphotungstic acid,[110] and polyoxometalates (POMs) such as $K_6SiW_{11}ZnO_{39}$.[111] Bioderived catalysts such as silicate-based (though containing other metal oxides such as calcium, potassium, iron, manganese and magnesium) bamboo ash and orange peel ash catalysts have also been reported.[112-114] It is clear, however, that metals such as zinc and manganese dominate the metal-based catalyst design space for PET glycolysis.

Microwave depolymerisation has been observed to lower the activation energy of the glycolysis reaction, increasing the efficiency of degradation.[115] This has allowed for lower catalysts amounts,[82] shorter timespan of reaction,[89] and lower temperature.[56] Another method by which PET depolymerisation has been accelerated is by melt compounding catalyst into the bulk substrate before the chemolysis step. This provides a low-energy method of improving the catalyst's availability, increasing its activity and lowering reaction times.[116, 117]

In 2011, organic bases in the form of 1,5,7-triazabicyclo-[4.4.0]-dec-5-ene (TBD) were introduced as single PET glycolysis catalysts by Fukushima *et al.*.[75] A subsequent work by this group[118] surveyed a variety of organic bases for PET glycolysis, in which 1,8-diazabicyclo[5.4.0]undec-7-ene (DBU) appeared as the most efficient single catalyst for EG-based glycolysis. However, for longer-chain diols (such as 1,6-hexanediol), TBD was significantly faster. The authors hypothesise that the bifunctionality of TBD aids in providing a directing effect for longer-chain diols. Additionally, the pK_{aH} of the base tended to correlate with activity, with high-basicity catalysts depolymerising PET faster. This is borne out by a later study by Nica *et al.,*[119] which also compared these organocatalysts with a metal catalyst, titanium tetraisopropoxide. The comparison favours the organocatalysts for all but imidazole, and is equivalent to 1,4-diazabicyclo[2.2.2]octane (DABCO). TBD has since been functionalised in a variety of ways using terephthalates, glycols and amines, which has been shown to improve reaction time significantly.[108] Nanoparticle catalysts in addition have recently shown to be variously effective as PET glycolysis catalysts.[120-124] There are now many extant PET glycolysis single organocatalysts: urea,[125] cyanamide (although the authors argue it is a dual catalyst),[126] 1,3-dimethylimidazolium-2-carboxylate,[127] tropine,[128] and strong phosphazene bases.[92]

PET can be more efficiently glycolysed if reacted in a cosolvent. The first reported case of this was xylene,[129] although more recent examples use greener solvents such as *N*-methylpyrrolidone,[130, 131] acetonitrile[132] or anisole.[97] Use of these solvents has allowed for a

significant reduction in operating temperature with little to no drop in activity; in the case of acetonitrile the operating temperature was reduced as low as 363 K (90 ˚C).

PET glycolysis using single catalysis broadly falls into two kinetic categories. The first is the same kinetic category as methanolysis; that is, integration of single-step shrinking-core approximations which can produce the pseudo-first-order rate constant found in Equation 3. This is confirmed by several literature examples.[88, 106, 133] This method is also the one utilised by melt PET glycolysis,[134] as well as BPA-PC glycolysis.[89] The other example of rate equation is that wherein surface area calculations yield an apparent rate constant given by plotting Equation 4, wherein *C* is PET conversion:[114, 130]

$$1 - (1 - C)^{2/3} = k''t \qquad 4$$

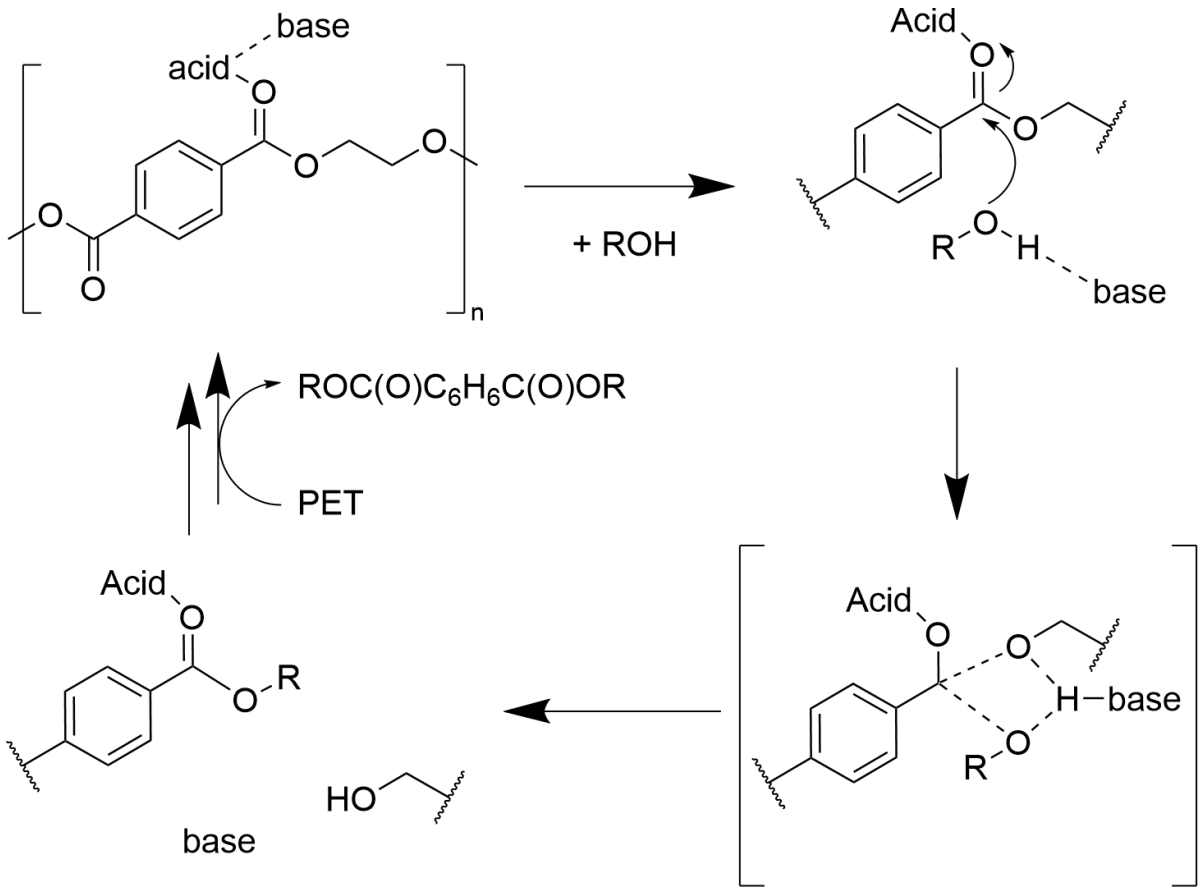
Another model is used in the case of heterogeneous PET glycolysis, known as the Avrami-Erofe'ev nucleation and growth model. A study by Sangalang *et al.* showed two of these Avrami-Erofe'ev models to be most applicable to heterogeneously catalysed PET glycolysis.[135]

Dual Catalysis

The chemical degradation of PET by alcoholysis or glycolysis are examples of trans-esterification reactions. Transesterification is a classic organic reaction which involves substitution of an alcohol into an ester group,[136] with the ester's parent alcohol being freed. Most often, a transesterification reaction is acid- or base-catalysed, as the free ester is quite stable in alcohol alone. This is also an immensely useful reaction for polymerisation, being used to form polyesters from monomers such as lactones and

lactides.[137, 138] It can also be used to polymerise methyl esters such as dimethyl terephthalate (DMT) with polyols or similar.[139]

Scheme 1.4. A typical dual-catalysed PET alcoholysis/glycolysis reaction mechanism.



Transesterification can also be catalysed by both an acid and a base simultaneously, known as dual or synergic catalysis (Scheme 1.4 represents the transesterification mechanism in PET glycolysis using an acid-base dual catalytic system).[140] Dual catalysts can be defined as one of four types:[141] Type I have no overlapping function, and neither alone can generate the product; in Type II one of the catalysts can promote the reaction, albeit inefficiently; Type III dual catalysts have both components which can promote the reaction, albeit inefficiently; Type IV allows one catalyst to form undesirable coproducts.

Type II and III dual catalysts have been employed successfully in polymerisation of lactide,[142] lactones,[143, 144] and DMT with diols.[145] The mechanism of transesterification has been extensively studied, especially in relation to acid-, base-, and acid/base dual catalysis.

These two types (Type II and Type III dual catalysts) have been extended to PET glycolysis catalysis. There are three categories of these dual catalysts as they are used for PET glycolysis: ionic liquids (ILs), organocatalysts and organometallic catalysts.

ILs are simply any liquid comprised of ionic components, and can be subdivided into those with metal components – such as 1-butyl-3-methylimidazolium tetrachloroferrate ([bmim] $FeCl_4$),[146] 1,3-diethylimidazolium triacetic metallates ([deim][$M(OAc)_3$]),[147] or di[bmim] metal chlorides[146, 148] – and those which are purely organic – such as [bmim]X^- or [deim]X^- ILs,[149, 150] amino acid- or urea-cholinium ILs,[151] 1,8-Diazabicyclo[5.4.0]undec-7-ene (DBU) phenol ILs,[65] and even poly(ionic liquids) (PILs) such as poly(1-vinyl-3-ethylimidazole) acetate (P[VEIm]Ac).[152]

Dual organocatalysts fall broadly into two categories: organic ILs, as discussed above, and organic salts of an acid and a base, such as TBD:methanesulfonic acid (TBD:MSA).[144] Many such organic salts have been developed, including the aforementioned TBD:MSA, which has been shown to repolymerise BHET as well as depolymerise PET, paving the way for a true PET circular economy. The authors extended their study to include differing stoichiometries and acid/base components.[83] Several similar acid:base salts have been subsequently developed,[153] such as TBD:trifluoromethanesulfonic acid (TBD:TfOH), TBD:benzylic acid (TBD:BA) and TBD:*p*-TSA; the authors report that the key component of a rapid, thermally-stable organic salt dual catalyst is high ΔpK_a values (≥16.9).

Generally, single-catalyst organic bases are faster at depolymerising PET, but degrade more rapidly and therefore have a lifetime of fewer catalytic cycles. The thermal stability of these dual catalysts is thus their ‘unique selling point’.

Organometallic dual catalysts usually include a metal salt and an organic base, principally involving $Zn(OAc)_2$ and a cocatalyst such as DBU,[102] N,N-dimethylaminopyridine (DMAP),[127] tropine,[154] urea[155] or 1,3-dimethylurea (DMU) (Figure 1.5.)[102] Alternatively, they may be ILs as discussed above. There is a distinct lack of any systematic screen of organometallic dual catalysts, with only delle Chiaie *et al.* reporting and directly comparing $Zn(OAc)_2$ / base combinations,[154] of which $Zn(OAc)_2$ / DMAP was found to be the most efficient, and Wang *et al.* comparing metal salts in combination with urea.[127]

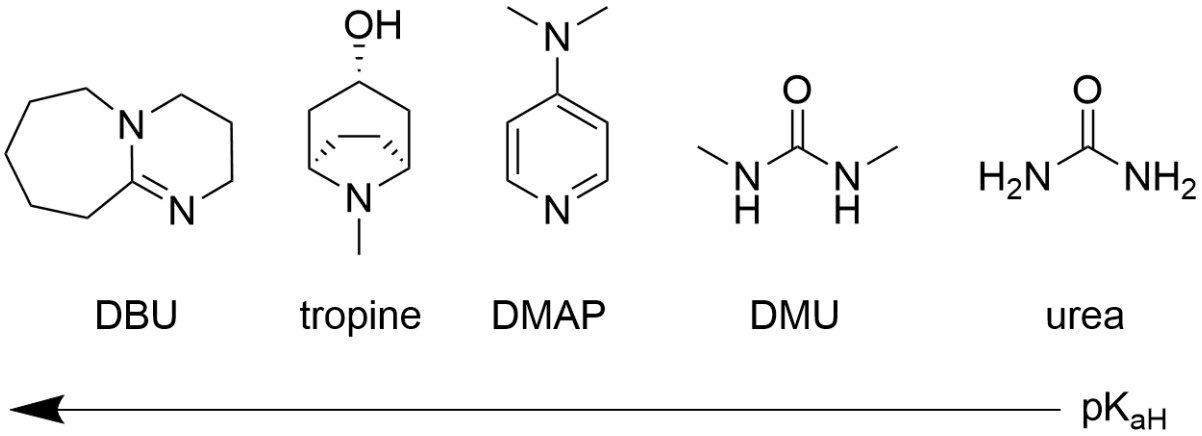


Figure 1.5. Bases used in combination with $Zn(OAc)_2$, in decreasing pK_{aH} order.

The mechanism of dual organometallic catalysis has been investigated in a few studies, one example being Deng *et al.*'s 2021 paper which utilised tropine as the base: they used DFT to propose a concerted mechanism in which tropine was simultaneously bound to the metal and acting as a base to deprotonate the glycol.[156] Similarly, Horn *et al*.'s earlier study investigated the role of TBD (single organocatalysed system) to act simultaneously as an acid and base, hydrogen-bonding to the carbonyl with its protonated amine, and deprotonating the glycol with its basic nitrogen.[153] Chen *et al.* speculate their reaction mechanism with $Zn(OAc)_2$ and DBU allows the acetate ligand to participate as a base, although this is likely a result of the 1:2 ratio of $Zn(OAc)_2$:DBU.[157] For non-$Zn(OAc)_2$ catalysts, Trejo-Carbajal *et al.* propose that the basic activity of *tert*-butylamine is entirely separate from the acidic activity of lithium bromide, as in the classic picture of dual catalysis;[158] however, this is not backed up with any computational methods, and it is possible the highly bulky *tert*-butyl group present on the amine prevents

association with the metal. The mechanism for dual organocatalysts is more fully understood. The DES choline acetate shows how the acetate ion acts as a base, whereas the cholinium ion acts as an acid.[153] A similar mechanism is proposed by Wang *et al.* for their DBU / phenol protic ionic liquid catalyst.

The kinetics of the dual catalysed reaction have been studied by Chen *et al.*, who concluded the surface-area-based Equation 1.4. was most appropriate for their $Zn(OAc)_2$ / DBU system.[151] Additionally, Wang *et al.* used the same model in their DBU / phenol catalyst's glycolysis kinetics.[159]

1.4.4 PET CRM Methods Energy Usage

The three methods of PET CRM (hydrolysis, methanolysis, glycolysis) all require different temperatures, pressures and timescales to complete depolymerisation. In order to properly compare these methods, a metric known as 'Environmental Energy Impact' (EEI), developed by Barnard *et al.* as a simple alternative to life-cycle analysis (LCA), was used.[117] This metric simply multiplies the operating temperature of the reaction by the time required to reach 100% conversion. Highlighted catalytic conditions for each method were selected and compared (Table 1.1.).

Table 1.1. Comparison of the most efficient hydrolysis, methanolysis and glycolysis conditions. [a]tetrabutylammonium iodide; [b]choline chloride; [c]1,3-dimethylurea

Solvent	Catalyst	Temperature / °C	Reaction Time / min	EEI / °C min
NaOH (aq)	TBAI[a]	90	45	1.6×10^4

NaOH (aq)	microwave	220	2	7.8×10^2
Na_2PO_3 (aq)	ICCG enzyme	65	900	4.7×10^6
MeOH	nanodisperse ZnO	170	15	2.0×10^3
MeOH	supercritical	300	70	2.6×10^4
2-ethylhexanol	$Zn(OAc)_2$ / ChCl[b]	185	160	1.9×10^4
EG	$Zn(OAc)_2$	196	60	4.9×10^3
EG	$Zn(OAc)_2$ microwave	196	35	4.3×10^3
EG	$Zn(OAc)_2$/1,3-DMU[c]	190	20	1.9×10^2
EG	TBD	190	210	2.5×10^4
EG	TBD:MSA	180	120	1.3×10^4

It is clear from these values that the most energy-efficient depolymerisation methods are those which employ high temperatures to ensure short reaction times; low-temperature solutions such as the enzymatic PET hydrolases require too much time, so that even at low temperatures they require more energy overall. Additionally, microwave synthesis appears to greatly reduce the required energy input; however, problems with scale-up of microwave systems make this a challenging approach to pursue.

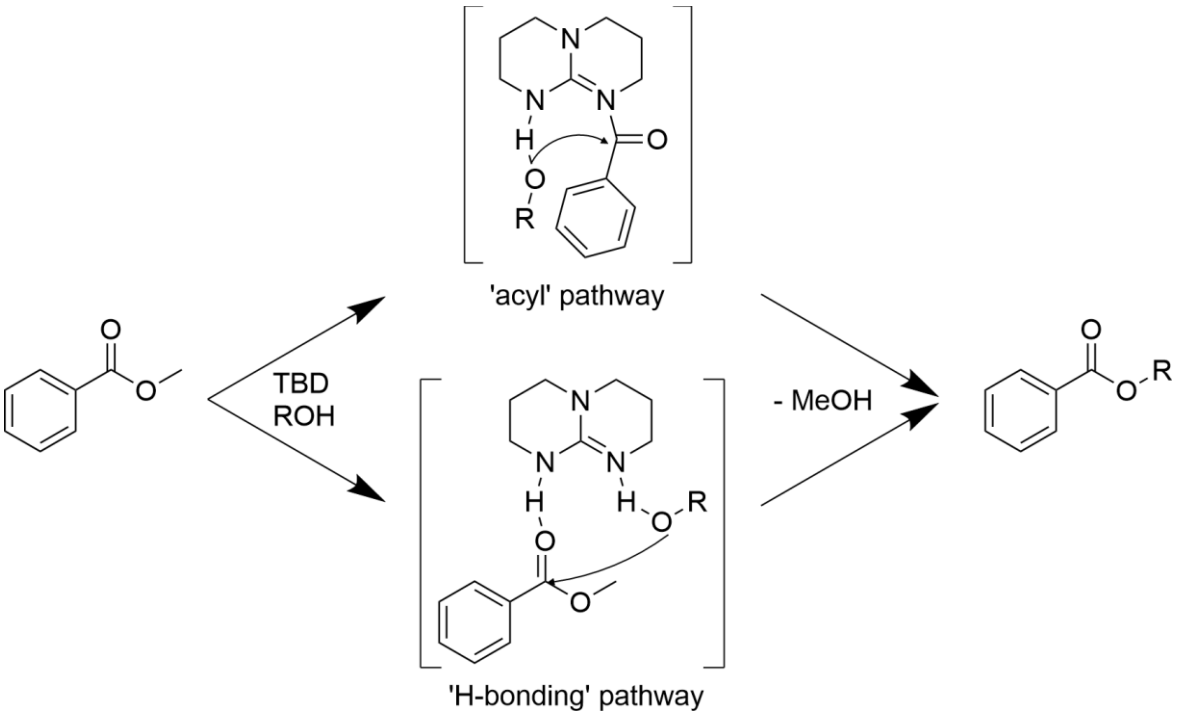
1.5 Use of Density Functional Theory in PET Depolymerisation Mechanistic Studies

Density Functional Theory (DFT) is a useful tool for elucidating mechanisms, energies and structures of chemical systems. It is an *ab initio* quantum chemistry technique, meaning it calculates electronic energies and therefore optimal geometries and rovibrational modes from first principles.

The majority of PET depolymerisation publications do not investigate the mecanism in great detail, and those that have were detailed in Section 1.4.1, aside from Fukushima *et al.*'s 2011 companion study to their seminal paper describing TBD's unusually high activity. In this work they use DMT and MeOH as model compounds of PET glycolysis to investigate the energy levels of the minimum energy pathway of the reaction. The results show the hydrogen-bonding pathway was significantly energetically superior to the TBD acyl-transfer pathway (Scheme 1.5.)[160]

Horn *et al.* later published work wherein they utilised DFT to study the trans-esterification of methyl benzoate and ethylene glycol as a model compound for PET glycolysis. It was found that an additional EG molecule acting as cocatalyst was responsible for a decrease in all intermediate and transition state energies, although the activation energy was lowest with one EG molecule.

Scheme 1.5. Examples of 'acyl' pathway *versus* 'Hydrogen-bonding' pathway of TBD-catalysed PET alcoholysis.



1.6 PET Upcycling

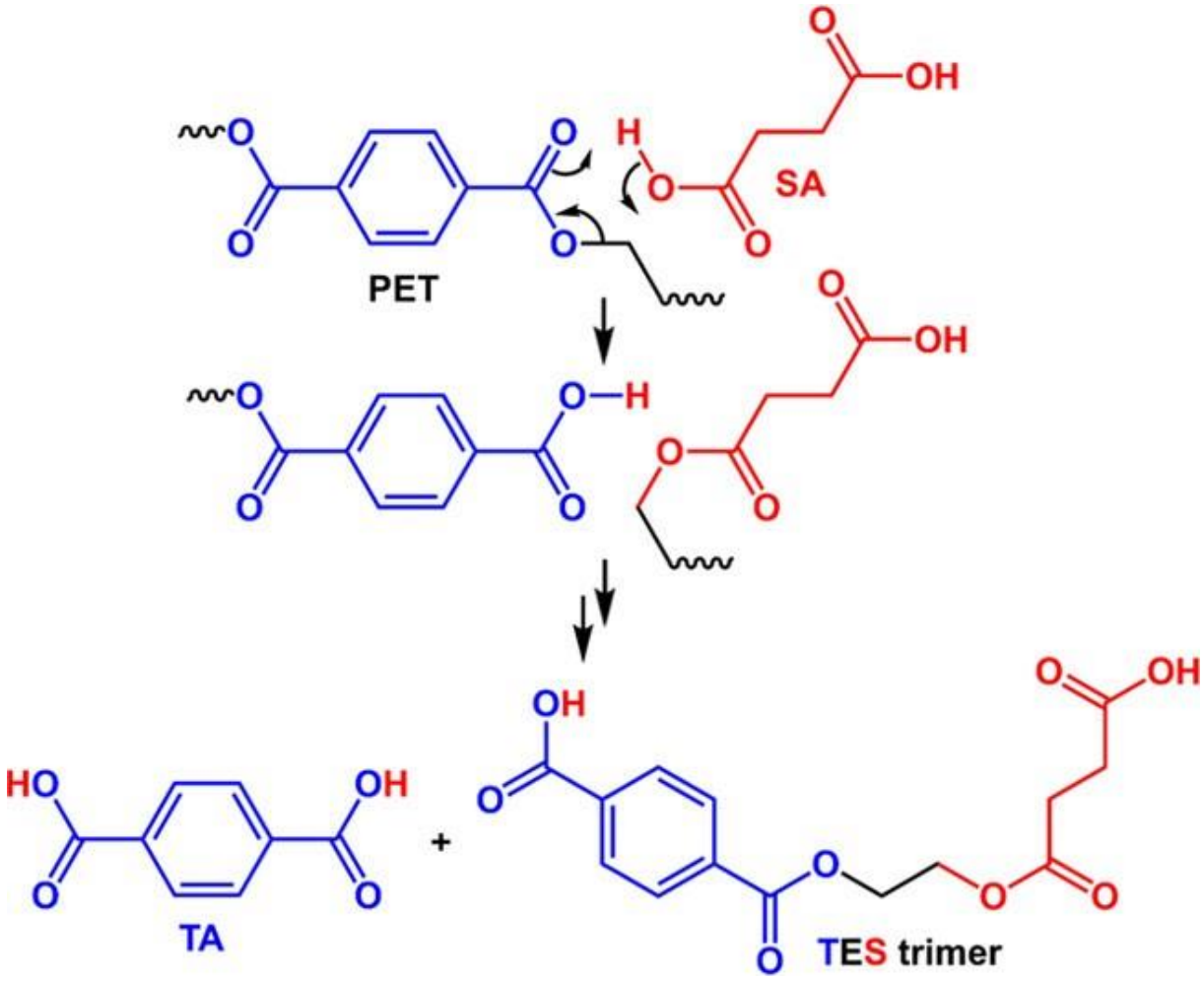
As aforementioned, PET upcycling is turning PET waste into more valuable chemicals than its corresponding monomer; this can be achieved with a variety of methods.

Ammonolysis is a difficult process because of the relative unreactivity of ammonia. Soni et al. were the first to characterise the terephthalamide resultant from ammonolysis of PET waste, catalysed by cetyl ammonium bromide.[161] Ammonolysis has since been shown to be catalysed by common glycolysis catalyst zinc acetate ($Zn(OAc)_2$).[162]

Aminolysis, on the other hand, is a rapid and easily catalysed process (requiring temperatures of only up to 373 K (100 °C)) for which the literature expounds on many examples. Aminolysis of PET was reported first in 1962,[163] with later developments bringing employment of ethanolamine and microwave heating.[164-167] Since then, aminolysis of PET has usually been posited as a form of upcycling, most commonly to form polyurethanes[168-170] or polyester-amides,[171-173] but also to develop antimicrobials and antifungals.[166, 174] Common catalysts employed in PET aminolysis are metal acetates (such as $Zn(OAc)_2$),[175-177] as well as ionic liquids[178] and Deep Eutectic Solvents (DESs),[179] and organocatalysts.[180, 181] Another subset of aminolysis is use of hydrazine to depolymerise PET, which allows access to a wide variety of products such as nitriles and hydrazones.[174, 177, 182]

Acidolysis is a relatively under-explored method of PET upcycling, introduced in 2022 by Hoang et al. as they depolymerised PET using adipic acid to oligo(ethylene adipate-co-terephthalate).[78] They then extended this method to succinic acid (Scheme 1.6).[183] The authors demonstrate the subsequent dicarboxylic acids ability to be used as curing agents for epoxy and other resins.

Scheme 1.6. Proposed mechanism of acidolytic upcycling of PET. Reproduced with permission from Hoang *et al.*[1] under Creative Commons Non-Commercial Attribution License.



A further, more destructive method of PET upcycling is *hydrogenolysis*, wherein the ester bond is fully reduced to alcohols (usually by a ruthenium catalyst as in Krall *et al.*'s 2014 work),[184] or a hydrocarbon/alcohol pair (as in subsequent literature),[185, 186] with catalysts including the near-ubiquitous $Zn(OAc)_2$.[187] Some latter work has reported the hydrogenation of PET into TA and hydrocarbons.[73, 188]

Precious little has been achieved in the field of PET upcycling *via* alcoholysis, mostly focusing on the use of dioctyl terephthalate as a plasticiser, as opposed to a monomer for PET repolymerisation.

[74, 176] There have also been many reported examples of BHET monomer being functionalised and modified post-depolymerisation,[189] as opposed to degrading PET directly into functionalised molecules. One example of this is the use of neopentyl glycol by Kathalewar *et al.* to glycolyse PET waste then prepare polyurethane materials used for coating applications.[190] Similar applications have been found for DEG glycolyzed products.[190, 191] Glycolysed PET waste has also been used to form heavy metal adsorbent microspheres,[192] as luminescent sensors,[193] and new copolymers with diols.[194] Melt chain scission in the absence of any other catalyst or solvent has been used to convert PET into a vitrimer network by trapping of the newly formed chain ends by epoxide N,N′-tetraglycidyldiaminodiphenyl methane (TGDDM).[195]

Hydrolysis is only possible by upcycling of the monomers into new fine chemicals, which can be achieved by enzymatic conversion. *G. oxydans* has been shown to convert EG into glycolic acid (a cosmetic ingredient), and other enzymes to convert TA into protocatechuic acid, alongside many other targets.[196]

As well as this, PET can be depolymerised partially into oligomers and repolymerised into upcycled materials. One such example is the use of linoleic acid-derived ‘dimer fatty acid’ to create what the authors call ‘PET-DFA segmented thermoplastic copolymer’.[197] The catalyst was chosen to be capable of both depolymerisation of PET and repolymerisation to their copolymer. Geyer *et al.* have used adipic acid as a chain scission agent which replaces terephthalate repeat units.[129] PET oligomers have also been copolymerised with poly(ethylene glycol) (PEG) to form PE-compatible block copolymers.[36]

PET can also be functionalised by chemical modification of the polymer without depolymerisation, but that is beyond the scope of this review.

1.7 Additive Manufacturing In Upcycling

Additive manufacturing, also known as 3D printing, is a method by which parts and materials are manufactured by addition of small amounts in points or layers to a build plate. In this way, shapes and structures which cannot be accessed by conventional manufacturing techniques can be assembled.

Chemolytic upcycling of polymers for 3D printing applications is a relatively unexplored field. Most publications focus on mechanically upcycling polymer and mixing with virgin polymer to form filament for fused deposition modelling (FDM) 3D printing. Shao *et al.* reported a method of PLA upcycling by aminolysis and subsequent esterification to form 3D-printable resins with notable mechanical properties.[36]

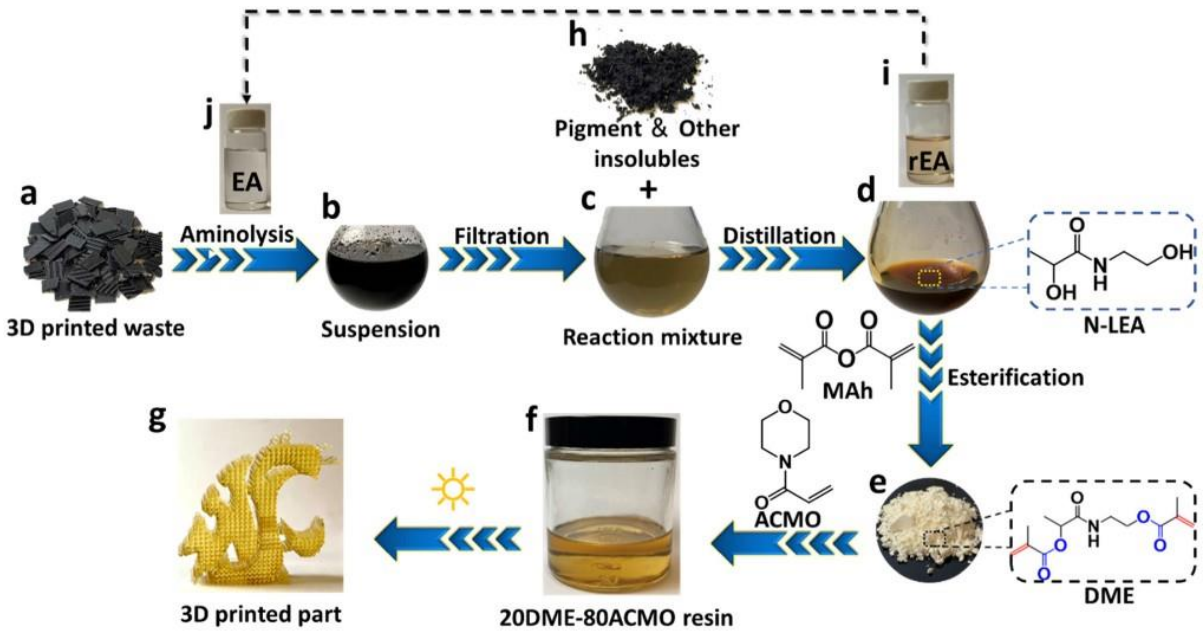


Figure 1.6. Aminolytic upcyclic of PLA to produce 3D-printable resins. Reproduced with permission from Shao *et al.*.[2]

1.8 Summary and Outlook

The degradability of polymers, and PET in particular, is a long-studied field, but has only become popular in recent years. There is, however, still room for novel efficient catalysts; in fact, it might be said that a breakthrough is direly needed for the design space to move forward. In the past 40 years, the major paradigm shifts have been the development of PETase enzymes for hydrolysis, and the introduction of near-room-temperature EG trapping in methanolysis or *via* use of cosolvents in the reaction. Little else has changed in the field of PET CRM, and especially in glycolysis, since $Zn(OAc)_2$ was introduced as a glycolysis catalyst. Despite the relative surge in dual catalysis development, only a few works have been performed to understand the mechanism and relationships between dual catalyst functionality and activity. This work hopes to build the basis of an understanding of PET glycolysis dual catalysis, thus developing a working knowledge from which novel, breakthrough catalysts can be discovered.

Upcycling of polymers has also entered a renaissance in recent years, with many publications modifying existing polymers chemically and physically. Few papers display full chemical degradation of polymers as a form of upcycling, and fewer still directly show the use cases of the resultant chemicals or materials. This work also illustrates a method of PET degradation *via* alcoholysis, a nearly totally unexplored method, which can be utilised for direct upcycling by repolymerisation into functional, 3D-printable materials.

1.9 References

1. OECD, *Global Plastics Outlook*, 2022.
2. R. Geyer, J. R. Jambeck and K. L. Law, *Science Advances*, 2017, **3**, e1700782.
3. T. R.-S. João Pinto Da Costa, Armando C. Duarte, *The environmental impacts of plastics and micro-plastics use, waste and pollution: EU and national measures*.
4. Y. Zhou, V. Ashokkumar, A. Amobonye, G. Bhattacharjee, R. Sirohi, V. Singh, G. Flora, V. Kumar, S. Pillai, Z. Zhang and M. K. Awasthi, *Environmental Pollution*, 2023, DOI: https://doi.org/10.1016/j.envpol.2023.121106, 121106.
5. J. Brahney, M. Hallerud, E. Heim, M. Hahnenberger and S. Sukumaran, *Science*, 2020, **368**, 1257-1260.

6. H. A. Leslie, M. J. M. van Velzen, S. H. Brandsma, A. D. Vethaak, J. J. Garcia-Vallejo and M. H. Lamoree, *Environment International*, 2022, **163**, 107199.
7. L. D. Ellis, N. A. Rorrer, K. P. Sullivan, M. Otto, J. E. McGeehan, Y. Román-Leshkov, N. Wierckx and G. T. Beckham, *Nature Catalysis*, 2021, **4**, 539-556.
8. J.-P. Lange, *ACS Sustainable Chemistry & Engineering*, 2021, **9**, 15722-15738.
9. M. R. Hannah Ritchie, *Journal*, 2018.
10. G. L. Huffman and D. J. Keller, in *Polymers and Ecological Problems*, ed. J. Guillet, Springer US, Boston, MA, 1973, DOI: 10.1007/978-1-4684-0871-3_10, pp. 155-167.
11. M. E. Dunn, M. Mills and D. Veríssimo, *Conservation Science and Practice*, 2020, **2**, e280.
12. P. Benyathiar, P. Kumar, G. Carpenter, J. Brace and D. K. Mishra, *Polymers*, 2022, **14**, 2366.
13. Z. O. G. Schyns and M. P. Shaver, *Macromolecular Rapid Communications*, 2021, **42**, 2000415.
14. R. Geyer, B. Kuczenski, T. Zink and A. Henderson, *Journal of Industrial Ecology*, 2016, **20**, 1010-1017.
15. W. McDonough and M. Braungart, *Cradle to Cradle: Remaking the Way We Make Things*, North Point Press, 2002.
16. S.-G. European Commission, *A European Strategy for Plastics in a Circular Economy*.
17. M. Crippa and B. Morico, in *Studies in Surface Science and Catalysis*, eds. A. Basile, G. Centi, M. D. Falco and G. Iaquaniello, Elsevier, 2020, vol. 179, pp. 215-229.
18. A. Merrington, in *Applied Plastics Engineering Handbook (Second Edition)*, ed. M. Kutz, William Andrew Publishing, 2017, DOI: https://doi.org/10.1016/B978-0-323-39040-8.00009-2, pp. 167-189.
19. N. Singh, D. Hui, R. Singh, I. P. S. Ahuja, L. Feo and F. Fraternali, *Composites Part B: Engineering*, 2017, **115**, 409-422.
20. G. W. Coates and Y. D. Y. L. Getzler, *Nature Reviews Materials*, 2020, **5**, 501-516.
21. C. Jehanno, J. W. Alty, M. Roosen, S. De Meester, A. P. Dove, E. Y. X. Chen, F. A. Leibfarth and H. Sardon, *Nature*, 2022, **603**, 803-814.
22. L. T. J. Korley, T. H. Epps, B. A. Helms and A. J. Ryan, *Science*, 2021, **373**, 66-69.
23. C. Jehanno, J. Demarteau, D. Mantione, M. C. Arno, F. Ruipérez, J. L. Hedrick, A. P. Dove and H. Sardon, *Angewandte Chemie International Edition*, 2021, **60**, 6710-6717.
24. M. Rehan, R. Miandad, M. A. Barakat, I. M. I. Ismail, T. Almeelbi, J. Gardy, A. Hassanpour, M. Z. Khan, A. Demirbas and A. S. Nizami, *International Biodeterioration & Biodegradation*, 2017, **119**, 162-175.
25. R. Miandad, M. Rehan, M. A. Barakat, A. S. Aburiazaiza, H. Khan, I. M. I. Ismail, J. Dhavamani, J. Gardy, A. Hassanpour and A.-S. Nizami, *Frontiers in Energy Research*, 2019, **7**.
26. T. Helmer Pedersen and F. Conti, *Waste Management*, 2017, **68**, 24-31.
27. M. Day, J. D. Cooney, C. Touchette-Barrette and S. E. Sheehan, *Journal of Analytical and Applied Pyrolysis*, 1999, **52**, 199-224.
28. A. Demirbas, M. A. Baluabaid, M. Kabli and W. Ahmad, *Petroleum Science and Technology*, 2015, **33**, 129-138.
29. P. McKeown and M. D. Jones, *Sustainable Chemistry*, 2020, **1**, 1-22.

30. Y.-T. Li, H.-Y. Yu, W.-B. Li, Y. Liu and X.-B. Lu, *Macromolecules*, 2021, **54**, 4641-4648.
31. J. G. Kim, *Polymer Chemistry*, 2020, **11**, 4830-4849.
32. J. Yuan, W. Xiong, X. Zhou, Y. Zhang, D. Shi, Z. Li and H. Lu, *Journal of the American Chemical Society*, 2019, **141**, 4928-4935.
33. Y. Wang, Y. Hou and H. Song, *Polymer Degradation and Stability*, 2017, **144**, 17-23.
34. S. Enthaler, *Journal of Applied Polymer Science*, 2014, **131**.
35. C. Jehanno, J. Demarteau, D. Mantione, M. C. Arno, F. Ruipérez, J. L. Hedrick, A. P. Dove and H. Sardon, *ACS Macro Letters*, 2020, DOI: 10.1021/acsmacrolett.0c00164, 443-447.
36. L. Shao, Y.-C. Chang, C. Hao, M.-e. Fei, B. Zhao, B. J. Bliss and J. Zhang, *Green Chemistry*, 2022, **24**, 8716-8724.
37. G. Celik, R. M. Kennedy, R. A. Hackler, M. Ferrandon, A. Tennakoon, S. Patnaik, A. M. Lapointe, S. C. Ammal, A. Heyden, F. A. Perras, M. Pruski, S. L. Scott, K. R. Poeppelmeier, A. D. Sadow and M. Delferro, *ACS Central Science*, 2019, **5**, 1795-1803.
38. E. Bäckström, K. Odelius and M. Hakkarainen, *Industrial and Engineering Chemistry Research*, 2017, **56**, 14814-14821.
39. D. Paszun and T. Spychaj, *Industrial and Engineering Chemistry Research*, 1997, **36**, 1373-1383.
40. G. P. Karayannidis, A. P. Chatziavgoustis and D. S. Achilias, *Advances in Polymer Technology*, 2002, **21**, 250-259.
41. S. Mishra and A. S. Goje, *Polymer Reaction Engineering*, 2003, **11**, 963-987.
42. S. Mishra, V. S. Zope and A. S. Goje, *Polymer International*, 2002, **51**, 1310-1315.
43. H. I. Khalaf and O. A. Hasan, *Chemical Engineering Journal*, 2012, **192**, 45-48.
44. *USA Pat.,* 1976.
45. W. Yang, J. Wang, L. Jiao, Y. Song, C. Li and C. Hu, *Green Chemistry*, 2022, DOI: 10.1039/D1GC04567A.
46. S. Yoshida, K. Hiraga, T. Takehana, I. Taniguchi, H. Yamaji, Y. Maeda, K. Toyohara, K. Miyamoto, Y. Kimura and K. Oda, *Science*, 2016, **351**, 1196.
47. F. Kawai, T. Kawabata and M. Oda, *Applied Microbiology and Biotechnology*, 2019, **103**, 4253-4268.
48. W. Zimmermann, *Philosophical Transactions of the Royal Society A: Mathematical, Physical and Engineering Sciences*, 2020, **378**, 20190273.
49. T. Tiso, T. Narancic, R. Wei, E. Pollet, N. Beagan, K. Schröder, A. Honak, M. Jiang, S. T. Kenny, N. Wierckx, R. Perrin, L. Avérous, W. Zimmermann, K. O'Connor and L. M. Blank, *Metabolic Engineering*, 2021, **66**, 167-178.
50. H. P. Austin, M. D. Allen, B. S. Donohoe, N. A. Rorrer, F. L. Kearns, R. L. Silveira, B. C. Pollard, G. Dominick, R. Duman, K. El Omari, V. Mykhaylyk, A. Wagner, W. E. Michener, A. Amore, M. S. Skaf, M. F. Crowley, A. W. Thorne, C. W. Johnson, H. L. Woodcock, J. E. McGeehan and G. T. Beckham, *Proceedings of the National Academy of Sciences*, 2018, **115**, E4350-E4357.
51. H. Lu, D. J. Diaz, N. J. Czarnecki, C. Zhu, W. Kim, R. Shroff, D. J. Acosta, B. R. Alexander, H. O. Cole, Y. Zhang, N. A. Lynd, A. D. Ellington and H. S. Alper, *Nature*, 2022, **604**, 662-667.
52. V. Tournier, C. M. Topham, A. Gilles, B. David, C. Folgoas, E. Moya-Leclair, E.

Kamionka, M. L. Desrousseaux, H. Texier, S. Gavalda, M. Cot, E. Guémard, M. Dalibey, J. Nomme, G. Cioci, S. Barbe, M. Chateau, I. André, S. Duquesne and A. Marty, *Nature*, 2020, **580**, 216-219.
53. R. Wei, G. von Haugwitz, L. Pfaff, J. Mican, C. P. S. Badenhorst, W. Liu, G. Weber, H. P. Austin, D. Bednar, J. Damborsky and U. T. Bornscheuer, *ACS Catalysis*, 2022, **12**, 3382-3396.
54. M. A. Mohsin, M. A. Alnaqbi, R. M. Busheer and Y. Haik, *Catalysis in Industry*, 2018, **10**, 41-48.
55. S. Thomas, A. Rane, K. Kanny, A. V.K. and M. G. Thomas, *Recycling of Polyethylene Terephthalate Bottles*, Elsevier Inc., 2018.
56. Z. Aayanifard, A. Khan, M. Naveed, J. Schager and M. Rabnawaz, *Polymer*, 2023, **265**, 125585.
57. T. Yoshioka, N. Okayama and A. Okuwaki, *Industrial & Engineering Chemistry Research*, 1998, **37**, 336-340.
58. T. Yoshioka, T. Motoki and A. Okuwaki, *Industrial & Engineering Chemistry Research*, 2001, **40**, 75-79.
59. D. Paszun and T. Spychaj, *Industrial & Engineering Chemistry Research*, 1997, **36**, 1373-1383.
60. D. S. Achilias and G. P. Karayannidis, *Water, Air and Soil Pollution: Focus*, 2004, **4**, 385-396.
61. I. M. Abdulagatov, N. G. Polikhronidi, A. Abdurashidova, S. B. Kiselev and J. F. Ely, *International Journal of Thermophysics*, 2005, **26**, 1327-1368.
62. H. Kurokawa, M.-a. Ohshima, K. Sugiyama and H. Miura, *Polymer Degradation and Stability*, 2003, **79**, 529-533.
63. J.-T. Du, Q. Sun, X.-F. Zeng, D. Wang, J.-X. Wang and J.-F. Chen, *Chemical Engineering Science*, 2020, **220**, 115642.
64. C. Liu, Y. Ling, Z. Wang, W. Zheng, W. Sun and L. Zhao, *Chemical Engineering Science*, 2022, **247**, 117024.
65. Z. Jiang, D. Yan, J. Xin, F. Li, M. Guo, Q. Zhou, J. Xu, Y. Hu and X. Lu, *Polymer Degradation and Stability*, 2022, DOI: https://doi.org/10.1016/j.polymdegradstab.2022.109905, 109905.
66. M. Genta, T. Iwaya, M. Sasaki, M. Goto and T. Hirose, *Industrial & Engineering Chemistry Research*, 2005, **44**, 3894-3900.
67. M. Goto, H. Koyamoto, A. Kodama, T. Hirose, S. Nagaoka and B. J. McCoy, *AIChE Journal*, 2002, **48**, 136-144.
68. S. Tanaka, J. Sato and Y. Nakajima, *Green Chemistry*, 2021, **23**, 9412-9416.
69. A. B. Raheem, Z. Z. Noor, A. Hassan, M. K. Abd Hamid, S. A. Samsudin and A. H. Sabeen, *Journal of Cleaner Production*, 2019, **225**, 1052-1064.
70. D. D. Pham and J. Cho, *Green Chemistry*, 2021, **23**, 511-525.
71. F. Tollini, L. Brivio, P. Innocenti, M. Sponchioni and D. Moscatelli, *Chemical Engineering Science*, 2022, **260**, 117875.
72. S. Liu, Z. Wang, L. Li, S. Yu, C. Xie and F. Liu, *Journal of Applied Polymer Science*, 2013, **130**, 1840-1844.
73. J. Chen, J. Lv, Y. Ji, J. Ding, X. Yang, M. Zou and L. Xing, *Polymer Degradation and Stability*, 2014, **107**, 178-183.
74. L. Zhou, X. Lu, Z. Ju, B. Liu, H. Yao, J. Xu, Q. Zhou, Y. Hu and S. Zhang, *Green Chemistry*, 2019, **21**, 897-906.

75. K. Fukushima, D. J. Coady, G. O. Jones, H. A. Almegren, A. M. Alabdulrahman, F. D. Alsewailem, H. W. Horn, J. E. Rice and J. L. Hedrick, *Journal of Polymer Science Part A: Polymer Chemistry*, 2013, **51**, 1606-1611.
76. Y. Ohki, Y. Ogiwara and K. Nomura, *Catalysts*, 2023, **13**, 421.
77. A. R. Ajitha, M. K. Aswathi, S. Bhandari, K. R. Chavan, C. J. Chirayil, A. Dey, K. G. Gopalakrishna, P. Gupta, M. Han, K. Kanny, S. Mandal, P. Manju, K. V. Marathe, R. K. Mishra, P. Nakhate, R. K. Padhan, D. Pant, A. Rane, N. Reddy, A. Sheel, A. Sreeram and S. Thomas, in *Recycling of Polyethylene Terephthalate Bottles*, eds. S. Thomas, A. Rane, K. Kanny, A. V.K and M. G. Thomas, William Andrew Publishing, 2019, DOI: https://doi.org/10.1016/B978-0-12-811361-5.00015-8, p. 96.
78. C. N. Hoang, N. T. Nguyen, S. T. Ta, N. N. Nguyen and D. Hoang, *ACS Omega*, 2022, **7**, 47285-47295.
79. X. Zhou, C. Wang, C. Fang, R. Yu, Y. Li and W. Lei, *Waste Management*, 2019, **85**, 164-174.
80. American Chemical Society National Historic Chemical Landmarks. Bakelite: The World's First Synthetic Plastic. , (accessed 11/10/22, 2022).
81. F. Pardal and G. Tersac, *Polymer Degradation and Stability*, 2006, **91**, 2567-2578.
82. D. S. Achilias, H. H. Redhwi, M. N. Siddiqui, A. K. Nikolaidis, D. N. Bikiaris and G. P. Karayannidis, *Journal of Applied Polymer Science*, 2010, **118**, 3066-3073.
83. S. Kaiho, A. A. R. Hmayed, K. R. Delle Chiaie, J. C. Worch and A. P. Dove, *Macromolecules*, 2022, **55**, 10628-10639.
84. U. R. Vaidya and V. M. Nadkarni, *Industrial & Engineering Chemistry Research*, 1987, **26**, 194-198.
85. U. R. Vaidya and V. M. Nadkarni, *Journal of Applied Polymer Science*, 1987, **34**, 235-245.
86. U. R. Vaidya and V. M. Nadkarni, *Journal of Applied Polymer Science*, 1988, **35**, 775-785.
87. S. Baliga and W. T. Wong, *Journal of Polymer Science Part A: Polymer Chemistry*, 1989, **27**, 2071-2082.
88. J. R. Campanelli, M. R. Kamal and D. G. Cooper, *Journal of Applied Polymer Science*, 1994, **54**, 1731-1740.
89. F. Chen, G. Wang, C. Shi, Y. Zhang, L. Zhang, W. Li and F. Yang, *Journal of Applied Polymer Science*, 2013, **127**, 2809-2815.
90. A. Aguado, L. Martínez, L. Becerra, M. Arieta-araunabeña, S. Arnaiz, A. Asueta and I. Robertson, *Journal of Material Cycles and Waste Management*, 2014, **16**, 201-210.
91. G. R. Lima, W. F. Monteiro, R. Ligabue and R. M. C. Santana, *Materials Research*, 2017, **20**, 588-595.
92. G. Güçlü, A. Kas¸göz, S. Özbudak, S. Özgümüs¸ and M. Orbay, *Journal of Applied Polymer Science*, 1998, **69**, 2311-2319.
93. J.-W. Chen and L.-W. Chen, *Journal of Applied Polymer Science*, 1999, **73**, 35-40.
94. G. Xi, M. Lu and C. Sun, *Polymer Degradation and Stability*, 2005, **87**, 117-120.
95. M. Ghaemy and K. Mossaddegh, *Polymer Degradation and Stability*, 2005, **90**, 570-576.
96. C.-H. Chen, *Journal of Applied Polymer Science*, 2003, **87**, 2004-2010.
97. R. López-Fonseca, I. Duque-Ingunza, B. de Rivas, L. Flores-Giraldo and J. I.

Gutiérrez-Ortiz, *Chemical Engineering Journal*, 2011, **168**, 312-320.
98. R. López-Fonseca, I. Duque-Ingunza, B. De Rivas, S. Arnaiz and J. I. Gutiérrez-Ortiz, *Polymer Degradation and Stability*, 2010, **95**, 1022-1028.
99. S. R. Shukla and A. M. Harad, *Journal of Applied Polymer Science*, 2005, **97**, 513-517.
100. K. Troev, G. Grancharov, R. Tsevi and I. Gitsov, *Journal of Applied Polymer Science*, 2003, **90**, 1148-1152.
101. N. D. Pingale, V. S. Palekar and S. R. Shukla, *Journal of Applied Polymer Science*, 2010, **115**, 249-254.
102. K. R. Delle Chiaie, F. R. McMahon, E. J. Williams, M. J. Price and A. P. Dove, *Polymer Chemistry*, 2020, **11**, 1450-1453.
103. M. Zhu, Z. Li, Q. Wang, X. Zhou and X. Lu, *Industrial & Engineering Chemistry Research*, 2012, **51**, 11659-11666.
104. M. Zhu, S. Li, Z. Li, X. Lu and S. Zhang, *Chemical Engineering Journal*, 2012, **185-186**, 168-177.
105. M. Imran, D. H. Kim, W. A. Al-Masry, A. Mahmood, A. Hassan, S. Haider and S. M. Ramay, *Polymer Degradation and Stability*, 2013, **98**, 904-915.
106. F. Chen, Q. Zhou, R. Bu, F. Yang and W. Li, *Fibers and Polymers*, 2015, **16**, 1213-1219.
107. M. A. H. Alzuhairi, B. I. Khalil and R. S. Hadi, *Engineering and Technology Journal*, 2017, **35**, 831-837.
108. L. Bartolome, M. Imran, K. G. Lee, A. Sangalang, J. K. Ahn and D. H. Kim, *Green Chemistry*, 2014, **16**, 279-286.
109. J. Gopal, G. Elumalai, A. A. H. Tajuddin, Y. Ito, S. Vajiravelu and D. Ravikumar, *Journal of Polymers and the Environment*, 2022, **30**, 2614-2630.
110. Y. Geng, T. Dong, P. Fang, Q. Zhou, X. Lu and S. Zhang, *Polymer Degradation and Stability*, 2015, **117**, 30-36.
111. K. K. Bhanderi, J. R. Joshi and J. V. Patel, *Journal of the Indian Chemical Society*, 2023, **100**, 100904.
112. S. Lalhmangaihzuala, Z. Laldinpuii, C. Lalmuanpuia and K. Vanlaldinpuia, *Polymers*, 2021, **13**, 37.
113. Z. Laldinpuii, S. Lalhmangaihzuala, Z. Pachuau and K. Vanlaldinpuia, *Waste Management*, 2021, **126**, 1-10.
114. A. Sangalang, L. Bartolome and D. H. Kim, *Polymer Degradation and Stability*, 2015, **115**, 45-53.
115. J. Y. Cho, C.-J. Hong and H.-M. Choi, *Industrial & Engineering Chemistry Research*, 2013, **52**, 2309-2315.
116. Z. Guo, K. Lindqvist and H. de la Motte, *Journal of Applied Polymer Science*, 2018, **135**, 46285.
117. K. Fukushima, O. Coulembier, J. M. Lecuyer, H. A. Almegren, A. M. Alabdulrahman, F. D. Alsewailem, M. A. McNeil, P. Dubois, R. M. Waymouth, H. W. Horn, J. E. Rice and J. L. Hedrick, *Journal of Polymer Science Part A: Polymer Chemistry*, 2011, **49**, 1273-1281.
118. S. Nica, A. Hanganu, A. Tanase, M. Duldner, S. Iancu, C. Draghici, P. I. Filip and E. Bartha, *Revista De Chimie*, 2015, **66**, 1105-1111.
119. S. Nica, M. Duldner, A. Hanganu, S. Iancu, B. Cursaru, A. Sarbu, P. Filip and E. Bartha, *Revista de Chimie*, 2018, **69**, 2613-2616.

120. L.-X. Yun, H. Wu, Z.-G. Shen, J.-W. Fu and J.-X. Wang, *ACS Sustainable Chemistry & Engineering*, 2022, **10**, 5278-5287.
121. Y. Li, K. Li, M. Li and M. Ge, *Advanced Powder Technology*, 2022, **33**, 103444.
122. F. R. Veregue, C. T. Pereira Da Silva, M. P. Moisés, J. G. Meneguin, M. R. Guilherme, P. A. Arroyo, S. L. Favaro, E. Radovanovic, E. M. Girotto and A. W. Rinaldi, *ACS Sustainable Chemistry & Engineering*, 2018, **6**, 12017-12024.
123. T. Wang, Y. Zheng, G. Yu and X. Chen, *European Polymer Journal*, 2021, **155**, 110590.
124. Q. Wang, X. Yao, S. Tang, X. Lu, X. Zhang and S. Zhang, *Green Chemistry*, 2012, **14**, 2559-2566.
125. Z. Wang, Y. Jin, Y. Wang, Z. Tang, S. Wang, G. Xiao and H. Su, *ACS Sustainable Chemistry & Engineering*, 2022, **10**, 7965-7973.
126. L. Wang, G. A. Nelson, J. Toland and J. D. Holbrey, *ACS Sustainable Chemistry & Engineering*, 2020, **8**, 13362-13368.
127. L. Deng, R. Li, Y. Chen, J. Wang and H. Song, *Journal of Molecular Liquids*, 2021, **334**, 116419.
128. C. Fan, L. Zhang, C. Zhu, J. Cao, Y. Xu, P. Sun, G. Zeng, W. Jiang and Q. Zhang, *Green Chemistry*, 2022, DOI: 10.1039/D1GC03885K.
129. J. Moncada and M. D. Dadmun, *Journal of Materials Chemistry A*, 2023, **11**, 4679-4690.
130. B. Liu, X. Lu, Z. Ju, P. Sun, J. Xin, X. Yao, Q. Zhou and S. Zhang, *Industrial & Engineering Chemistry Research*, 2018, **57**, 16239-16245.
131. J. Huang, D. Yan, Q. Zhu, X. Cheng, J. Tang, X. Lu and J. Xin, *Polymer Degradation and Stability*, 2023, **208**, 110245.
132. N. H. Le, T. T. Ngoc Van, B. Shong and J. Cho, *ACS Sustainable Chemistry & Engineering*, 2022, **10**, 17261-17273.
133. S. Javed, J. Fisse and D. Vogt, *Polymers*, 2023, **15**, 687.
134. D. Kim, B.-K. Kim, Y. Cho, M. Han and B.-S. Kim, *Industrial and Engineering Chemistry Research*, 2009, **48**, 685-691.
135. J. Otera, *Chemical Reviews*, 1993, **93**, 1449-1470.
136. E.-J. Choi, J.-K. Park and H.-N. Chang, *Journal of Polymer Science Part B: Polymer Physics*, 1994, **32**, 2481-2489.
137. O. Coulembier and P. Dubois, in *Handbook of Ring-Opening Polymerization*, 2009, DOI: https://doi.org/10.1002/9783527628407.ch9, pp. 227-254.
138. E. Santacesaria, F. Trulli, L. Minervini, M. Di Serio, R. Tesser and S. Contessa, *Journal of Applied Polymer Science*, 1994, **54**, 1371-1384.
139. A. E. Allen and D. W. C. MacMillan, *Chemical Science*, 2012, **3**, 633-658.
140. F. Romiti, J. del Pozo, P. H. S. Paioti, S. A. Gonsales, X. Li, F. W. W. Hartrampf and A. H. Hoveyda, *Journal of the American Chemical Society*, 2019, **141**, 17952-17961.
141. F. M. Lamberti, A. Ingram and J. Wood, *Processes*, 2021, **9**, 921.
142. B. G. G. Lohmeijer, R. C. Pratt, F. Leibfarth, J. W. Logan, D. A. Long, A. P. Dove, F. Nederberg, J. Choi, C. Wade, R. M. Waymouth and J. L. Hedrick, *Macromolecules*, 2006, **39**, 8574-8583.
143. S. Naumann, P. B. V. Scholten, J. A. Wilson and A. P. Dove, *Journal of the American Chemical Society*, 2015, **137**, 14439-14445.
144. A. Basterretxea, C. Jehanno, D. Mecerreyes and H. Sardon, *ACS Macro Letters*,

2019, **8**, 1055-1062.
145. H. Wang, R. Yan, Z. Li, X. Zhang and S. Zhang, *Catalysis Communications*, 2010, **11**, 763-767.
146. X. Zhou, X. Lu, Q. Wang, M. Zhu and Z. Li, *Pure and Applied Chemistry*, 2012, **84**, 789-801.
147. T. Wang, C. Shen, G. Yu and X. Chen, *Polymer Degradation and Stability*, 2021, DOI: https://doi.org/10.1016/j.polymdegradstab.2021.109751, 109751.
148. Q. Wang, Y. Geng, X. Lu and S. Zhang, *ACS Sustainable Chemistry & Engineering*, 2015, **3**, 340-348.
149. H. Wang, Y. Liu, Z. Li, X. Zhang, S. Zhang and Y. Zhang, *European Polymer Journal*, 2009, **45**, 1535-1544.
150. S. Marullo, C. Rizzo, N. T. Dintcheva and F. D'Anna, *ACS Sustainable Chemistry & Engineering*, 2021, DOI: 10.1021/acssuschemeng.1c04060.
151. T. Wang, C. Shen, G. Yu and X. Chen, *Polymer Degradation and Stability*, 2022, **203**, 110050.
152. C. Jehanno, I. Flores, A. P. Dove, A. J. Müller, F. Ruipérez and H. Sardon, *Green Chemistry*, 2018, **20**, 1205-1212.
153. W. Chen, M. Li, X. Gu, L. Jin, W. Chen and S. Chen, *Polymer Degradation and Stability*, 2022, **206**, 110168.
154. Q. Wang, X. Yao, Y. Geng, Q. Zhou, X. Lu and S. Zhang, *Green Chemistry*, 2015, **17**, 2473-2479.
155. B. Liu, W. Fu, X. Lu, Q. Zhou and S. Zhang, *ACS Sustainable Chemistry & Engineering*, 2019, **7**, 3292-3300.
156. H. W. Horn, G. O. Jones, D. S. Wei, K. Fukushima, J. M. Lecuyer, D. J. Coady, J. L. Hedrick and J. E. Rice, *The Journal of Physical Chemistry A*, 2012, **116**, 12389-12398.
157. N. Trejo-Carbajal, K. I. Ambriz-Luna and A. M. Herrera-González, *European Polymer Journal*, 2022, DOI: https://doi.org/10.1016/j.eurpolymj.2022.111388, 111388.
158. Y. Liu, X. Yao, H. Yao, Q. Zhou, J. Xin, X. Lu and S. Zhang, *Green Chemistry*, 2020, **x**, xx.
159. E. Barnard, J. J. Rubio Arias and W. Thielemans, *Green Chemistry*, 2021, **23**, 3765-3789.
160. R. K. Soni and S. Singh, *Journal of Applied Polymer Science*, 2005, **96**, 1515-1528.
161. A. Jain and R. K. Soni, *Journal of Polymer Research*, 2007, **14**, 475-481.
162. G. Farrow, D. A. S. Ravens and I. M. Ward, *Polymer*, 1962, **3**, 17-25.
163. S. R. Shukla and A. M. Harad, *Polymer Degradation and Stability*, 2006, **91**, 1850-1854.
164. N. D. Pingale and S. R. Shukla, *European Polymer Journal*, 2009, **45**, 2695-2700.
165. Y. Zhang, F. Tian, Z. Wu, X. Li, X. Liu and Y. He, *Materials Today Communications*, 2022, **32**, 104045.
166. L.-n. Zhang, L.-z. Liu, Q.-f. Yue and C.-c. Zhu, *Polymers and Polymer Composites*, 2014, **22**, 13-16.
167. G. M. M. Sadeghi, R. Shamsi and M. Sayaf, *J Polym Environ*, 2011, **19**, 522-534.
168. E. Bulak and I. Acar, *Polymer Engineering & Science*, 2014, **54**, 2272-2281.
169. R. Shamsi, M. Abdouss, G. M. M. Sadeghi and F. A. Taromi, *Polymer International*, 2009, **58**, 22-30.

170. V. Jamdar, M. Kathalewar and A. Sabnis, *Journal of Polymers and the Environment*, 2018, **26**, 2601-2618.
171. J. Natarajan, G. Madras and K. Chatterjee, *ACS Applied Materials & Interfaces*, 2017, **9**, 28281-28297.
172. S. M. Elsaeed and R. K. Farag, *Journal of Applied Polymer Science*, 2009, **112**, 3327-3336.
173. J. P. K. Tan, J. Tan, N. Park, K. Xu, E. D. Chan, C. Yang, V. A. Piunova, Z. Ji, A. Lim, J. Shao, A. Bai, X. Bai, D. Mantione, H. Sardon, Y. Y. Yang and J. L. Hedrick, *Macromolecules*, 2019, **52**, 7878-7885.
174. N. Tarannum, R. Khan, S. Ansari, R. Agrawal, S. Mishra, M. Ubaidullah and A. A. Al-Kahtani, *Journal of King Saud University - Science*, 2022, **34**, 101739.
175. K. Chan and A. Zinchenko, *Journal of Environmental Chemical Engineering*, 2022, **10**, 107749.
176. K. K. Bhanderi, J. R. Joshi and J. V. Patel, *Journal of the Indian Chemical Society*, 2023, **100**, 100843.
177. V. S. Palekar, R. V. Shah and S. R. Shukla, *Journal of Applied Polymer Science*, 2012, **126**, 1174-1181.
178. R. M. Musale and S. R. Shukla, *International Journal of Plastics Technology*, 2016, **20**, 106-120.
179. K. Fukushima, J. M. Lecuyer, D. S. Wei, H. W. Horn, G. O. Jones, H. A. Al-Megren, A. M. Alabdulrahman, F. D. Alsewailem, M. A. McNeil, J. E. Rice and J. L. Hedrick, *Polymer Chemistry*, 2013, **4**, 1610-1616.
180. J. Demarteau, I. Olazabal, C. Jehanno and H. Sardon, *Polymer Chemistry*, 2020, **11**, 4875-4882.
181. H. Zahn and H. Pfeifer, *Polymer*, 1963, **4**, 429-432.
182. C. N. Hoang, N. T. Nguyen, T. Q. Doan and D. Hoang, *Polymer Degradation and Stability*, 2022, DOI: https://doi.org/10.1016/j.polymdegradstab.2022.110175, 110175.
183. E. M. Krall, T. W. Klein, R. J. Andersen, A. J. Nett, R. W. Glasgow, D. S. Reader, B. C. Dauphinais, S. P. Mc Ilrath, A. A. Fischer, M. J. Carney, D. J. Hudson and N. J. Robertson, *Chemical Communications*, 2014, **50**, 4884-4887.
184. J. A. Fuentes, S. M. Smith, M. T. Scharbert, I. Carpenter, D. B. Cordes, A. M. Z. Slawin and M. L. Clarke, *Chemistry – A European Journal*, 2015, **21**, 10851-10860.
185. B. F. S. Nunes, M. C. Oliveira and A. C. Fernandes, *Green Chemistry*, 2020, **22**, 2419-2425.
186. A. C. Fernandes, *ChemSusChem*, 2021, **14**, 4228-4233.
187. Y. Kratish, J. Li, S. Liu, Y. Gao and T. J. Marks, *Angewandte Chemie International Edition*, 2020, **59**, 19857-19861.
188. Y. Kratish and T. J. Marks, *Angewandte Chemie International Edition*, 2022, **61**, e202112576.
189. M. Kathalewar, N. Dhopatkar, B. Pacharane, A. Sabnis, P. Raut and V. Bhave, *Progress in Organic Coatings*, 2013, **76**, 147-156.
190. P. K. Roy, R. Mathur, D. Kumar and C. Rajagopal, *Journal of Environmental Chemical Engineering*, 2013, **1**, 1062-1069.
191. J. D. Estrada-Flores, M. C. García-López, P. Elizondo-Martínez, N. A. Pérez-Rodríguez, J. R. De la Rosa and M. G. Sánchez-Anguiano, *Journal of Polymers and*

the Environment, 2020, **28**, 1654-1663.
192. C. H. Flores-Tamez, P. Elizondo-Martínez, R. M. Jiménez-Barrera, I. Moggio, E. Arias, M. G. Sánchez-Anguiano, M. C. García-López and R. Chan-Navarro, *Optical Materials*, 2023, **137**, 113516.
193. P. Huang, J. Pitcher, A. Mushing, F. Lourenço and M. P. Shaver, *Resources, Conservation and Recycling*, 2023, **190**, 106854.
194. S.-S. Wu, Y.-D. Li, Z. Hu and J.-B. Zeng, *ACS Sustainable Chemistry & Engineering*, 2023, **11**, 1974-1984.
195. H. T. Kim, J. K. Kim, H. G. Cha, M. J. Kang, H. S. Lee, T. U. Khang, E. J. Yun, D.-H. Lee, B. K. Song, S. J. Park, J. C. Joo and K. H. Kim, *ACS Sustainable Chemistry & Engineering*, 2019, **7**, 19396-19406.
196. A. A. Karanastasis, V. Safin and L. M. Pitet, *Macromolecules*, 2022, DOI: 10.1021/acs.macromol.1c02338.
197. B. Geyer, S. Röhner, G. Lorenz and A. Kandelbauer, *Journal of Applied Polymer Science*, 2014, **131**.

2 Low-temperature Upcycling of PET: Novel Materials Derived from Functional and Renewably Sourced Alcohols

Post-consumer waste (PCW) plastic is commonly discarded, however it also represents an untapped feedstock to create unique functional building blocks for use as new platform chemicals and/or in materials synthesis via catalytic upcycling. Poly(ethylene terephthalate) (PET) is an important commodity plastic, though it is conventionally 'downcycled' by mechanical recycling as this presents an economical route for its reuse. In this study, an efficient procedure for the alcoholysis of PET is presented, accomplished by increasing the particle surface area and employing an inexpensive, highly active Zn/DMAP dual catalyst. The rapid depolymerisation (>80% conversion, 5 h) of PET proceeded under mild reaction temperatures (120 °C), enables application of low boiling and thermally unstable alcohols as alcoholysis reagents. Introducing alkene groups through depolymerisation with prenol and perillyl alcohol allowed their respective bisterephthalates to be crosslinked into new, upcycled materials, using radical thiol-ene chemistry to yield a robust rubbery material and a strong plastic. Formulation into a resin suitable for additive manufacturing further shows the potential of this methodology. This study establishes emerging opportunities for mild PET upcycling using renewable alcohols and highly active catalysts.

2.1 Introduction

In the past 70 years, over 8 billion tonnes of plastic has been produced, consumed, and – for the most part – discarded.[6] A recent analysis suggested that only 9% of historical plastic has been recycled, and of that fraction, 90% was only recycled once before entering the waste stream.[7-11] As such, there exists a vast untapped stream of valuable post-consumer waste (PCW) plastic that could serve as an alternative chemical feedstock platform for new materials

synthesis. The predominant method to reuse PCW plastic is *via* mechanical recycling or 'downcycling', where plastics are thermally reprocessed into equal or lower-value materials. Even when PCW plastic can be mechanically recycled in a 'closed-loop' process (*i.e.* to afford useful plastic for similar application) the production of virgin plastic is often less expensive. Pyrolysis of waste materials, where polymers are cracked into hydrocarbon fuels and chemicals under low oxygen environments, provides an alternate treatment for PCW plastics. However, the process requires high reaction temperatures (in excess of 300 °C), which makes it energetically demanding, and acidic impurities/products can be detrimental to the process. Chemical recycling to monomer (CRM) is another emergent closed-loop recycling process to recycle the PCW plastic to virgin plastic after repolymerisation of the recovered monomer. This approach has been successfully applied to polymers with low ceiling temperatures and/or reactive backbone compositions. Chemical 'upcycling', which seeks to transform PCW plastic into useful chemical feedstocks where the products are distinct from the initial monomer (or polymer), presents a further interesting alternative to CRM.[12] While this process is not 'closed-loop', it could substantially increase the sustainability of the materials economy by providing new sources of high-performance materials or platform chemicals. Polar PCW polymers, *i.e.* carbonyl-containing plastics, are excellent candidates for chemical upcycling strategies on account of the reactive motifs in the polymer backbone. Bisphenol-A polycarbonate (BPA-PC) has been upcycled using a variety of simple alcohols, diols,[17, 18] and heterolytic nucleophiles and also *via* dehydrogenative processes.[21] Polyurethanes (PU) have been upcycled into new materials using both alcoholysis[22] and aminolysis[24, 25], and polyoxymethylenes have been selectively transformed into acetal products.

PET has also been widely studied for upcycling as its labile ester moiety engenders it amenable to well-controlled depolymerisation with nucleophiles. The majority of PET upcycling research has focused on aminolysis to afford amide products, as the reaction is generally faster and more

thermally accessible than transesterification methods with alcohols. Tan *et al.* reported the depolymerisation of PET by catalyst-free aminolysis to produce antimicrobial polyionenes,[26, 27] and Fukushima *et al.* created a library of terephthalic diamides using the same method, albeit catalysed by 1,5,7-triazabicyclo[4.4.0]dec-5-ene (TBD). Demarteau *et al.* also applied a protic organocatalyst to make a small set of aminolysed PET products.[28, 29] Several groups have also used aminolysis of PET as a way of accessing sustainable feedstocks for PU synthesis, as well as for epoxy resin and paint additives. Despite this focus on aminolysis, alcoholysis of PET potentially provides a more attractive upcycling process on account of the synthetic simplicity (amines are often synthesised from alcohols), greater potential for biomass derivation and generally lower toxicity of alcohols compared to amines.[36] On the other hand, the lower nucleophilicity of alcohols (compared to amines) in PET depolymerisation creates a challenge for their use. Even in the presence of catalysts, alcoholysis typically requires temperatures close to 200 °C to obtain suitable reaction kinetics and conversions.[38] In turn, this limits the potential pool of alcohols that can be applied on account of their low boiling points and/or low degradation temperatures. While ethylene glycol (EG) has been studied to depolymerize PET to bis(2-hydroxyethyl)terephthalate (BHET) as a CRM method,[18] other alcohols such as methanol,[41] benzyl alcohol, 1-octanol, 1,3-propanediol, 1,6-hexanediol,[42] and butanol[43] have been employed with some success, albeit at high pressures (since reaction temperatures commonly exceed 190 °C).

It was sought to expand the potential for PET upcycling through alcoholysis by developing a milder, lower temperature procedure employing inexpensive dual catalysts[34] that would enable access to a wider range of alcohols to be used in the depolymerisation process and, in turn, allow new upcycled materials to be generated. the application of a previously reported dual catalysis approach was reported that is based on commercially available metal salts and amines.[34] Since depolymerisation by hydrolysis is a surface-based process,[34] a hypothesis was

developed that the analogous glycolysis/alcoholysis reactions would be similar, and thus an increase in PET surface area would lead to a substantial increase in reaction rate. By using finely ground PET in combination with the highly active dual catalyst, the efficient transesterification of PET with ethylene glycol was accomplished at 120 °C in under 24 h. In turn, this enabled PET depolymerisation using a range of functional alcohol substrates. When prenol and perillyl alcohol, both renewably sourced terpenoid alcohols, were employed as the nucleophile, it afforded functional and reactive depolymerisation upcycled products. The prenol- and perillyl-based compounds were subsequently crosslinked using photoinitiated thiol-ene chemistry to produce a tough, rubbery material and a semicrystalline polymer network, respectively. Finally, the perillyl-derived monomer was formulated into a resin for Digital Light Processing (DLP) additive manufacturing (3D printing) by utilising the radical thiol-ene click reaction.

2.2 Results & Discussion

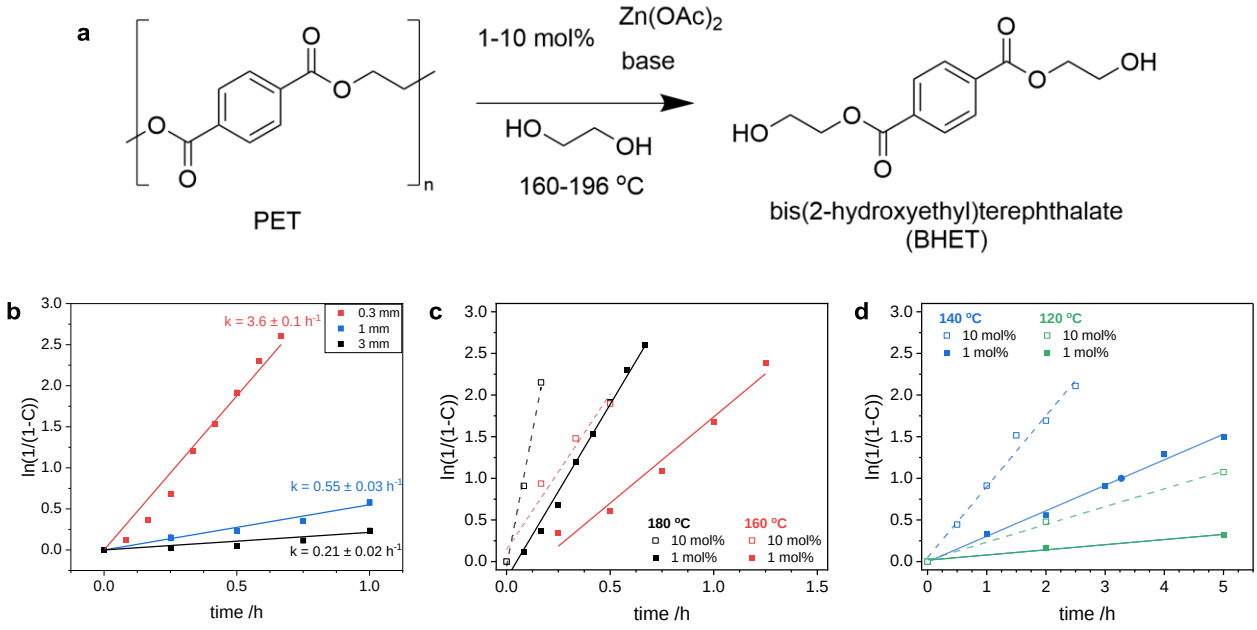


Figure 2.1. a) Scheme for commonly employed conditions for PET glycolysis. b) PET depolymerisation at 180 °C by glycolysis of 3 mm PET pellets, 1 mm PET pellets, and 0.3 mm PET powder. Catalyst loading = 1 mol%. c) First-order rate plots for PET depolymerisation by glycolysis at 180-160 °C. Catalyst loading = 1-10 mol%. d) First-order rate plots for PET depolymerisation by glycolysis at 140-120 °C. Catalyst loading = 1-10 mol%.

Dual catalysis has previously been employed in PET glycolysis (Figure 2.1a) with a variety of catalysts, principally involving zinc acetate and a cocatalyst such as DBU,[34] DMAP,[34] tropine, urea[34] or 1,3-dimethylurea,[34] however all these have been employed at relatively high temperature (≥160 °C), and all with simple alcohols, most commonly ethylene glycol. There is therefore scope for catalysts with lower active temperatures within the design space, which allows for access to the synthesis of functional monomers *via* sustainable alcohols. PET depolymerisation *via* glycolysis was initially investigated to readily explore the effect of reaction conditions. Using 3 mm diameter plastic pellets and 1 mol% Zinc acetate dihydrate / *N*,*N*-dimethylaminopyridine (Zn/DMAP) dual catalyst system at 180 °C (Figure 2.1b), PET conversion was measured by periodically sampling the reaction mixture and analysing the aliquot using ^{1}H NMR spectroscopy. Since PET is insoluble in the reaction medium, sample conversion was quantified by integrating the aromatic signals of the generated bis(2-

hydroxyethyl)terephthalate (BHET) at δ = 8.1 ppm with respect to an internal standard (*N*-methylpyrrolidone (NMP)) at δ = 2.8 ppm (Figure S2.6). Under these conditions, the reaction was initially slow (20% conversion at 1 h), which may be explained by swelling of the pellets, but then accelerated to afford high conversion (*ca.* 90%) within *ca.* 2 h.

To investigate if the depolymerisation of PET *via* glycolysis was a surface-based process, the 3 mm diameter pellets were frozen in liquid N_2 and manually ground to approx. 1 mm diameter pellets then reacted under the same conditions. The smaller pellets were observed to depolymerise at a faster initial rate compared to the large pellets (40% conversion at 1 h), but

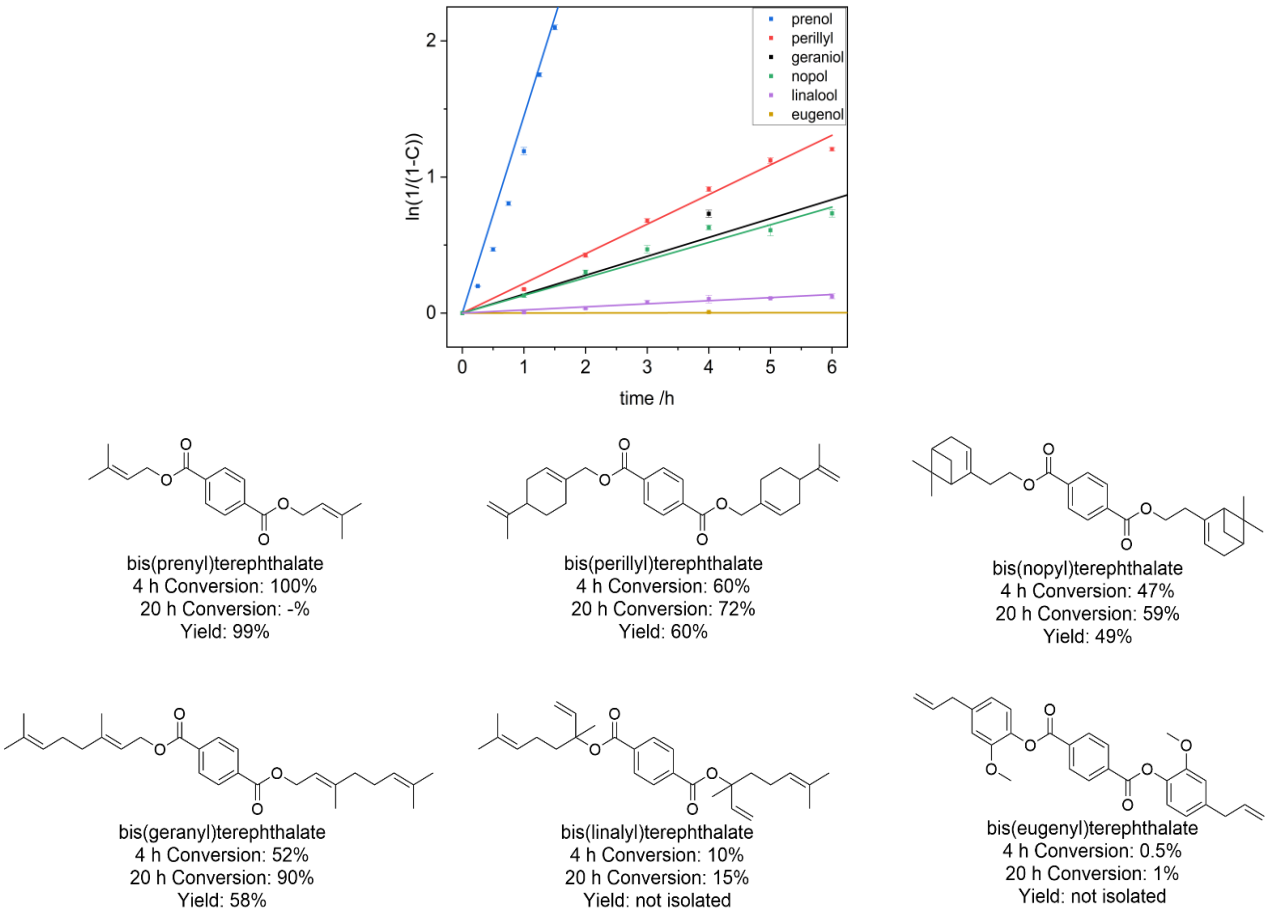


Figure 2.2. a) PET depolymerisation at 120 °C by alcoholysis. Catalyst loading = 10 mol%. b) functionalised monomers, their respective conversions at 4 and 20 h measured by FTIR spectroscopy, and their final product yields (if isolated).

the reaction similarly plateaued at *ca.* 2 h. Therefore, a finer PET particle size (300 μm) was tested and found to have a significantly higher rate of depolymerisation compared to the pelletised samples, reaching high conversion to BHET (*ca.* 90%) within just 0.5 h (Figure 1b). Inspired by the rapid depolymerisation of PET powder, the glycolysis was screened at lower temperatures (120 – 160 °C) to determine if the reaction could proceed efficiently under milder conditions (Figure 2.1c & d). As the temperature was decreased, the dual catalyst system remained active, albeit with significant increases in reaction time (*ca.* 48 h, 120 °C) required to achieve high conversions (≥ 80%) (Figure 2.1d). In order to decrease the reaction time, the catalyst loading was increased to 10 mol%, which notably increased the rate, especially at reaction lower temperatures.

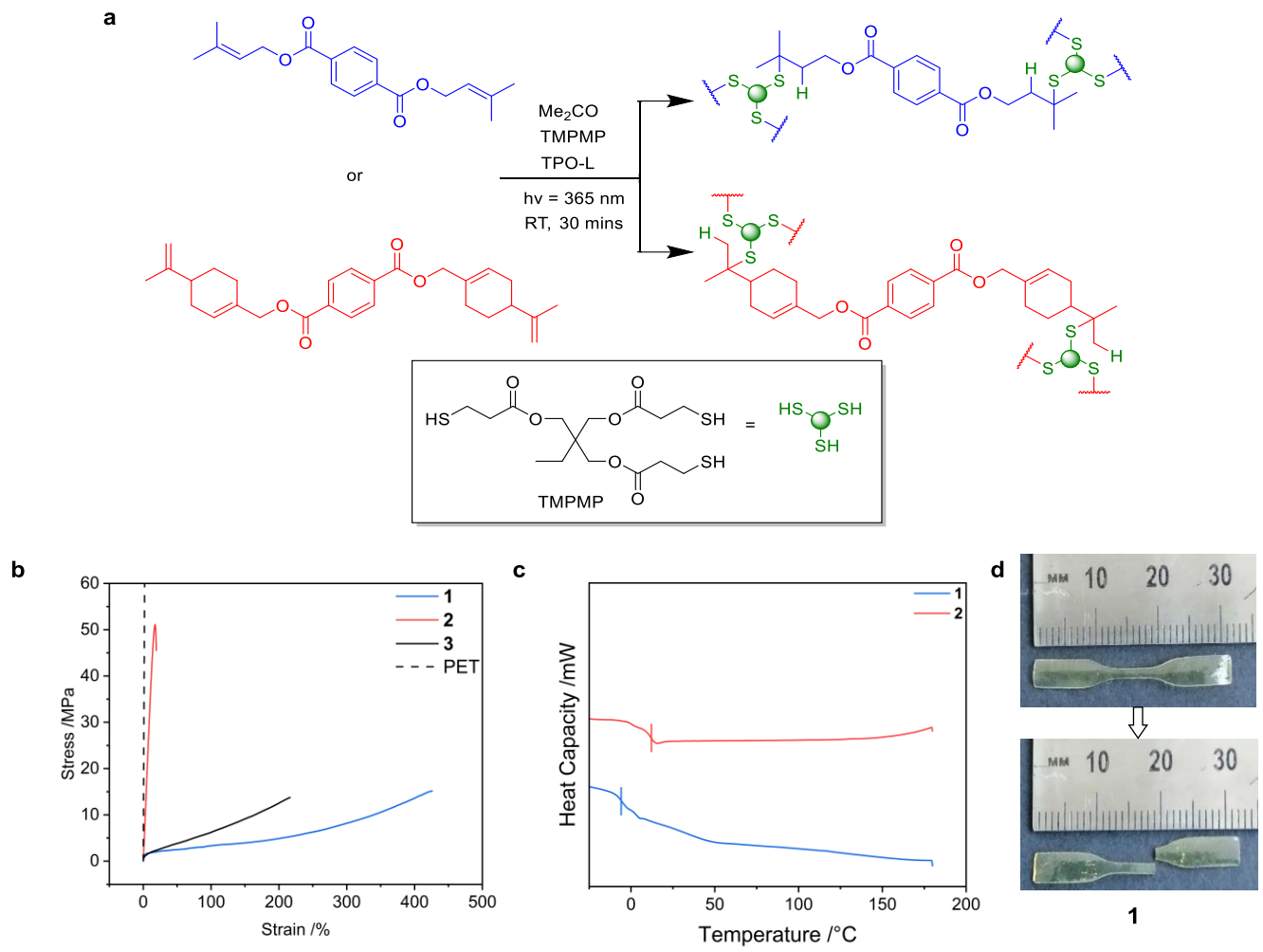


Figure 2.3. a) The upcycling of PET depolymerisation product into a crosslinked network. Radical thiol-ene reaction between prenol- and perillyl-based monomer and trimethylolpropane tris(3-mercaptopropionate) (TMPMP) (1:1 thiol:alkene stoichiometry) at 22 °C, 10 min. b) The upcycling of PET depolymerisation product into crosslinked networks: Uniaxial tensile testing at 21 ± 1 °C, 10 mm min^{-1} strain rate c) DSC thermogram for 1st heating cycle from −100 to 200 °C, 10 °C min^{-1}. d) Images of dogbone samples before and after tensile testing to show elastic recovery.

Kim et al. demonstrated that despite the heterogeneity of the system (with respect to polymer), the depolymerisation could still be treated using pseudo-1st order kinetic analysis. As such, the rate of each depolymerisation was determined using Equation 2.1, where *C* is total conversion and *k* is the first-order rate constant:

$$\ln\left(\frac{1}{1-C}\right) = k' \times t \qquad 2.1$$

The derived rate constants (Figure 2.1b-d) show that the glycolysis of PET can be fitted to a linear approximation of 1st order rate. The rate constants from these analyses were used to approximate the activation energy of the depolymerisation reaction at each respective catalyst loading using an Arrhenius plot (ln(k) versus 1/T). The activation energy for glycolysis using 1 mol% and 10 mol% Zn/DMAP were found to be 107 ± 11 and 102 ± 2 kJ mol^{-1} respectively, which are within error, confirming the mechanism is consistent regardless of catalytic loading (Figure S2.16).

The reasonably high activity of this catalyst system for depolymerisation at 120 °C and 10 mol% catalyst loading allowed us to investigate the upcycling of PET with a range of alcohols to afford various bis(alkyl) terephthalate esters. To this end, a selection of alcohols were screened with lower thermal stability than EG (Figure 2.2a) to expand the scope of products that could be obtained from this reaction (Figure 2.2b). These alcohols were chosen to illustrate the range of sustainably sourced alcohols which can be used when the depolymerisation temperature is reduced. The conversion to the corresponding bis(terephthalate ester) was monitored by FT-IR spectroscopy and benchmarked against ^{1}H NMR spectra in the same way as for the glycolysis reactions, using NMP as an internal standard (Figure S2.6). PET was depolymerised by prenol (quantitative conversion) within 2 h, whereas perillyl alcohol required 20 h to reach high conversion (Figure 2.2). Nopol and geraniol reached moderate conversions (>60%) within 20 h, but only the nopyl terephthalate was easily isolable. Linalool and eugenol only depolymerised PET very slowly and thus were excluded from further investigation. The general trend was that both the steric availability and nucleophilicity of the nucleophile were positively correlated to the rate of depolymerisation (and overall conversion) for PET. Notably, isolation of the bis(alkyl) terephthalate esters from depolymerisation with prenol, perillyl alcohol and nopol was simply achieved in high yield, as the esters precipitated from the depolymerisation solution upon cooling to room temperature and addition of methanol or 1:1 water:methanol. This provides a

simple and scalable method to create these products and facilitates their further study as upcycled monomers.

Further upcycling of the bis(terephthalate ester)s into potentially useful polymeric materials was demonstrated by reacting the prenol and perillyl alcohol-based diesters with a multi-valent thiol through a photoinitiated radical thiol-ene coupling to afford crosslinked networks of bis(prenyl)terephthalate (**1**) and of bis(perillyl)terephthalate (**2**) (Figure 2.3). Reaction with the nopyl terephthalate ester was also attempted, but a crosslinked film was not able to be synthesised because of poor reactivity, most likely a result of the sterically hindered double bond. The materials were annealed, at either ambient temperature or at 120 °C, and the thermomechanical properties of the network were thoroughly characterised. Both of the 120 °C-annealed materials displayed adequate thermal stability with 50% degradation temperatures above 300 °C (Figure S2.18). However, the annealing temperature significantly altered the glass transition temperature (T_g) of the networks (Figure 3c, Figures S2.19 & S2.20). Both materials were amorphous according to differential scanning calorimetry (DSC) analysis (Figure 2.3c). Uniaxial tensile testing of the 120 °C annealed sample showed that the resultant material **1** was strong (ultimate tensile strength of **1** = 16.2 ± 3.4 MPa), with high extensibility (elongation at break of **1** = 459 ± 21%), whereas **2** was stiff (Ultimate tensile strength of **2** = 36.1 ± 8.7 MPa) with low elasticity (elongation at break of **2** = 19.0 ± 1.0%) (Figure 4a, Figures S2.21 & S2.22). Furthermore, the prenyl-derived material still maintained rubbery behaviour (similar to the sample annealed at ambient temperature) as evidenced by excellent recovery after elongation (Figure 2.3d).

Similarly to PET, the upcycled networks contain terephthalate esters, and hence it was hypothesised that they would be able to be depolymerised in a comparable manner to PET to regenerate the bisterephthalate ester, i.e. closing the loop and regenerating monomer. To this end, network **1** was heated with Zn/DMAP catalyst in excess prenol for 1 h. Depolymerisation of

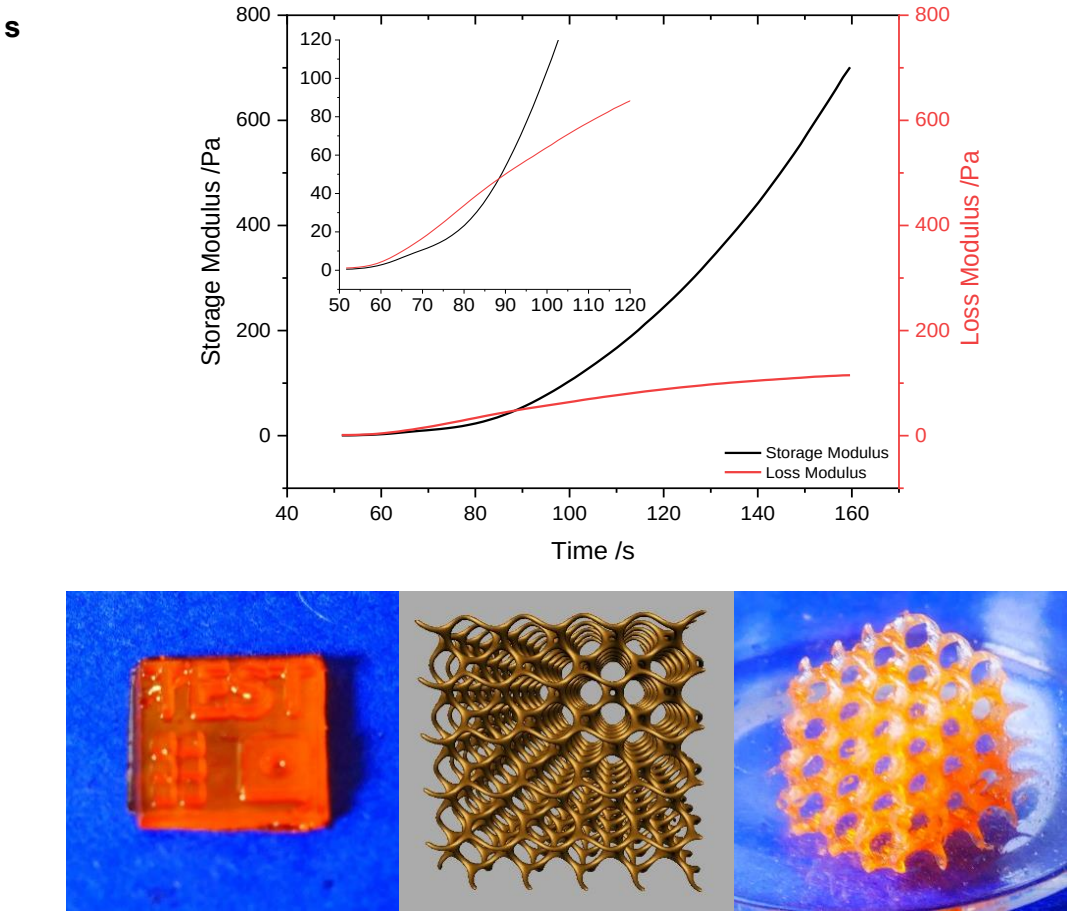


Figure 2.4. a) Photorheology of the formulation for 3D printing b) test square print with pyrogallol 1wt% + Sudan II 0.03 wt%; the 3D digital render; and printed cube of the (10,3)-a structure.

the network was observed visually and the reaction solution became homogeneous. However, unlike the depolymerisation of PET under the same conditions, upon cooling, the prenyl terephthalate did not precipitate in high yield and pure prenyl terephthalate was only isolated in low yields (*ca*. 13%). Similar results were also obtained when depolymerising network **2** in perillyl alcohol. It was hypothesised that this lower recovery yield is a consequence of the altered polarity of the depolymerisation medium that leads to an increased solubility of the bis(alkyl) terephthalate esters, thus hindering their recovery without extensive purification.

The rapid nature of the formation of robust network materials by photoinitiated thiol-ene polymerisation led us to investigate if these monomers could be applied in the generation of a

photocurable resin that would be suitable for additive manufacturing (3D printing) using a light based process such as DLP. To this end, the prenyl terephthalate monomer was selected as it has terminal alkene functionalities, which displayed higher reactivity towards the thiol-ene crosslinking reaction. Rheological analysis of the mixture of prenyl terephthalate, TMPMP and NMP indicated an initial viscosity of 0.41 mPa.s which is in an appropriate range for application DLP.[34] Furthermore in, studying the photorheology of the formation of **1** indicated a gelation point (where the storage modulus overtakes the loss modulus) at approximately 1.5 min, which is sufficiently rapid for translation to DLP (Figure 2.4a). While these studies demonstrated the ability to photocure the material in a suitable timeframe, the formulation of a resin that would be suitable for DLP required the optimisation of both Z-resolution and X,Y-resolution. Initial attempts to photopattern a test plaque (Figure 2.4b) led to a poor resolution in which the features could not be easily identified. Commonly, red coloured additives are included into such resins in order to improve the Z-resolution on account of their ability to absorb the blue/violet light typically used in these processes and reduce 'cure-through'.[1] These dyes can also improve X,Y-resolution. Often additional radical inhibitors are required to prevent early gelation, but a side-effect of this is the reduction of diffusion of radicals, hence enabling better X-Y resolution. To this end, X,Y-resolution was improved by addition of pyrogallol (1 wt%), and both X,Y- and Z-resolution were significantly improved by addition of the red dye Sudan II (0.03 wt%) (Figure 4b). With this formulation in hand, a Hart cube was printed, which is a gyroid structure that is based on the *(10,3)-a* crystal structure (also known as *srs* or K_4) that demonstrates the ability of the resin to be printed with high resolution (Figure 2.4b).

2.3 Conclusions

The increase of depolymerisation rate that was afforded by exploiting higher surface area of PET enabled depolymerisation reactions to be undertaken at temperatures as low as 120 °C while maintaining reasonable reaction times. In turn, this advance has enabled us to

depolymerise PET with a wider range of alcohols that would not be able to be applied at typical glycolysis temperatures of 180 °C. The inclusion of naturally sourced terpenoid alcohols has subsequently enable the creation of products that are derived from naturally occurring chemicals and waste plastic. The use of alkene-containing alcohols subsequently enabled the creation of upcycled monomers for further polymerisation. The application of these monomers to create photocured materials in 2D and 3D, through resin formulation for DLP, further extends the utility of this methodology to a viable path toward practical upcycled materials.

2.4 References

1. K. R. Delle Chiaie, F. R. McMahon, E. J. Williams, M. J. Price and A. P. Dove, *Polymer Chemistry*, 2020, **11**, 1450-1453.
2. A. L. Allred, *Journal of Inorganic and Nuclear Chemistry*, 1961, **17**, 215-221.
3. R. D. Shannon, *Acta Crystallographica Section A*, 1976, **32**, 751-767.
4. R. D. Shannon and C. T. Prewitt, *Acta Crystallographica Section B Structural Crystallography and Crystal Chemistry*, 1969, **25**, 925-946.
5. R. G. Pearson, *Inorganic Chemistry*, 1988, **27**, 734-740.
6. M. Cranmer, *Journal*, 2020, DOI: 10.5281/zenodo.4041459.
7. M. M. Noack, I. Humphrey, elliottperryman, R. Pandolfi and MarcusMichaelNoack, *Journal*, 2022, DOI: 10.5281/zenodo.6147361.
8. P. Anggo Krisbiantoro, Y.-W. Chiao, W. Liao, J.-P. Sun, D. Tsutsumi, H. Yamamoto, Y. Kamiya and K. C.-W. Wu, *Chemical Engineering Journal*, 2022, **450**, 137926.
9. L. Bartolome, M. Imran, K. G. Lee, A. Sangalang, J. K. Ahn and D. H. Kim, *Green Chemistry*, 2014, **16**, 279-286.
10. W. McDonough and M. Braungart, *Cradle to Cradle: Remaking the Way We Make Things*, North Point Press, 2002.
11. S.-G. European Commission, *A European Strategy for Plastics in a Circular Economy*.
12. P. McKeown and M. D. Jones, *Sustainable Chemistry*, 2020, **1**, 1-22.
13. Z. O. G. Schyns and M. P. Shaver, *Macromolecular Rapid Communications*, 2021, **42**, 2000415.
14. R. Geyer, B. Kuczenski, T. Zink and A. Henderson, *Journal of Industrial Ecology*, 2016, **20**, 1010-1017.
15. P. Benyathiar, P. Kumar, G. Carpenter, J. Brace and D. K. Mishra, *Polymers*, 2022, **14**, 2366.
16. A. Demirbas, M. A. Baluabaid, M. Kabli and W. Ahmad, *Petroleum Science and Technology*, 2015, **33**, 129-138.
17. C. Jehanno, J. Demarteau, D. Mantione, M. C. Arno, F. Ruipérez, J. L. Hedrick, A. P. Dove and H. Sardon, *ACS Macro Letters*, 2020, DOI: 10.1021/acsmacrolett.0c00164, 443-447.

18. L. Shao, Y.-C. Chang, C. Hao, M.-e. Fei, B. Zhao, B. J. Bliss and J. Zhang, *Green Chemistry*, 2022, **24**, 8716-8724.
19. C. Jehanno, J. Demarteau, D. Mantione, M. C. Arno, F. Ruipérez, J. L. Hedrick, A. P. Dove and H. Sardon, *Angewandte Chemie International Edition*, 2021, **60**, 6710-6717.
20. T. Helmer Pedersen and F. Conti, *Waste Management*, 2017, **68**, 24-31.
21. M. Day, J. D. Cooney, C. Touchette-Barrette and S. E. Sheehan, *Journal of Analytical and Applied Pyrolysis*, 1999, **52**, 199-224.
22. G. Celik, R. M. Kennedy, R. A. Hackler, M. Ferrandon, A. Tennakoon, S. Patnaik, A. M. Lapointe, S. C. Ammal, A. Heyden, F. A. Perras, M. Pruski, S. L. Scott, K. R. Poeppelmeier, A. D. Sadow and M. Delferro, *ACS Central Science*, 2019, **5**, 1795-1803.
23. M. Rehan, R. Miandad, M. A. Barakat, I. M. I. Ismail, T. Almeelbi, J. Gardy, A. Hassanpour, M. Z. Khan, A. Demirbas and A. S. Nizami, *International Biodeterioration & Biodegradation*, 2017, **119**, 162-175.
24. S. Baliga and W. T. Wong, *Journal of Polymer Science Part A: Polymer Chemistry*, 1989, **27**, 2071-2082.
25. C.-H. Chen, *Journal of Applied Polymer Science*, 2003, **87**, 2004-2010.
26. M. A. Beckett, G. C. Strickland, J. R. Holland and K. Sukumar Varma, *Polymer*, 1996, **37**, 4629-4631.
27. S. Tshepelevitsh, A. Kütt, M. Lõkov, I. Kaljurand, J. Saame, A. Heering, P. G. Plieger, R. Vianello and I. Leito, *European Journal of Organic Chemistry*, 2019, **2019**, 6735-6748.
28. M. Lõkov, S. Tshepelevitsh, A. Heering, P. G. Plieger, R. Vianello and I. Leito, *European Journal of Organic Chemistry*, 2017, **2017**, 4475-4489.
29. A. Albert, *Heterocyclic Chemistry*, Athlone Press, 2nd edn., 1968.
30. I. Kaljurand, A. Kütt, L. Sooväli, T. Rodima, V. Mäemets, I. Leito and I. A. Koppel, *The Journal of Organic Chemistry*, 2005, **70**, 1019-1028.
31. C. Jehanno, I. Flores, A. P. Dove, A. J. Müller, F. Ruipérez and H. Sardon, *Green Chemistry*, 2018, **20**, 1205-1212.
32. D. D. Pham and J. Cho, *Green Chemistry*, 2021, **23**, 511-525.
33. S. Mishra, V. S. Zope and A. S. Goje, *Polymer International*, 2002, **51**, 1310-1315.
34. J.-P. Lange, *ACS Sustainable Chemistry & Engineering*, 2021, **9**, 15722-15738.
35. D. S. Achilias and G. P. Karayannidis, *Water, Air and Soil Pollution: Focus*, 2004, **4**, 385-396.
36. D. Paszun and T. Spychaj, *Industrial & Engineering Chemistry Research*, 1997, **36**, 1373-1383.
37. M. Goto, H. Koyamoto, A. Kodama, T. Hirose, S. Nagaoka and B. J. McCoy, *AIChE Journal*, 2002, **48**, 136-144.
38. T. Yoshioka, N. Okayama and A. Okuwaki, *Industrial & Engineering Chemistry Research*, 1998, **37**, 336-340.
39. I. M. Abdulagatov, N. G. Polikhronidi, A. Abdurashidova, S. B. Kiselev and J. F. Ely, *International Journal of Thermophysics*, 2005, **26**, 1327-1368.
40. M. Genta, T. Iwaya, M. Sasaki, M. Goto and T. Hirose, *Industrial & Engineering Chemistry Research*, 2005, **44**, 3894-3900.
41. Z. Aayanifard, A. Khan, M. Naveed, J. Schager and M. Rabnawaz, *Polymer*, 2023,

265, 125585.
42. F. Tollini, L. Brivio, P. Innocenti, M. Sponchioni and D. Moscatelli, *Chemical Engineering Science*, 2022, **260**, 117875.
43. Z. Jiang, D. Yan, J. Xin, F. Li, M. Guo, Q. Zhou, J. Xu, Y. Hu and X. Lu, *Polymer Degradation and Stability*, 2022, DOI: https://doi.org/10.1016/j.polymdegradstab.2022.109905, 109905.

2.5 Instrumentation

Nuclear Magnetic Resonance Spectrometry (NMR). All ^{1}H and ^{13}C NMR spectra were recorded using a Bruker Avance III 400 spectrometer equipped with a QNP probe operating at 400 MHz at 298 K. ^{1}H spectra were referenced against solvent residual proton signals: δ = 7.26 ppm ($CDCl_3$) and δ = 2.50 ppm (DMSO-d_6); ^{13}C spectra were referenced against solvent residual signals: δ = 77.16 ppm (CDCl3) and δ = 39.52 ppm (DMSO-d_6). Spectra were processed using MestReNova 12.0.03 software. Resonance multiplicities are described as s (singlet), d (doublet), t (triplet), q (quartet), p (pentet), or m (multiplet).

High Resolution Mass Spectrometry (HRMS). Mass spectrometry was performed using a Waters Xevo G2-XS QTof with Atmospheric Solids Analysis Probe Positive (ASAP+) for direct solid sampling. m/Z scan completed from 0 to 1200 m/Z.

Fourier-Transform Infrared Spectroscopy (FT-IR). FT-IR spectroscopy was carried out using an Agilent Technologies Cary 630 FTIR spectrometer. 16 Scans from 600 to 4000 cm^{-1} were taken at a resolution of 4 cm^{-1}, and the spectra were corrected for background absorbance. Peaks above 1000 cm-1 are reported in wavenumber (cm^{-1}) with the strength notated as weak (w), medium (m) or strong (s), as well as broad peaks (br).

Flash Column Chromatography. Flash chromatography was performed on a Teledyne ISCO CombiFlash Rf+ Lumen equipped with nm) and an internal evaporative light scattering detector (ELSD) with two UV detectors (254 nm and 280 nm) and RediSep RF normal phase columns.

Thermogravimetric Analysis (TGA). TGA thermograms were obtained using a TGA/DSC 1 - Thermogravimetric Analyzer (Mettler Toledo). Thermograms were recorded under an N_2 atmosphere at a heating rate of 10 ^{o}C min^{-1}, from 10 - 600 ^{o}C, with an average sample weight of *ca.* 10 mg. Aluminium pans were used for all samples. Decomposition temperatures were reported as the 5% weight loss temperature (T_d, 5%).

Differential Scanning Calorimetry (DSC). The thermal characteristics of the polymers were determined using differential scanning calorimetry (STARe system DSC3, Mettler Toledo) from -50 to 150 ^{o}C at a heating rate of 10 ^{o}C min^{-1} for two heating/cooling cycles unless otherwise specified. The glass transition temperature (T_g) was determined from the inflection points in the first and second heating cycles of DSC.

Uniaxial Tensile Testing (UTT). Dumbbell-shaped samples were cut directly from the synthesized films using a custom ASTM Die D-638 Type V. Tensile tests at different stretching speed were carried out using a Testometric M350-5CT universal mechanical testing instrument fitted with a load cell of 5 kN at room temperature (21 ± 1 ^{o}C). The gauge length was set as 6.3 mm and the crosshead speed was set 10 mm min^{-1}. The dimensions of the neck of the specimens were 6.3 mm in length, 1.6 mm in width and 0.4-0.7 mm in thickness. The reported results are average values from at least three individual measurements (n = 5).

Dynamic Mechanical Analysis (DMA). Dynamic mechanical thermal analysis (DMTA) data were obtained using a Mettler Toledo DMA 1 star system and analyzed using the software

package STARe V13.00a (build 6917). Thermal sweeps were conducted using films (L × W × thickness = 9.00 mm × 6.00 mm × 0.5–0.7 mm) cooled to -50 °C and held isothermally for *ca.* 5 minutes. Storage and loss moduli, as well as the loss factor (ratio of *E*" and *E*', tan *δ*) were probed as the temperature was swept from -50 to 150 °C, 5 °C min^{-1}, 1 Hz.

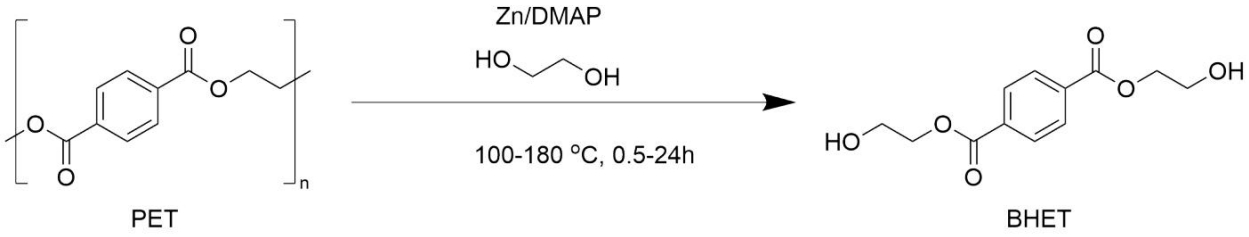
2.6 Materials

Ethylene glycol anhydrous (EG, >98.5%), 4-(dimethylamino)pyridine (DMAP, >99%), zinc acetate dihydrate ($Zn(OAc)_2 \cdot 2H_2O$, >99.9%), *S*-(–)-perillyl alcohol (>95%), geraniol (98%), 3-methyl-2-buten-1-ol (prenol, 99%), (1R)-(–)-nopol (nopol, 98%), linalool (97%), 1-methyl-2-pyrrolidone (NMP, 99.5%), and trimethylolpropane tris(3-mercaptopropionate) (TMPMP, >95.0%) were purchased from Sigma Aldrich Company. Poly(ethylene terephthalate) (PET) was purchased from Goodfellow Company.

2.7 Synthetic Methods

2.7.1 General Procedure for the Glycolysis of PET

Scheme S2.1. Scheme of PET glycolysis reaction using $Zn(OAc)_2$ / DMAP at various temperatures.



A 20 mL scintillation vial was charged with ethylene glycol (2.8 mL, 3120 mg, 50 mmol, 20 equiv.), $Zn(OAc)_2 \cdot 2H_2O$ (5.5-55 mg, 0.025-0.25 mmol, 0.01-0.10 equiv.), 4 (N,N dimethylamino)pyridine (DMAP) (3.1-31 mg, 0.025-0.25 mmol, 0.01-0.10 equiv.) and *N* methyl pyrrolidone (0.024 mL, 25 mg, 0.25 mmol, 0.10 equiv., as internal standard) and sealed with a screw cap. The mixture was brought to the desired temperature (100 - 180 °C) in a pre-heated

metal heating block. PET (480 mg, 2.5 mmol, 1 equiv.) was added to the solution and stirred at this temperature for 2 h. Aliquots of 0.1 mL were taken at regular timepoints, and prepared for ^{1}H NMR spectroscopic analysis by dilution in in DMSO-d_6. Once all the PET had been depolymerised, water (15 mL) was added to the solution and cooled to 4 ^{o}C for 18 h, and the resulting crystals of bis(2-hydroxyethylene)terephthalate (BHET) (561 mg, 2.4 mmol, 96%) were recovered by vacuum filtration, washing with water (5 mL) and drying under reduced pressure. Analysis of BHET recovered was consistent with that previously reported.

BHET: **^{1}H NMR** (400 MHz, DMSO-d_6, 298 K) δ = 8.12 (s, 4H; Ar-H), 4.96 (t, 2H; OH), 4.32 (m, 4H; CH_2), 3.72 (m, 4H; CH_2).

^{13}C NMR (400 MHz, DMSO-d_6, 298 K) δ = 165.17 (C**C**(O)O), 133.75 (C=**C**(C)C), 129.52 (C=**C**C), 67.03 (O**C**C), 58.98 (C**C**OH).

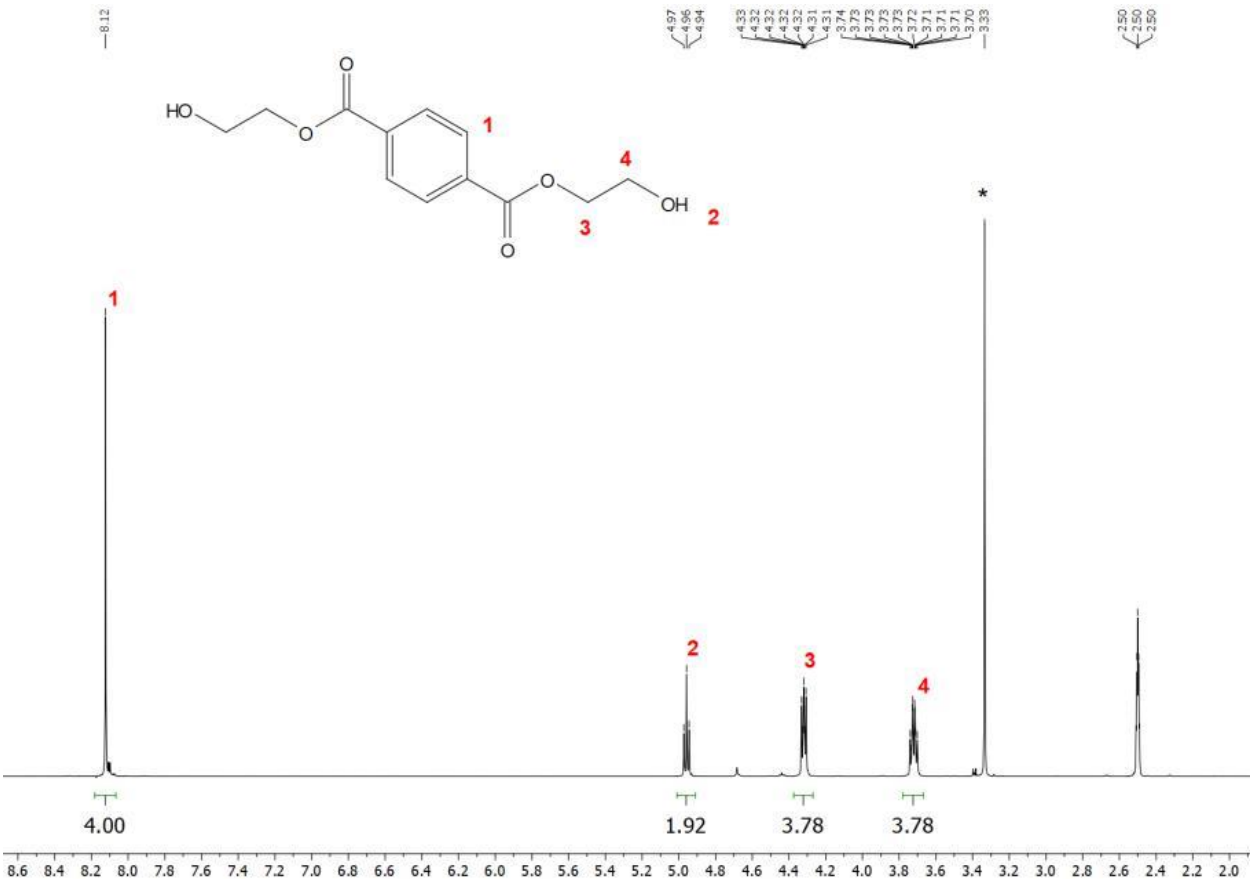


Figure S2.4. ^{1}H NMR spectrum of bis(2-hydroxyethyl)terephthalate (400 MHz, DMSO-d_6, 298 K). * = H_2O

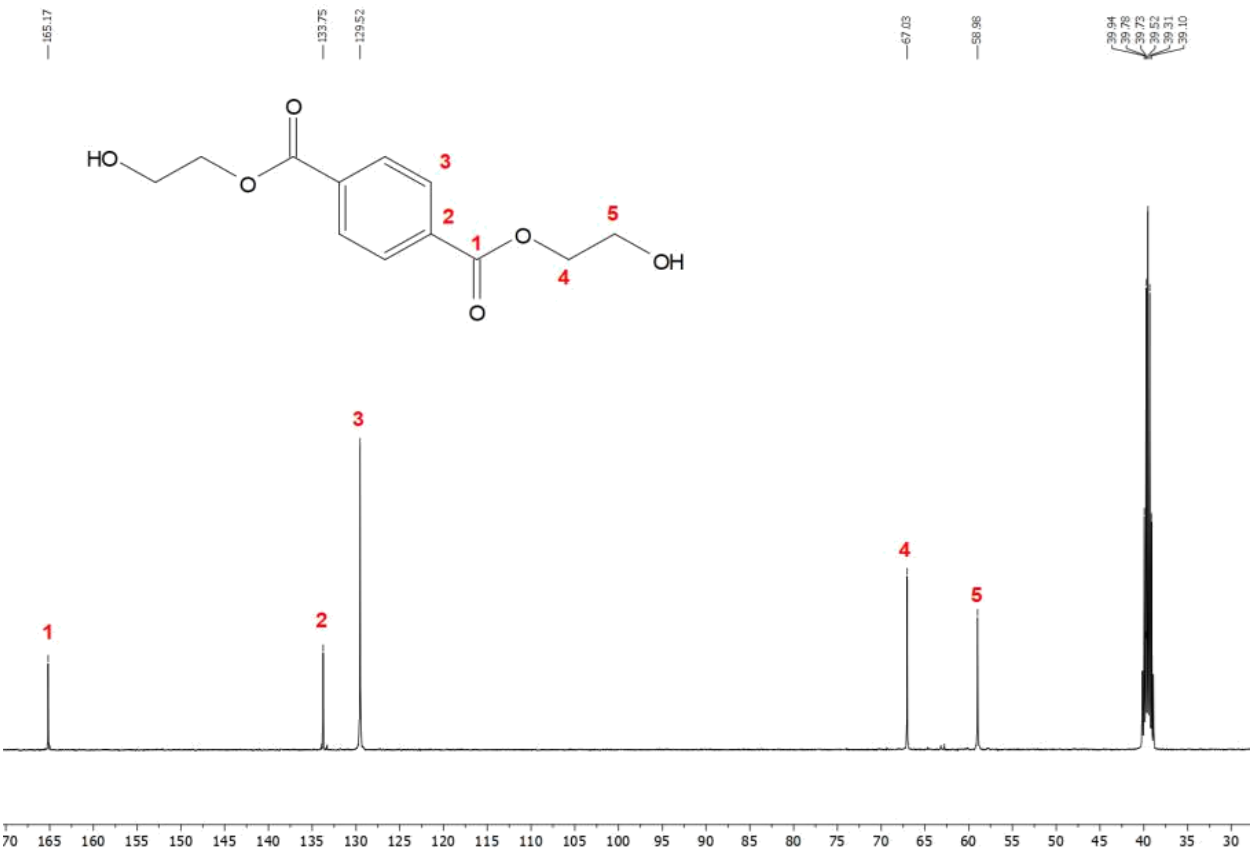


Figure S2.5. ^{13}C NMR spectrum of bis(2-hydroxyethyl)terephthalate (100 MHz, DMSO-d$_6$, 298 K).

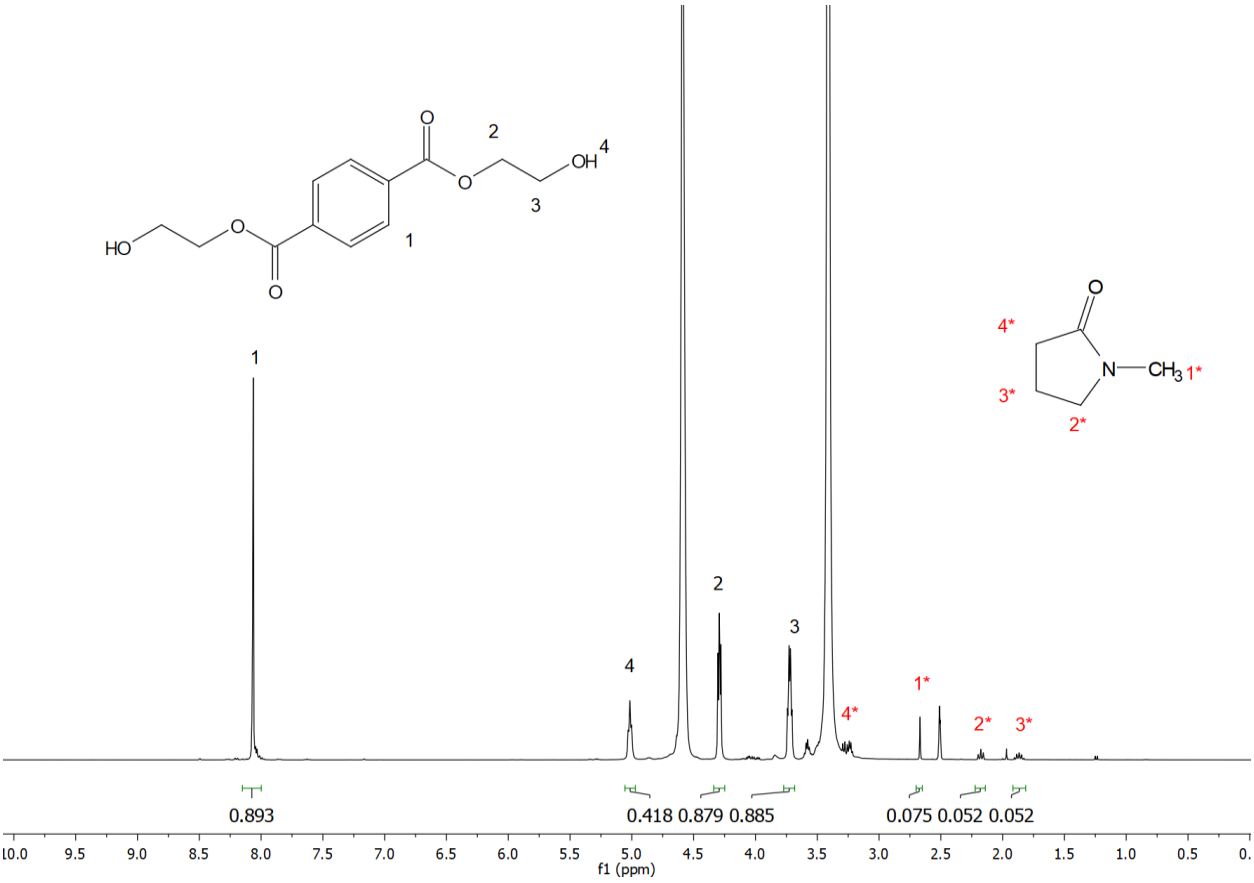


Figure S2.6. Example ^{1}H NMR spectrum of glycolysis reaction mixture aliquot (400 MHz, DMSO-d6, 298 K).

1. J.-P. Lange, *ACS Sustainable Chemistry & Engineering*, 2021, **9**, 15722-15738.

2.7.2 Generic Depolymerisation of PET by alcoholysis (10 mol% catalyst loading)

A 20 mL scintillation vial was charged with an alcohol (50 mmol, 20 equiv.), $Zn(OAc)_2 \cdot 2H_2O$ (55 mg, 0.25 mmol, 0.10 equiv.), 4-(N,N-dimethylamino)-pyridine (DMAP) (31 mg, 0.25 mmol, 0.10 equiv.) and N-methyl-pyrrolidone (0.024 mL, 25 mg, 0.25 mmol, 0.10 equiv., as internal standard) and sealed with a screw cap. The mixture was brought to the desired temperature (100 - 180 ^{o}C) in a pre-heated metal heating block. PET (480 mg, 2.5 mmol, 1 equiv.) was added to the solution and stirred at this temperature for 2 h. Aliquots of 0.1 mL were taken at regular timepoints, and prepared for ^{1}H NMR spectroscopic analysis in DMSO-d_6. Once all the PET had been depolymerised the workup was conducted in one of two ways (1) a 1:1 methanol:water (15 mL) mixture was added to the solution and the resulting crystals (yield in table below) were recovered by vacuum filtration and washed with water (5 mL); or (2) the mixture was washed with water (20 mL) before the solvent was distilled off at low pressure and the crude product was purified by column chromatography (0-50% ethyl acetate in hexane). The product was dried under high vacuum. Some products were not isolated.

Table S1 Yields of functionalised monomers derived from PET powder alcoholysis.

Compound	Yield / g	% Yield
Bis(prenyl)terephthalate	0.506	67
Bis(perillyl)terephthalate	0.654	60
Bis(geranyl)terephthalate	0.630	58
Bis(nopyl)terephthalate	0.564	49
Bis(eugenyl)terephthalate	n/a	n/a
Bis(linalyl)terephthalate	n/a	n/a

Bis(prenyl)terephthalate: ^{1}H NMR (400 MHz, Chloroform-d) δ = 8.11 (s, 4H; Ar-H), 5.50 (ddp, J = 8.6, 5.7, 1.4 Hz, 2H; C=CH), 4.86 (dt, J = 7.3, 0.9 Hz, 4H; OCH_2), 1.81 (dd, J = 7.2, 1.3 Hz, 12H; CH_3), 1.57 (s; H_2O).

^{13}C NMR (100 MHz, Chloroform-d, 298 K) δ = 165.92 (CC(O)O), 139.57 (C=C(C)(C)), 134.19 (C=C(C)C), 129.51 (C=CC), 118.39 (CC=C(C)(C)), 62.30 (OCC=C), 25.82 (C=C(C)(C)), 18.14 (C=C(C)(C)).

FT-IR Wavenumber / cm^{-1}: 2903 (w, br, C-H), 1715 (s, C=O), 1501 (w, C=C), 1447 (m), 1402 (m), 1382 (m), 1369 (m), 1324 (m), 1265 (s), 1238 (s), 1196 (m), 1127 (s), 1116 (s), 1100 (s), 1042 (m), 1019 (m).

HRMS (ASAP): *m/z* calcd. for $C_{18}H_{22}O_4$+H^+: 303.1596 $[M+H]^+$; found: 303.1600.

Bis(geranyl)terephthalate: ^{1}H NMR (400 MHz, Chloroform-d, 298 K) δ = 8.09 (s, 4H; Ar-H), 5.47 (tq, J = 7.1, 1.3 Hz, 2H; C=CH), 5.09 (tq, J = 4.6, 1.5 Hz, 2H; C=CH), 4.86 (d, J = 7.1 Hz, 4H; OCH2), 2.15 – 2.05 (m, 8H; CH_2), 1.77 (s, 8H; CH_2), 1.67 (d, J = 1.3 Hz, 6H; CH_3), 1.60 (t, J = 2.1 Hz, 12H; CH_3).

^{13}C NMR (100 MHz, Chloroform-d, 298 K) δ = 166.02 (CC(O)O), 142.92 (OCC=C(C)C), 134.3 (C=C(C)C), 132.03, 129.64, 123.82 (CC=C(C)(C)), 118.24 (OCC=C(C)), 62.42 (OCC=C(C)), 39.69 (C=C(C)CCC=C), 26.41 (C=C(C)CCC=C), 25.81 (CC=C(C)(C)), 17.84 (CC=C(C)(C)), 16.71 (OCC=C(C)C).

FT-IR Wavenumber / cm^{-1}: 2960 (m, C-H), 2910 (m, C-H), 2848 (m, C-H), 1714 (s, C=O), 1667 (w, C=C), 1575 (w, C=C), 1500 (w, C=C), 1438 (m, br), 1405 (m), 1374 (m), 1339 (w), 1260 (s), 1243 (s), 1112 (s), 1096 (s, br), 1016 (s).

HRMS (ASAP): m/Z calcd. for $C_{28}H_{38}O_4$+H^+: 439.2848 $[M+H]^+$; found: 439.2850.

Bis(perillyl)terephthalate: ^{1}H NMR (400 MHz, Chloroform-d, 298 K) δ = 8.14 (s, 3H; Ar-H), 5.88 (s, 2H; C=CH), 4.76 (dd, *J* = 4.8, 1.4 Hz, 8H; OCH_2; $C=CH_2$), 2.21 (s, 6H; CH_2; CH), 2.05 (d, *J* = 14.7 Hz, 4H; CH_2), 1.95 – 1.87 (m, 4H; CH_2), 1.77 (dd, *J* = 1.5, 0.8 Hz, 6H; CH_3).

^{13}C NMR (100 MHz, Chloroform-d, 298 K) δ = 165.72, 149.54, 134.16, 132.42, 129.59, 126.17, 108.87, 69.33, 40.83, 30.49, 27.32, 26.49, 20.78.

FT-IR Wavenumber / cm^{-1}: 3033 (w, br, C-H), 1796 (s, C=O), 1708 (m), 1625 (w, C=C), 1486 (w), 1460 (w), 1424 (m), 1292 (s), 1208 (w), 1134 (s), 1046 (m)

HRMS (ES+): m/Z calcd. for $C_{29}H_{30}O_4$+Na^+: 457.2368 $[M+Na]^+$; found: 457.2365.

Bis(nopyl)terephthalate: ^{1}H NMR (400 MHz, Chloroform-d, 298 K) δ = 8.10 (s, 4H; Ar-H), 5.39 (tt, *J* = 3.0, 1.4 Hz, 2H; C=CH), 4.38 (td, *J* = 6.9, 2.8 Hz, 4H; OCH_2), 2.52 – 2.36 (m, 4H; CH_2), 2.35 – 2.18 (m, 2H; CH), 2.14 (qd, J = 6.1, 2.6 Hz, 4H; CH_2), 1.30 (s, 6H; CH_3), 1.19 (d, *J* = 8.5 Hz, 2H; CH), 0.85 (s, 6H; CH_3).

^{13}C NMR (100 MHz, Chloroform-d, 298 K) δ = 165.80, 144.09, 134.15, 129.49, 119.10, 63.73, 45.77, 40.73, 38.04, 36.00, 31.71, 31.40, 26.27, 21.16.

FT-IR Wavenumber / cm^{-1}: 3077 (m, br, C-H), 1801 (s, C=O), 1727 (s), 1526 (w, C=C), 1489 (w), 1435 (m), 1416 (m), 1311 (m), 1157 (w), 1067 (s)

HRMS (ES+): m/Z calcd. for $C_{30}H_{38}O_4$+Na^+: 463.2848 $[M+Na]^+$; found: 463.2851.

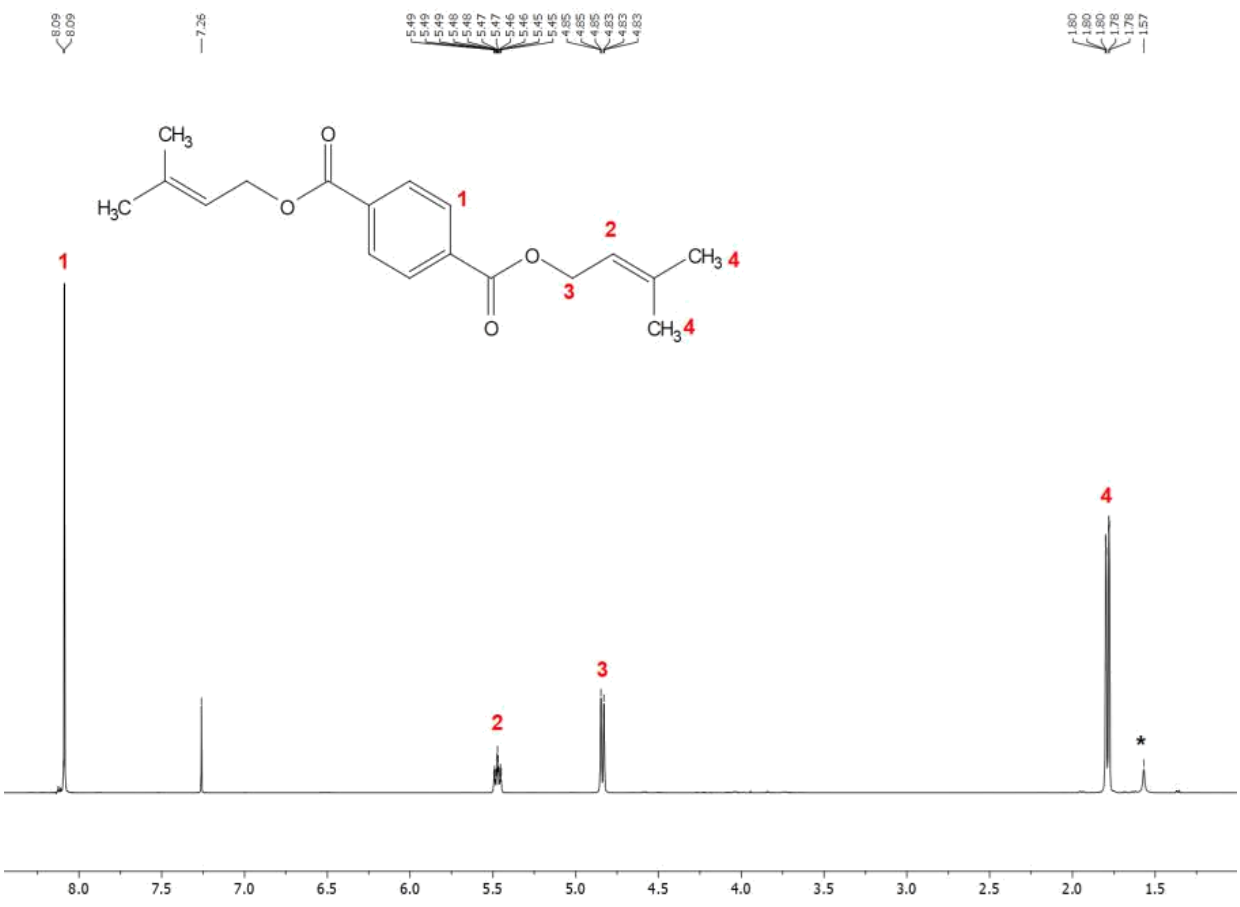


Figure S2.7 ^{1}H NMR spectrum of bis(prenyl)terephthalate (400 MHz, $CDCl_3$, 298 K). * = H_2O

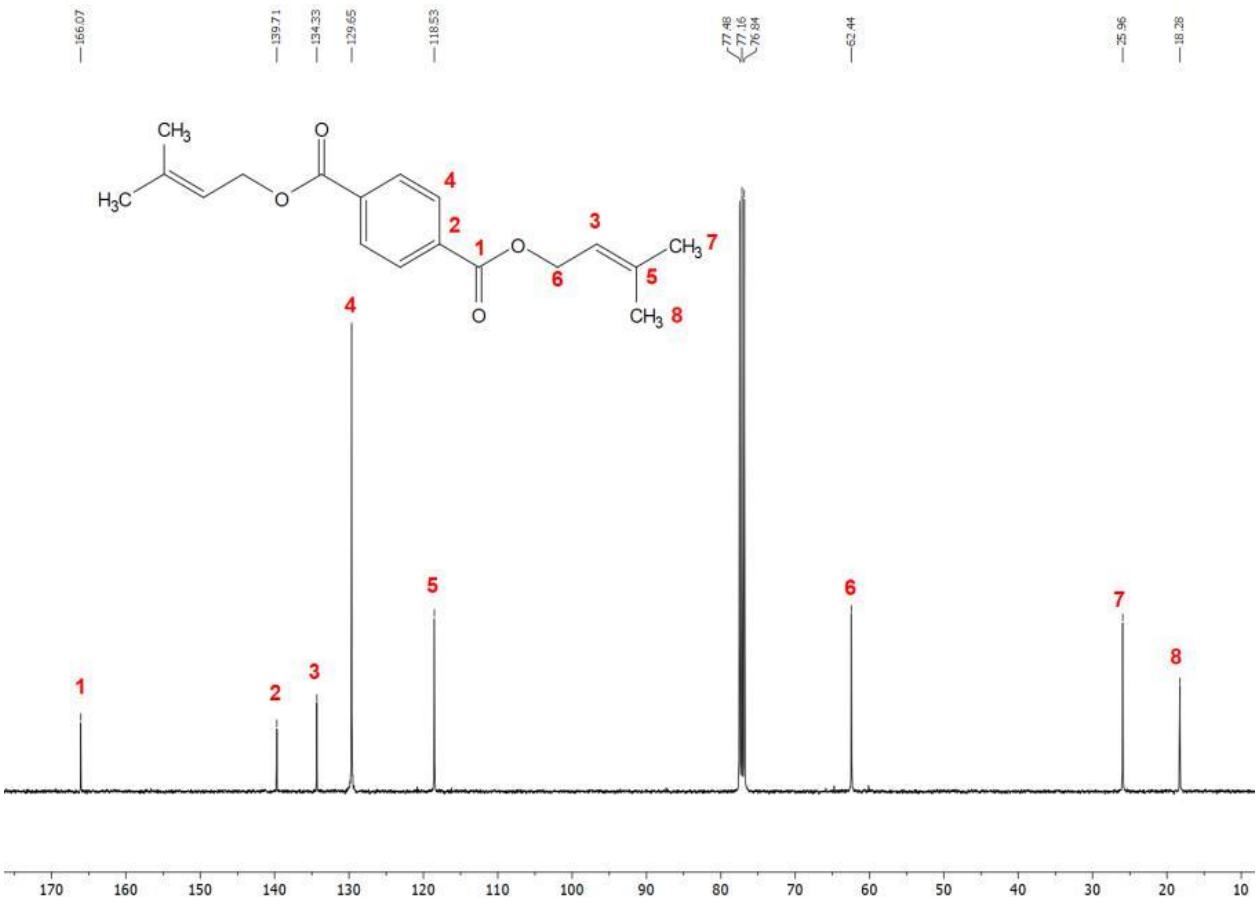


Figure S2.8 ^{13}C NMR spectrum of bis(prenyl)terephthalate (100 MHz, $CDCl_3$, 298 K).



Figure S2.9 ^{1}H NMR spectrum of bis(geranyl)terephthalate (400 MHz, $CDCl_3$, 298 K).

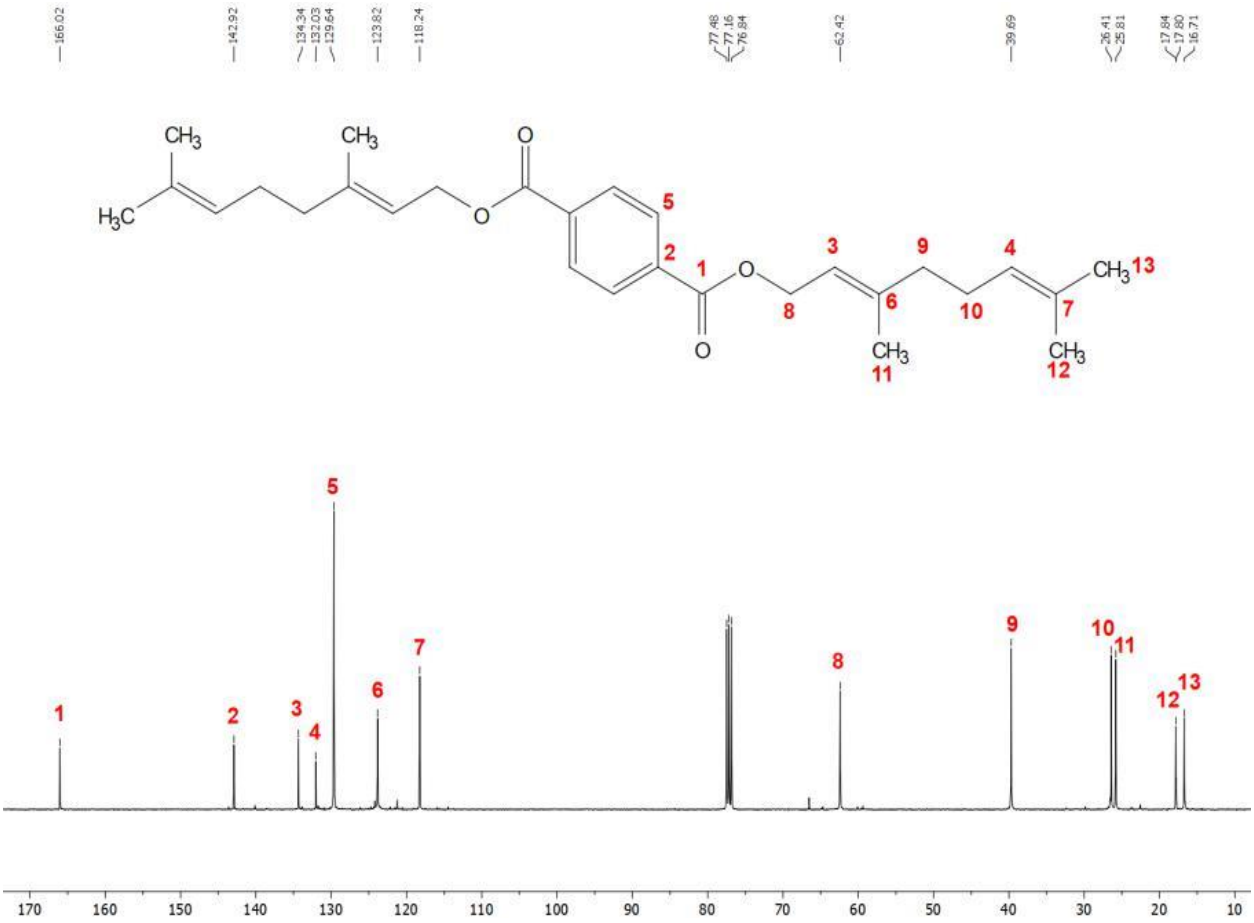


Figure S2.10 ^{13}C NMR spectrum of bis(geranyl)terephthalate (100 MHz, $CDCl_3$, 298 K).

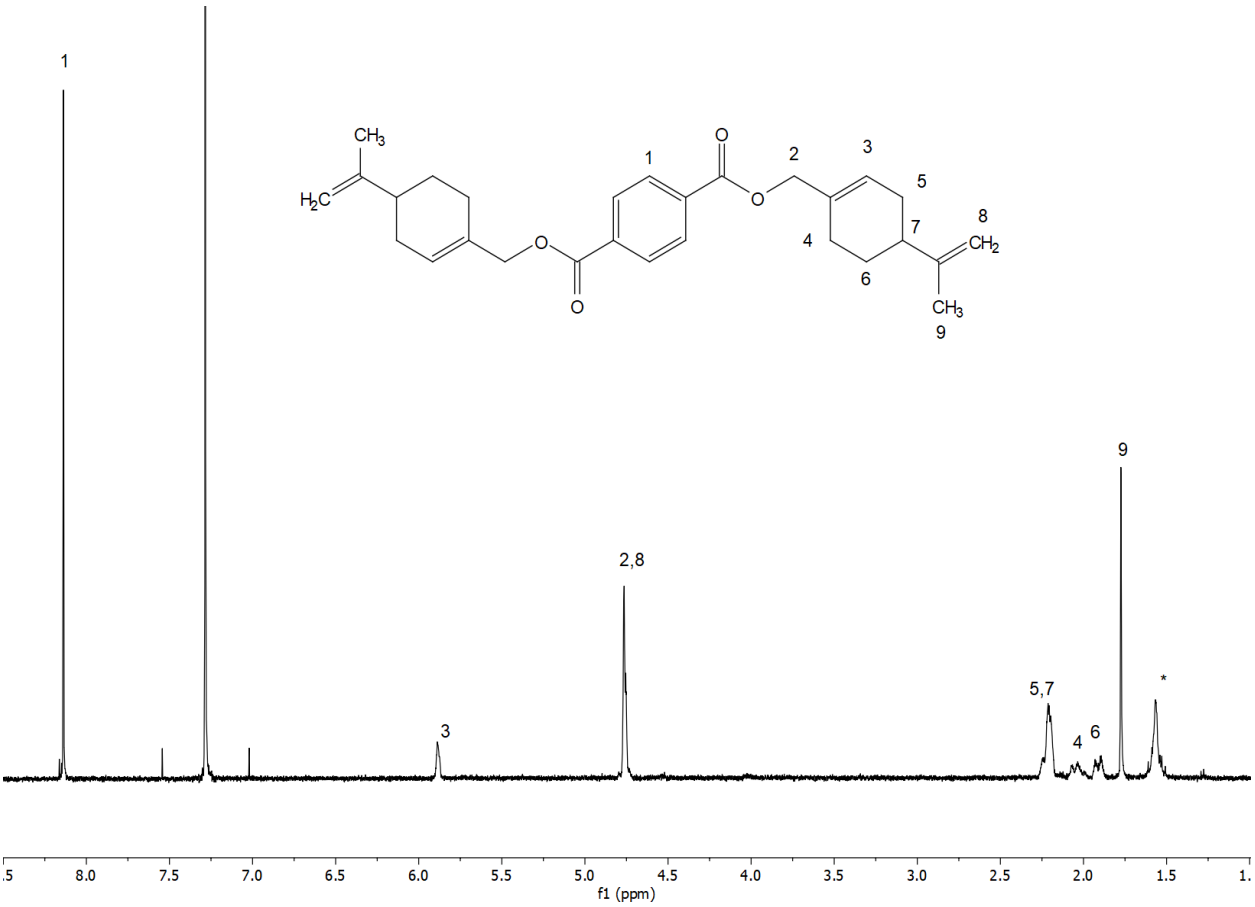


Figure S2.11 ^{1}H NMR spectrum of bis(perillyl)terephthalate (400 MHz, $CDCl_3$, 298 K). * = H_2O

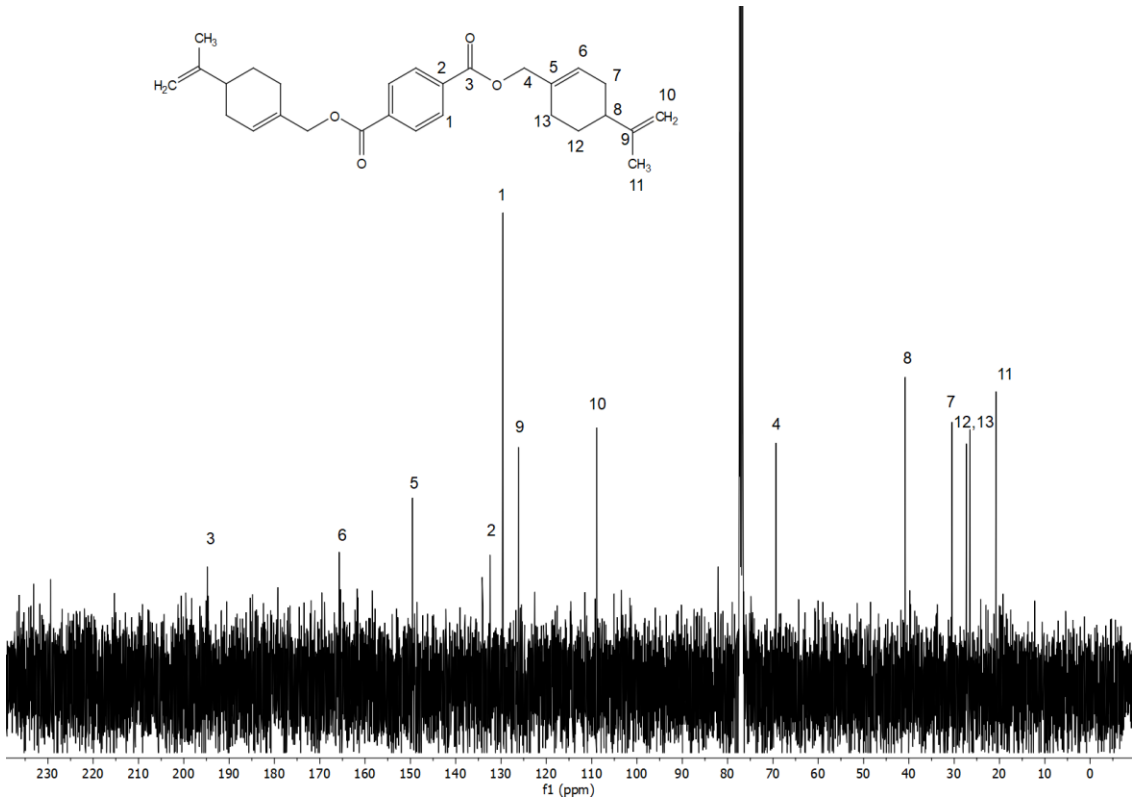


Figure S2.12 ^{13}C NMR spectrum of bis(perillyl)terephthalate (100 MHz, $CDCl_3$, 298 K).

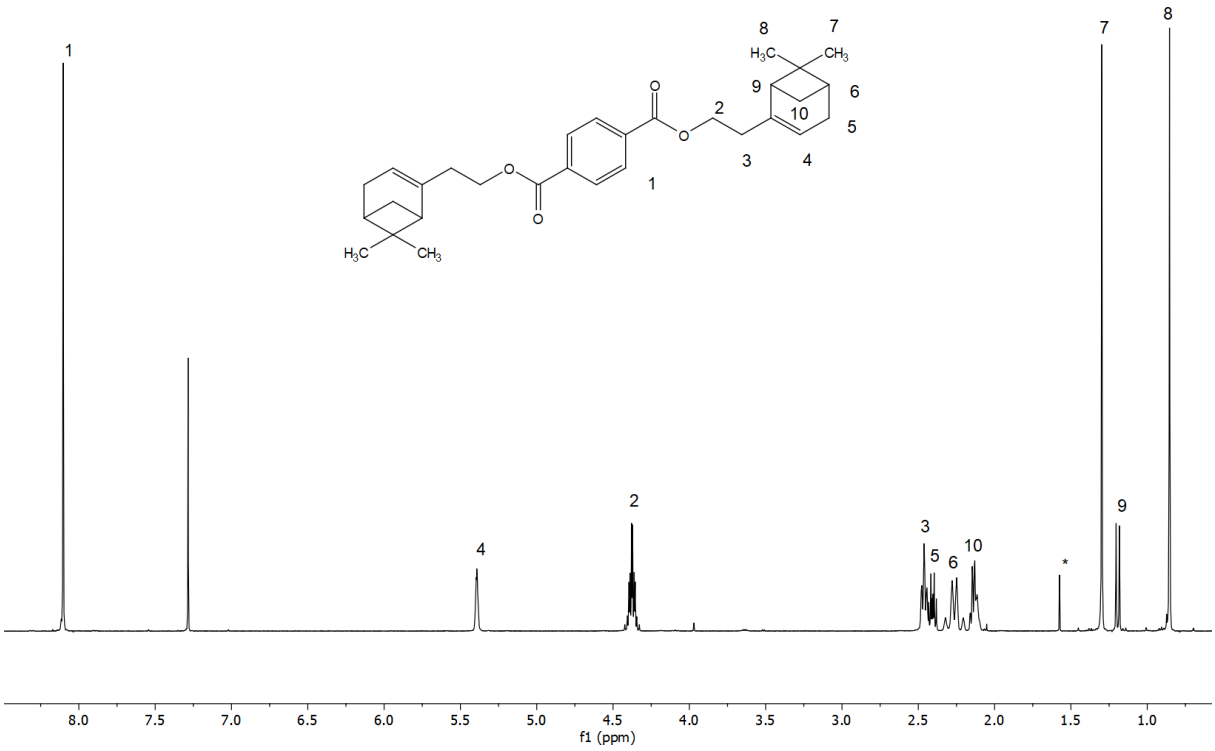


Figure S2.13 ^{1}H NMR spectrum of bis(nopyl)terephthalate (400 MHz, $CDCl_3$, 298 K). * =

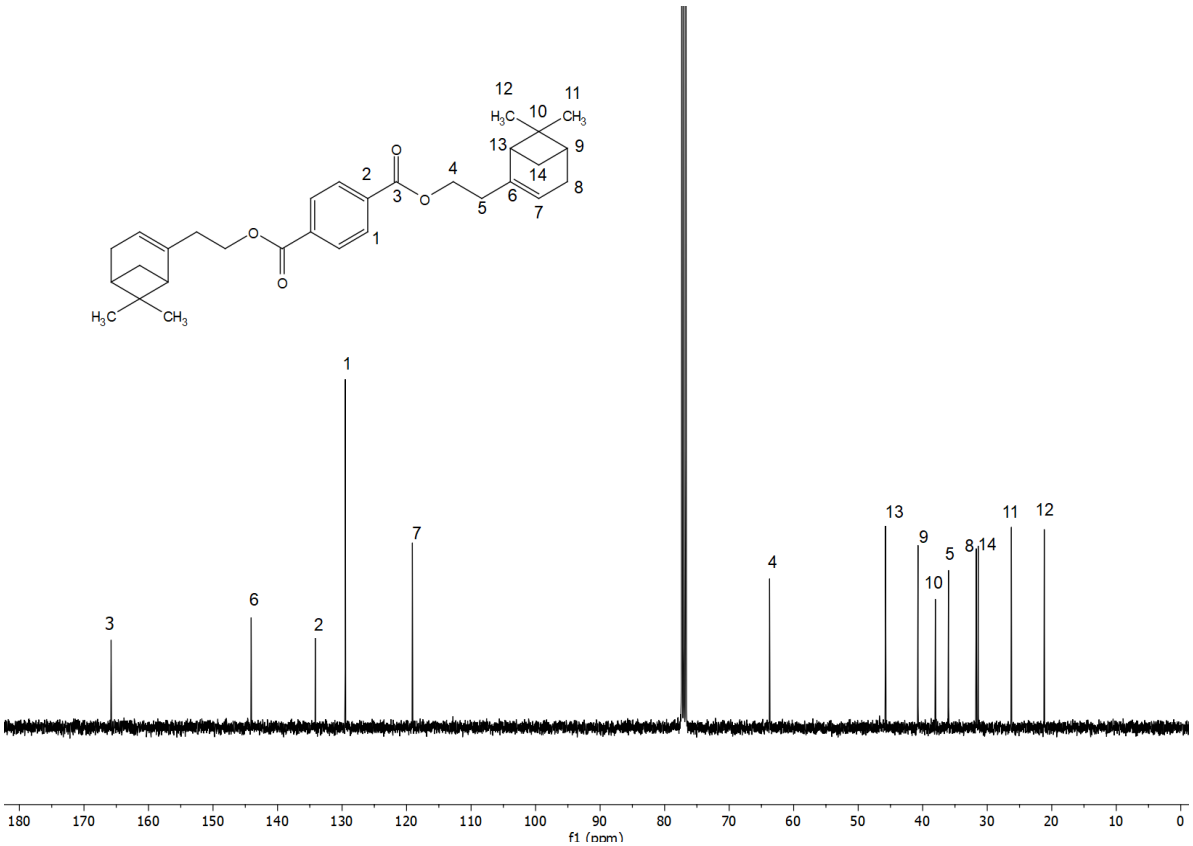


Figure S2.14 ^{1}H NMR spectrum of bis(nopyl)terephthalate (100 MHz, $CDCl_3$, 298 K).

2.7.3 Synthesis of Crosslinked Networks

A beaker was charged with bis(perillyl)terephalate (435 mg, 1.0 mmol, 3.0 equiv.) or bis(prenyl)terephthalate (302 mg, 1.0 mmol, 3.0 equiv.), trimethylolpropane tris(3-mercaptopropionate) (TMPMP) (0.214 mL, 0.67 mmol, 2.0 equiv.), ethyl (2,4,6-trimethylbenzoyl) phenylphosphinate photoinitiator (Irgacure® TPO-L) (0.018 mL, 2.5-3.5 wt%) and acetone (0.80 mL). The mixture was sonicated for 5-15 minutes until dissolved, then placed in a UV light box (λ = 405 nm, Formlabs Form Cure) for 30 minutes (gelation typically occurred within a few minutes, but the sample was further irradiated to ensure higher reaction conversion). The resultant film was left to dry at ambient temperature for 24 h, then further post-cured in a vacuum oven at 120 °C for 24 hours.

2.7.4 Synthesis of Blended Crosslinked Networks

A beaker was charged with bis(perillyl)terephalate (218 mg, 0.5 mmol, 1.5 equiv.) and bis(prenyl)terephthalate (151 mg, 0.5 mmol, 1.5 equiv.), trimethylolpropane tris(3-mercaptopropionate) (TMPMP) (0.214 mL, 0.67 mmol, 2.0 equiv.), ethyl (2,4,6-trimethylbenzoyl) phenylphosphinate photoinitiator (Irgacure® TPO-L) (0.018 mL, 3.1 wt%) and acetone (0.80 mL). The mixture was sonicated in a water bath at 37 kHz for 5-15 minutes until dissolved, then placed in a UV light box (λ = 405 nm, Formlabs Form Cure) for 30 minutes (gelation typically occurred within a few minutes, but the sample was further irradiated to ensure higher reaction conversion). The resultant film was left to dry at ambient temperature for 24 h, then further post-cured in a vacuum oven at 120 °C for 24 h.

2.7.5 Formulation of resin for 3D Printing

A 20 mL scintillation vial was charged with bis(perillyl)terephalate (1000 mg, 33 wt%), trimethylolpropane tris(3-mercaptopropionate) (TMPMP) (1.11 mL, 33 wt%), ethyl (2,4,6-trimethylbenzoyl) phenylphosphinate photoinitiator (Irgacure® TPO-L) (0.0667 mL, 2.2 wt%), N-methylpyrrolidone (0,97 mL, 33 wt%), pyrogallol (30 mg, 1 wt%) and Sudan II dye (1 mg, 0.03 wt%). The mixture was stirred and heated at 60 °C for 0.5 h.

2.7.6 Depolymerisation of Crosslinked Networks

A 20 mL scintillation vial was charged with C.BPrT or C.BPeT (0.50 mmol, 1 equiv.), prenol or perillyl alcohol (10 mmol, 20 equiv.), zinc acetate dihydrate (11.0 mg, 0.05 mmol, 0.1 equiv.), DMAP (6.2 mg, 0.05 mmol, 0.1 equiv.) and N methyl pyrrolidone (0.024 mL, 25 mg, 0.25 mmol, 0.10 equiv.) and sealed. The mixture was brought to 180 °C and stirred at this temperature for 1 h. Once the crosslinked material had visibly disappeared, the mixture was cooled to room temperature and 1:1 methanol:water (8 mL) was added, to yield a dark yellow powder (yields in Table S2).

Table S2.1 Yields of functionalised monomers derived from crosslinked network alcoholysis.

Compound	Yield / g	% Yield
Bis(prenyl)terephthalate	0.019	13
Bis(perillyl)terephthalate	0	0

2.8 Additional Data

2.8.1 Conversion Plots

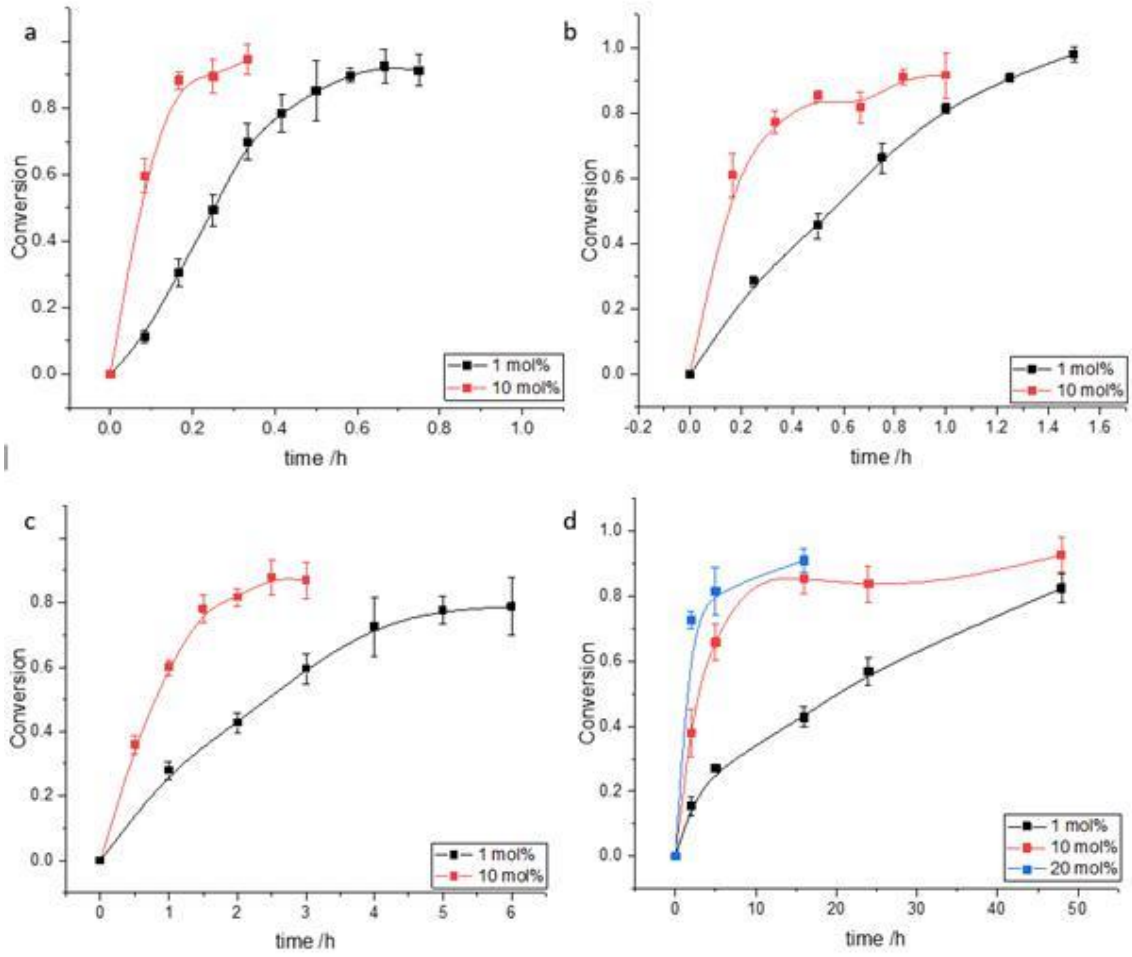


Figure S2.15 PET depolymerisation by glycolysis using Zn/DMAP catalyst at various loading, at a) 180 °C, b) 160 °C, c) 140 °C, d) 120 °C.

2.8.2 Arrhenius Plot

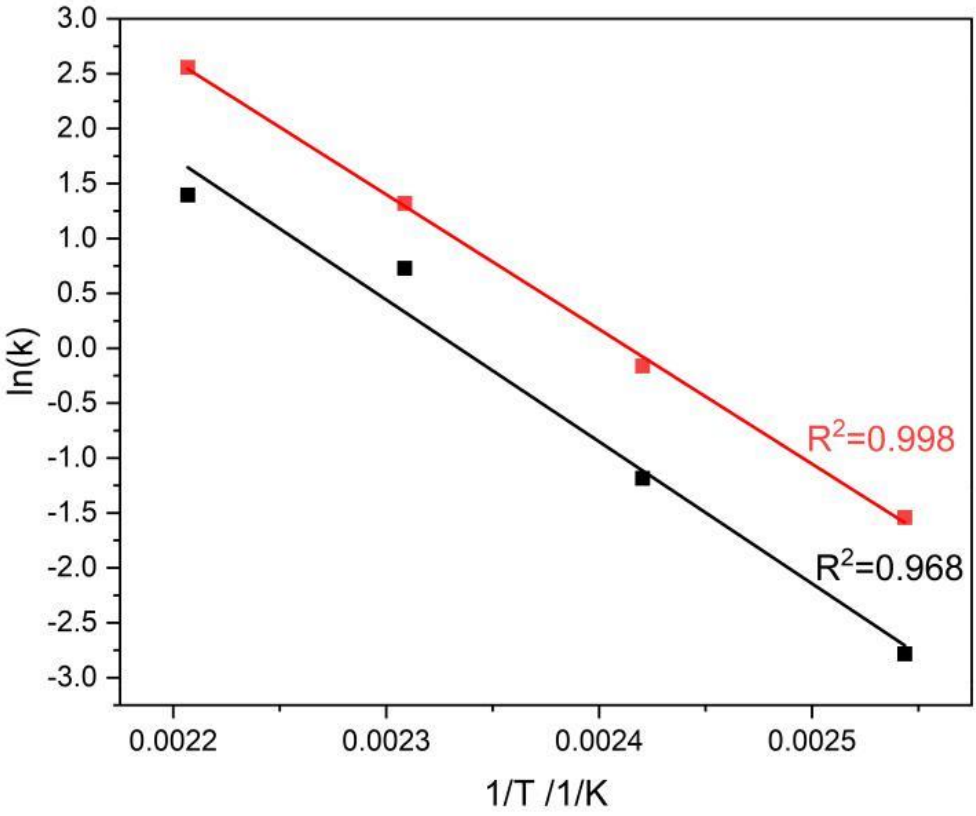


Figure S2.16 Arrhenius Plots of PET powder depolymerisation using Zn/DMAP catalyst at 1 mol% and 10 mol%. 1 mol% E_a = 107 11 kJ mol^{-1}; 10 mol% E_a = 102 ±2 kJ mol^{-1}.

2.8.3 TGA Plots

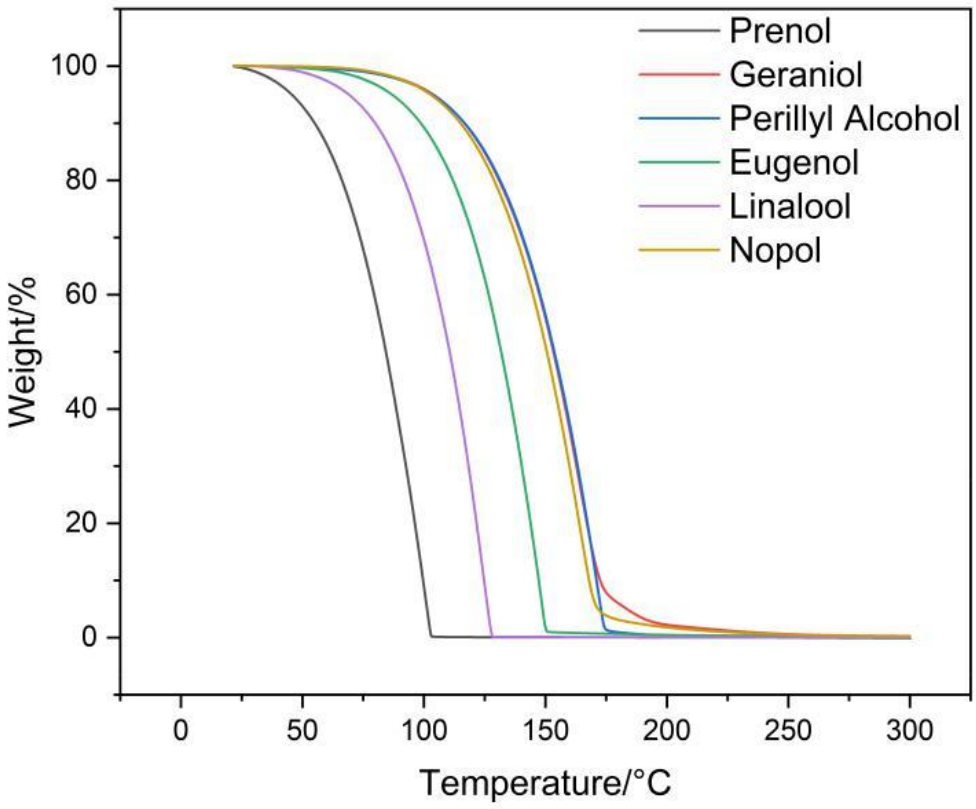


Figure S2.17 TGA thermograms of alcohols, from 25 to 600 °C, 10 °C min^{-1}.

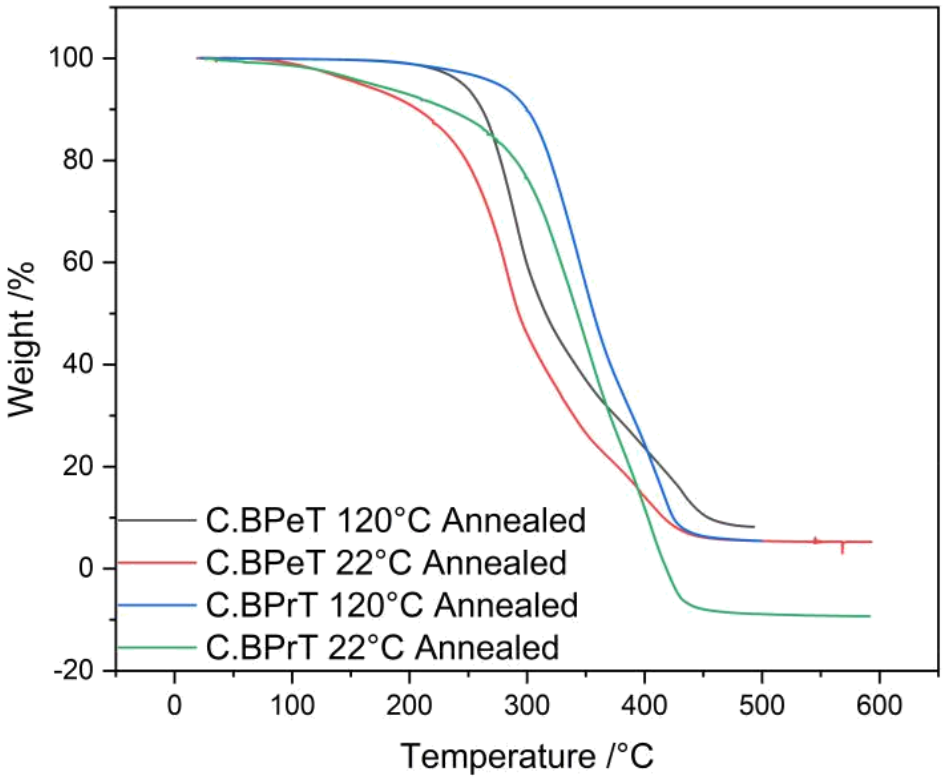


Figure S2.18 TGA thermograms of networks annealed at 22 °C and 120 °C, from 25 to 600 °C, 10 °C min^{-1}.

2.8.4 DSC Plots

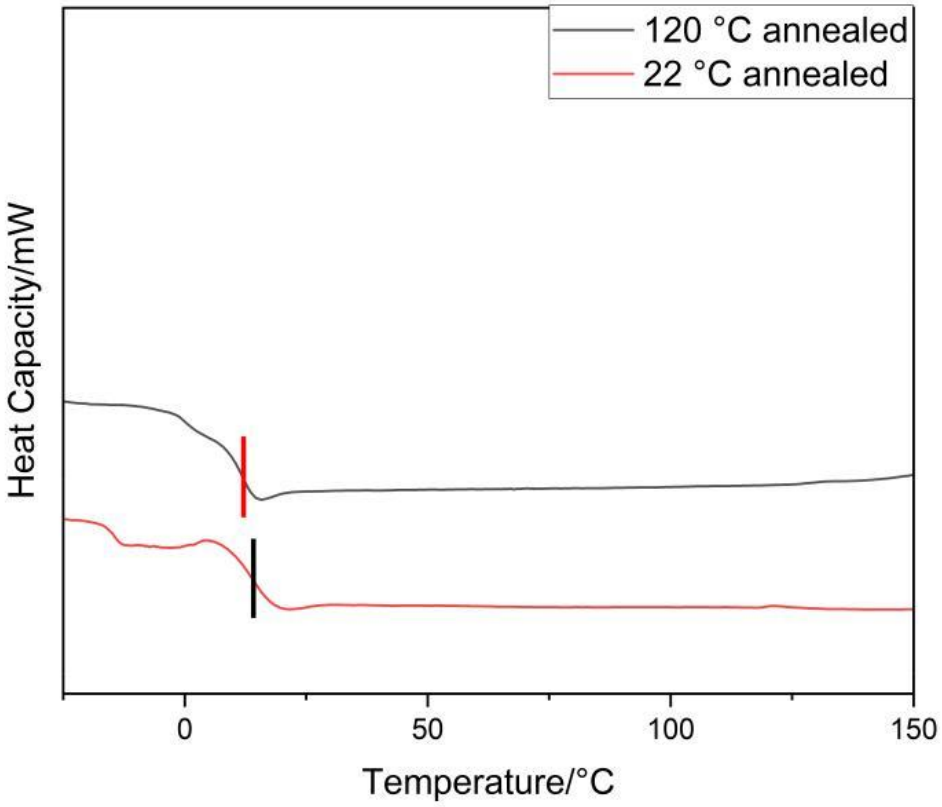


Figure S2.19 DSC thermograms of network 1 (BPrT) annealed at 22 °C and at 120 °C from -25 to 150 °C, 10 °C min^{-1}. Position of T_g is indicated with vertical hashmark.

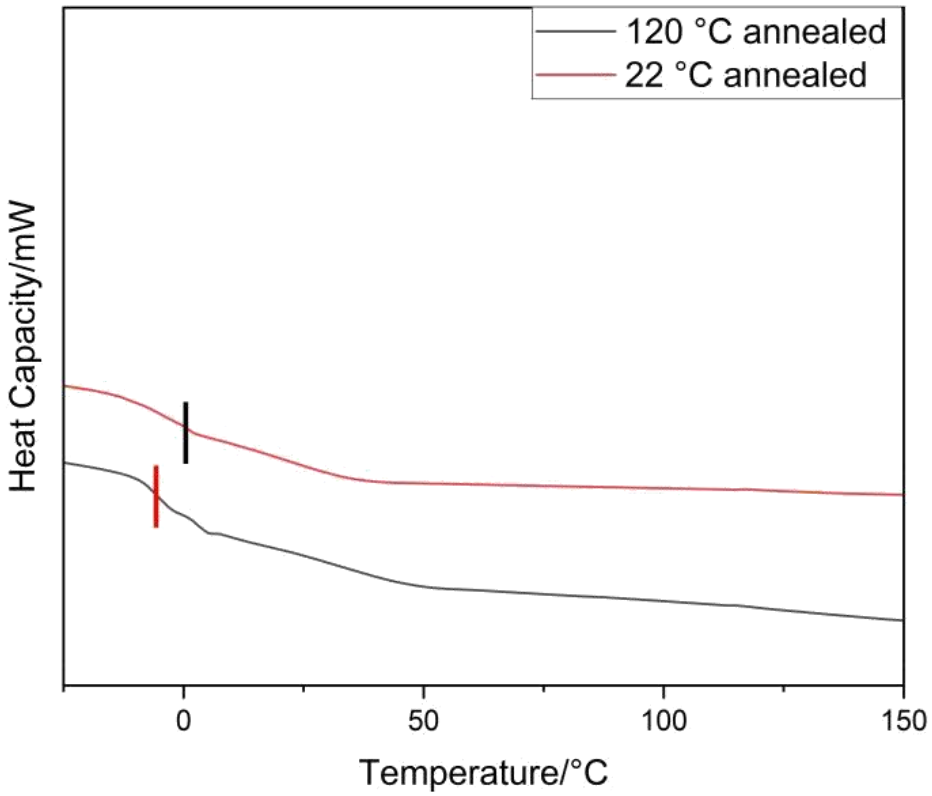


Figure S2.20 DSC thermograms of network 2 (BPeT) annealed at 22 °C and at 120 °C from -25 to 150 °C, 10 °C min^{-1}. Position of T_g is indicated with vertical hashmark.

2.8.5 Tensile Testing Plots

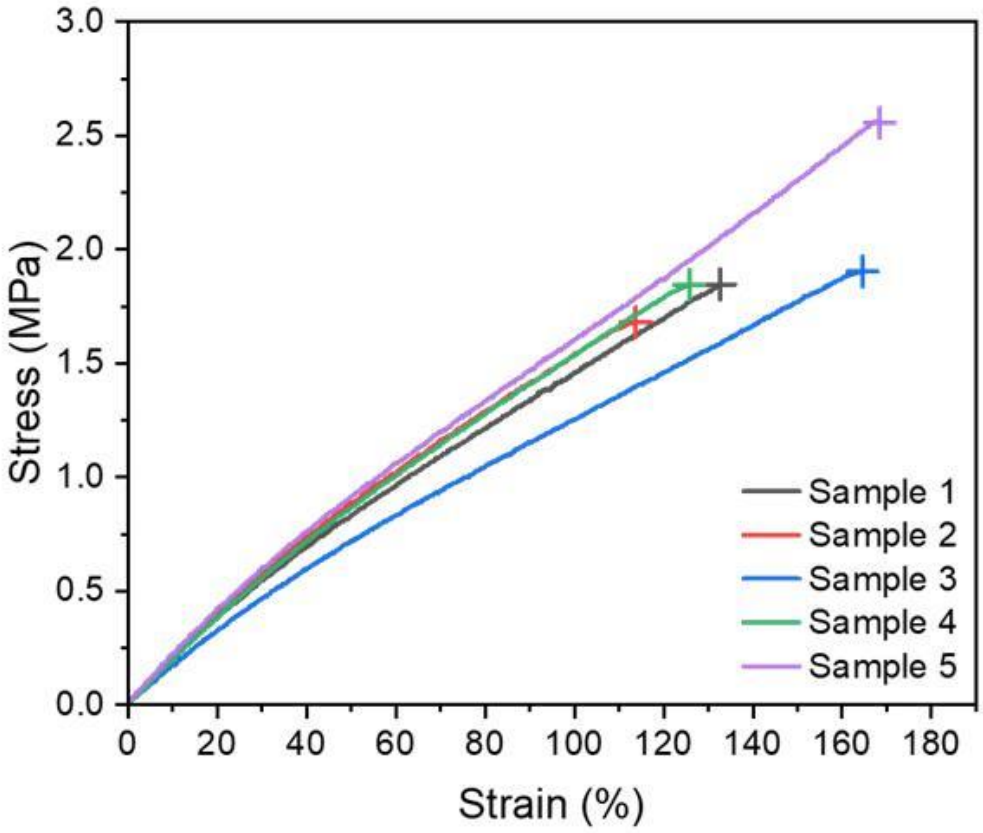


Figure S2.21 Stress vs strain curves of network **1** samples (BPrT) annealed at 22 °C tested at 10 mm min^{-1} strain rate (n = 5). Summary of results are shown in Table S3

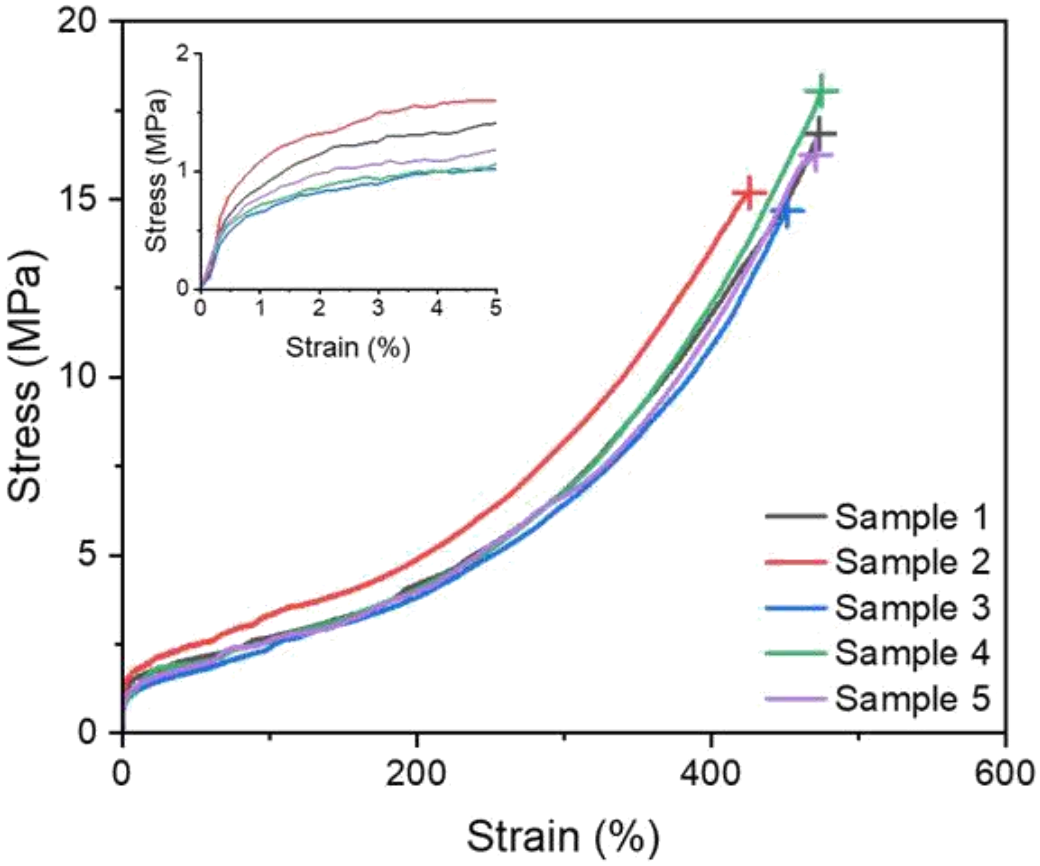


Figure S2.22 Stress vs strain curves of network **2** (BPrT) samples annealed at 120 °C tested at 10 mm min^{-1} strain rate (n = 5). Summary of results are shown in Table S3

2.8.6 DMA Plots

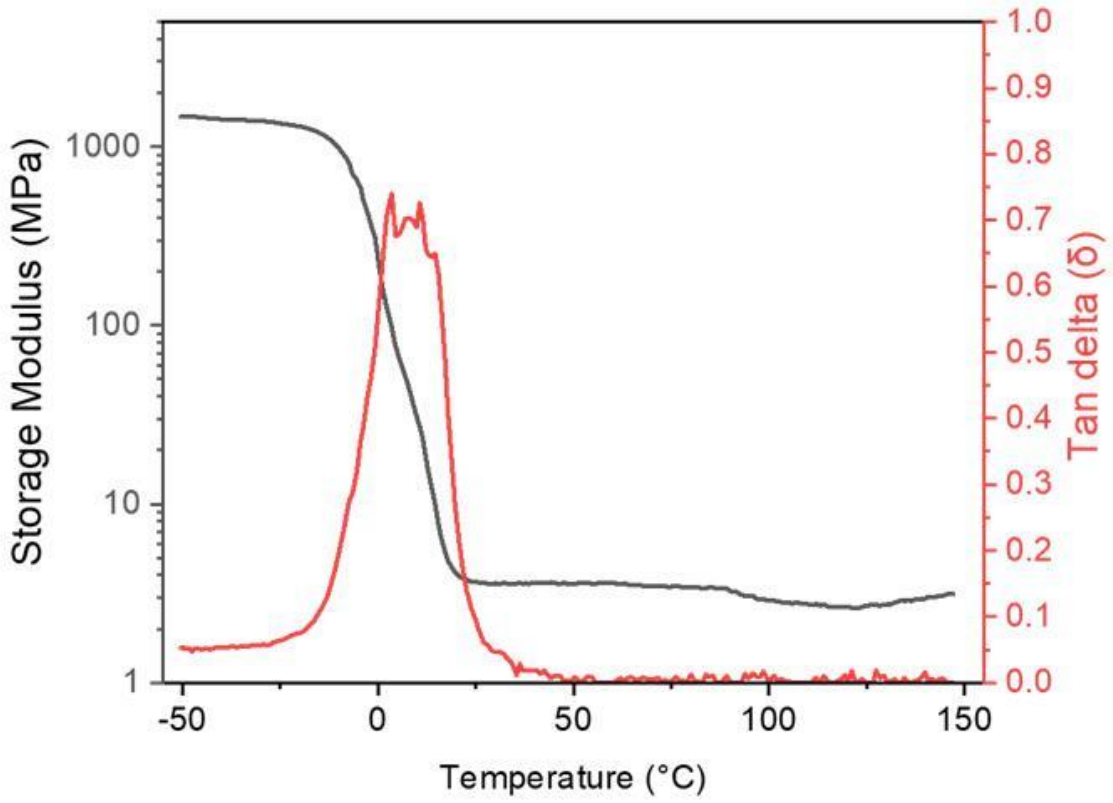


Figure S2.23 DMA temperature sweep of network **1** (BPrT) sample annealed at 22 °C from 50 to 150 °C, 5 °C min^{-1}.

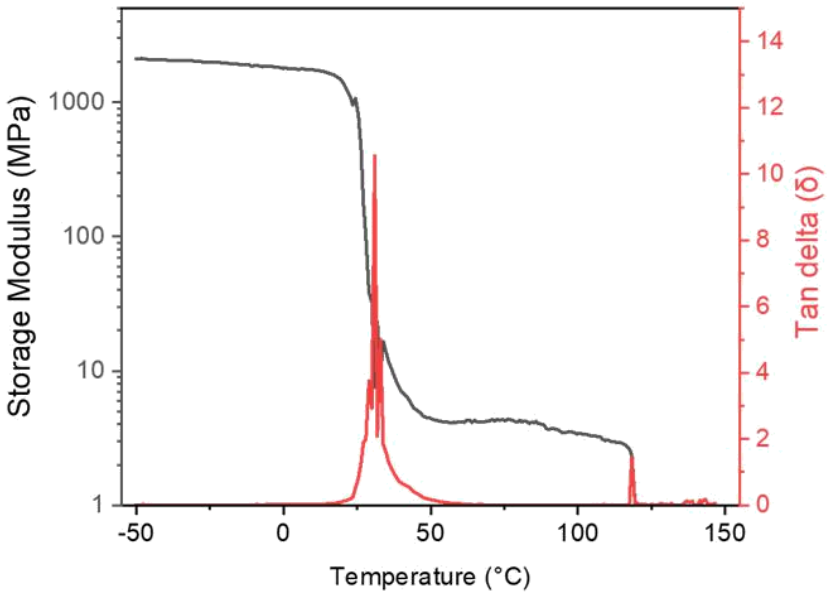


Figure S2.24 DMA temperature sweep of network **1** (BPrT) sample annealed at 120 °C from 50 to 150 °C, 5 °C min^{-1}.

2.8.7 Mechanical Properties Summary

Table S2.2. Summary of thermomechanical properties for crosslinked networks. [a]Glass transition temperature determined from inflection point in DSC thermogram from -100 to 150 °C, 10 °C min^{-1}. [b]Strain at break and stress at break determined from uniaxial tensile testing at 21 ±1 °C, 10 mm min^{-1} strain rate. All uncertainties are reported as 1 S.D.

Network	Sample Annealing Temperature / °C	[a]T_g 1st heat / °C	[b]Strain at Break / %	[b]Stress at Break / MPa	Tensile Toughness / MJ m^{-3}
1 (BPrT)	22 °C	-6	141 ±24	2.0 ±0.3	154 ±43
	120 °C	1	459 ±21	16.2±1.3	2840 ±217
2 (BPeT)	22 °C	14	82 ±11	1.31±0.35	59 ±19
	120 °C	12	29 ±2	41.9±9.2	477 ±92

2.8.8 Photorheology Plots

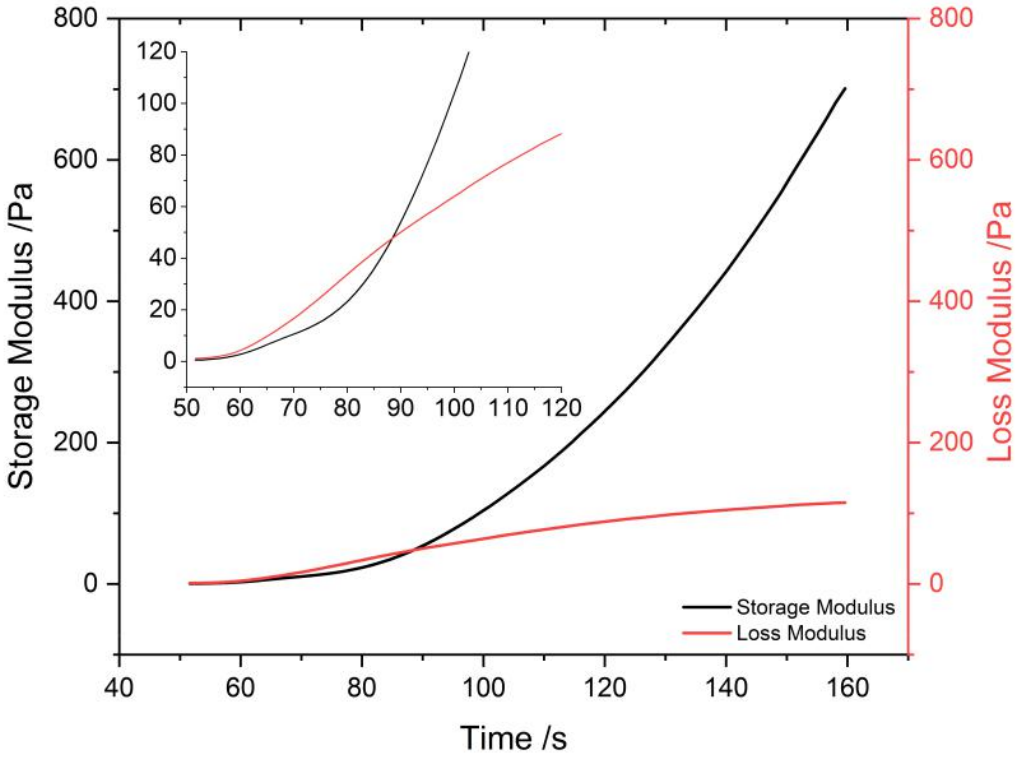


Figure S2.25 Photorheology of 3D printing formulation showing storage/loss modulus crossover point at *ca.* 88 s.

2.8.9 UV/Vis Plots

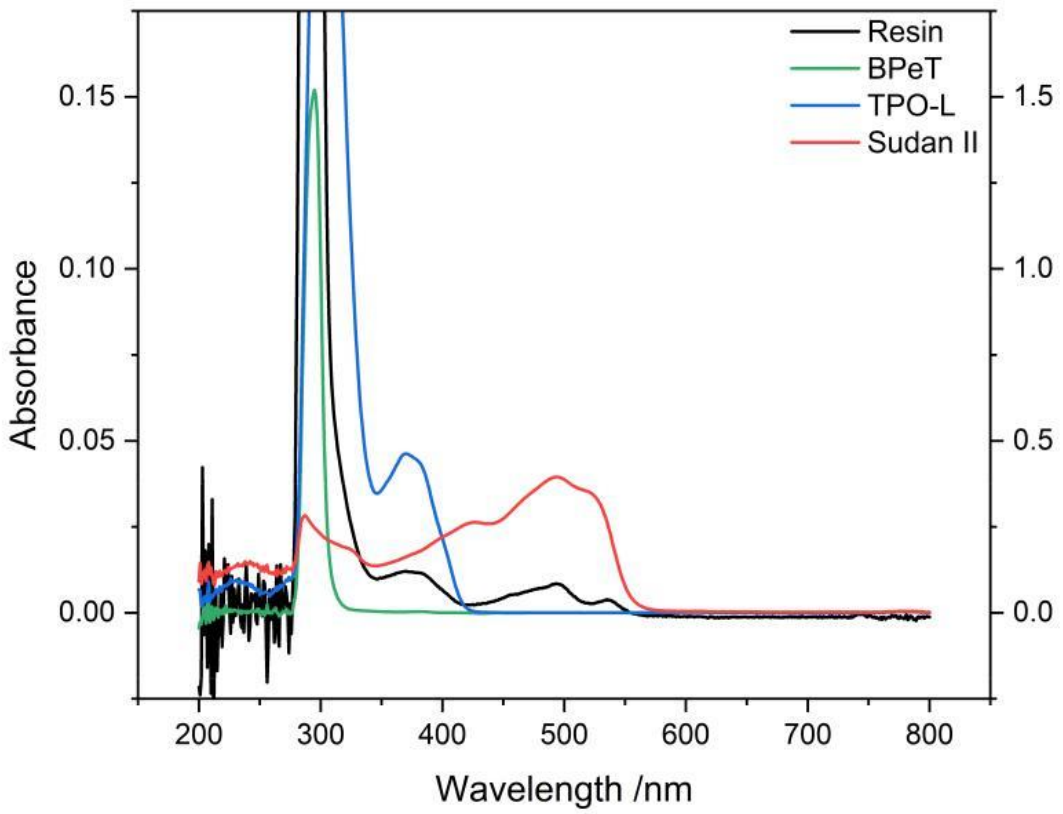


Figure S2.26 UV/Vis spectra of 3D printing resin formulation, alongside its UV-active components (BPeT monomer, TPO-L radical initiator, Sudan II dye).

2.8.10 UV Cure Working Cure Plots

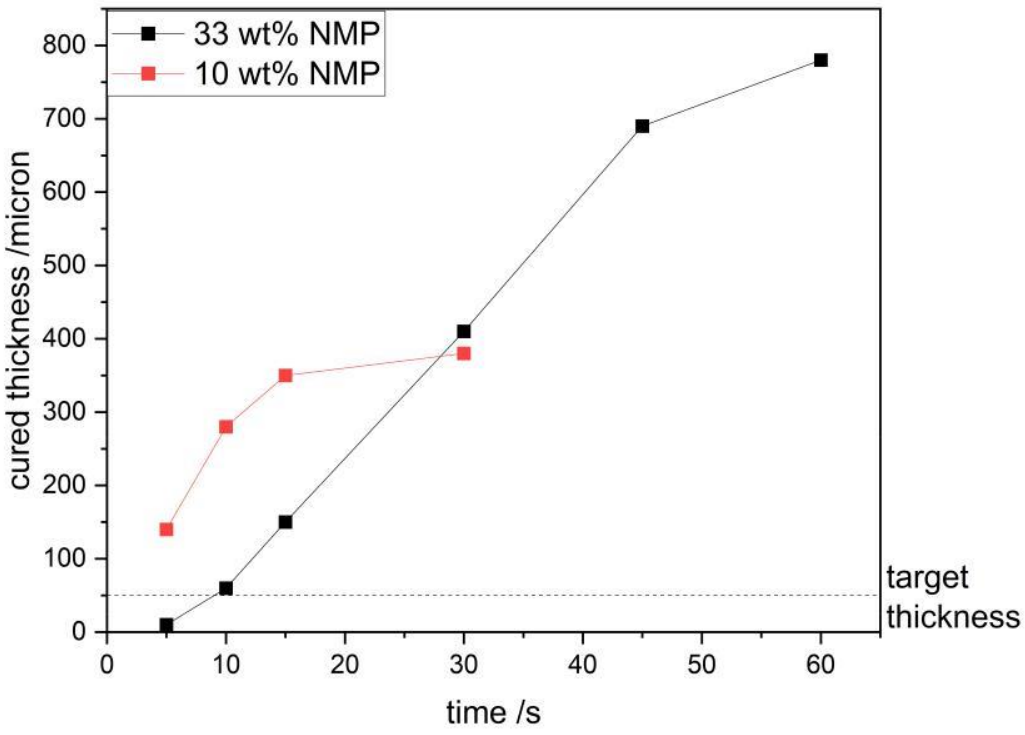


Figure S2.27 UV curing time of 3D printing resin formulation with respect to thickness cured, at 900% intensity.

2.9 References

1. P. Anggo Krisbiantoro, Y.-W. Chiao, W. Liao, J.-P. Sun, D. Tsutsumi, H. Yamamoto, Y. Kamiya and K. C.-W. Wu, *Chemical Engineering Journal*, 2022, **450**, 137926.

2. L. Bartolome, M. Imran, K. G. Lee, A. Sangalang, J. K. Ahn and D. H. Kim, *Green Chemistry*, 2014, **16**, 279-286.

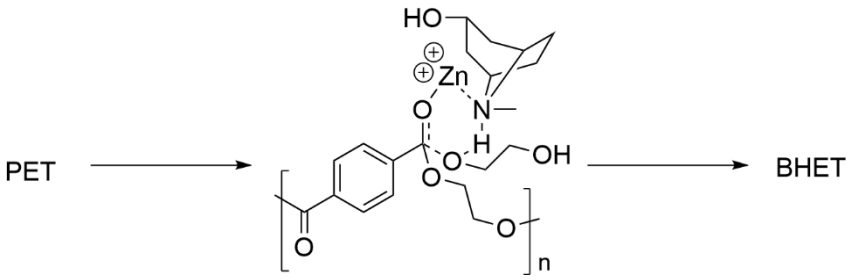
3. S. M. June, P. Bissel, T. E. Long, *J. of Polym. Sci. Part A: Polym. Chem.* **2012**, *50*, 3797-3805.

3. Dual Catalysis of PET Glycolysis

3.1. Introduction

Few studies have been undertaken into the structure-activity and property-activity relationships of dual catalysts for PET glycolysis. Of those which have been reported, Kaiho *et al.* screened a range of organocatalysts, wherein stoichiometric organic salts made up of organic acids and bases were surveyed. The pK_as of the acids ranged from -14 to 4.2, and the pK_{aH}s of the bases from 5.1 to 14.5, for a maximum ΔpK_a of 28.5. These salts were almost all found to be more stable than their component parts, and all but the TBD:weak acid salts were found to be active towards BHET repolymerisation.

Several studies have focused on a specific metal-organic catalyst system.[1] Of these, work by Deng *et al.* on base- and dual-catalysed PET glycolysis screened several metal acetates (manganese(II), copper(II) and nickel(II)) in dual catalysts in combination with tropine for the base component. The work found that zinc acetate ($Zn(OAc)_2$) / tropine was the most efficient catalyst combination. A mechanism of action was proposed, wherein the tropine acts both as a ligand to the zinc ion and as a base which deprotonates the EG attacking into the electrophilic carbonyl centre, in a six-membered concerted transition state (Scheme 3.1). Deng *et al.* found conversion rates of metal acetate / tropine complexes to be in the order: zinc > manganese >



Scheme 3.1. $Zn(OAc)_2$ / tropine mechanism proposed by Deng *et al.*

copper > nickel. However, the authors have not proposed a relationship between metal acetate properties and activities.

There is no clear consensus from the literature regarding the mechanism by which the dual catalyst acts, and none have attempted to survey a wide variety of dual catalysts aside from the 2020 work by Delle Chiaie *et al.,*[3] which forms the starting point for this study. The authors assessed metal salts and concluded that the metal acetate salts were most active. They observed an induction period in the depolymerisation kinetics of the non-acetate catalysts. A mechanism was suggested wherein the transesterification location forms a carboxylate which replaces the ligand on the metal; the depolymerisation kinetics catalysed by the metal acetates did not possess such an induction period. The study then screened organic base catalysts in combination with the most active metal acetate salt, $Zn(OAc)_2$. $Zn(OAc)_2$ / DMAP and $Zn(OAc)_2$ / ABCO were found to be the most efficient. The higher activity of these combinations was postulated to be a result of a qualitative peak function of activity with respect to basicity as a result of a 'Goldilocks Zone' of Lewis acid and base strength. However, a systematic quantitative model was not developed.

In this work the PET glycolysis dual catalyst design space will be surveyed, in order to develop a working understanding of how the interaction between an acid and a base would affect the activity of the combinations. In order to compare and contrast how the degradation process for each metal acetate / base dual catalyst combination proceeded, two separate models of PET degradation were utilised. The first was a surface-and-bulk degradation model, and the second a surface-only degradation model. The results of the property-activity relationships involving both Lewis acids and bases included in this study are significantly more complex than use of simple regression analysis would allow. Therefore, theoretical calculations were initiated to attempt to elucidate the more intricate relationships between structure, properties and activity,

the details of which are expanded upon in Chapter 4. The understanding of the activity-property relationships was further aided by M^2E^3D, a powerful tool for deriving equations.

3.2. Results and Discussion

3.2.1. Depolymerisation of PET by Dual Catalysis – Methodology

Many of the previous PET glycolysis methodologies involve weighing dried PET samples before and after degradation. This method requires a large number of experiments and produces high

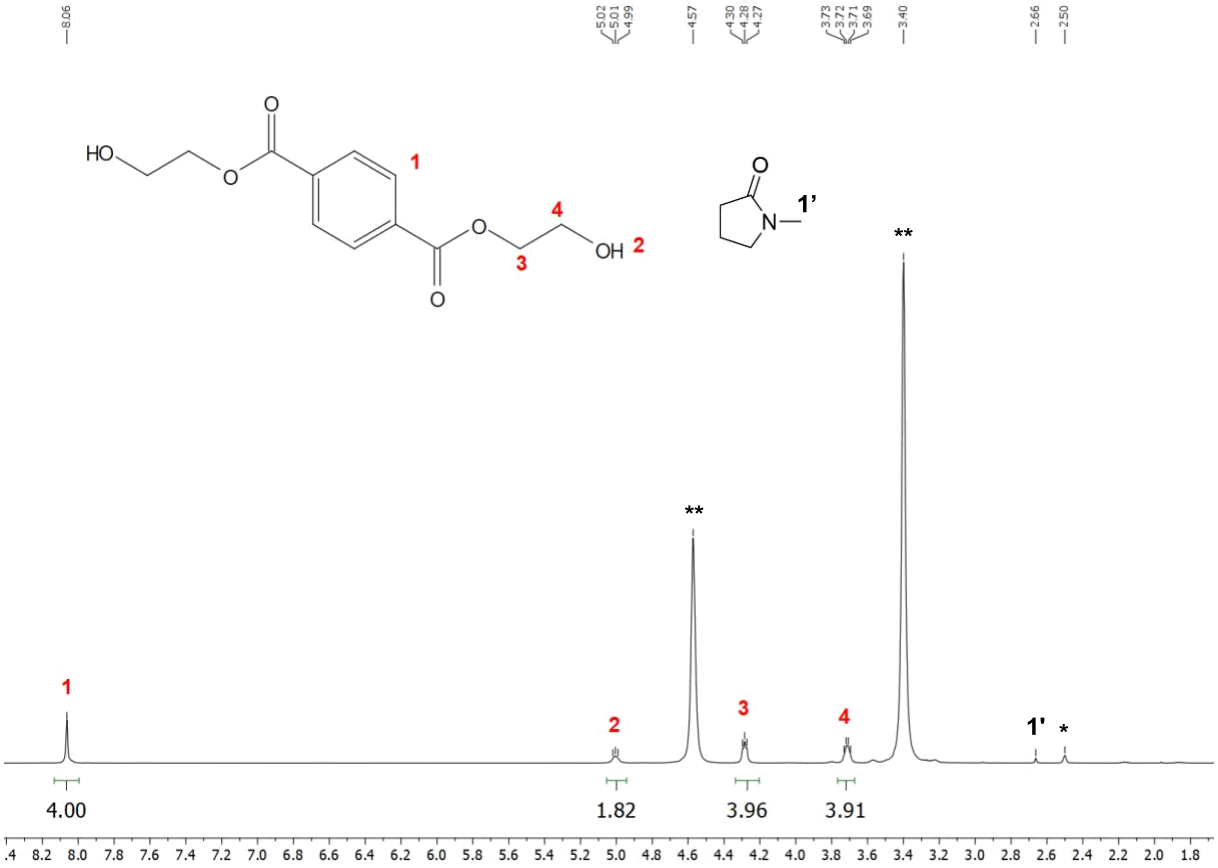


Figure 3.1**.** Exemplar ^{1}H NMR (400 MHz, DMSO-d_6, 298 K) spectrum of glycolysis reaction mixture aliquot. * = DMSO; ** = EG

levels of chemical waste, because of the requirement to perform an individual experiment for every timepoint in the kinetic profile. Therefore, a method was used which was developed in the

Dove group by Delle Chiaie *et al.* using nuclear magnetic resonance (NMR) spectroscopy, integrating against an internal standard. *N*-methylpyrrolidone (NMP) was used as a stable, unreactive internal standard for the PET depolymerisation reactions at 10 mol% (with respect to PET repeat unit), and used to measure BHET concentration in NMR spectroscopy samples made up from aliquots taken from the reaction mixture (Figure 3.1).

The pre-reaction mixture (all reagents excepting PET) was homogeneous at reaction temperature (180 °C) for all catalysts, while PET was insoluble in the reaction medium and hence, once added, the reaction became heterogeneous. While PET was being depolymerised, samples were taken at regular intervals and quenched and prepared for NMR spectroscopy by dilution with DMSO-d_6. The PET particles were small enough that they were taken up into the samples, and so the ratio of internal standard to PET was not altered. In each NMR spectrum, the NMP methyl (-CH_3) peak was integrated, usually falling in the range δ = 2.70 – 2.65 ppm. The BHET aromatic peak (4 hydrogens) was then integrated, usually in the range of δ = 8.1 – 8.0 ppm, and the conversion was calculated from this.

Previous literature[4, 5] suggested that PET depolymerisation by glycolysis occurs *via* one of two primary degradation behaviours: surface-bulk, or surface-only, each of which possesses an equation of rate. It is, however, unknown whether the degradation proceeds *via* a surface-only or surface-bulk pattern for all catalysts, or whether the catalysts differ between one another. Therefore (in order to compare models for each catalyst), once the conversions were calculated, they were plotted against time, and semi-log plots of conversion vs time were drawn up based on the simple kinetic equation below (Equation 3.1), where *C* is reaction conversion.[6] Using the semi-log plots for each catalyst, initial straight lines could be fited to the points, from which the pseudo-first order rate constant *k*' could be derived for each catalyst combination. This is referred to hereafter as 'Model 1'. Model 1 is a surface-bulk model, so it can be assumed that

any catalysts for which kinetic data fits this model with low error, proceed *via* a surface-bulk degradation pattern.

$$\ln\left(\frac{1}{1-C}\right) = k't \qquad 3.1$$

An alternative model of PET degradation, referred to as 'Model 2', uses surface area calculations to determine rate of degradation, and culminates in Equation 2 below. Model 2 is a surface-only mediated process, so it can be assumed that any catalyst for which kinetic data fits this model proceeds *via* a surface-only degradation pattern.

$$1 - (1 - C)^{2/3} = k''t \qquad 3.2$$

For each catalyst combination *k*' and *k*'' were derived from the semi-log and conversion-time plots, and the pseudo-first order rate constant (and therefore activity) values and trends were therefore able to be evaluated by comparison of *k*' values. Values of *k*'' were able to be similarly compared, although comparison of *k*' with *k*'' is not possible, because they are calculated using differing dimensions of conversion. There is still an open debate regarding the best kinetic model of PET degradation to be used,[7] although the vast majority of studies predict that degradation begins as a surface erosion process. Additionally, some models (such as the shrinking-core model)[8-11] propose that surface erosion continues for the entire process. Others suggest swelling and cracking of the polymer particle are included as secondary processes. However, given the variety of activity of catalysts screened, these simpler models seemed most appropriate to acquire a single number which could be used to compare catalysts. Both of these models line up with existing models, assuming the PET equilibrium conversion is approximated to 1 (which, given the excess of reagent and relatively high temperature, is a reasonable assumption).

The state of the art reviews a range of metal salts; metal acetates typically displayed the highest PET glycolysis activity in metal salt catalysts,[12, 13] so metal acetate salts were selected for study.

On top of this they are cheap, commercially available salts. The PET depolymerisation was thus explored using a range of readily available metal acetate catalysts, and a wide range of properties were considered as possible 'proxy variables' for metal acetate Lewis acidity (Table 3.1). Pauling electronegativity is a quantitative relative measure of the degree to which an atom or functional group attracts electrons by use of the dissociation and valence bond energies (here measured relative to Hydrogen). The Gagné-Hawthorne parameter is a fitted constant for the exponential bond-length-valence curve with a fixed value of average bond length derived from a large empirical data set of species bonded to oxygen. Shannon-Prewitt effective ionic radius is a measurement of the effective radius of, in this case, a 6-valent metal ion. Pearson hardness is a derived quantity of charge density per unit volume of an ion, using half the difference between ionisation potential and electron affinity. Although these properties can all be used to approximate Lewis acidity, there is no universal measure of electrophilicity.

Table 3.1. Metal acetates chosen and their physicochemical properties, where χ = electronegativity.

Metal ion	Pauling χ	Gagné-Hawthorne Parameter / Å	Shannon-Prewitt Ionic Radius (6-valent) / Å	Pearson Hardness / eV
zinc (II)	1.65	0.405	0.740	4.94
magnesium (II)	1.31	0.337	0.720	3.90
manganese (III)	1.55	0.513	0.645	3.72
lanthanum (III)	1.10	0.343	1.032	2.60

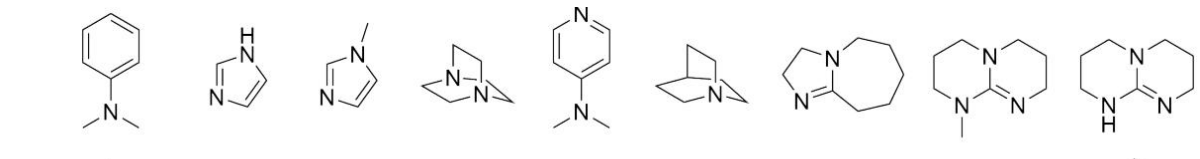
3.2.2. $Zn(OAc)_2$ / Base-Catalysed Glycolysis

It was hypothesised that dual catalytic glycolysis of PET proceeds *via* a mechanism in which the Lewis acid and base act as separate entities, but in tandem. Within this, it was postulated that

the Lewis acid activates the carbonyl group (electrophilic centre) of the substrate (PET) by reducing its electron density and lowering the energy of the Lowest Unoccupied Molecular Orbital (LUMO). The base activates the nucleophile (EG) by deprotonation, increasing the electron density on the oxygen (nucleophilic centre) and raising the energy of the Highest Occupied Molecular Orbital (HOMO). This would mean that the energy overlap between HOMO and LUMO increases, decreasing activation energy and increasing rate. It would therefore follow that the activity of a dual catalyst can be described as some function of Lewis acidity and basicity. This hypothesis will herein be tested by measurement of the activity of a range of Lewis acids and bases, and the dual catalysts formed by 1:1 combination of these, and use of linear regression with the aim to develop a model of activity prediction for PET glycolysis dual catalysts.

Given the status of $Zn(OAc)_2$ as a highly efficient metal salt catalyst for PET glycolysis, it was decided to use it as a basis for the initial dual catalyst screening, in combination with a range of bases with pK_{aH} from 5.1 to 15.2. The bases chosen are reported in Scheme 3.2 and were, in order of basicity (starting lowest): *N,N*-dimethylaniline (DMA); Imidazole (Im); *N*-methylimidazole (NMI); 1,4-diazabicyclo[2.2.2]octane (DABCO); *N,N*-dimethylaminopyridine (DMAP); quinuclidine or azabicyclo[2.2.2]octane (ABCO); 1,8-diazabicyclo[5.4.0]undec-7-ene (DBU); 1,5,7-triazabicyclo[4.4.0]dec-5-ene (TBD). 7-Methyl-1,5,7-triazabicyclo[4.4.0]dec-5-ene (MTBD) was also chosen as a base to test any model developed. These bases cover a wide range of the pK_{aH} scale and present relatively sterically available nitrogens. The catalyst combinations

Scheme 3.2. Range of bases used in the study, and their pK_{aH} in water.



base:	DMA	Im	NMI	DABCO	DMAP	ABCO	DBU	MTBD	TBD
pK_{aH}:	5.1	7.0	7.4	8.8	9.6	11.0	13.5	15.0	15.2

were screened at 1 mol% using the methodology described in Section 3.7.1, and the initial values of *k*' and *k*'' were derived from the conversion-time plots, an example of which for $Zn(OAc)_2$ / DMA is shown in Figure 3.2.

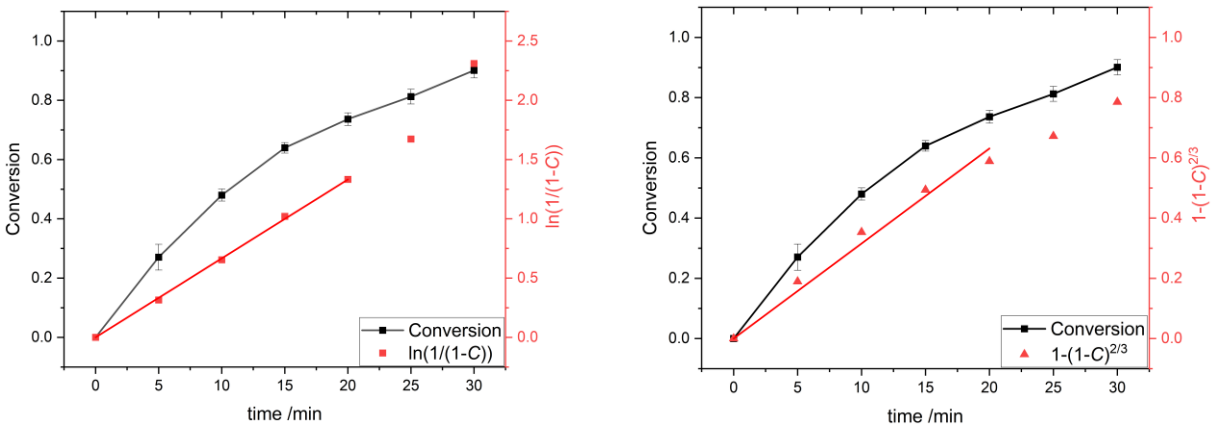


Figure 3.2. Conversion-time (black) and initial rate constant (red) plots of $Zn(OAc)_2$ / DMA-catalysed PET glycolysis as described by Model 1 (left) and Model 2 (right).

The values of *k*' and *k*'' were calculated in this way for each combination of $Zn(OAc)_2$ and base, so that the values of R^2 were maximised for each gradient calculation (see Table 3.2 for specific values). These values of *k*' and *k*'' (Table 3.2; Figure 3.3) were then compared to gain a greater understanding of the relationship between properties such as basicity and activity in $Zn(OAc)_2$-based dual catalysts.

Table 3.1. Range of bases used in the study, and their *k*' and *k*'' values.

Base	**pK_{aH} (in water)**	***k*' / min^{-1} (Model 1)**	**Adjusted R^2 (Model 1)**	***k*'' / min^{-1} (Model 2)**	**Adjusted R^2 (Model 2)**
DMA	5.0	0.067±0.007	1.000	0.0316±0.0012	0.992
Im	7.0	0.126±0.003	0.998	0.0416±0.0014	0.994
NMI	7.4	0.120±0.013	0.952	0.0308±0.0010	0.992
DABCO	8.8	0.050±0.005	0.957	0.0199±0.0013	0.970
DMAP	9.6	0.074±0.004	0.989	0.0249±0.0007	0.995

ABCO	11.0	0.062±0.003	0.995	0.0238±0.0006	0.995
DBU	13.5	0.107±0.003	0.996	0.0415±0.0019	0.989
MTBD	15.0	0.100±0.004	0.992	0.0396±0.0011	0.996
TBD	15.2	0.097±0.006	0.958	0.0258±0.0007	0.995

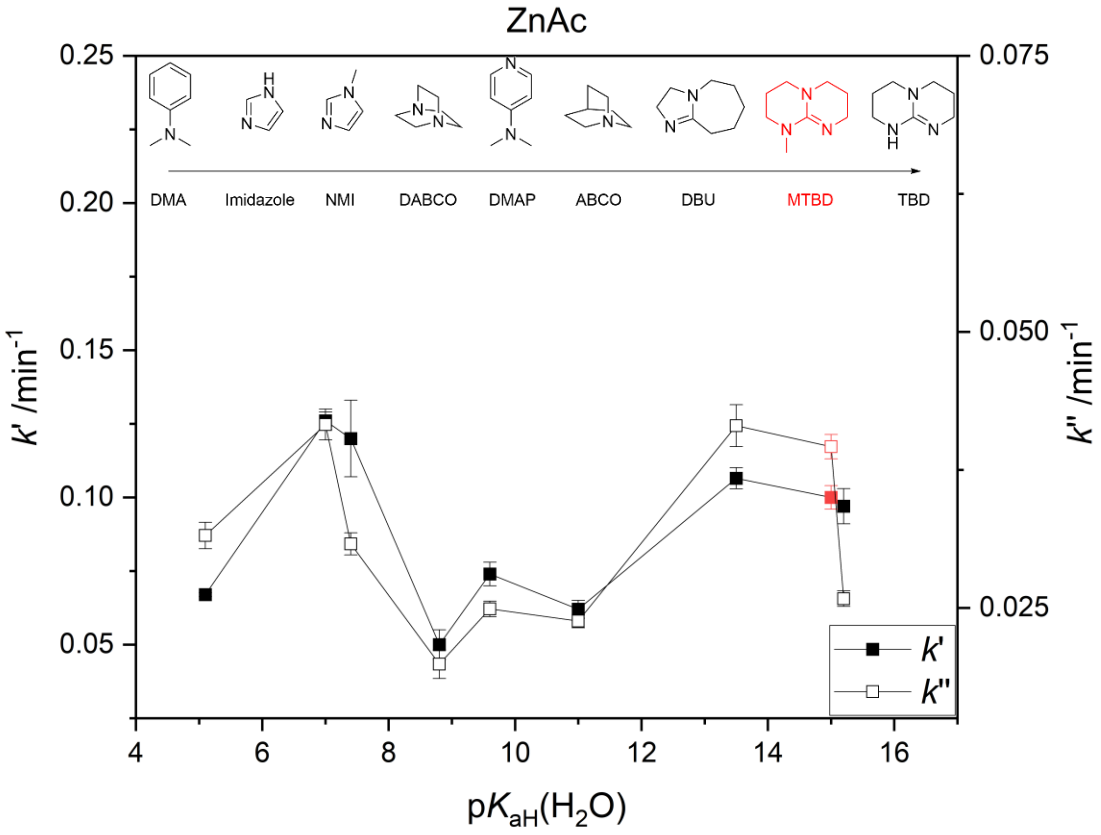


Figure 3.3. Values of *k*' and *k*'' for each $Zn(OAc)_2$ / base combination catalysed PET glycolysis.

It was revealed that the combination $Zn(OAc)_2$ / Im was the most active of the $Zn(OAc)_2$ / base combinations using Model 1 and Model 2, an unusual result given that imidazole is a weak base. As they are derived from the same data, the correlations between *k*' or *k*'' and pK_{aH} are relatively similar in shape. MTBD was added to the study later as a test of certain predictive capabilities, so has been highlighted in red. These complex correlations (or lack thereof) suggest the property-activity relationships are more than the simple separated function of acid and base that was hypothesised. An investigation was therefore begun into the mechanistic

details of the PET glycolysis reaction as catalysed by these metal acetate / base dual catalysts, which included theoretical chemical calculations. These are further detailed in Chapter 4.

In order to find a more accurate method of activity prediction, an investigation into the specifics of the relationships between activity and various parameters was begun using the Python-based M^2E^3D software tool, developed by A. L. Nicusan using the PySR library.[17-20] This tool allows a user to analyse an *N*-dimensional problem and generate equations of varying complexity and fit to a pre-existing data set. Hence it was used to generate relationship equations between $Zn(OAc)_2$ / base activities and a variety of variables, including calculated cone angle, Zn-N bond length, Lewis acidity proxy variables, and basicity of the base. The results of this experiment produce equations, each with a 'score'. This score is a function of both the simplicity of the equation and its ability to fit the data provided. The best scoring functions were extracted and plotted (Figures 3.4a and 3.4b). For $Zn(OAc)_2$ / base data, both models 1 and 2 were tested with an array of data (Table 3.2). The calculated cone angle (the maximum steric angle the ligand takes up) and calculated Zn-N bond length are derived from the Section 4.2.1 of Chapter 4, the optimisation of $Zn(OAc)_2$ / base bound states.

Table 3.2. Parameters used in M^2E^3D analysis of $Zn(OAc)_2$ / base property-activity relationships.

Catalyst	**Base pK_{aH}**	**Zn-N Bond Length / Å**	**Base Cone Angle / °**
$Zn(OAc)_2$ / DMA	5.0	2.155	103.5
$Zn(OAc)_2$ / Im	7.0	1.996	81.7
$Zn(OAc)_2$ / NMI	7.4	1.983	81.9
$Zn(OAc)_2$ / DABCO	8.8	2.072	87.1
$Zn(OAc)_2$ / DMAP	9.6	1.995	88.7
$Zn(OAc)_2$ / ABCO	11.0	2.040	88.3
$Zn(OAc)_2$ / DBU	13.5	1.960	102.3
$Zn(OAc)_2$ / TBD	15.2	1.979	110.3

The standout best-scoring equations (score = 0.603) were fits of Model 1 data (*k*') to Equation 3.4a and 3.4b, where *L* is Zn-N bond length:

$$k' \approx \frac{2.70 \times 1.61^{\frac{1.67}{\sqrt{\exp(pK_{aH})}}}}{L} - 1.27 \qquad 3.4a$$

$$k' \approx \frac{\left(\frac{2.06}{L} pK_{aH}\right) - 0.446}{pK_{aH}} \qquad 3.4b$$

It can be seen from Equations 3.4a and 3.4b and Figure 3.4 that for a $Zn(OAc)_2$ / base system,

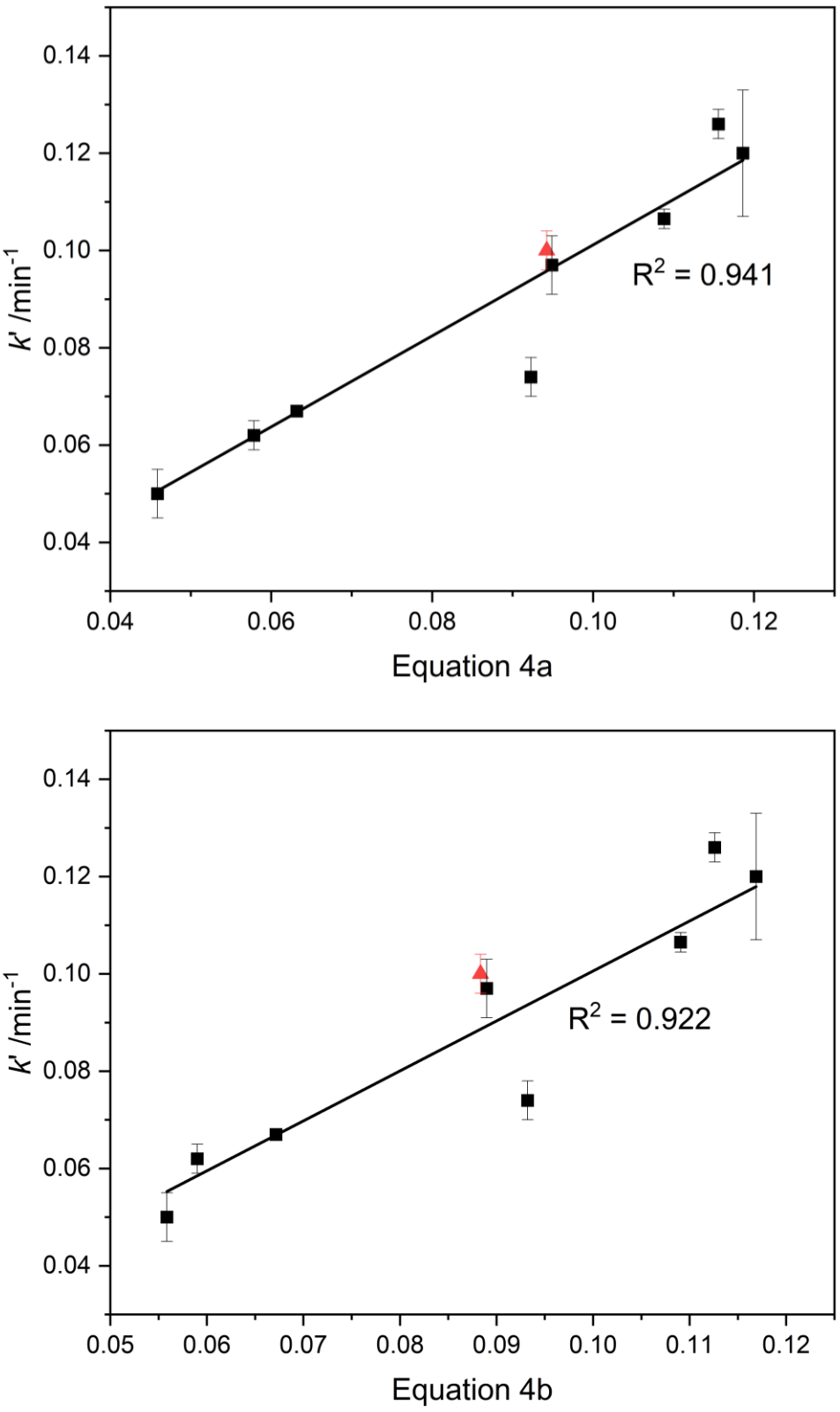


Figure 3.4. Plot of predictive equation for *k*' for $Zn(OAc)_2$ / base. $Zn(OAc)_2$ / MTBD given in red.

the activity can be predicted with relatively high accuracy given the calculated Zn-N bond length and the pK_{aH} of the base. Equation 3.4a is marginally better correlated than Equation 3.4b, although 4b is a simpler equation and produces similarly shaped results. Both relationships are inverse with respect to Zn-N bond length, suggesting a shorter bond length produces a higher rate. It is hypothesised that the shorter bond length leading to higher rate is a result of back-bonding between the base and the Zn *d* orbitals. This reduces the electron density on the Zn ion, tightening the binding with the acetate ligands and therefore tightening the transition state. This in turn directs the nucleophile more closely into the electrophilic centre. Additionally, pK_{aH} of the base has a complex relationship with activity, having an inverse exponential relationship in

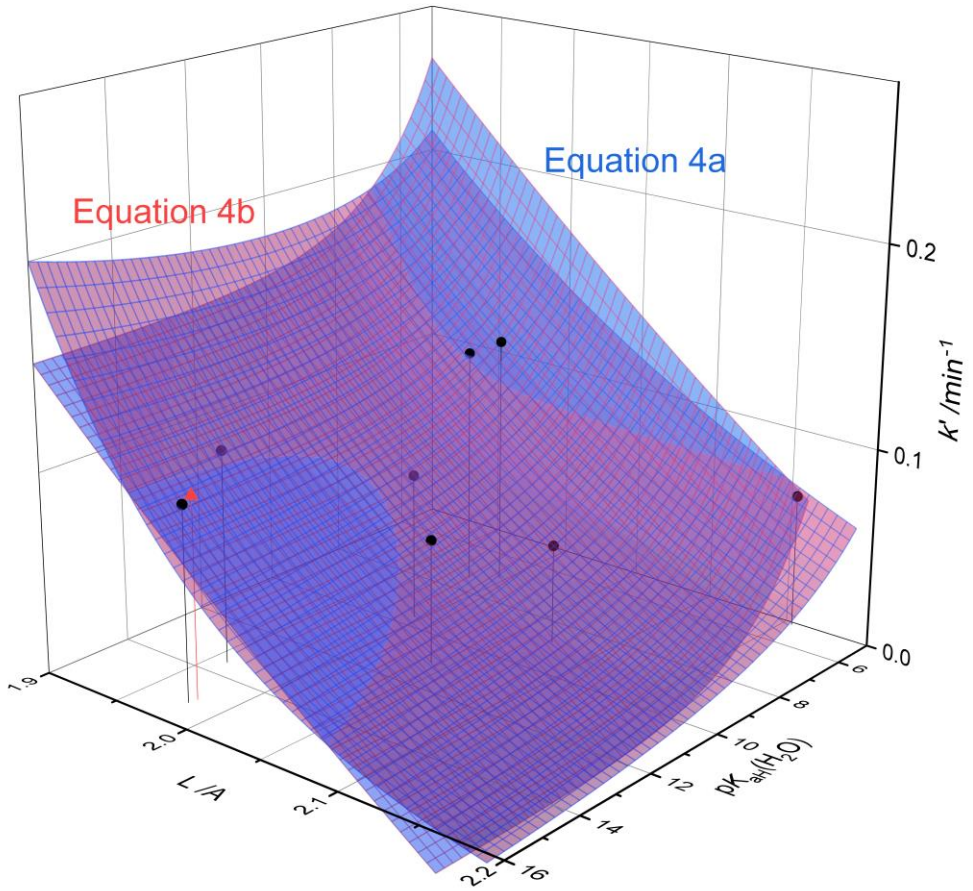


Figure 3.5. Contour plots of Equations 3.4a and 3.4b, and the positions of the data points on the curves. $Zn(OAc)_2$ / MTBD marked as a red triangle.

Equation 3.4a but a power-reciprocal relationship in Equation 3.4b. Both relationships, however, provide similar downward curves (Figure 3.5).

It can be seen from the mesh plots that smaller Zn-N bonds translate to higher activity in both cases, and that basicity is a low-priority parameter in Equation 3.4b, but low-basicity bases have higher activity using Equation 3.4a. Therefore using Equation 3.4a (the more well-fitted equation) it can be predicted that low-basicity bases with short bonds to the Zn ion will be most active; these are likely to be those with additional bonding parameters such as back-bonding, as weaker bases generally have longer bonds to Zn.

$Zn(OAc)_2$ / MTBD was chosen as a new combination to test the predictive equations (Table 3.4). The error in Equation 3.4a was 0.0058 min^{-1}, *cf.* 0.0058 min^{-1} average for the other 8 dual catalysts, which reinforces the predictive ability of this equation. The error in Equation 3.4b was slightly higher, at 0.012 min^{-1}. Regardless, these equations appear to have the ability to predict new combinations of dual catalyst components with relatively high accuracy.

Table 3.3. Parameters used in M^2E^3D analysis of $Zn(OAc)_2$ / MTD property-activity relationship.

Catalyst	Base pK_{aH}	Zn-N Bond Length / Å	Base Cone Angle / °
$Zn(OAc)_2$ / MTBD	15.0	1.980	128.5

3.2.3. Metal Acetate Standalone Catalysis

Metal acetates other than $Zn(OAc)_2$ are known to have activity with respect to PET glycolysis, so it was hypothesised that metal activity would correlate with some measure of Lewis acidity. A few metal acetates were therefore chosen to be studied in greater detail. These metal acetates, magnesium acetate ($Mg(OAc)_2$), manganese acetate ($Mn(OAc)_2$) and lanthanum acetate ($La(OAc)_3$), were first screened at 1 mol% catalyst loading, both to determine if there is a significant link between physicochemical properties of a metal and its PET glycolysis activity, as

well as to provide control experiments for the dual catalyst screenings. The results found were that (in terms of activity) $Mn(OAc)_2$ > $Mg(OAc)_2$ > $Zn(OAc)_2$ ≈ $La(OAc)_3$. These results bear notable differences from the literature's usual choice of $Zn(OAc)_2$ as the staple; however, it does agree with the reported works of others which place $Mn(OAc)_2$ as more efficient than $Zn(OAc)_2$. Furthermore, there were no significant simple correlations between *k*' or *k*'' of a metal acetate and the proxy variables to Lewis acidity chosen (Figures 3.6 & 3.7).

Table 3.4. Metal acetate-only catalysed glycolysis first order rate constants *k*' and *k*''.

Metal Acetate	**Model 1 *k*' / min^{-1}**	**Model 1 Adjusted R^2**	**Model 2 *k*'' / min^{-1}**	**Model 2 Adjusted R^2**
$Zn(OAc)_2$	0.058±0.006	0.965	0.0202±0.0013	0.975
$Mg(OAc)_2$	0.109±0.004	0.995	0.0358±0.0010	0.996
$Mn(OAc)_2$	0.130±0.012	0.958	0.0443±0.0010	0.997
$La(OAc)_3$	0.042±0.004	0.982	0.0241±0.0006	0.996

The physicochemical properties were used as proxy variables for the Lewis acidity of the metal acetate, as Lewis acidity is a relative variable and has no absolute scale which encompasses all the metal acetates tested. Measurement of the Lewis acidity of the metal acetates was therefore attempted by the Gutmann-Beckett method, wherein ^{31}P NMR is used to measure the shift of triethylphosphine oxide bound to the metal.[21] This method was attempted for three of the four above metal acetates ($Mn(OAc)_2$ was insufficiently soluble in the NMR solvent to gather data), but the values found did not correlate well with activity (Supplementary Figure S3.17).

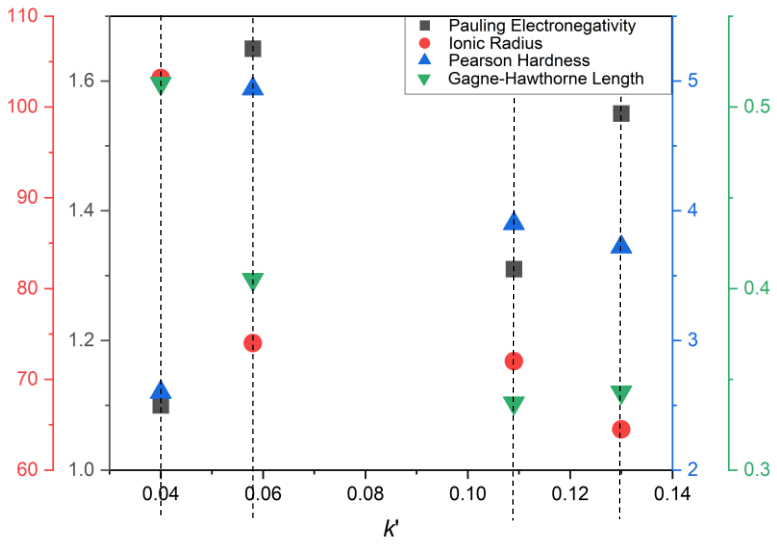


Figure 3.6. a) Scatter plot of shown physicochemical properties with respect to the first-order rate constant *k*' of the metal acetate-catalysed glycolysis reaction (from left to right: La, Zn, Mg, Mn).

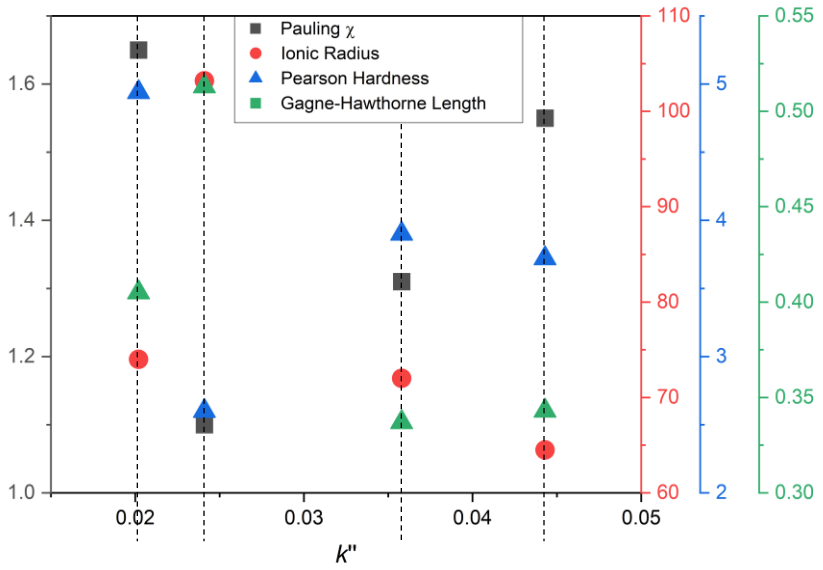


Figure 3.7. b) Scatter plot of shown physicochemical properties with respect to the first-order rate constant *k*'' of the metal acetate-catalysed glycolysis reaction (from left to right: Zn, La, Mg, Mn).

The lack of correlation between activity and any Lewis acidity proxy variable was unexpected, so further study was needed to develop a predictive model of metal acetate PET glycolysis catalysis activity. To this end, a linear regression analysis of the proxy variables with activity was performed. As the results yielded were not as successful as anticipated, with a maximum achieved R^2 value of 0.685, the M^2E^3D tool was once again used to derive a relationship between metal acetate-only catalysed Model 1 activity (*k*') and some combination of proxy variables. One high-scoring equation was derived, Equation 3.5 (score = 1.38):

$$k' \approx \exp\left(-0.0303 \times \left(r + \left(\chi^{(1/2\chi^{\eta})}\right)\right)\right) \qquad 3.5$$

where r = ionic radius, χ = Pauling electronegativity and η = Pearson hardness (Figure 3.8). The function is an exponential decay curve in all dimensions decreasing with increasing ionic radius and electronegativity, with an asymptote at $k' = 0$.

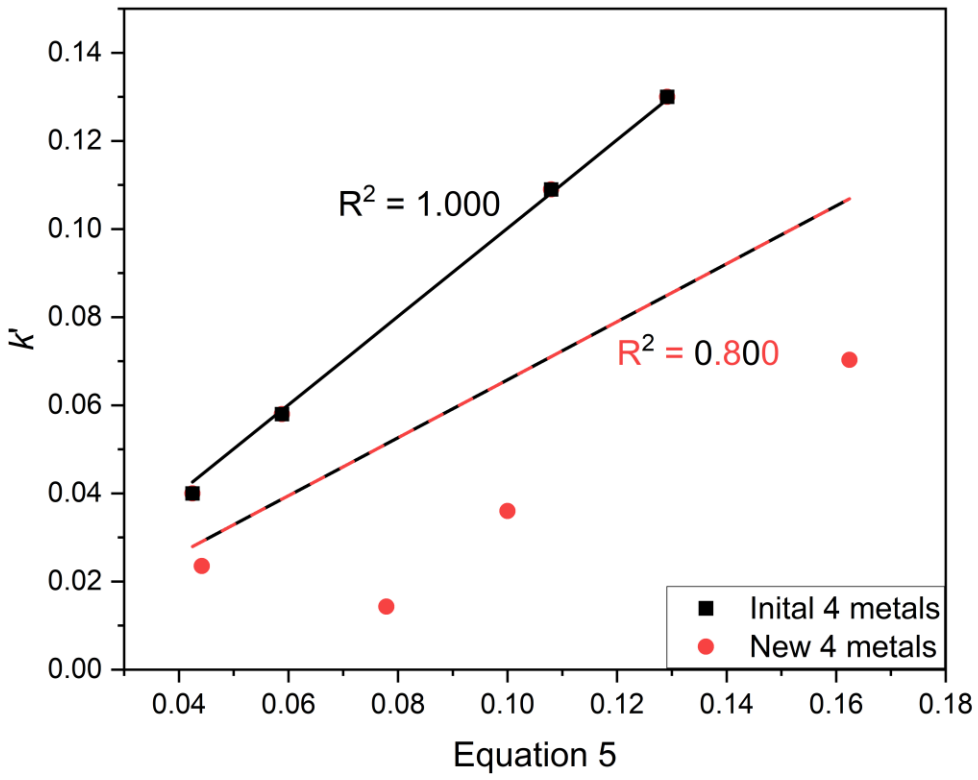


Figure 3.8. Comparison of Equations 5 for the 4-metal ($Zn(OAc)_2$, $Mn(OAc)_2$, $Mg(OAc)_2$, $La(OAc)_2$) initial data and the 8-metal (+ $Sc(OAc)_3$, $In(OAc)_3$, NaOAc, LiOAc) total data sets.

This model was tested using other readily available metal acetates with a wide range of electronegativities: scandium acetate ($Sc(OAc)_3$), indium acetate ($In(OAc)_3$), sodium acetate (NaOAc), and lithium acetate (LiOAc). These new 4 metal acetates fell off the curve by a significant margin. The M^2E^3D program was therefore run again, this time including all 8 metals tested so far, and a new predictive equation was derived, Equation 3.6 (score = 0.659):

$$k' \approx \frac{5.00\left(\sqrt{\eta} - 1.79\right)}{r\chi\left(\sqrt{\eta} - 1.88\right)} \qquad 3.6$$

where r = ionic radius, χ = Pauling electronegativity and η = Pearson hardness.

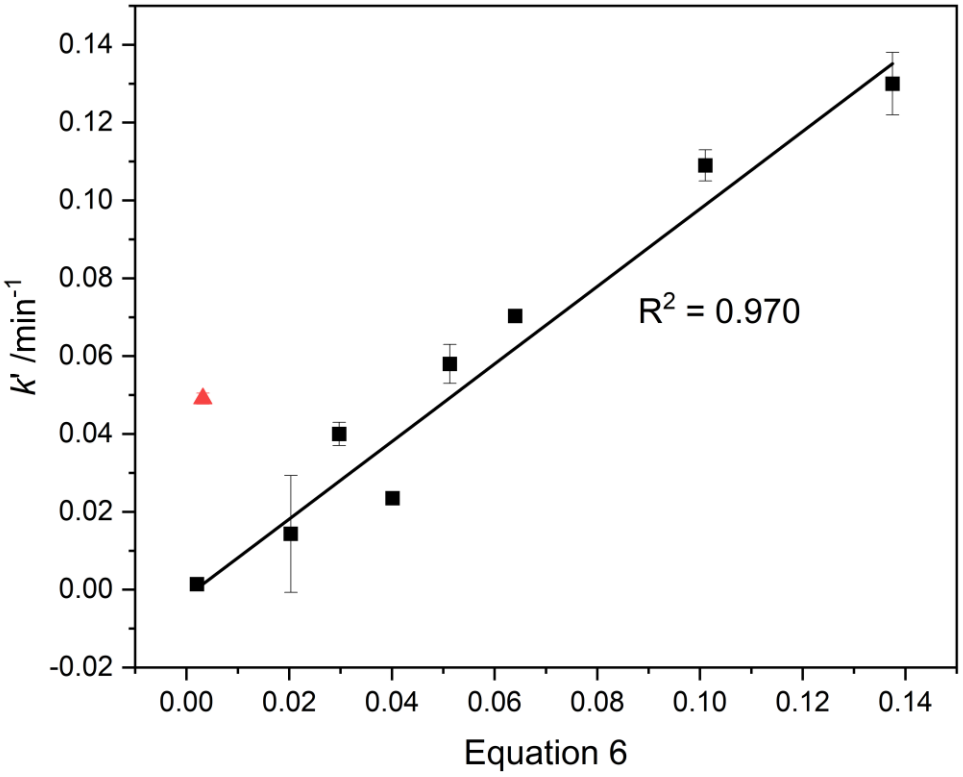


Figure 3.9. Improved predictive equation for metal acetate catalysed PET glycolysis activity. YAc given as the red triangle.

This produces a much better prediction curve (Figure 3.9), although it is more complex an equation and thus the physical representation is more difficult to untangle. The equation represents an inversely proportional relationship with both electronegativity and ionic radius, implying that a smaller, less electronegative metal ions have higher activity; this is unexpected, as electronegativity is used as a proxy for Lewis acidity, and it was expected that higher Lewis acidity would correlate with higher activity. However, it is modified by the function (√(*η*)-1.79)/(√(*η*)-1.88), a diagonal parabolic function with an asymptote at *ca.* 3.20. This is unusual as

well, as the activity would, with increasing η (hardness), first decrease rapidly, then jump to a very high value. Hardness is still an important factor, as reduced electronegativity and smaller ionic radius both correlate with increased activity, which indicates metal acetate salts with borderline hard-soft metal ions are the most effective catalysts.

In order to test this new equation, a ninth metal acetate was chosen to screen, yttrium acetate (YAc) (Figure 3.7, given in red). The error (difference between Equation 3.6 prediction and *k*') for YAc is 0.037 min^{-1}, compared with an average error for the existing 8 metals of 0.010 min^{-1}. This suggests more screening is necessary to confirm this model, and that the model may be over-fitted. It also highlights the power of this tool to extract complex physicochemical property-activity relationships.

3.2.4. Base Standalone Catalysis

A range of bases were screened, for which basicity can be ascribed to the presence of a lone pair on the nitrogen atom. Additionally, these bases were chosen so that their basicity (measured as pK_{aH}) fit a wide range without large gaps (as illustrated in Scheme 3.2).[1] Their activities as single catalyst systems towards PET glycolysis were therefore explored.

Table 3.5. Base-only catalysed glycolysis first order rate constants *k*' and *k*''.

Base	***k*' / min^{-1} (Model 1)**	**Adjusted R^2 (Model 1)**	***k*' / min^{-1} (Model 2)**	**Adjusted R^2 (Model 2)**
DMA	0.0019±0.00013	0.978	0.00127±0.00008	0.992
Im	0.00063±0.00004	0.964	0.00041±0.00002	0.978
NMI	0.00036±0.00002	0.913	0.00024±0.00002	0.971
DABCO	0.00175±0.00010	0.955	0.00113±0.00012	0.922
DMAP	0.00214±0.00007	0.996	0.00143±0.00017	0.909

ABCO	0.00361±0.00006	0.990	0.00237±0.00005	0.997
DBU	0.0319±0.007	0.890	0.0116±0.0016	0.878
MTBD	0.0450±0.005	0.955	0.0215±0.0018	0.956
TBD	0.0386±0.004	0.925	0.0183±0.002	0.906

These bases were screened both to determine relationships with activity as well as to provide controls for the activity of the dual catalysts. They were screened as standalone PET glycolysis

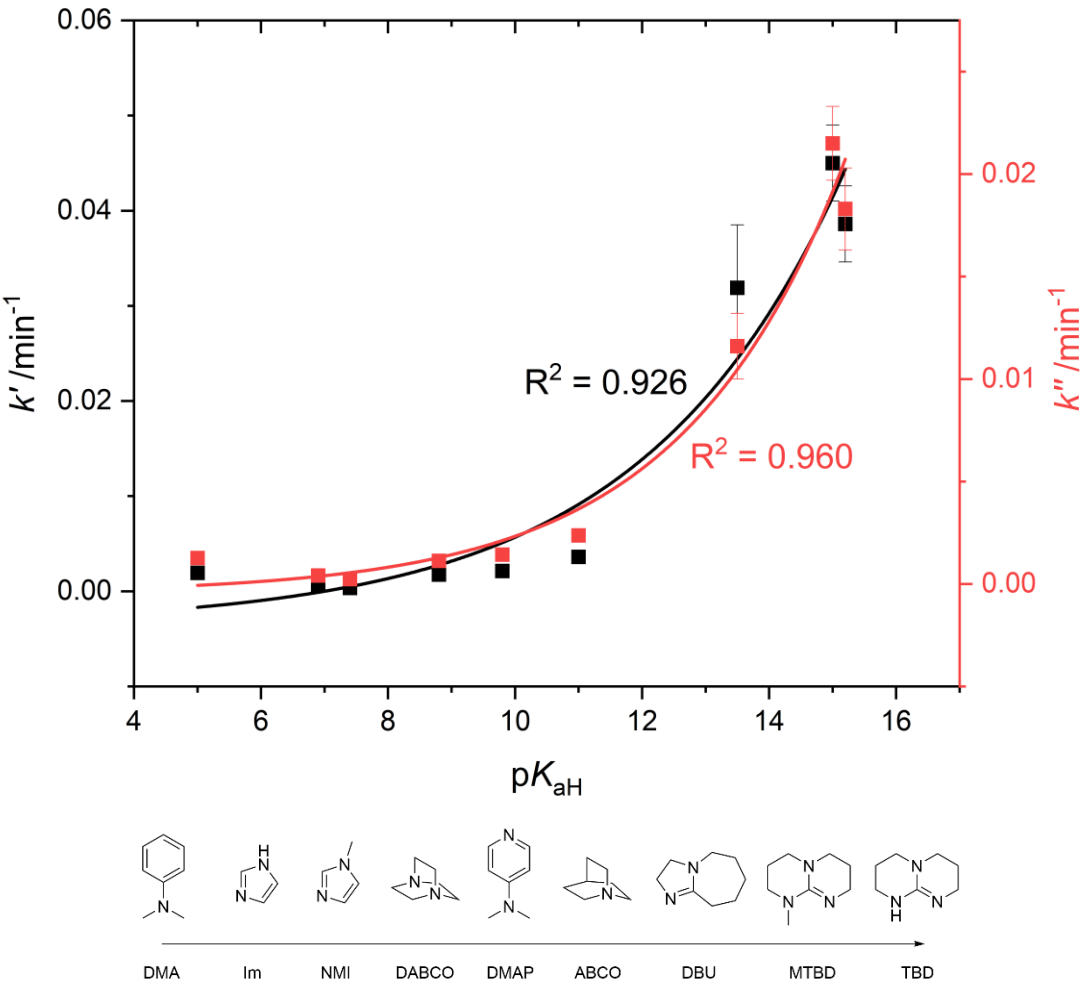


Figure 3.10. Pseudo-first-order rate constants (*k*' and *k*'') of standalone base-catalysed PET glycolysis *versus* pK_{aH}.

catalysts at 1 mol% loading (with respect to PET repeat unit). It was hypothesised that the stronger a base, the higher its activity. It was unknown, however, what precise form this relationship would take.

The activity of base-only catalysed PET glycolysis correlated strongly with basicity, in an exponential function in the case of both *k*' and *k*'' (Figure 3.10), although *k*'' is more well-correlated with this function. This is a chemically sensible relationship as pK_{aH} is a logarithmic scale, so an increase in pK_{aH} of 1 represents a tenfold increase in basicity. This means strong bases rapidly increase in activity because they are orders of magnitude more basic than weak bases. This fits our hypothesis of how basic PET glycolysis functions, as the more basic a base catalyst is, the better it is at deprotonating the nucleophilic species (in this case EG), thus increasing the electron density on the oxygen (the actual nucleophile) when it attacks the electrophilic carbonyl centre of the polymeric chains.

3.2.5. Metal Acetate / Base Dual Catalyst Kinetics

Given the strong correlation of PET glycolysis activity with basicity, it was anticipated there being a similar trend when the bases were combined with the metal acetates (still at 1 mol% with respect to PET repeat unit) in catalysing PET glycolysis. It was hypothesised that the dual catalysts acted in a 'separate but in tandem' approach wherein the Lewis acid acted to activate the substrate, and the base acted to activate the nucleophile, but neither interacts with each other. With this hypothesis in place, it was expected to see direct addition of activity between Lewis acid and base, and so an exponential curve with varying baseline dependent on the metal acetate component of the dual catalyst. However, the relationship appears to be significantly

more complex than an increase in activity with basicity and metal acetate Lewis acidity (Figures 3.11-3.13).

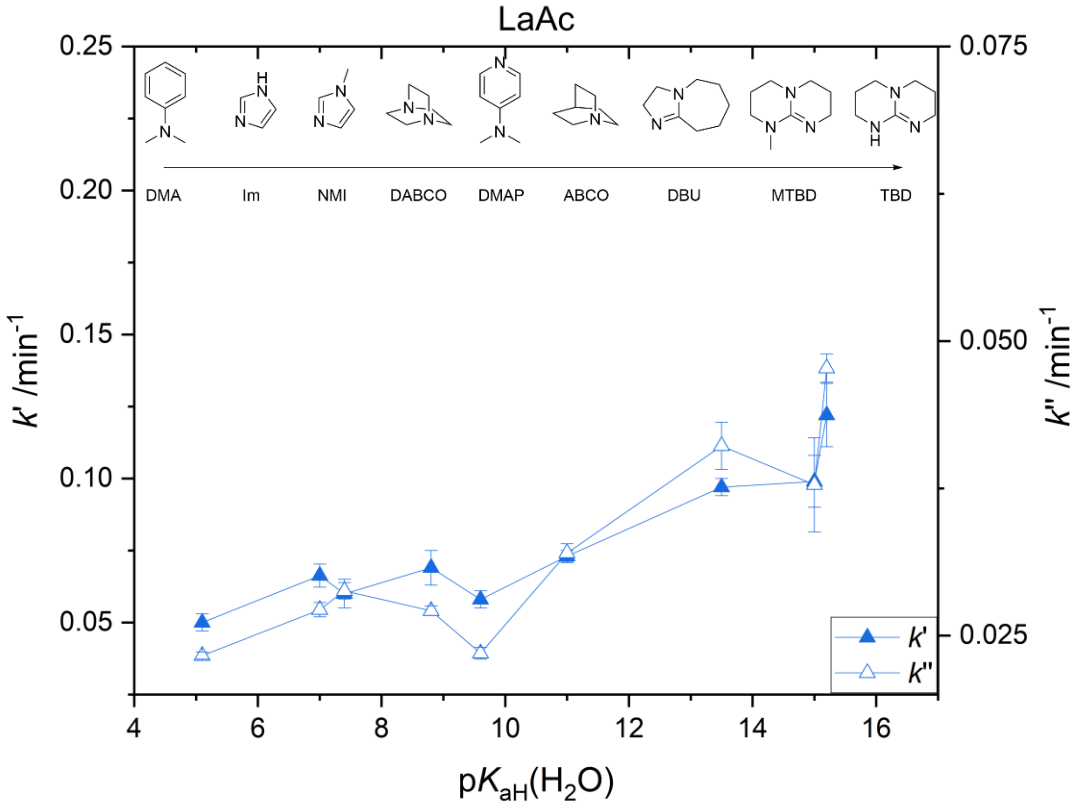


Figure 3.11. Pseudo-first-order rate constants (*k*' and *k*'') of catalyst combinations for $La(OAc)_3$.

Using Model 1, the most active catalyst combination for three of the four metal acetate series uses TBD or MTBD, suggesting basicity has a significant effect on activity; however there is not a clear trend of decreasing activity with decreasing basicity in all dual catalyst systems.

$La(OAc)_3$ / base dual catalysts do have a relatively clear trend of basicity correlating with activity for both Model 1 and 2 (Figure 3.11, Supplementary Figure S3.19), likely because of the relative weakness of $La(OAc)_3$ as a Lewis acid and poor activity as a glycolysis catalyst. Model 2 has more variation in the trend, however, with decreased activity in comparison to the trend when using MTBD and DMAP. This could be because of the relatively high steric demand of these bases in combination with the large ionic radius of lanthanum in $La(OAc)_3$ causing the catalyst to be less strongly bound to the substrate. It follows that the base is likely the more important component in the $La(OAc)_3$-based dual catalysts.

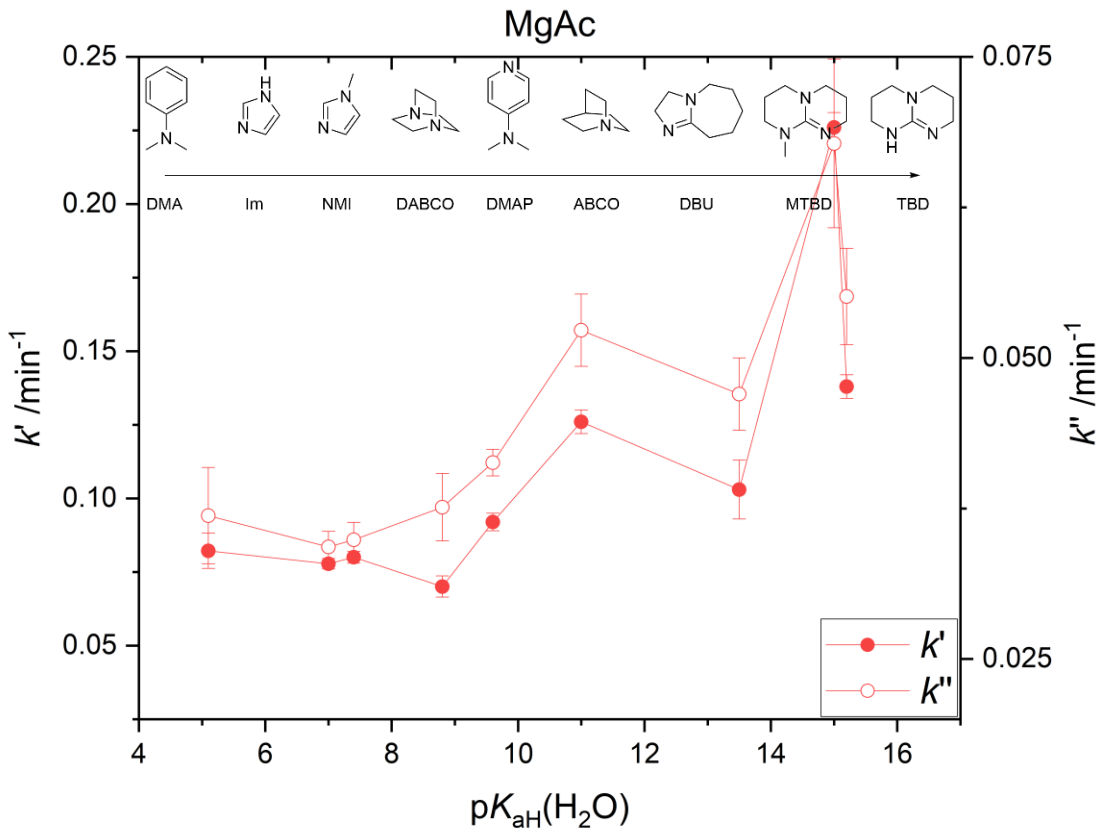


Figure 3.12. Pseudo-first-order rate constants (*k*' and *k*'') of catalyst combinations for $Mg(OAc)_2$.

$Mg(OAc)_2$ / base catalysts are similar to $La(OAc)_3$ / base catalysts in both models in that their activity scales with basicity (Figure 3.12), but with outliers in $Mg(OAc)_2$ / DBU and $Mg(OAc)_2$ / TBD, which have activity much lower than expected (Figure 6b). Using the M^2E^3D software, the

highest-scoring equation for $La(OAc)_3$-based dual catalysts showed *k*' as proportional to pK_{aH} alone (score = 0.700), and for $Mg(OAc)_2$ *k*'' was proportional to √(Cone Angle)+pK_{aH} (Supplementary Figure S3.18) in Equation 3.7 (score = 0.860):

$$k'' \approx 0.00224 \times \left(\sqrt{Cone_{Angle}} + pK_{aH}\right) \quad 3.7$$

The *k*'' values of $Mg(OAc)_2$ / base catalysts having the stronger relationship indicates the process is a surface-only one, as opposed to $Zn(OAc)_2$- and $La(OAc)_3$-based catalysts having strong relationships with *k*' only, indicating they proceed *via* a more surface-bulk pattern of degradation. This could be a product of $Mg(OAc)_2$ being less soluble in the reaction mixture than $Zn(OAc)_2$ and $La(OAc)_3$.

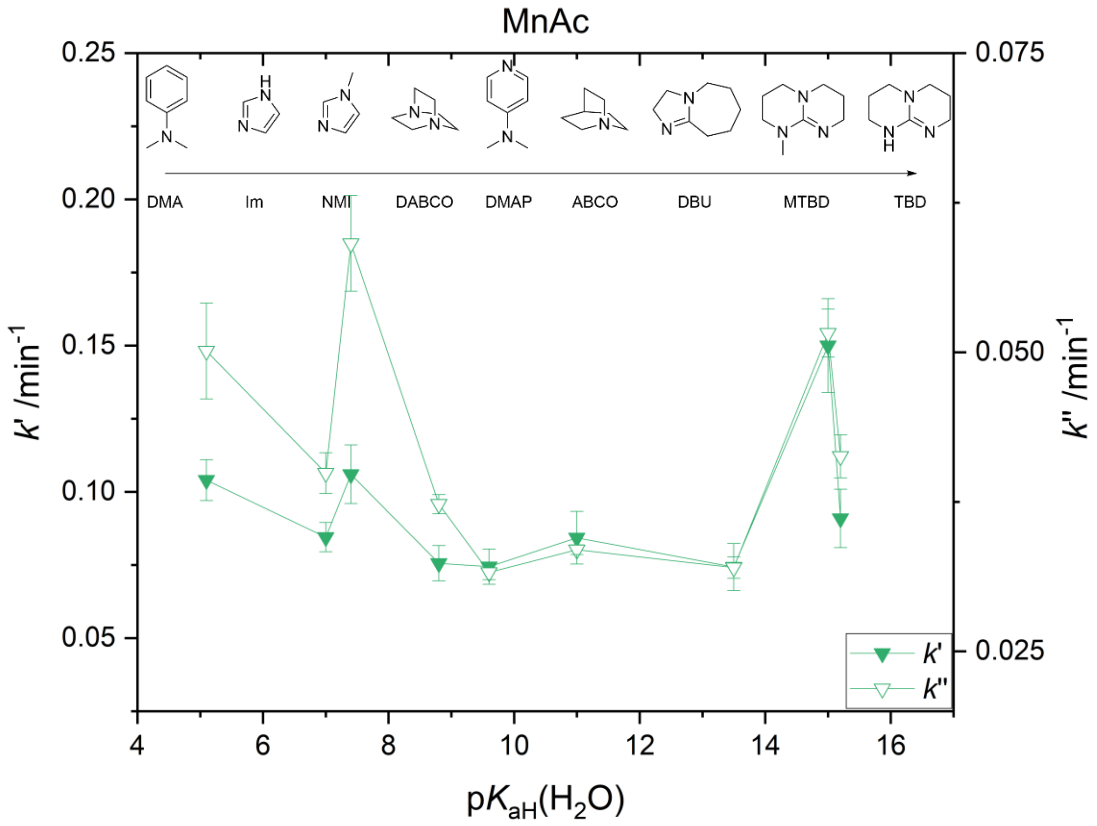


Figure 3.13. Pseudo-first-order rate constants (*k*' and *k*'') of catalyst combinations for $Mn(OAc)_2$.

The trends of $Zn(OAc)_2$ / base- and $Mn(OAc)_2$ / base-catalysed PET glycolysis activity did not at all correlate to basicity of the base, indicating there must be a more complicated relationship between the basicity of the base, Lewis acidity of the metal acetate, and the interaction between the two. This will be discussed later on in Chapter 4. It is possible that both have a relationship with imidazoles which produces highly active catalysts, as both show spikes in activity around Im and NMI (Figure 3.13).

$Zn(OAc)_2$ / base activity was found to have a specific relationship to basicity and Zn-N bond length (derived from DFT calculations in Chapter 4). However, M^2E^3D was unable to find a suitable equation for $Mn(OAc)_2$ / base activity; the maximum achieved R^2 was equal to 0.500.

As an alternative analysis, MTBD and TBD can be discounted for another interesting approach to the results. In this case, the peak activities of both Model 1 and Model 2 occur when using $La(OAc)_3$ / DBU (pK_{aH} = 13.5), $Mg(OAc)_2$ / ABCO (pK_{aH} = 11.0), $Mn(OAc)_2$ / NMI (pK_{aH} = 7.4) and $Zn(OAc)_2$ / Im (pK_{aH} = 7.0); these will be referred to henceforth as the 'weak base' peaks. If these peaks are plotted against the various Lewis acidity proxy variables, it can be seen that this yields some interesting results (Figure 3.14).

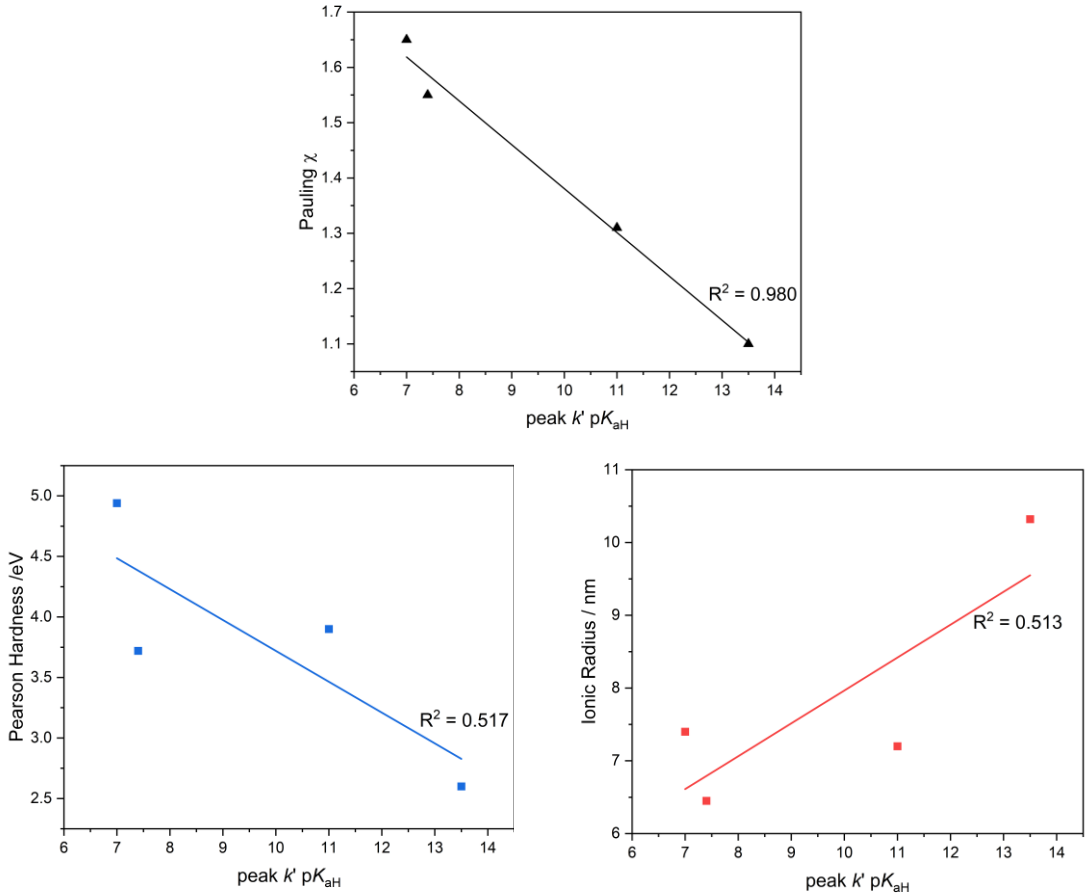


Figure 3.14. 'Weak base' peak combinations measured against proxy Lewis acidity variables.

It is clear from these plots that Pauling electronegativity (χ) has a high correlation with the pK_{aH} of the weak base peak. It is proposed that these peak activities are a result of a 'Goldilocks effect', wherein the activity peaks when the strength of the Lewis acid balances the strength of the base. This allows them to be highly active without being so strongly and closely bound that

they are sterically hedged from binding well to the substrate, or that they bind so strongly to the substrate that the monomer poisons the catalyst.

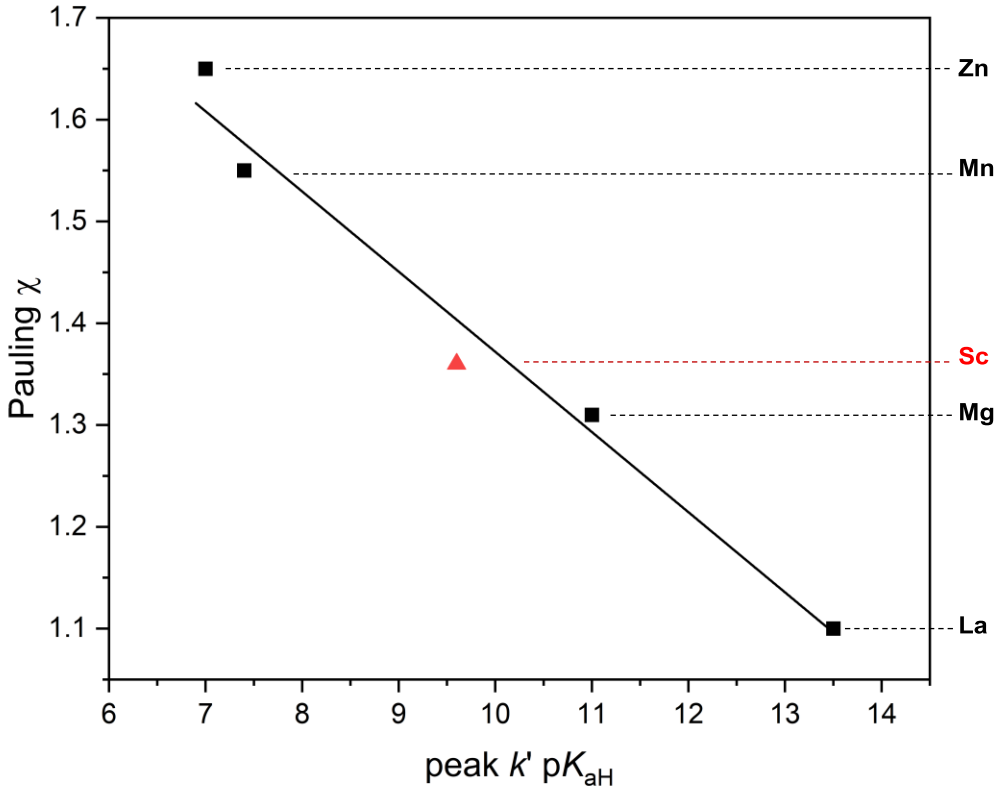


Figure 3.15. 'Weak base' peak basicity plotted against Pauling electronegativity, with the $Sc(OAc)_3$ peak highlighted as a red triangle.

In order to test this theory, scandium acetate ($Sc(OAc)_3$) was employed alongside already screened bases to determine the peak weak base combination. It was found that the most active combination of the screened $Sc(OAc)_3$ / base combinations was $Sc(OAc)_3$ / DMAP (base pK_{aH} = 9.6), which falls close to the linear relationship between peak *k*' pK_{aH} and χ (Figure 3.15), thus lending evidence to this theory of a 'Goldilocks effect' between the weak bases and the metal acetates.

3.2.6. Metal Acetate / TBD and MTBD Combinations

When taken in isolation, the combinations of metal acetates with MTBD and TBD illustrate well the stabilising effect the metal salt has on the base – *i.e.,* the combination is more able to withstand high temperatures for greater lengths of time than the bases alone. This effect also appears when using DBU. TBD, MTBD and DBU alone (at 1 mol% loading) all show a characteristic drop-off in activity after 5 mins of heating at 180 °C (Figure 3.16a). When in combination with $Mg(OAc)_2$ or $Zn(OAc)_2$, however, the high activity is maintained throughout (Figure 3.16b & c).

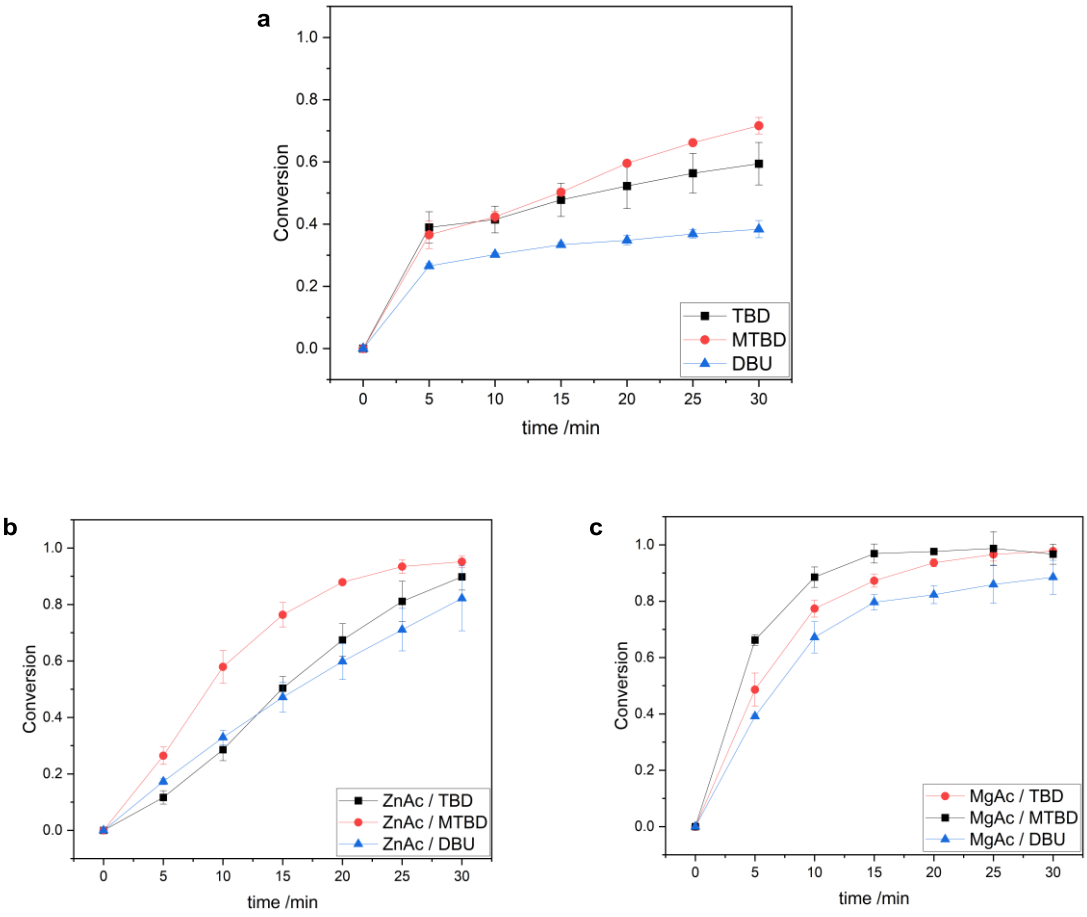


Figure 3.16. Conversion-time graphs for a) 'strong bases' alone, and in combination with b) $Zn(OAc)_2$ or c) $Mg(OAc)_2$.

It is proposed that the increase in activity and lack of rate reduction is a result of the metal acetate and base forming a metal-organic salt, increasing its heat stability (an effect well-illustrated in literature).[5, 6] This effect is also borne out by the binding Density Functional Theory calculations performed in Chapter 4, wherein the $Zn(OAc)_2$ and $Mg(OAc)_2$ / TBD, MTBD or DBU all have positive binding energies, meaning they are more stable as bound species and would require energy input to be unbound.

This increased heat stability allows for more extended high activity with no reduction in rate. In fact, in the cases of combination with $Mg(OAc)_2$ there is actually an increase in rate (also known as a 'synergy' effect). These dual catalyst combinations therefore have an increased potential lifespan and number of effective catalytic cycles.

3.3. Conclusions

Dual catalysts were selected for screening. Activity towards PET glycolysis was measured by two different degradation models, which were found to be variously effective based on the catalyst employed. $Zn(OAc)_2$ was screened in combination with a range of amine bases, and Model 1 pseudo-first-order rate constants (*k*') were found to be predictable with an R^2 value of 0.941, and to predict the value of *k*' for a newly added dual catalyst to within 0.0058 min^{-1}.

Metal acetates were screened as single catalysts for activity towards PET glycolysis, once again using two models of degradation; the first model was again found to have a better prediction model, with an R^2 value of 0.970. The value of *k*' was able to be predicted within 0.037 min^{-1}. When there is a relationship this complex, there is always the concern of overfitting. In this case, a continuation of the metal acetate screening would be useful to verify this model. These are the first such quantitative predictive models of such metal acetate and dual catalysts known to us.

As a follow-on study, the nine selected bases were combined with $Mn(OAc)_2$, $Mg(OAc)_2$ and $La(OAc)_3$ to form a screen of nearly 40 dual catalysts in total. The lanthanum-based dual catalysts followed a linear or exponential trend of decreasing *k*' with decreasing pK_{aH}, both with equal R^2 values of 0.852. $Mg(OAc)_2$-based catalysts showed correlation with a function of Cone Angle and pK_{aH}.

Imidazoles showed a peak in activity when paired with transition metal acetates ($Zn(OAc)_2$ and $Mn(OAc)_2$). Therefore a more tightly-focused screen of imidazoles is likely to be useful future work for this project, providing greater insight into the specifics of both sterics and electronic influences over the dual catalysts from the base.

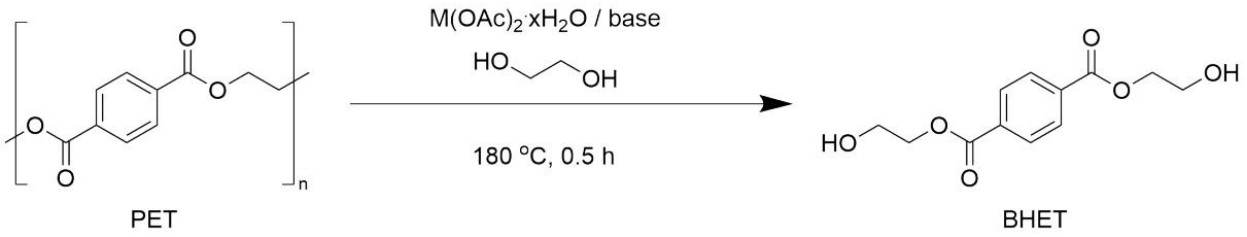
'Synergic' effects were revealed in some combinations, *i.e.* activity that is more than the sum of its parts. $Mg(OAc)_2$ / MTBD especially displayed significant synergy, as well as $Zn(OAc)_2$ / Im and $Mn(OAc)_2$ / NMI.

A separation between 'strong' and 'weak' bases appeared to resolve itself in the results also, wherein the strong bases 'die off' but are stabilised by the metal acetate, and the weak bases show a strong correlation between peak pK_{aH} and Pauling electronegativity. The metal acetates $Zn(OAc)_2$ and $Mg(OAc)_2$ were shown to have a stabilising effect on the strong base catalysts DBU, MTBD and TBD. Future work will include thermogravimetric analysis and catalyst recycling studies of these catalysts.

3.4. Supporting Information

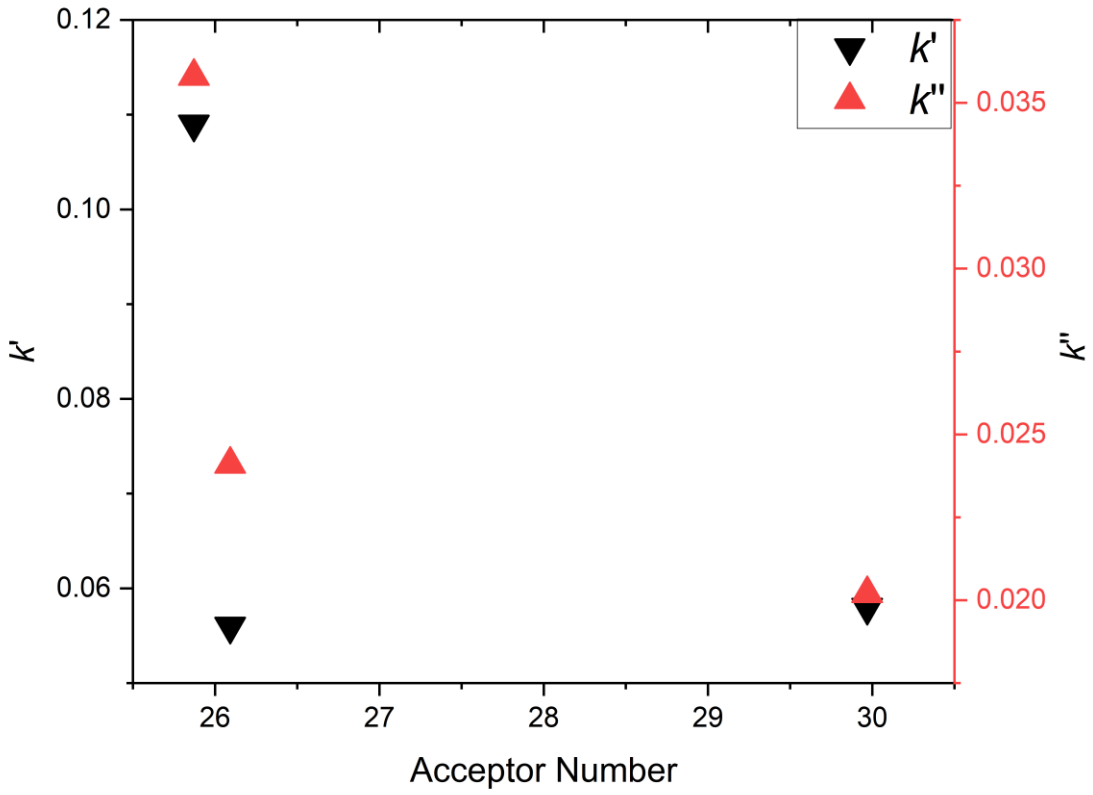
3.4.1. Generic PET Dual-Catalysed Glycolysis Reaction

Scheme S3.3. Generic scheme of PET glycolysis by organometallic dual catalysis.

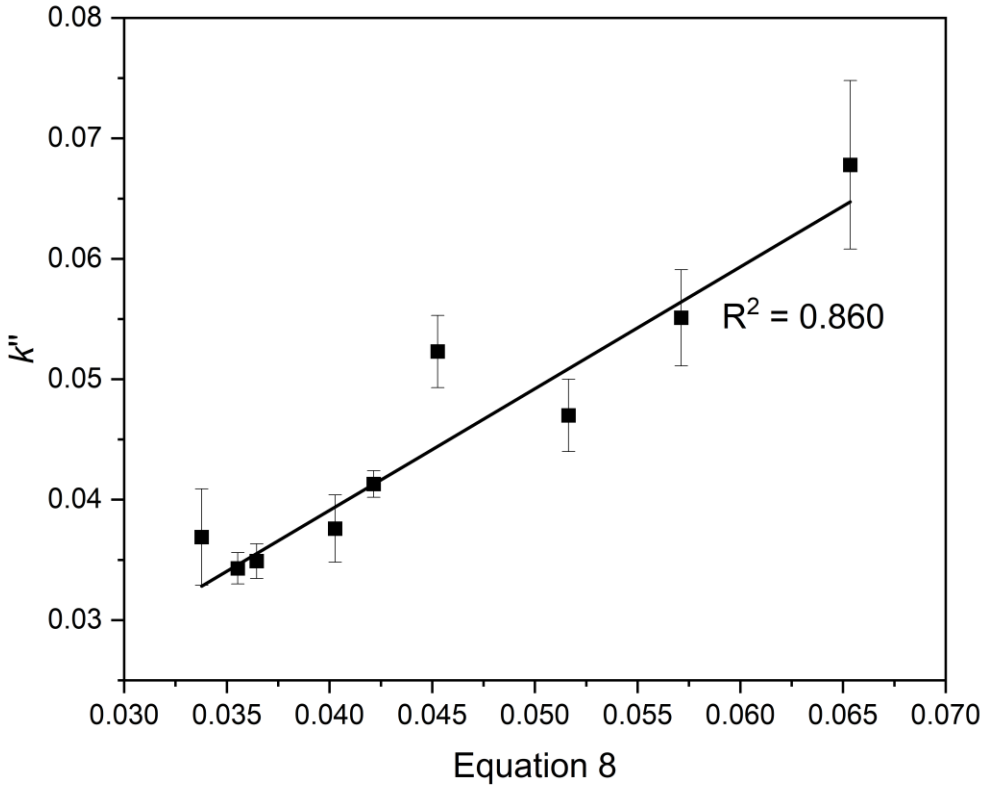


A 20 mL scintillation vial was charged with ethylene glycol (2.8 mL, 3120 mg, 50 mmol, 20 equiv.), metal acetate hydrate ($M(OAc)_{2\text{-}3}{\cdot}xH_2O$) (0.025-0.25 mmol, 0.01-0.10 equiv.), base (0.025-0.25 mmol, 0.01-0.10 equiv.) and N-methyl-pyrrolidone (0.024 mL, 25 mg, 0.25 mmol, 0.10 equiv.) and sealed with a screw cap. The mixture was brought to 180 °C. PET (480 mg, 2.5 mmol, 1 equiv.) was added to the solution and stirred at this temperature for 0.5 h. Aliquots of 0.1 mL were taken at regular timepoints, and prepared for ^{1}H NMR spectroscopic analysis in DMSO-d_6. Once all the PET had been depolymerised, water (15 mL) was added to the solution and cooled to 4 °C for 18 h, and the resulting crystals of bis(2-hydroxyethylene)terephthalate (BHET) (561 mg, 2.4 mmol, 96%) were recovered by vacuum filtration, washing with cold water (5 mL) and drying under reduced pressure.

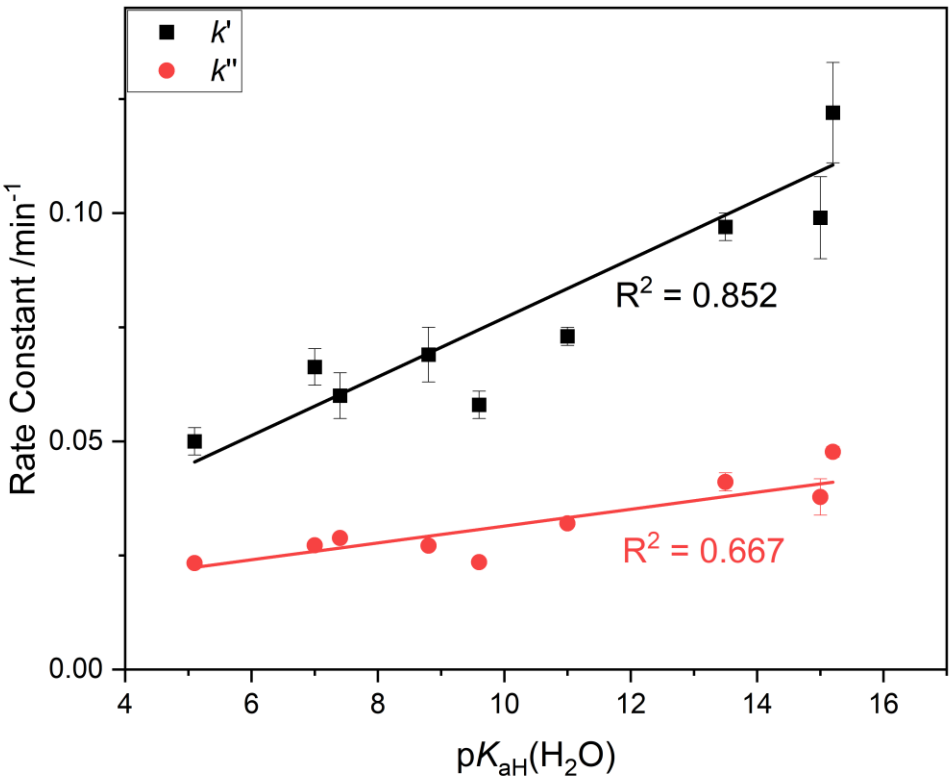
For those mixtures with paramagnetic catalysts ($Mn(OAc)_2$), each sample was filtered over silica to remove the metal acetate catalyst; this was also performed on a non-paramagnetic sample to verify the process did not alter the monomer amounts.



Supplementary Figure S3.17. Gutmann-Beckett Acceptor Number *versus* *k*' and *k*'' values for $La(OAc)_3$, $Zn(OAc)_2$, and $Mg(OAc)_2$.



Supplementary Figure S3.18. $Mg(OAc)_2$ / base activity prediction curve.



Supplementary Figure S3.19. $La(OAc)_3$ / base activity (*k*' and *k*'') prediction curve.

3.5. References

1. J.-P. Lange, *ACS Sustainable Chemistry & Engineering*, 2021, **9**, 15722-15738.
2. S. M. Blinder, *Journal*, 2011.
3. D. Paszun and T. Spychaj, *Industrial and Engineering Chemistry Research*, 1997, **36**, 1373-1383.
4. A. Aguado, L. Martínez, L. Becerra, M. Arieta-araunabeña, S. Arnaiz, A. Asueta and I. Robertson, *Journal of Material Cycles and Waste Management*, 2014, **16**, 201-210.
5. R. Wei, G. von Haugwitz, L. Pfaff, J. Mican, C. P. S. Badenhorst, W. Liu, G. Weber, H. P. Austin, D. Bednar, J. Damborsky and U. T. Bornscheuer, *ACS Catalysis*, 2022, **12**, 3382-3396.
6. H. Lu, D. J. Diaz, N. J. Czarnecki, C. Zhu, W. Kim, R. Shroff, D. J. Acosta, B. R. Alexander, H. O. Cole, Y. Zhang, N. A. Lynd, A. D. Ellington and H. S. Alper, *Nature*, 2022, **604**, 662-667.
7. V. Tournier, C. M. Topham, A. Gilles, B. David, C. Folgoas, E. Moya-Leclair, E. Kamionka, M. L. Desrousseaux, H. Texier, S. Gavalda, M. Cot, E. Guémard, M. Dalibey, J. Nomme, G. Cioci, S. Barbe, M. Chateau, I. André, S. Duquesne and A. Marty, *Nature*, 2020, **580**, 216-219.
8. H. P. Austin, M. D. Allen, B. S. Donohoe, N. A. Rorrer, F. L. Kearns, R. L. Silveira, B. C. Pollard, G. Dominick, R. Duman, K. El Omari, V. Mykhaylyk, A. Wagner, W. E. Michener, A. Amore, M. S. Skaf, M. F. Crowley, A. W. Thorne, C. W. Johnson, H. L. Woodcock, J. E. McGeehan and G. T. Beckham, *Proceedings of the National Academy of Sciences*, 2018, **115**, E4350-E4357.
9. S. Mishra and A. S. Goje, *Polymer Reaction Engineering*, 2003, **11**, 963-987.
10. S. Tanaka, J. Sato and Y. Nakajima, *Green Chemistry*, 2021, **23**, 9412-9416.
11. C. N. Hoang, N. T. Nguyen, S. T. Ta, N. N. Nguyen and D. Hoang, *ACS Omega*, 2022, **7**, 47285-47295.
12. T. Yoshioka, T. Motoki and A. Okuwaki, *Industrial & Engineering Chemistry Research*, 2001, **40**, 75-79.
13. H. Kurokawa, M.-a. Ohshima, K. Sugiyama and H. Miura, *Polymer Degradation and Stability*, 2003, **79**, 529-533.
14. C. Liu, Y. Ling, Z. Wang, W. Zheng, W. Sun and L. Zhao, *Chemical Engineering Science*, 2022, **247**, 117024.
15. S. Liu, Z. Wang, L. Li, S. Yu, C. Xie and F. Liu, *Journal of Applied Polymer Science*, 2013, **130**, 1840-1844.
16. A. B. Raheem, Z. Z. Noor, A. Hassan, M. K. Abd Hamid, S. A. Samsudin and A. H. Sabeen, *Journal of Cleaner Production*, 2019, **225**, 1052-1064.
17. Y. Ohki, Y. Ogiwara and K. Nomura, *Catalysts*, 2023, **13**, 421.
18. U. R. Vaidya and V. M. Nadkarni, *Journal of Applied Polymer Science*, 1987, **34**, 235-245.
19. F. Chen, G. Wang, C. Shi, Y. Zhang, L. Zhang, W. Li and F. Yang, *Journal of Applied Polymer Science*, 2013, **127**, 2809-2815.
20. S. Kaiho, A. A. R. Hmayed, K. R. Delle Chiaie, J. C. Worch and A. P. Dove,

Macromolecules, 2022, **55**, 10628-10639.
21. Z. Jiang, D. Yan, J. Xin, F. Li, M. Guo, Q. Zhou, J. Xu, Y. Hu and X. Lu, *Polymer Degradation and Stability*, 2022, DOI: https://doi.org/10.1016/j.polymdegradstab.2022.109905, 109905.

4. Density Functional Theory

4.1. Introduction

Density Functional Theory (DFT) is a computational chemistry methodology wherein:

a) a 'basis set' of Gaussian functions are used to approximate the Atomic Orbitals (AOs) of an atom in Gaussian-Type Orbitals (GTOs) (Figure 4.1).

b) a 'density functional' is used to approximate the exchange-correlation interactions between electrons both within atoms and between atoms.

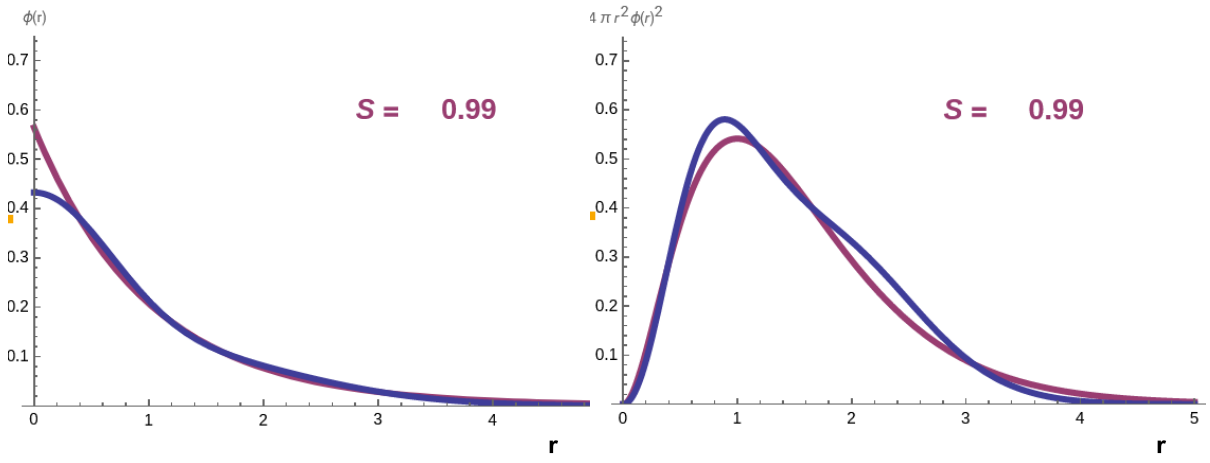


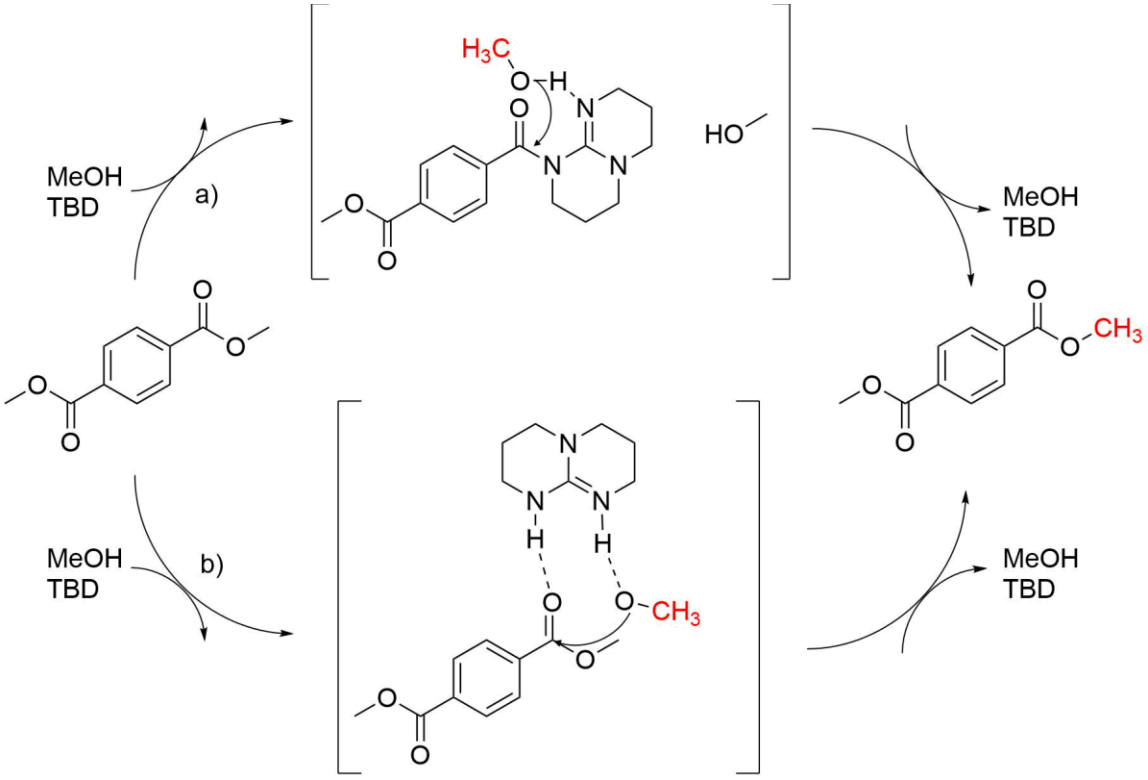
Figure 4.1**.** Wavefunction and Radial Density Function AOs (pink) approximated by 3G GTOs (purple).

A functional is a mathematical operator which takes a function as an input and yields a number as an output. Using these functionals on the Gaussian type functions, a total electron density is derived for each electron across the system, instead of attempting to solve the very highly computationally intense equations that come from trying to determine the potentials and positions of an n-body system using the wavefunction. This electron density is much easier to calculate. The derivation equations can be found in Section 4.4.1. By use of a starting

approximation and self-consistent (*i.e.* iterative) field calculations, the energy minimum and therefore optimal geometry of a system can be approximated to a high degree of accuracy.

DFT has therefore been exploited in the elucidation of the mechanism of PET glycolysis in several literature examples. The earliest examples of this investigated TBD as an organocatalyst for PET glycolysis. Calculations done by Fukushima *et al.* lent evidence for a hydrogen-bond stabilisation of the substrate pathway being the lowest-energy pathway (activation energy ($\Delta G^{\ddagger}$) = 15.9 kcal mol^{-1}), instead of an acyl-transfer pathway ($\Delta G^{\ddagger}$ = 24.8 kcal mol^{-1}) by use of dimethyl terephthalate and methanol as a model reaction (Scheme 4.1).

Scheme 4.1. Two possible mechanisms of TBD-catalysed transesterification: a) acyl-transfer; b) Hydrogen-bond stabilisation.



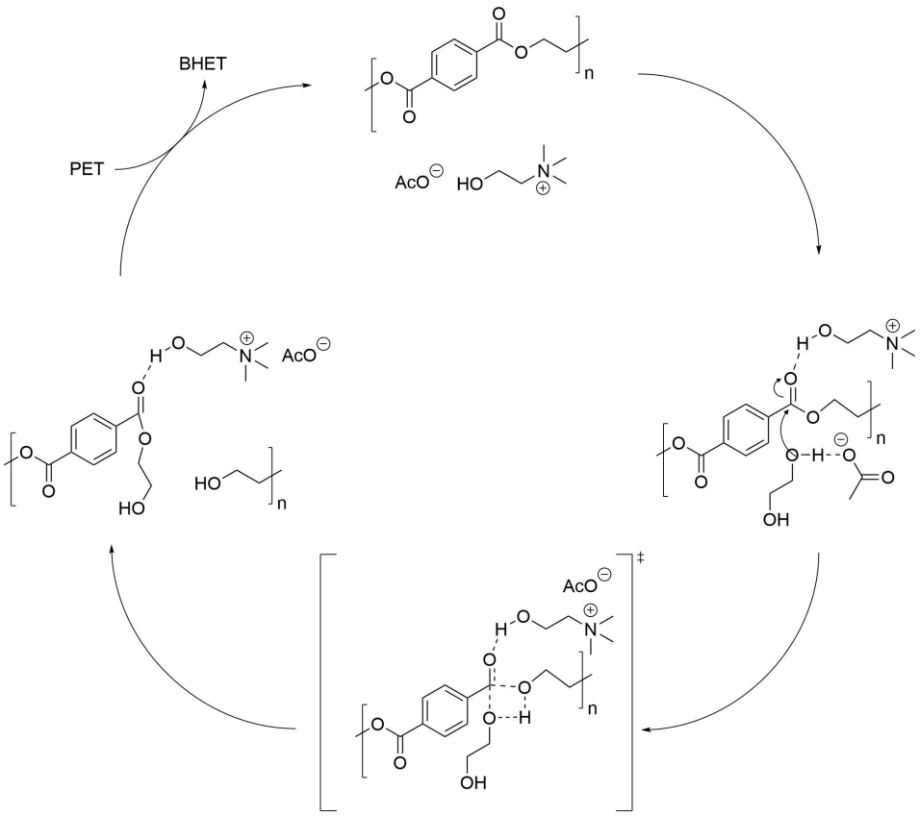
Horn *et al.* reported a methyl benzoate and ethylene glycol model reaction, and found a $\Delta G^{\ddagger}$ = 19.0-19.3 kcal mol^{-1}. Both works used the B3LYP functional (a simple functional for organic systems) with the 6-31+G(d) basis set (a medium-sized basis set with diffuse functions and a single polarisation function included) for geometry optimisation. They then used the same

functional with aug-cc-pVTZ (a larger ‘triple-zeta’ basis set with diffuse functions and a polarisation function) for single-point energy (SPE) calculations. The authors suggested 6-31+G(d) is a sufficiently large basis set for geometry optimisation calculations, but a larger set is required for SPE calculations. Both works also used the Conductor-like Polarisable Continuum Model (CPCM) of solvation to model the ethylene glycol (EG) solution, which assumes a polarised conductor as the solvent and surrounds the molecule(s) with a solvation ‘shell’ which applies a fixed external electrostatic field to the energy calculations.

Wang *et al.* reported in 2015 a series of metal salt / urea dual catalysts which could rapidly glycolyse PET.[8] $ZnCl_2$ / urea was employed in calculations at the B3LYP/6-311++G(d,p) level, although the transition states (TS) were not determined and so an activation energy could not be calculated.

The ionic liquid choline acetate was reported by Liu *et al.*[9] to glycolyse PET with an apparent experimental activation energy of 31.4 kcal mol^{-1}. DFT calculations were performed at the B3LYP/6-31++G(d,p) level on a PET dimer model compound to propose a 'separate but in tandem' mechanism of the catalyst, wherein the components of the dual catalyst act separately but both act at the same time (Scheme 4.2). In this mechanism the cholinium ion acts as a Lewis acid by hydrogen-bonding to the substrate, and the acetate ion acts as a base to stabilise the deprotonated EG.

Scheme 4.2. Catalytic cycle choline acetate-catalysed PET glycolysis, as proposed by Liu *et al.*



In another case reported by Jehanno *et al.*,[10, 11] DFT was used to calculate the minimum energy pathway of TBD:MSA 1:1 catalysed depolymerisation of PET and BPA-PC by glycolysis. A model reaction using methyl benzoate (MB) and EG was employed to simplify the calculations. From these calculations it was shown that the protonated TBD acted as a Lewis acid (stabilising the carbonyl), and the deprotonated MSA acted as a base (deprotonating, and therefore activating, the EG) (Figure 4.2). This mechanism lends credence to the separated dual catalyst mechanistic hypothesis, wherein each component acts separately but in tandem. The overall $\Delta G^{\ddagger}$ of this PET glycolysis pathway was calculated to be 20.5 kcal mol^{-1} from isolated reactants,

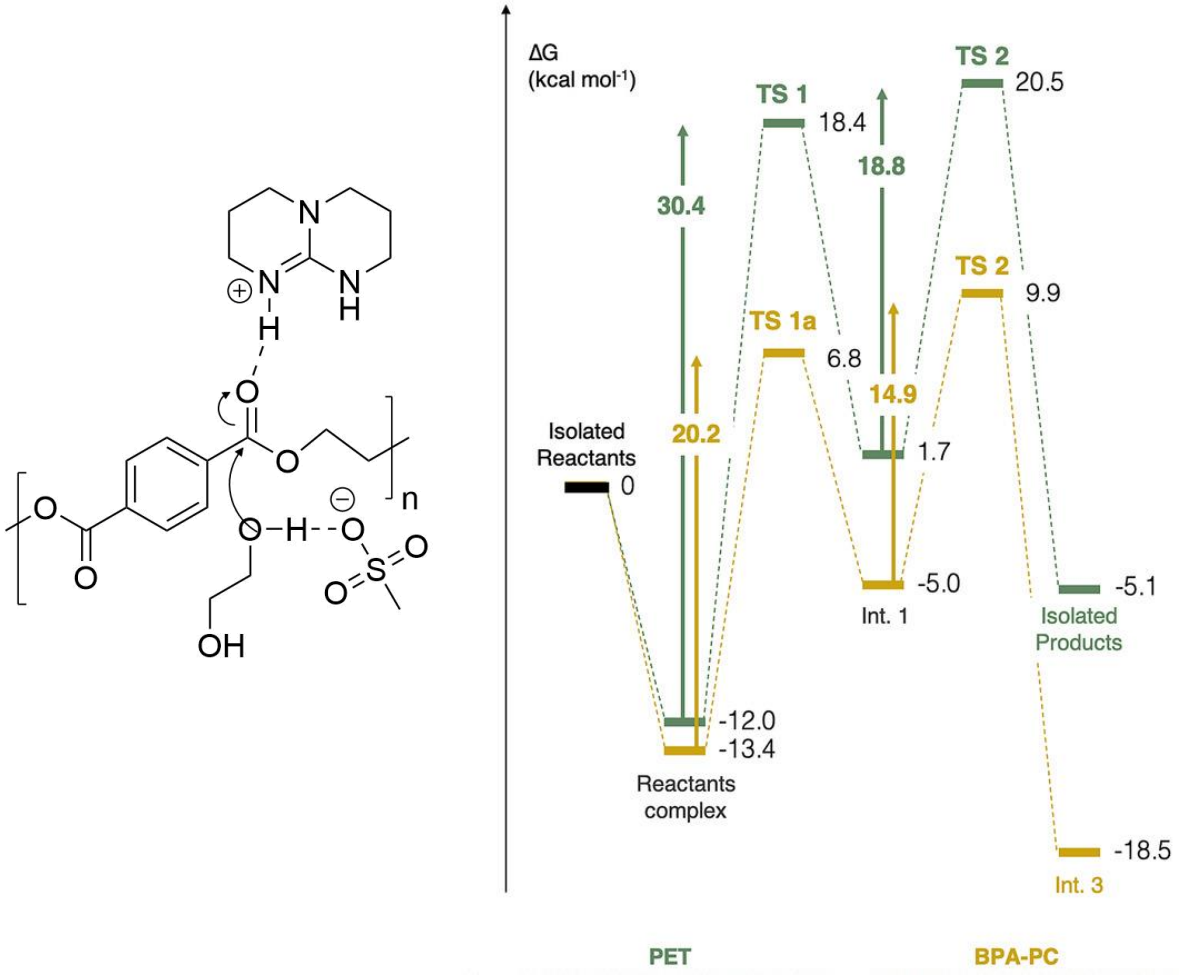


Figure 4.2. left: TBD:MSA glycolysis proposed TS; right: DFT calculations for the glycolysis of BPA-PC (yellow) and PET (green) using the Minnesota MN12SX functional in conjunction with the Pople 6-311+G(d,p) triple-zeta basis set. Reproduced with permission from Jehanno *et al.*

or 32.5 kcal mol^{-1} from complexed reactants (Figure 4.2). Given the authors only evaluate the reaction at a single temperature, it is impossible to determine whether this value of $\Delta G^{\ddagger}$ is accurate.

In the present study, in order to elucidate the mechanism of alcoholysis using the $Zn(OAc)_2$ / DMAP dual catalyst system, DFT was employed to discover the optimal structure of the catalyst. The most energetically favourable pathway *via* which the PET glycolysis reactions can proceed was also elucidated. They were calculated using the ωB97XD functional theory, which includes Grimme D2 long-range dispersion forces[13] by default and is useful for metal-containing catalysts.[13] The organic standard B3LYP functional was rejected because of its inaccuracy in metal-based systems.[14] The M06 family of theories was also considered for their accurate prediction of metal-containing systems, but ultimately avoided because of known integration grid issues.[15-17] The inclusion of long-range forces in ωB97XD also provided the potential for extension to polymer substrate studies in the future.

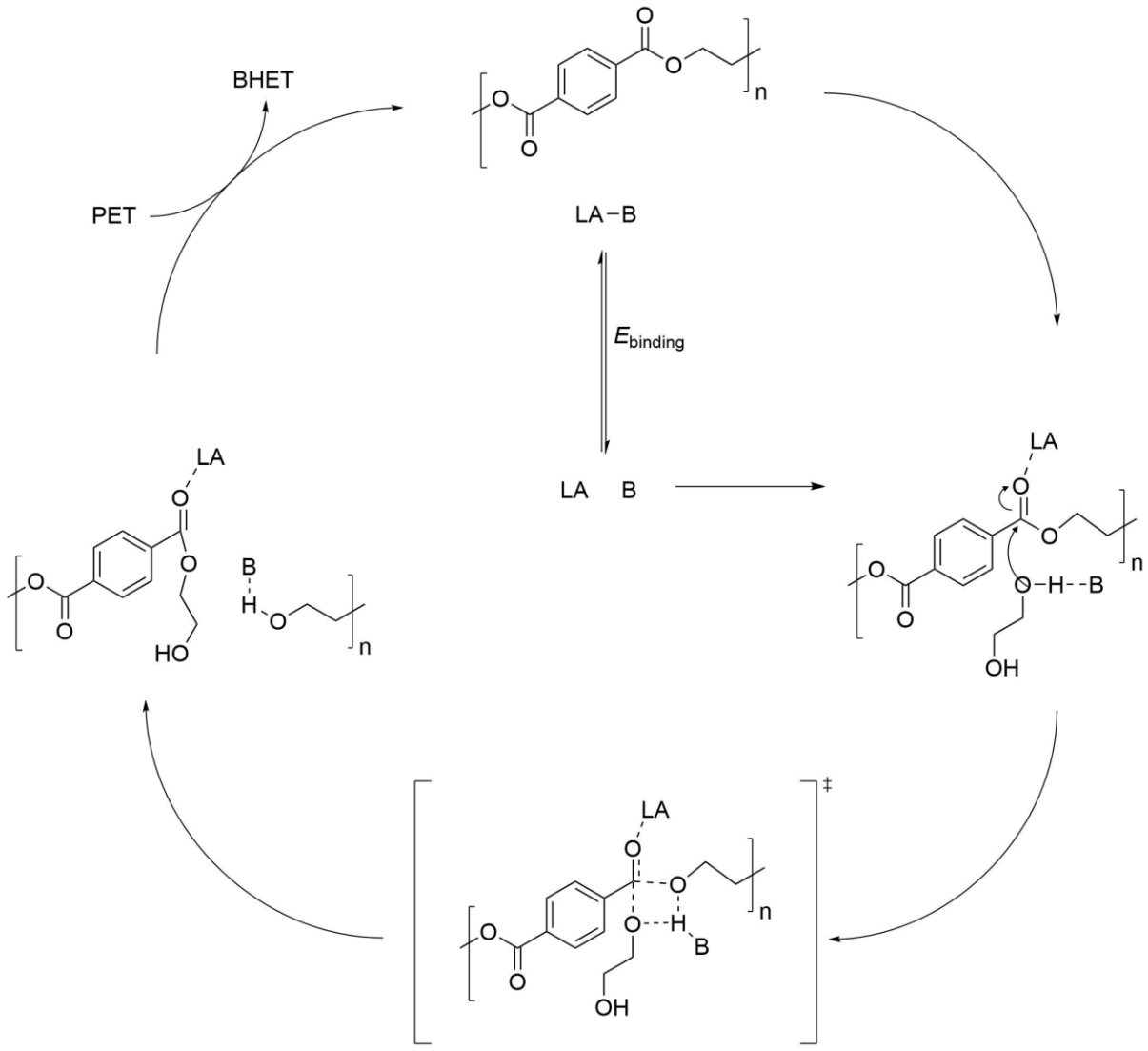
The basis set used was the literature standard double-zeta Pople basis set 6-31+g(d) because of its updated polarisation functions and split-valence orbitals for 3rd- and 4th-row atoms, which includes zinc. It also includes diffuse functions for proton affinity and ion geometries.[6] This basis set has been utilised effectively in the past for PET analogue studies.[18]

Additionally, the CPCM[6] method of solvation was used, and EG chosen as CPCM solvent and modified to have a dielectric permittivity (ε) of 19.1,[19] to model a continuum dielectric which more closely matches the conditions of the glycolysis reaction.

The catalysts were expected to be bound at room temperature but to unbind at the reaction temperature of 453 K. The minimum energy pathway was hypothesised to be one in which the Lewis acid and base act in a ‘separate but in tandem’ fashion, wherein the Lewis acid activates the carbonyl by stabilisation of the LUMO, whilst the base acts to raise the nucleophile’s HOMO

(Scheme 4.3). This increases the energy overlap between the MOs, lowering the $\Delta G^{\ddagger}$ and raising the rate.

Scheme 4.3. Generic Lewis acid/base-catalysed PET glycolysis catalytic cycle, wherein the Lewis acid and Base act in a 'separate but in tandem' fashion.



4.2. Results and Discussion

4.2.1. Catalyst Binding

Catalyst structures were calculated for each of the combinations of $Zn(OAc)_2$ or $Mg(OAc)_2$ and bases as detailed in Chapter 3 (DMA, Im, NMI, DABCO, DMAP, ABCO, DBU, MTBD, TBD). The catalysts' geometries were optimised and energies were calculated both as an bound pair wherein the most available nitrogen lone pair is bound to the zinc or magnesium ion, and as infinitely separated unbound species. Additionally, the binding modes of a variety of EG-based ligands were tested for $Zn(OAc)_2$ alone; ultimately it was found that no EG binding to $Zn(OAc)_2$ was energetically favourable.

The value of $\Delta G_{binding}$ of metal acetate and base was found to vary significantly depending on the sterics and strength of the base, although a general trend can be observed that the stronger the base (i.e. the higher its pK_{aH}), the stronger the binding and the shorter the metal-N bond (Figure 4.3).

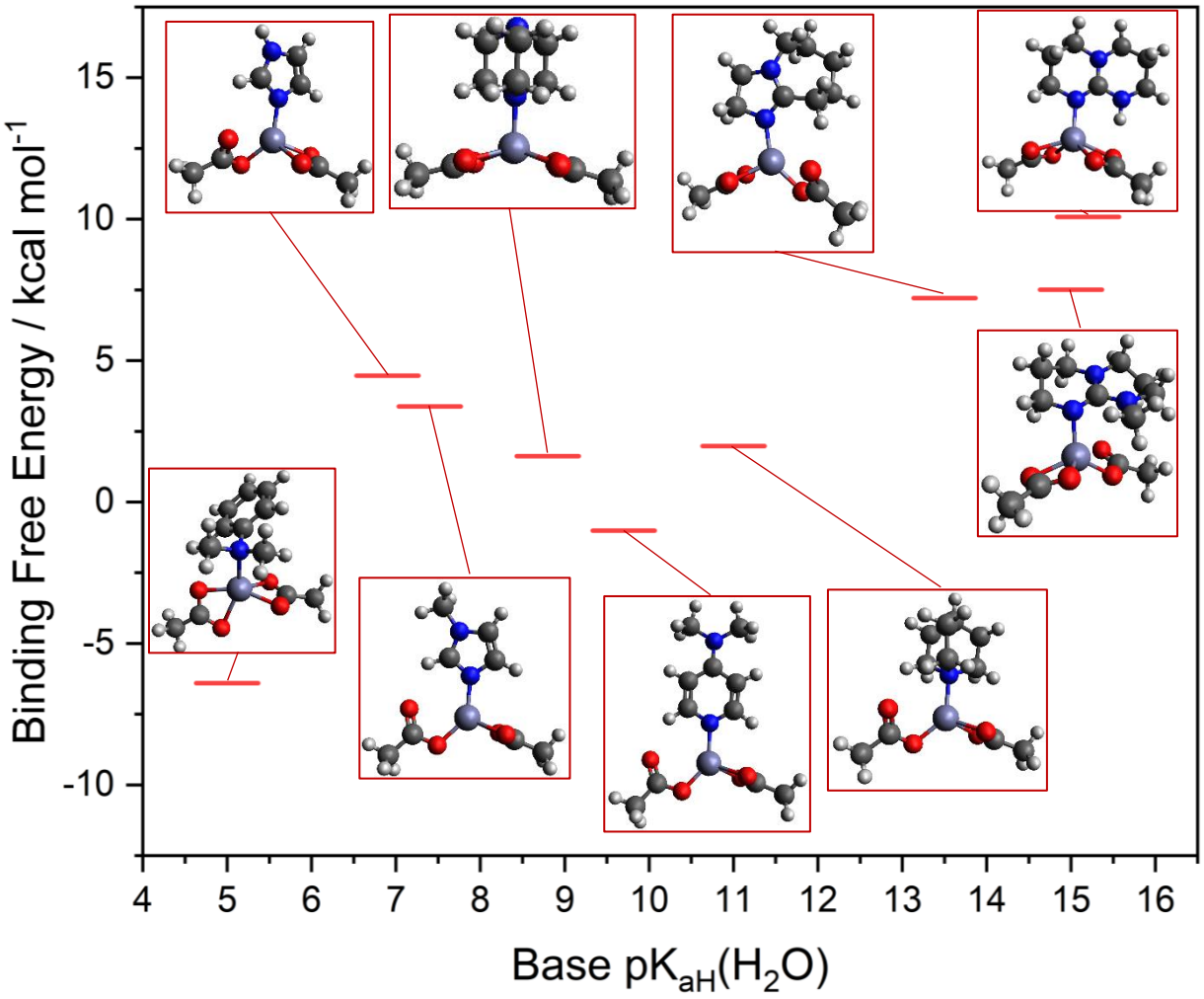


Figure 4.3. $Zn(OAc)_2$-base binding free energy ($\Delta G_{binding}$) *versus* basicity of the base, alongside geometries; grey = C, white = H, blue = N, red = O.

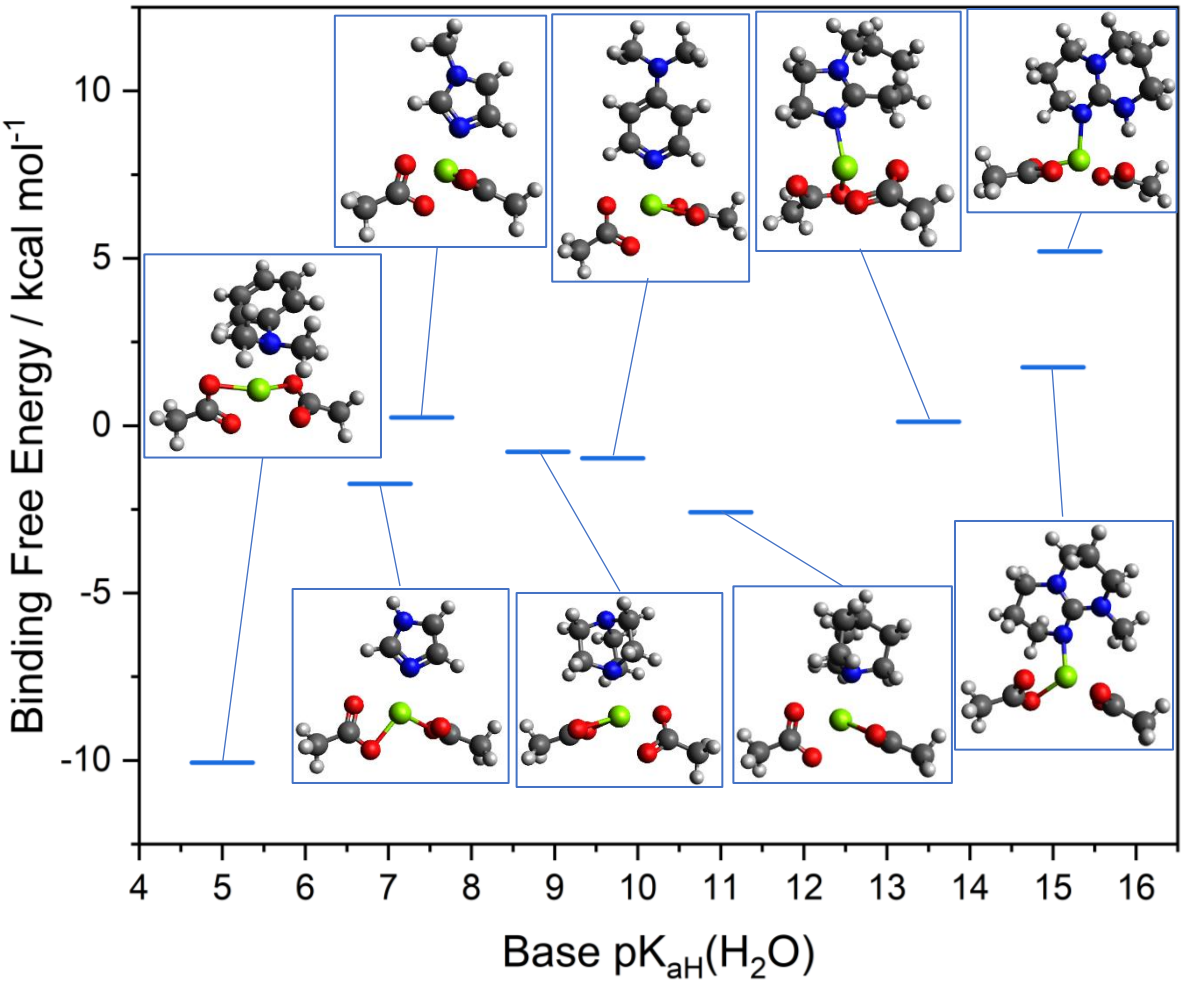


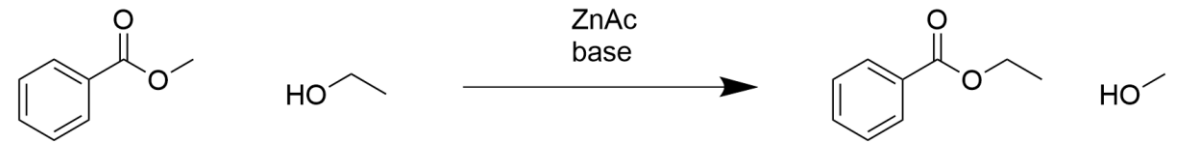
Figure 4.4. $Mg(OAc)_2$-base binding free energy ($\Delta G_{binding}$) *versus* basicity of the base, alongside geometries.

This is to be expected as a stronger base should have a more available nitrogen lone pair (as basicity and nucleophilicity broadly correlate),[6] and thus stronger donation to the metal and a shorter bond.

4.2.2. Model Compounds

Once the catalyst binding mode was elucidated, the mode of catalyst binding to the polymer substrate and the lowest-energy pathway was sought. In order to reduce the computational load for the calculations, small molecule model compounds were used in place of the polymer substrate and nucleophile. For the polymer substrate, methyl benzoate was used, as there is precedent for this small molecule to be used in DFT calculations in place of PET, as it models much of the desired structure of the active polymer cleavage site.[20] In place of EG, ethanol was used to avoid complicating hydrogen bonding with the inactive end of the diol, to genericise the alcohol used in the reaction, and to differentiate the final product (ethyl benzoate) from the reactant substrate (methyl benzoate (MB)) (Scheme 4.4). The full catalyst structure itself was kept, so as to maintain any effects of the acetate ligands.

Scheme 4.4. Model reaction used to simplify polymer substrate.



methyl benzoate ethanol ethyl benzoate methanol

Transition states and reactive intermediates were calculated for both the bound and unbound catalyst modes, wherein the nitrogen base acts either as a ligand to the metal (bound), or as a base (unbound) in the ‘separate but in tandem’ mechanism.

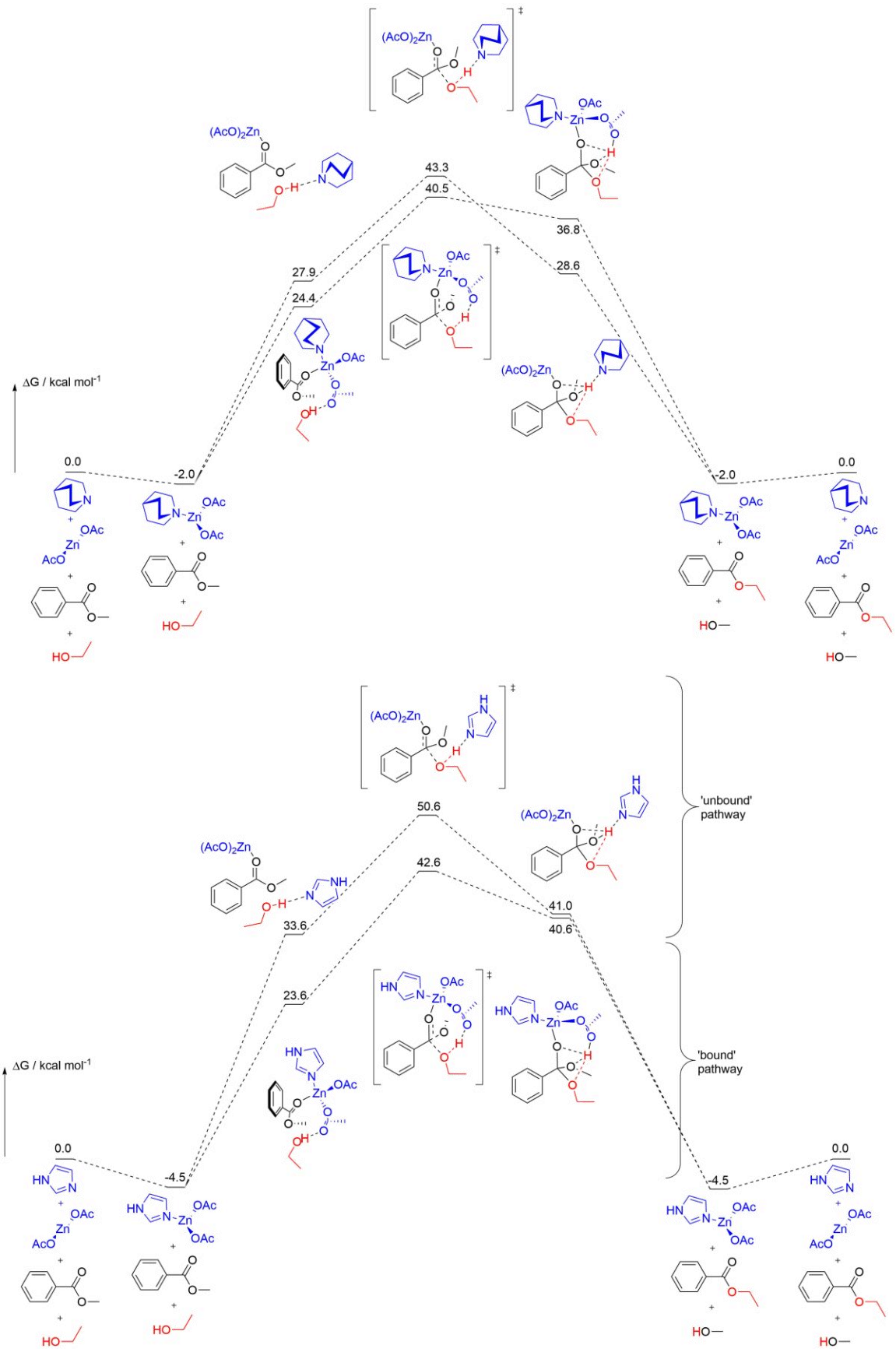


Figure 4.5. Minimum energy pathways for a) $Zn(OAc)_2$ / ABCO; b) $Zn(OAc)_2$ / Im.

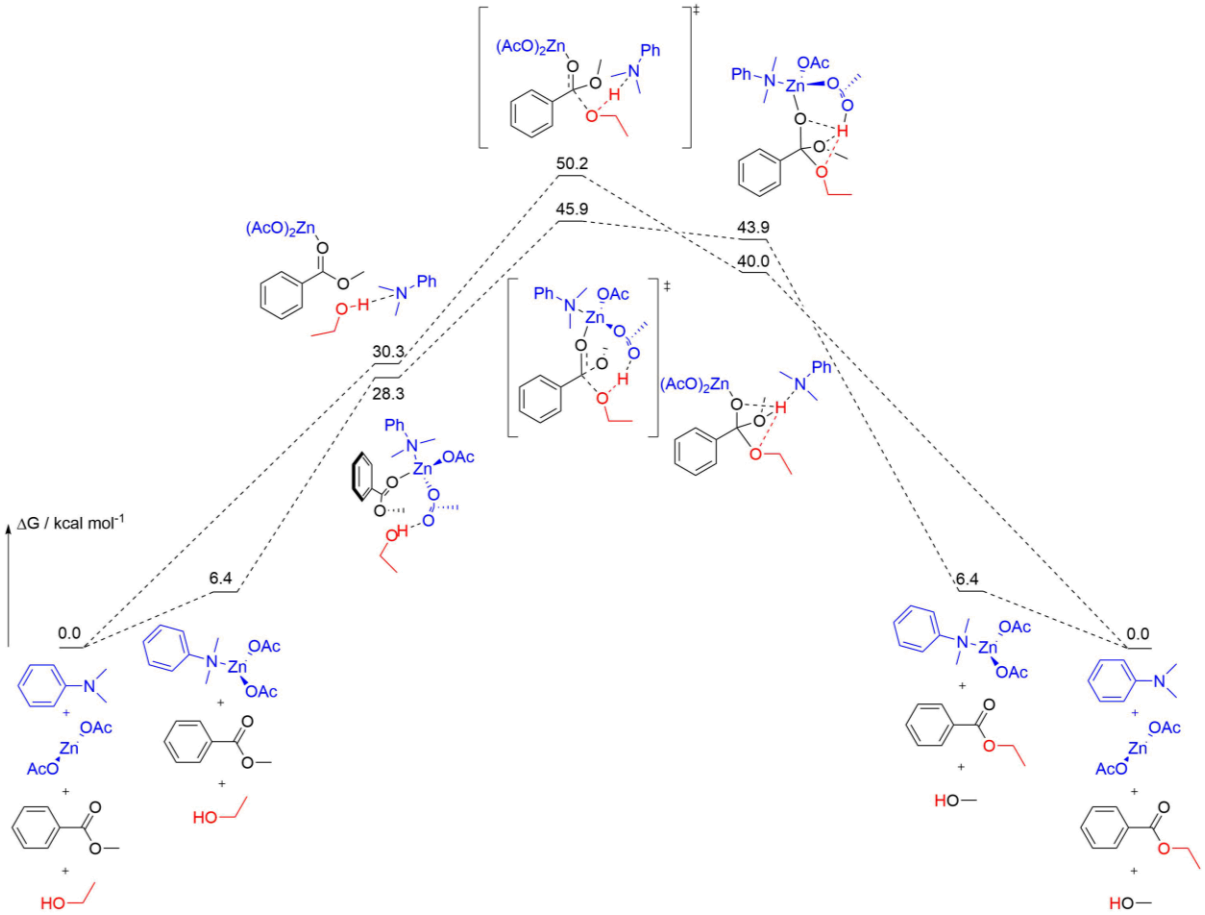


Figure 4.6. Minimum energy pathway for c) $Zn(OAc)_2$ / DMA.

The catalysts were chosen to be $Zn(OAc)_2$-based, and the bases sampled were DMA, Im and ABCO. Im was chosen as it was the highest-activity base in combination with $Zn(OAc)_2$, and the remaining bases were chosen as two bases which flank this peak: DMA at lower and ABCO at higher pK_{aH}.

All three combinations' transition state (TS) geometry were optimised using the theory and basis set as described above. The optimised structure was confirmed to be a saddle point on the potential energy surface (PES), as well as the imaginary vibrational mode calculated being confirmed to have chemically sensible bond changes. These bond changes showed the acetate-H bond shortening and the H-O_{EG} bond lengthening (representing deprotonation), as the oxygen-carbonyl carbon bond forms and shortens.

Next, intermediates were optimised using starting points from the extreme points of the TS imaginary vibrational mode. These geometries were then used for frequency calculations as above. These intermediates and TSs were used to construct energy level diagrams for each of the studied metal / base systems (Figure 4.3).

The $\Delta G^{\ddagger}$ for $Zn(OAc)_2$ / ABCO was found to be 40.5 kcal mol^{-1} (169 kJ mol^{-1}); the $\Delta G^{\ddagger}$ for $Zn(OAc)_2$ / Im was found to be 42.6 kcal mol^{-1} (178 kJ mol^{-1}); the $\Delta G^{\ddagger}$ for $Zn(OAc)_2$ / DMA was found to be 45.9 kcal mol^{-1} (192 kJ mol^{-1}). These values of $\Delta G^{\ddagger}$ are all significantly higher than those found by other literature examples starting from infinitely separated reactants. They also do not correspond properly to the observed experimental activity; *i.e.* $Zn(OAc)_2$ / Im should have the lowest $\Delta G^{\ddagger}$ as the dual catalyst with highest activity. The binding energies are yet to be included in the $\Delta G^{\ddagger}$s, however. When including these, the $\Delta G^{\ddagger}$ for $Zn(OAc)_2$ / ABCO becomes 42.5 kcal mol^{-1}; the $\Delta G^{\ddagger}$ for $Zn(OAc)_2$ / Im becomes 46.5 kcal mol^{-1} (Figure 4.4); the $\Delta G^{\ddagger}$ for $Zn(OAc)_2$ / DMA remains 45.9 kcal mol^{-1} (as the unbound state remains the most stable). These actually correlate inversely with activity, and therefore conversely with what is expected. These values of $\Delta G^{\ddagger}$ are also not consistent in size with those found in Chapter 2. There are several possibilities for what could have caused this. One possibility is that, while CPCM was used to create a solvent shell, presence of excess reagent such as EG was not taken into account and so the entropic contribution to energy was underestimated. Another option is that only the TSs wherein the base was *cis* to the ester were considered, and perhaps the *trans* transition structures have energy levels more consistent with the experimental values. Additionally, extrapolating from the calculations done by Jehanno *et al.*, it is possible that the bases are protonated by the excess EG, so they are acting as co-Lewis acids alongside the metal salts. This possibility could not have appeared in the existing calculations as discrete excess EG was not included, only the solvation shell using CPCM.

The lowest-energy TSs were all shown to be the ones in which the catalyst remained bound, which is to say the base acted as a ligand to the zinc. Additionally, in these structures it was shown that the acetate ligand on the zinc acts as a base, deprotonating the alcohol prior to its attack into the carbonyl centre (Figure 4.5).

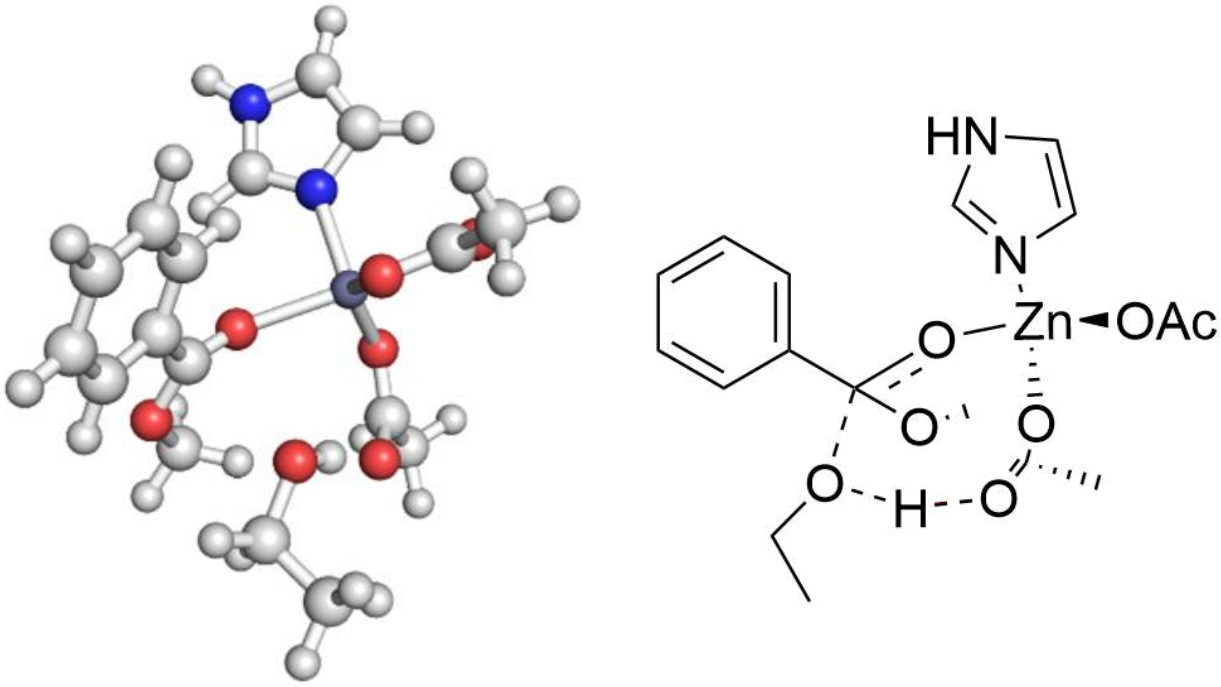


Figure 4.7. Three-dimensional structure and simplified scheme of the $Zn(OAc)_2$ / Im catalysed reaction's lowest-energy TS, showing the direction of the alcohol by the acetate ligand; white = H, grey = C, blue = N, red = O.

It was proposed that the bonding of the base to the zinc modified the acetate bonding to the zinc in such a way as to affect the acetate's ability to deprotonate the alcohol and direct the EG into the reactive centre, therefore changing the overall activation energy of the reaction and thus the activity of the catalyst. The bond lengths between the bases' nitrogen atom and the Lewis acid's zinc atom were measured, as well as the Zn-O(Ac) bond length, and these were compared with the activity of the catalyst.

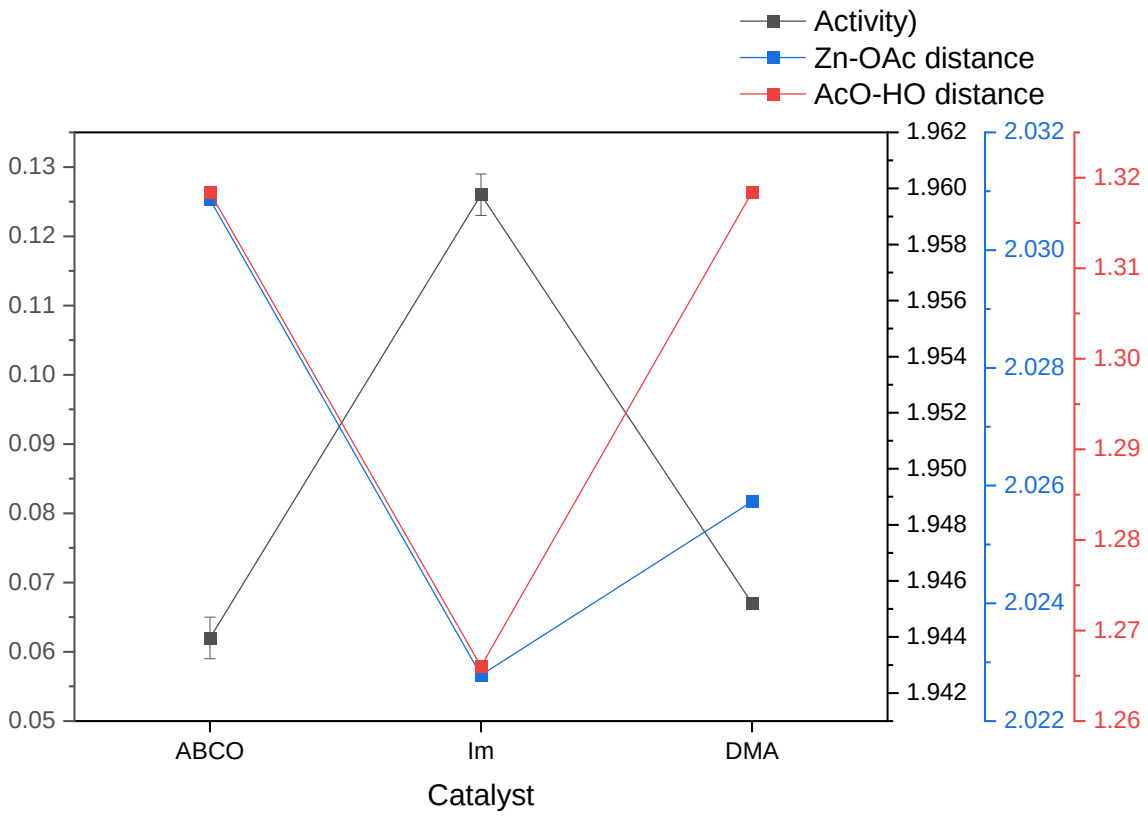


Figure 4.8. Comparison of activity with: Zn-O(Ac) distance (blue); (Ac)O-H(OR) distance (hydrogen bond) (red)

It can also be qualitatively derived that the relative activity decreases when the AcO-Zn bond length is long (Figure 4.6). The ligand which is able to π-electron back-bond (Im) therefore has lesser metal electron density, causing the metal-oxygen(acetate) bond to be shorter as the oxygen can donate more into the metal (Figure 4.7c). This produces a tighter transition state and the hydrogen bond is able to more closely direct the nucleophile into the substrate's C=O π* LUMO. This more closely approximates the ideal intramolecular Bürgi-Dunitz angle of attack of 105° (Figure 4.7d). It is supposed that the ability of zinc to back-bond into the Im and NMI produces a better TS geometry which translates into a faster reaction. It is possible this back-bonding effect is also why MnAc / NMI is such an effective combination.

The binding energies of $Zn(OAc)_2$ / Im and $Zn(OAc)_2$ / NMI support this theory, as they are significantly stronger than the basicity of the imidazoles would suggest they should be. This implies a stronger bond, perhaps as a result of back-bonding.

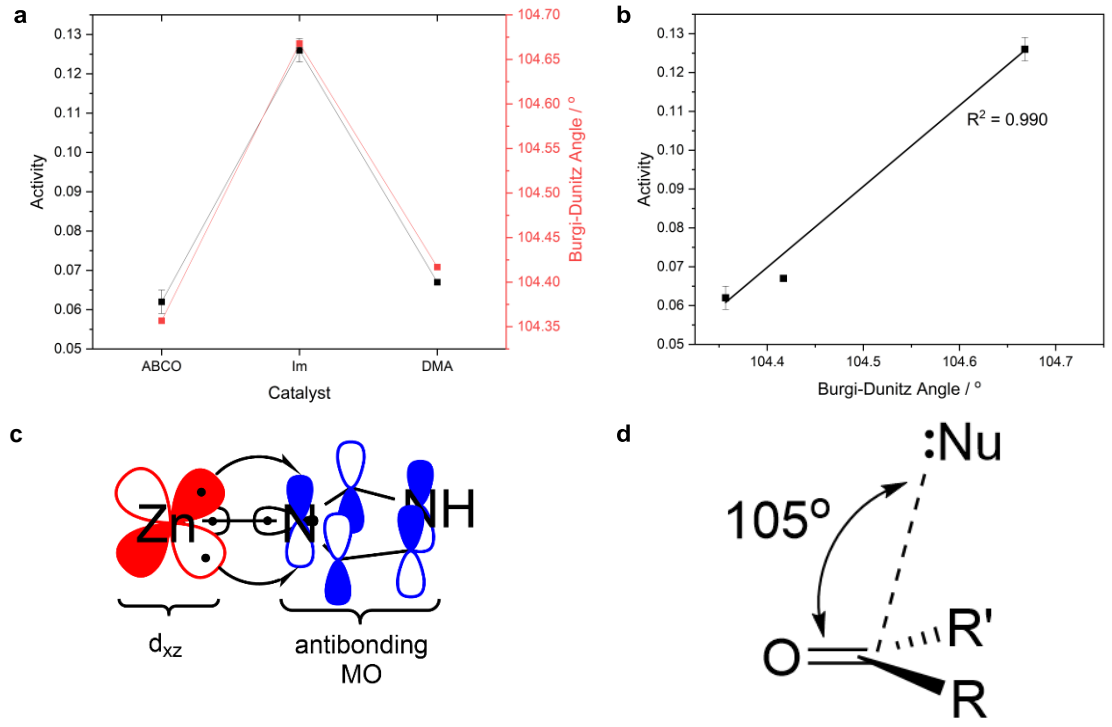


Figure 4.9. a) & b) Comparisons of activity *versus* Bürgi-Dunitz Angle; c) diagram of back-bonding of metal d-electrons; d) diagram of ideal intramolecular Bürgi-Dunitz Angle.

The lower reaction barrier of $Zn(OAc)_2$ / ABCO indicates a possibility of why MgAc / ABCO is an off-trend high activity combination. It is not possible for Mg^{2+} to back-bond with the ligands because of its lack of d orbitals, therefore the imidazoles are not highly active as they do not produce tightly bound TSs. It is also likely that La^{2+} is a poor back-bonder because of its very diffuse orbitals, hence the lack of 'imidazole spike' in the LaAc activity profile.

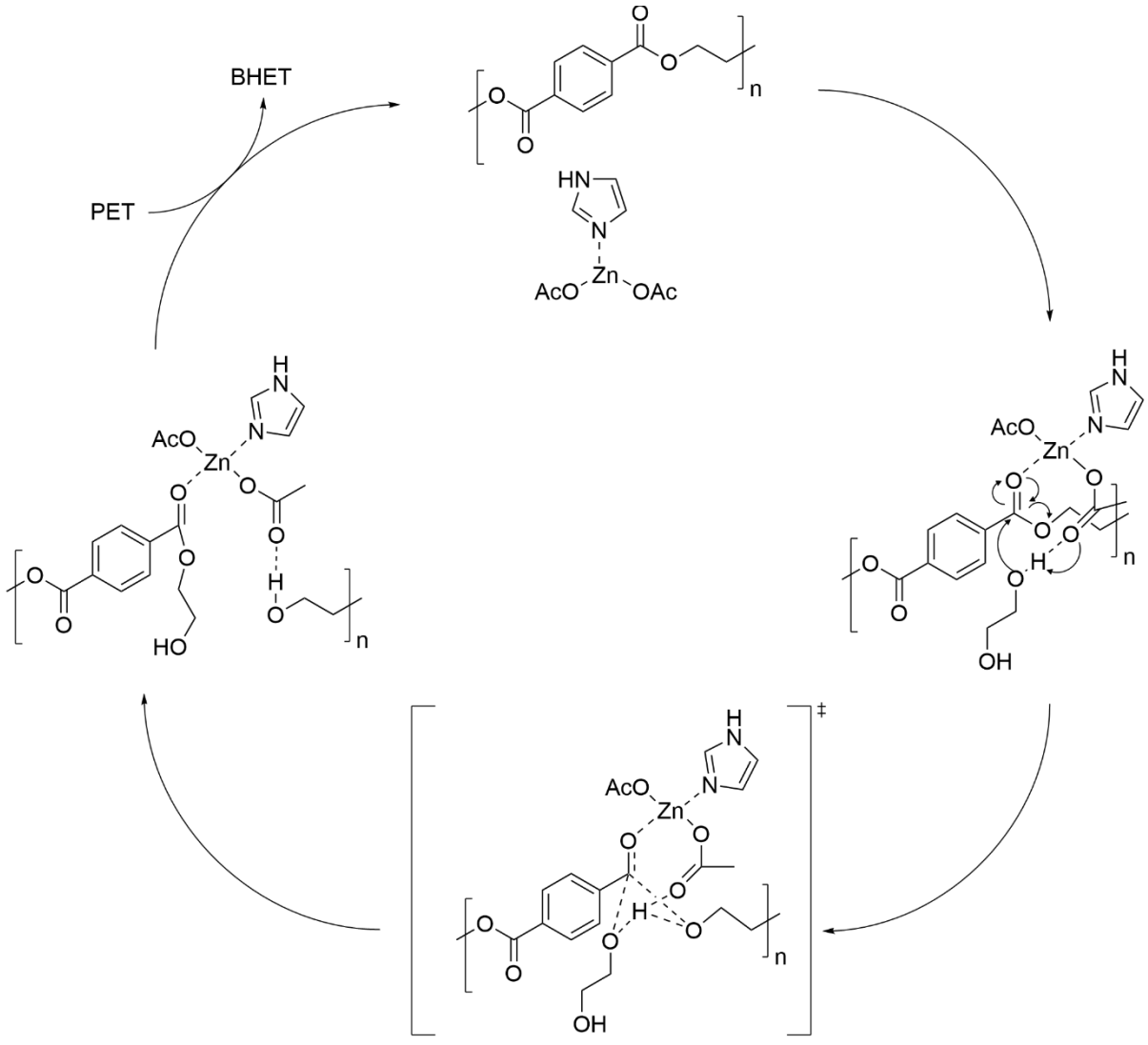
The TS energies were then confirmed *via* SPE calculations for $Zn(OAc)_2$ / Im using the larger, triple-zeta Pople basis set 6-311+d(g). The differences in $\Delta G^{\ddagger}$ between double-zeta and triple-zeta basis set calculations were found to be less than 1 kcal mol^{-1} (4 kJ mol^{-1}).

Next, intermediates were optimised using starting points from the extreme points of the TS imaginary vibrational mode. These geometries were then used for SPE calculations as above, and the $\Delta G^{\ddagger}$ values were all also found to be within 1 kcal mol^{-1} (4 kJ mol^{-1}) of those found by using the smaller basis set.

4.2.3. Mechanistic Deductions

The discrepancy between the calculated values of $\Delta G^{\ddagger}$ and the experimentally observed reactivity necessitates caution when deriving conclusions from these computational data.

Scheme 4.5. Proposed catalytic cycle of the $Zn(OAc)_2$ / Im-catalysed PET glycolysis reaction.



However, an attempt will be made to deduce various mechanistic features from the structures of the TSs, and a catalytic cycle was hence constructed (Scheme 4.5). Accordingly, the acetate acts both as a base and a proton transfer agent between the EG and the exiting chain end.

In the first step, the catalyst complex binds to the PET substrate *via* the zinc ion, and the acetate hydrogen-bonds to the EG and directs it towards the carbonyl's electrophilic centre. In the TS, the carbon-oxygen bond from the EG to the electrophilic centre forms as the oxygen-hydrogen bond extends and the hydrogen transfers to the exiting chain end. The second intermediate is a tetrahedral structure around the electrophilic ex-carbonyl carbon, which rapidly transitions to a new carbonyl with the EG forming an ester instead of the exiting chain end.

4.3. Conclusions

DFT calculations were performed on a range of metal acetate / base dual catalysts. It was initially hypothesised that the dual catalyst combinations would not remain bound at the temperature the reaction was performed at; however, the binding energy depended strongly on base basicity, with weaker bases unbound at temperature and stronger bases remaining bound.

Calculations were then performed on a model system designed to mimic PET glycolysis. The mechanism was shown to follow a similar profile to the hypothesised 'separate but in tandem' model of acid-base catalysis, excepting that the acetate acts as the base and remains bound to the metal ion acid, whilst the base component of the dual catalyst acts merely as a ligand. The ligand likely modifies the steric and electronic properties of the metal ion and the acetate such that the activity is modulated.

It is clear from the results of the $\Delta G^{\ddagger}$ studies that either the theory or basis set or both are insufficient for this type of study; it is recommended that the same studies be undertaken using

a wider variety of functionals (such as M06-L, B3LYP and PBE0) and/or a larger basis set (such as 6-311+G(d) or 6-311+G(d,p)).

It is recommended that future work in this area focuses on covering the dual catalysts comprised of metal acetates not included in this study (principally $Mn(OAc)_2$ and $La(OAc)_3$), in combination with the same bases. A more tightly-focused study of functional group effect on energy levels could also be undertaken, possibly in tandem with a screen of substituted imidazoles.

4.4. Supporting Information

4.4.1. DFT Derivation Equations

$$\hat{H}\Psi = E\Psi = \left[\hat{T} + \hat{V} + \hat{U}\right]\Psi = \left[-\frac{1}{2}\sum_{i=1}^{N}\nabla_i^2 + \sum_{i=1}^{N}V(\boldsymbol{r_i}) + \sum_{i<j}^{N}\frac{1}{|\boldsymbol{r_i} - \boldsymbol{r_j}|}\right]\Psi \qquad S4.1$$

Where Ψ is the wavefunction, $\hat{H}$ is the Hamiltonian, E is the total energy, $\hat{T}, \hat{V}, \hat{U}$ are kinetic energy, potential energy from the nuclei, and electron-electron interaction energy respectively.

$$n(\boldsymbol{r}) = N\int d^3\boldsymbol{r}_2 \cdots \int d^3\boldsymbol{r}_N \Psi^*(\boldsymbol{r}, \boldsymbol{r_2}, \cdots, \boldsymbol{r_N})\Psi(\boldsymbol{r}, \boldsymbol{r_2}, \cdots, \boldsymbol{r_N}) \qquad S4.2$$

is the electron density for an electron in an N-electron system. The ground state wavefunction and thus the ground state energy can be found from this equation:

$$\Psi_0 = \Psi[n_0] \qquad S4.3$$

$$E_0 = E[n_0] = \left\langle \Psi_0 \middle| \hat{T} + \hat{V} + \hat{U} \middle| \Psi_0 \right\rangle \qquad S4.4$$

If this principle is extended *via* the Kohn-Sham Equations,[1] using orbitals to avoid having to solve the Schrödinger Equation, the energy of the system can be found using the charge density:

$$E[\rho] = T_s[\rho] + E_{ext}[\rho] + E_H[\rho] + E_{XC}[\rho] \geq E_0 \qquad S4.5$$

(where E_{XC} is the error in using non-interaction in the kinetic energy plus the error in using classical electron-electron interaction). The Kohn-Sham variational theorem follows directly from the variational theorem of the Schrödinger Equation. The energy of an orbital ε can be found using the orbital function $\varphi(\boldsymbol{r})$:

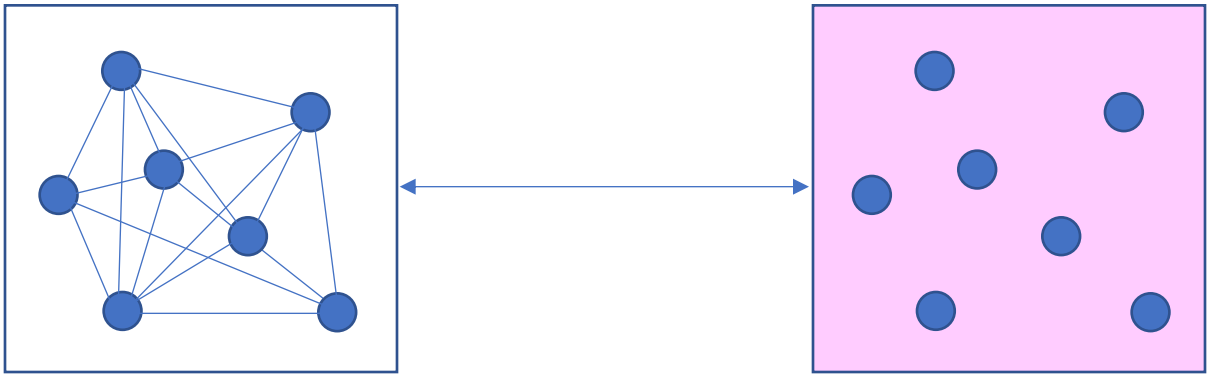
$$\left(-\frac{\bar{h}^2}{2m_i}\nabla_i^2 + v_{eff}\right)\varphi_i(\boldsymbol{r}) = \varepsilon_i\varphi_i(\boldsymbol{r}) \qquad S4.6$$

$$v_{eff}(\boldsymbol{r}) = v_{ext}(\boldsymbol{r}) + \int \frac{\rho(\boldsymbol{r}')}{|\boldsymbol{r}-\boldsymbol{r}'|}d\boldsymbol{r}' + \frac{\delta E_{XC}[\rho]}{\delta\rho(\boldsymbol{r})}\rho(\boldsymbol{r}) \qquad S4.7$$

where v_{ext} is the external potential, ρ is the charge density and E_{XC} is the exchange-correlation energy. This set of equations describes the behaviour of non-interacting Fermions in a local potential. The single-particle potential, v_{eff}, can be displayed as a sum of components:

$$v_{eff}(\boldsymbol{r}) = V(\boldsymbol{r}) + V_H(\boldsymbol{r}) + V_{XC}[n(\boldsymbol{r})] \qquad S4.8$$

As the Hartree component (V_H) and the exchange-correlation component (V_{XC}) depend on $n(\mathbf{r})$, which itself depends on the orbitals, the solution must be approached in a self-consistent manner.



Supporting Figure S4.10. The Schrödinger picture of interacting electrons, and the Kohn-Sham picture of non-interacting electrons in a constant potential (pink).

4.4.2. Typical Gaussian Input Commands

%nprocshared=20
%mem=6GB
# opt rwb97xd/6-31+g(d)
scrf=(cpcm,solvent=1,2-ethanediol,read) nosymm geom=(connectivity,nocrowd)
int=grid=ultrafine temperature=453

Title

0 1

xyzcoord

Eps=19.1

4.4.3. Cartesian Coordinates of Optimised Structures

$Zn(OAc)_2$ / ABCO I1b

C	-2.31377	1.54497	0.35933
C	-3.05471	1.89762	1.48278
C	-4.02529	1.02754	1.97809
C	-4.26359	-0.19237	1.34261
C	-2.54707	0.32124	-0.27312
C	-3.53099	-0.54511	0.21451
C	-1.73355	-0.04598	-1.45206
H	-1.56378	2.22749	-0.02516
H	-2.87097	2.84968	1.97128
H	-3.70455	-1.49626	-0.27694
H	-4.59856	1.29990	2.85936
H	-5.01838	-0.87015	1.72922
O	-2.28834	-0.94451	-2.23582
O	-0.65176	0.46989	-1.74089
C	-1.51106	-1.38609	-3.36463
H	-2.08740	-2.19755	-3.80502
H	-0.53099	-1.73119	-3.02784
H	-1.39665	-0.56572	-4.07601
Zn	1.14226	1.08885	-0.87526
O	-0.50068	-2.15381	-0.03248
C	-1.10259	-3.40423	-0.31735
C	-0.20689	-4.58476	0.03450
H	-1.39184	-3.45668	-1.37760
H	-2.02468	-3.43871	0.27254
H	0.05905	-4.56379	1.09702
H	0.71669	-4.55682	-0.55443
O	0.93525	0.97001	1.03865
C	0.69136	2.04619	1.71402
O	2.57815	-0.00415	-1.64246
C	2.51752	-1.21978	-2.05061
C	3.70543	-1.67378	-2.87538
C	0.40449	1.81789	3.18330
H	4.63456	-1.47929	-2.33135
H	3.74265	-1.09238	-3.80290
H	3.63413	-2.73541	-3.11702
H	0.36236	2.76404	3.72531
H	1.16323	1.16617	3.62572
H	-0.56161	1.30888	3.27660

O	1.57804	-2.00413	-1.82521
O	0.66111	3.18132	1.21942
H	0.27062	-2.03365	-0.62699
H	-0.71931	-5.53080	-0.17648
C	2.51408	3.51470	-1.77467
C	0.10443	3.62892	-2.02493
C	1.41666	2.25622	-3.53345
C	2.78224	4.62667	-2.81476
H	2.34523	3.92167	-0.77438
H	3.34938	2.81112	-1.71520
H	-0.75302	3.05397	-2.38605
H	-0.04736	3.84117	-0.96457
C	0.30918	4.92080	-2.84830
C	1.40800	3.44293	-4.52420
H	0.58985	1.56654	-3.72173
H	2.34608	1.68488	-3.59320
C	1.55425	4.74568	-3.72691
H	2.97518	5.57801	-2.30785
H	3.66894	4.38961	-3.41348
H	-0.57181	5.11726	-3.46847
H	0.44017	5.78298	-2.18449
H	0.47365	3.46112	-5.09666
H	2.22866	3.33978	-5.24199
H	1.66534	5.59679	-4.40529
N	1.29342	2.73525	-2.12618

$Zn(OAc)_2$ / ABCO I1u

C	-2.74224	1.10088	0.56632
C	-3.84753	1.94542	0.59023
C	-4.62308	2.11393	-0.55879
C	-4.28785	1.42521	-1.72226
C	-2.39743	0.41474	-0.60107
C	-3.18070	0.57449	-1.74210
C	-1.15700	-0.48067	-0.55781
H	-2.12856	0.97986	1.45428
H	-4.10087	2.47913	1.50231
H	-2.91892	0.04206	-2.64999
H	-5.48244	2.77861	-0.54497
H	-4.88707	1.54920	-2.62022
O	-0.91580	-0.92298	-1.87537
O	-0.08898	0.14680	-0.01235
C	0.24033	-1.72992	-2.02763
H	0.29865	-1.97775	-3.08900
H	0.16061	-2.65415	-1.44260
H	1.14287	-1.18737	-1.72901
Zn	0.65961	1.80126	-0.64902
O	-1.37854	-1.60143	0.29765
C	-2.43220	-2.48583	-0.05897
C	-2.48895	-3.58310	0.98566
H	-2.24602	-2.90612	-1.05544

H	-3.38353	-1.93830	-0.09663
H	-2.70717	-3.16803	1.97527
H	-1.53674	-4.12249	1.03466
O	0.04037	3.35494	0.73723
C	-0.66851	3.83144	-0.19592
O	1.98404	1.44208	-2.30722
C	2.95462	1.44012	-1.49467
C	4.34762	1.12143	-1.97007
C	-1.58843	4.99711	0.05222
H	5.09206	1.64889	-1.37033
H	4.46575	1.36966	-3.02631
H	4.51532	0.04513	-1.84908
H	-1.59014	5.67375	-0.80555
H	-1.30668	5.53555	0.95846
H	-2.60564	4.60820	0.17484
O	2.74434	1.67233	-0.26281
O	-0.62908	3.30110	-1.35133
H	0.53538	-0.64350	1.24223
H	-3.27688	-4.30024	0.73316
C	2.12897	-0.14335	2.48563
C	1.71632	-2.33541	1.45754
C	0.16448	-1.46190	3.14136
C	3.07460	-0.87021	3.46240
H	2.63346	0.24139	1.59687
H	1.59777	0.68641	2.95781
H	0.92149	-2.89839	0.96556
H	2.42323	-2.00071	0.69481
C	2.39755	-3.11509	2.59962
C	1.00486	-1.96995	4.33019
H	-0.52021	-2.21552	2.75094
H	-0.41451	-0.56788	3.38074
C	2.44268	-2.21752	3.84643
H	4.05199	-1.03539	2.99743
H	3.23413	-0.25436	4.35221
H	1.84323	-4.03317	2.81980
H	3.40865	-3.40531	2.29996
H	0.56880	-2.89283	4.72359
H	1.00609	-1.23493	5.14151
H	3.02769	-2.69756	4.63493
N	1.08320	-1.10529	2.02008

$Zn(OAc)_2$ / ABCO TSb

C	-1.69994700	-0.39795500	1.25426000
C	-2.35819600	0.00590600	2.41328900
C	-3.64248800	0.54357800	2.34007800
C	-4.26662700	0.67176400	1.09995500
C	-2.32322000	-0.27314300	0.01095800
C	-3.61067800	0.26301700	-0.06006300
C	-1.58260400	-0.59341900	-1.28009100
H	-0.69734600	-0.80708800	1.31650400

H	-1.86546500	-0.10100800	3.37554900
H	-4.09873700	0.36270100	-1.02437500
H	-4.15435100	0.85974000	3.24450500
H	-5.26729500	1.08917200	1.03350200
O	-2.46985700	-1.11033100	-2.19296300
O	-0.77436300	0.31476500	-1.73955900
C	-1.98682400	-1.21884500	-3.52972600
H	-2.77754700	-1.72261800	-4.08619900
H	-1.06916800	-1.81599900	-3.56886100
H	-1.79433400	-0.23166500	-3.95622500
Zn	0.77057000	1.10291300	-0.84505700
O	-0.61614000	-1.82622100	-0.88335600
C	-1.19426900	-3.13383200	-0.71409400
C	-0.26615100	-3.98063900	0.13313800
H	-1.36728300	-3.57625600	-1.70016400
H	-2.15939500	-2.98827200	-0.22341300
H	-0.11896700	-3.52541700	1.11726400
H	0.70864400	-4.10006700	-0.34968800
O	1.09197200	1.45471100	1.03914600
C	0.36331200	2.39618200	1.54298900
O	2.30107700	-0.16522400	-1.26191700
C	2.36780200	-1.18564700	-2.00249600
C	3.67654000	-1.46398400	-2.69949800
C	0.52107100	2.59866900	3.03535100
H	4.51613100	-1.14409600	-2.07909400
H	3.70132700	-0.87891300	-3.62640400
H	3.77078500	-2.52020300	-2.95692500
H	-0.05864200	3.45722100	3.37797200
H	1.57662000	2.73990100	3.28701100
H	0.17788700	1.69946100	3.55789200
O	1.40587300	-1.98342500	-2.22284800
O	-0.41845600	3.09098400	0.87639900
H	0.30438200	-1.83387800	-1.51400000
H	-0.70431000	-4.97434100	0.27088200
C	2.20161800	3.56987500	-1.55056200
C	-0.03582700	3.41237200	-2.47538300
C	1.76314700	2.09234800	-3.42163100
C	2.67265800	4.62634600	-2.57634300
H	1.71769400	4.03005900	-0.68482900
H	3.03565200	2.96395300	-1.18490900
H	-0.69778800	2.72731000	-3.01172800
H	-0.51307100	3.66533400	-1.52622400
C	0.29310900	4.66837600	-3.31407000
C	1.93097500	3.20218800	-4.48454800
H	1.09041900	1.30062000	-3.76418500
H	2.72075700	1.62974500	-3.16941100
C	1.74538800	4.56232600	-3.79794300
H	2.64648400	5.62525000	-2.12839100
H	3.70680800	4.43262300	-2.88307400
H	-0.38980800	4.74276300	-4.16701000
H	0.16642500	5.57695100	-2.71423400

H	1.19126500	3.08615600	-5.28478600
H	2.92271800	3.13641900	-4.94429400
H	1.97670700	5.37437700	-4.49360400
N	1.20378800	2.64707200	-2.15798000

$Zn(OAc)_2$ / ABCO TSu

C	-1.98317200	1.04317700	0.49991000
C	-3.14797900	1.61882500	0.99431500
C	-4.33592200	1.52317800	0.26755100
C	-4.34864900	0.84899100	-0.95200500
C	-1.99360000	0.36116000	-0.71787700
C	-3.18165400	0.26537900	-1.44366000
C	-0.72200200	-0.26218400	-1.20812000
H	-1.05612900	1.12618000	1.05623300
H	-3.12943700	2.14218000	1.94602000
H	-3.19443600	-0.26287700	-2.39078500
H	-5.24672700	1.97399900	0.65082000
H	-5.26902400	0.77404500	-1.52364600
O	-0.86960100	-0.84766900	-2.40237500
O	0.40782200	0.17713500	-0.85076700
C	0.31859000	-1.36840500	-3.00213100
H	-0.00637000	-1.83375700	-3.93220100
H	0.77010000	-2.11220700	-2.34126100
H	1.02816800	-0.56327500	-3.20599500
Zn	1.22067900	1.96653600	-1.01247300
O	-0.74404000	-1.88059200	-0.10922500
C	-1.97990100	-2.54921000	-0.01827400
C	-1.82063700	-4.01111400	0.38007800
H	-2.46614300	-2.49660400	-1.00258300
H	-2.64602900	-2.03713000	0.69609000
H	-1.43624200	-4.11120100	1.40107800
H	-1.13094000	-4.52300200	-0.29977500
O	0.92843000	2.88896800	0.93278600
C	0.10312900	3.66430000	0.36962000
O	2.04534400	1.92793600	-2.99343500
C	3.16449400	1.65058200	-2.46928400
C	4.36310300	1.36413200	-3.33251500
C	-0.67934300	4.67594100	1.16039200
H	5.28706800	1.62372100	-2.81257300
H	4.29541500	1.90177300	-4.27994800
H	4.38319300	0.29013700	-3.54936600
H	-0.65185500	5.64762900	0.66057300
H	-0.29480800	4.76490500	2.17707600
H	-1.72555400	4.35355600	1.19871500
O	3.26243900	1.58057800	-1.20249700
O	-0.09005300	3.56595000	-0.88572000
H	-0.17735900	-1.68502800	0.97078400
H	-2.79039300	-4.52080500	0.34049000
C	1.32295000	-0.37764100	2.07144800
C	1.21209400	-2.78354900	2.32334300

C	-0.61595700	-1.39747100	3.12888000
C	2.15980700	-0.35510000	3.36992000
H	1.94051400	-0.43922900	1.17347600
H	0.70518600	0.51644300	1.97598000
H	0.57170100	-3.64575700	2.12487900
H	2.01789800	-2.79327200	1.58448500
C	1.75126300	-2.78120200	3.77085700
C	0.05463200	-1.09631700	4.48733000
H	-1.19067600	-2.32790800	3.15533900
H	-1.29269800	-0.59909300	2.81269800
C	1.56020800	-1.37218300	4.35228700
H	3.20462800	-0.61070800	3.16142200
H	2.14984200	0.64993500	3.80382900
H	1.21497900	-3.51434000	4.38352100
H	2.80970700	-3.05982200	3.77864200
H	-0.38267200	-1.72355600	5.27059900
H	-0.10851400	-0.05177500	4.77435500
H	2.04843100	-1.29407300	5.32772700
N	0.41573800	-1.55477400	2.07235900

$Zn(OAc)_2$ / ABCO I2b

C	-1.75188	-0.43211	1.24612
C	-2.39429	0.09425	2.36559
C	-3.58724	0.80021	2.22114
C	-4.13454	0.97353	0.94944
C	-2.29696	-0.26527	-0.02780
C	-3.49307	0.44221	-0.16782
C	-1.53818	-0.73666	-1.27320
H	-0.81539	-0.96863	1.36219
H	-1.95946	-0.04598	3.35143
H	-3.92060	0.57732	-1.15650
H	-4.08751	1.21307	3.09272
H	-5.06383	1.52316	0.82687
O	-2.50210	-1.20709	-2.18301
O	-0.75786	0.21040	-1.80564
C	-2.01116	-1.48559	-3.48481
H	-2.84877	-1.91746	-4.03561
H	-1.18728	-2.20947	-3.45652
H	-1.66928	-0.57381	-3.98292
Zn	0.66177	1.08497	-0.87401
O	-0.65851	-1.84116	-0.92053
C	-1.26425	-3.08903	-0.57386
C	-0.23485	-3.92875	0.15652
H	-1.61165	-3.59085	-1.48438
H	-2.13570	-2.90133	0.06300
H	0.09249	-3.42987	1.07449
H	0.64246	-4.11114	-0.47273
O	1.08201	1.32949	1.00748
C	0.37191	2.27270	1.53317
O	2.35284	-0.13484	-1.35080

C	2.51445	-1.12984	-2.06343
C	3.80643	-1.40135	-2.77022
C	0.54245	2.45686	3.02519
H	4.59306	-0.75889	-2.37544
H	3.66982	-1.18807	-3.83607
H	4.08404	-2.45330	-2.67359
H	-0.09861	3.25792	3.39629
H	1.58792	2.68913	3.25249
H	0.29558	1.52272	3.53942
O	1.58394	-2.02268	-2.28927
O	-0.39720	2.99013	0.87443
H	0.73090	-1.83870	-1.78593
H	-0.66955	-4.89720	0.42453
C	2.15505	3.54379	-1.52696
C	-0.08536	3.42333	-2.45159
C	1.70378	2.11527	-3.43194
C	2.63243	4.61853	-2.53097
H	1.67511	3.98885	-0.65123
H	2.98542	2.92471	-1.17555
H	-0.75086	2.75572	-3.00551
H	-0.56176	3.65597	-1.49694
C	0.25041	4.69862	-3.25746
C	1.86887	3.24822	-4.47032
H	1.02998	1.33092	-3.78881
H	2.66400	1.65056	-3.19509
C	1.69954	4.59277	-3.74996
H	2.61872	5.60708	-2.06011
H	3.66317	4.42127	-2.84687
H	-0.43550	4.80112	-4.10505
H	0.13367	5.59162	-2.63284
H	1.12074	3.15617	-5.26583
H	2.85568	3.18563	-4.94098
H	1.93503	5.41962	-4.42648
N	1.14997	2.64194	-2.15347

$Zn(OAc)_2$ / ABCO I2u

C	-1.98805	1.02733	0.35736
C	-3.17512	1.34689	1.00576
C	-4.39657	1.11979	0.37079
C	-4.42901	0.57280	-0.91238
C	-2.01919	0.47328	-0.92499
C	-3.24300	0.24518	-1.56140
C	-0.73917	0.10887	-1.56597
H	-1.03441	1.19446	0.84684
H	-3.14795	1.76756	2.00639
H	-3.26557	-0.18978	-2.55462
H	-5.32461	1.36862	0.87688
H	-5.37982	0.39734	-1.40589
O	-0.85610	-0.51534	-2.71248
O	0.36689	0.38532	-1.08460

C	0.36209	-0.92699	-3.35731
H	0.04662	-1.39460	-4.28774
H	0.88139	-1.64317	-2.71833
H	0.99480	-0.05883	-3.55091
Zn	1.43234	2.10824	-0.90874
O	-0.76116	-2.37356	-0.33458
C	-2.09570	-2.71082	-0.00340
C	-2.21232	-4.07399	0.66650
H	-2.66307	-2.70356	-0.94098
H	-2.53378	-1.93491	0.64349
H	-1.66705	-4.09003	1.61724
H	-1.79886	-4.85735	0.02178
O	0.97336	2.83076	1.02645
C	0.18517	3.67116	0.49310
O	2.26704	2.19815	-2.86220
C	3.33184	1.69977	-2.38731
C	4.48864	1.37284	-3.28999
C	-0.64382	4.59203	1.34265
H	5.42487	1.34527	-2.73033
H	4.55397	2.09424	-4.10677
H	4.31637	0.38236	-3.72586
H	-0.70759	5.58091	0.88345
H	-0.23834	4.66647	2.35243
H	-1.65945	4.18429	1.39995
O	3.39849	1.44665	-1.14260
O	0.07334	3.69631	-0.77163
H	-0.28734	-2.12812	0.50662
H	-3.26220	-4.31272	0.87405
C	1.42080	-0.59906	1.90034
C	1.19718	-2.90096	2.55363
C	-0.56997	-1.34292	3.02693
C	2.19523	-0.32952	3.21676
H	2.09770	-0.84257	1.07528
H	0.84874	0.28057	1.59528
H	0.51064	-3.75386	2.52941
H	2.00272	-3.11200	1.84241
C	1.75241	-2.66280	3.98284
C	0.05050	-0.87774	4.37062
H	-1.21423	-2.21750	3.16917
H	-1.18552	-0.55815	2.57600
C	1.55706	-1.17803	4.32736
H	3.25382	-0.59474	3.10918
H	2.15119	0.73418	3.47688
H	1.22483	-3.28658	4.71427
H	2.81424	-2.92874	4.03424
H	-0.41812	-1.39829	5.21350
H	-0.10953	0.19655	4.52119
H	2.01728	-0.94904	5.29382
N	0.47409	-1.71748	2.05757

$Zn(OAc)_2$ / Im I1b

C	-2.48352200	1.44039500	-0.28889300
C	-3.45341400	1.92322300	0.58349200
C	-4.58624600	1.15735900	0.85880700
C	-4.75166000	-0.09201500	0.25899100
C	-2.64882400	0.18999300	-0.89056900
C	-3.78696300	-0.57634800	-0.61806300
C	-1.60423300	-0.29676700	-1.81750900
H	-1.59809200	2.03007500	-0.50092500
H	-3.32482300	2.89549400	1.04902700
H	-3.90884500	-1.54816600	-1.08389700
H	-5.34174600	1.53411200	1.54208100
H	-5.63239100	-0.68858800	0.47584200
O	-1.95162200	-1.35797600	-2.51658300
O	-0.52145500	0.26193200	-1.99375100
C	-0.95222700	-1.91472700	-3.38629200
H	-1.40586800	-2.81158200	-3.80392800
H	-0.05735400	-2.16086400	-2.81078500
H	-0.70590200	-1.20310100	-4.17655200
Zn	1.21030400	0.97296900	-0.97057700
N	1.05147600	2.80238700	-1.85051100
O	-0.53714900	-1.99583500	0.11745100
C	-1.04305600	-3.31222800	-0.01768100
C	-0.35930800	-4.30286900	0.91544900
H	-0.94950700	-3.65309400	-1.05928600
H	-2.11280500	-3.25131800	0.20945600
H	-0.47559900	-3.99194600	1.95943300
H	0.71142100	-4.36836900	0.69122900
O	0.67216700	1.15291200	0.93070600
C	1.74540900	1.63537100	1.45054000
O	2.47145600	-0.09998700	-1.99038800
C	2.59945400	-1.37369200	-1.88105900
C	3.63527600	-1.99349900	-2.79676500
C	1.70742600	1.95483100	2.92535300
H	4.59303300	-1.47692700	-2.68470800
H	3.31610600	-1.86909400	-3.83705500
H	3.76048600	-3.05619300	-2.58371600
H	2.67881400	2.30588600	3.27604700
H	1.41017600	1.06568200	3.48931600
H	0.95309100	2.72648700	3.10976400
O	1.93936300	-2.09260200	-1.10794700
O	2.76559500	1.83750800	0.75880500
C	0.22520800	3.14223800	-2.82674500
C	1.77866100	3.93173800	-1.53421400
C	1.37715500	4.95935300	-2.33724800
N	0.39479400	4.43633000	-3.14541200
H	-0.11761900	4.93502900	-3.85954200
H	-0.48772800	2.48812700	-3.30495800
H	2.52563700	3.91265800	-0.75523600
H	1.69054900	5.98868900	-2.40654900
H	0.36672600	-1.96438200	-0.25963600

H	-0.79480900	-5.30247800	0.80043300

$Zn(OAc)_2$ / Im I1u

C	-1.76777300	0.72061800	0.48778200
C	-2.86052900	0.92049200	1.32218100
C	-4.15372500	0.83635600	0.80572300
C	-4.35290900	0.54759200	-0.54503400
C	-1.96553500	0.42842800	-0.86369700
C	-3.26163100	0.33862900	-1.38162000
C	-0.78297500	0.18297300	-1.71125200
H	-0.76064600	0.76347400	0.88635700
H	-2.70310500	1.13128200	2.37541600
H	-3.41326200	0.10492900	-2.42974800
H	-5.00843600	0.99175000	1.45737400
H	-5.35970700	0.48100400	-0.94526900
O	-1.05058900	-0.28450300	-2.90775600
O	0.38010100	0.39334700	-1.35026400
C	0.06884900	-0.54347400	-3.77476700
H	-0.37102800	-0.86440200	-4.71657600
H	0.68598100	-1.33442100	-3.34532500
H	0.65832500	0.36545000	-3.90685500
Zn	1.59975700	1.94973600	-0.85329300
N	0.55827300	-1.94508900	1.74215300
O	-0.83911000	-2.66255000	-0.66726400
C	-2.15793200	-2.87476300	-0.18529400
C	-2.31398300	-4.21419300	0.52201200
H	-2.81528700	-2.82412500	-1.05927900
H	-2.44770700	-2.05650400	0.49004700
H	-1.65670500	-4.26818500	1.39775600
H	-2.05912500	-5.04033000	-0.15073000
O	1.43041400	2.59246500	1.15079200
C	0.48398500	3.37502400	0.80469800
O	2.48571300	2.29808200	-2.75257200
C	3.46205100	1.57813300	-2.38348400
C	4.58392100	1.26576800	-3.33371900
C	-0.25902100	4.15787200	1.84759300
H	5.51547100	1.09594600	-2.79105400
H	4.70794300	2.06803200	-4.06306900
H	4.33087200	0.34690300	-3.87446900
H	-0.77602800	5.00919000	1.40316700
H	0.42001300	4.49009700	2.63536400
H	-1.00480800	3.49577800	2.30260800
O	3.46632200	1.09250900	-1.20762800
O	0.16252300	3.44119100	-0.41630500
C	1.31885100	-0.88327600	1.54911300
C	-0.22315200	-1.64036000	2.83655400
C	0.07835000	-0.38588800	3.29546500
N	1.06990900	0.07824600	2.46574800
H	1.41972500	1.03213700	2.41114800
H	2.04726600	-0.76262000	0.75994200

H	-0.95400900	-2.33797400	3.22126100
H	-0.31485500	0.20609300	4.10750100
H	-0.26519900	-2.51941000	0.11398300
H	-3.34723700	-4.34975500	0.86263500

$Zn(OAc)_2$ / Im TSb

C	-2.33121100	0.34364900	0.67308000
C	-3.35525700	0.70674900	1.54277000
C	-4.68763000	0.47006800	1.19851600
C	-4.98723600	-0.13387200	-0.02015800
C	-2.63013800	-0.26459500	-0.54966700
C	-3.96101400	-0.50346900	-0.89137500
C	-1.48774100	-0.61396900	-1.49486100
H	-1.29684400	0.53065500	0.94800000
H	-3.11315700	1.17591800	2.49242800
H	-4.19582900	-0.97729800	-1.83815100
H	-5.48598100	0.75495200	1.87801800
H	-6.02085600	-0.32206500	-0.29666500
O	-1.98619200	-1.34987700	-2.54785700
O	-0.67036400	0.34410000	-1.81291500
C	-1.09869400	-1.55926900	-3.64079300
H	-1.65575200	-2.16175400	-4.35900500
H	-0.20221500	-2.10201300	-3.32242600
H	-0.80594100	-0.60884300	-4.09349300
Zn	0.90589700	1.11874300	-0.94225600
N	1.07130400	2.77209300	-2.08216500
O	-0.59504700	-1.64320200	-0.63500600
C	-1.16534900	-2.92625600	-0.31650200
C	-0.49867500	-3.46754100	0.93227400
H	-1.03344200	-3.59395400	-1.17450500
H	-2.23525100	-2.77292200	-0.15755500
H	-0.65632500	-2.78796500	1.77550700
H	0.57748200	-3.59637000	0.78030600
O	0.88911900	1.17364300	1.00958900
C	1.83669300	1.88999800	1.52032100
O	2.43463400	-0.06317000	-1.54033600
C	2.52147600	-1.30222300	-1.73663100
C	3.80872300	-1.85383300	-2.29482200
C	1.85183300	1.94770000	3.03381100
H	4.62171900	-1.13571100	-2.18103500
H	3.66521600	-2.05872300	-3.36152500
H	4.06250000	-2.79727700	-1.80612300
H	2.67033800	2.57279400	3.39420600
H	1.95800900	0.93659600	3.43965500
H	0.89916800	2.34595000	3.39720000
O	1.59063200	-2.14366300	-1.52094600
O	2.68001500	2.49246900	0.83972500
C	0.33169400	2.99957100	-3.15641000
C	1.94494500	3.83301100	-1.96410900
C	1.72002300	4.70681800	-2.98768300

N	0.69671000	4.15925200	-3.72735100
H	0.28322000	4.55845800	-4.55850100
H	-0.45130400	2.35447500	-3.52535500
H	2.65090400	3.87702600	-1.14893200
H	2.17962200	5.64587200	-3.25145700
H	0.46115700	-1.78210300	-1.07776200
H	-0.92857500	-4.44248800	1.18417100

$Zn(OAc)_2$ / Im TSu

C	-1.86975400	0.89506800	0.70188300
C	-2.94232200	1.57620500	1.26850200
C	-4.13166200	1.72652000	0.55421500
C	-4.24056200	1.18793300	-0.72632600
C	-1.97642300	0.35231900	-0.58032000
C	-3.16762600	0.49863600	-1.29150700
C	-0.78439900	-0.38747100	-1.15935100
H	-0.94021700	0.79408900	1.25117000
H	-2.84746100	1.99511900	2.26637000
H	-3.25433000	0.08069700	-2.28855400
H	-4.96786500	2.26254500	0.99398800
H	-5.16210800	1.30307600	-1.28964300
O	-1.03147900	-0.71388400	-2.46384500
O	0.40281300	0.02604300	-0.84795400
C	0.06600900	-1.27366600	-3.18318400
H	-0.33098400	-1.53188200	-4.16528000
H	0.43358600	-2.17361400	-2.68142900
H	0.87406800	-0.54522900	-3.28475500
Zn	1.14833800	1.80992400	-1.10505700
N	0.23276400	-1.59956200	1.85689600
O	-0.80298600	-1.87164300	-0.41537900
C	-2.03659800	-2.60470900	-0.36535500
C	-1.73611200	-4.08070300	-0.18832400
H	-2.55130000	-2.41852500	-1.31099500
H	-2.65367400	-2.21351900	0.45196800
H	-1.19051100	-4.26726800	0.74233100
H	-1.13719800	-4.45453900	-1.02422300
O	0.98330100	2.78174800	0.85275300
C	0.13031100	3.54487500	0.31860400
O	1.97933200	1.88460500	-3.07471300
C	3.10458400	1.58814500	-2.57119400
C	4.29779600	1.36156400	-3.46027600
C	-0.60636500	4.57877600	1.12611000
H	5.22685100	1.56670100	-2.92548300
H	4.23222400	1.97769600	-4.35907800
H	4.30414600	0.31001400	-3.76864900
H	-0.58458700	5.54324400	0.61175700
H	-0.17970500	4.67711900	2.12509600
H	-1.65449100	4.27219800	1.21078500
O	3.21062800	1.45017300	-1.31231100
O	-0.13149200	3.42393100	-0.92325100

C	1.20073500	-0.73408400	2.10336300
C	-0.06205600	-2.22357400	3.04843900
C	0.74857400	-1.72068900	4.02578300
N	1.53724000	-0.78077600	3.40449400
H	2.24998300	-0.21628000	3.84566300
H	1.64667500	-0.07050900	1.37871600
H	-0.82913700	-2.97995400	3.12067900
H	0.83441100	-1.93822800	5.07841300
H	-0.34830700	-1.75679800	0.59766400
H	-2.67405300	-4.64415300	-0.15115400

$Zn(OAc)_2$ / Im I2b

C	-2.26250700	0.10141600	0.77550200
C	-3.23701200	0.65764600	1.60070600
C	-4.53686700	0.84160000	1.12745900
C	-4.85193800	0.46365300	-0.17653500
C	-2.57420700	-0.27968800	-0.53299600
C	-3.87547900	-0.09570400	-1.00213100
C	-1.45933300	-0.79919800	-1.44951800
H	-1.25025900	-0.02977400	1.14713700
H	-2.98027600	0.94773500	2.61612000
H	-4.12561900	-0.39169500	-2.01535000
H	-5.29747600	1.27508700	1.77094700
H	-5.86136200	0.60149200	-0.55468900
O	-2.08381900	-1.54001800	-2.47070600
O	-0.67471800	0.17104800	-1.92380000
C	-1.22653800	-1.97497600	-3.51252500
H	-1.86550500	-2.48395200	-4.23645900
H	-0.47223400	-2.68045300	-3.14251100
H	-0.72366000	-1.12907600	-3.99004700
Zn	0.67594600	1.11227000	-0.92575800
N	0.86573300	2.73754800	-2.10354200
O	-0.59338700	-1.69453200	-0.69388300
C	-1.16733200	-2.90512100	-0.19591700
C	-0.31171200	-3.39712500	0.95481700
H	-1.21331000	-3.64465000	-1.00457000
H	-2.19059200	-2.70533200	0.14002500
H	-0.29400800	-2.65866600	1.76291200
H	0.71731600	-3.58238200	0.62930900
O	0.89962800	1.01084400	0.99176800
C	1.71471600	1.83648700	1.56394300
O	2.42264600	0.05991200	-1.55070100
C	2.67530300	-1.11603700	-1.82105000
C	4.00806300	-1.54628800	-2.35325000
C	1.84645800	1.65270800	3.06286400
H	4.68227700	-0.69294600	-2.41618000
H	3.87600300	-1.98981000	-3.34472200
H	4.43407400	-2.31430700	-1.70160100
H	2.51939700	2.39729100	3.49114400
H	2.22944700	0.64963800	3.27700600

H	0.86179300	1.73269300	3.53411600
O	1.82403300	-2.10321800	-1.67819500
O	2.35047000	2.71325800	0.96314300
C	0.22291100	2.86817800	-3.25359800
C	1.66121400	3.85481100	-1.95815000
C	1.48821800	4.66430900	-3.04291800
N	0.57531800	4.02040200	-3.84711400
H	0.22364300	4.35402100	-4.73378200
H	-0.48182100	2.15831200	-3.65965400
H	2.28061600	3.97767000	-1.08275100
H	1.91706400	5.61661500	-3.31103600
H	0.92494400	-1.82120800	-1.32583400
H	-0.71924800	-4.33435500	1.34780000

$Zn(OAc)_2$ / Im I2u

C	-2.55357600	1.28128900	0.75858000
C	-3.65913800	2.10529300	0.94768900
C	-4.60674800	2.24794100	-0.06745900
C	-4.44162600	1.55469900	-1.26477800
C	-2.37903000	0.59089300	-0.44322000
C	-3.33394700	0.72561500	-1.45026600
C	-1.14151300	-0.29919300	-0.58520100
H	-1.80625500	1.18317400	1.54001100
H	-3.77793800	2.64350400	1.88426000
H	-3.20705400	0.18925200	-2.38442200
H	-5.46705800	2.89602700	0.07537300
H	-5.17523900	1.65845100	-2.05967300
O	-1.04053700	-0.65103100	-1.95135900
O	-0.01965900	0.23244300	-0.08562800
C	0.08543700	-1.44909100	-2.27461000
H	0.03819600	-1.61954500	-3.35164800
H	0.05183800	-2.41481100	-1.75440300
H	1.02065000	-0.93746600	-2.02419700
Zn	0.70279700	1.91306800	-0.64471900
N	1.18366900	-2.11092000	1.23199100
O	-1.32751500	-1.50492000	0.19327100
C	-2.42885300	-2.34794700	-0.12777200
C	-2.23847100	-3.66225700	0.60358900
H	-2.46808000	-2.50518300	-1.21189000
H	-3.36151400	-1.85873400	0.18138700
H	-2.16680300	-3.50005500	1.68444000
H	-1.32909500	-4.16862000	0.26156900
O	0.12287900	3.49346400	0.68554300
C	-0.60918800	3.96221700	-0.23694600
O	2.21812500	1.83832200	-2.09344300
C	3.10515000	1.59285800	-1.21879200
C	4.52536500	1.31844400	-1.63761800
C	-1.51395500	5.13618400	0.02632100
H	5.22486900	1.77960800	-0.93666700
H	4.71442500	1.67580100	-2.65099800

H	4.69106300	0.23548000	-1.61117900
H	-1.58403600	5.77479400	-0.85704100
H	-1.16997700	5.71382000	0.88591200
H	-2.51612600	4.74902600	0.24361600
O	2.78446900	1.54658500	0.00637500
O	-0.60500200	3.41412400	-1.38189500
C	2.24326300	-1.31420300	1.18622600
C	1.52188800	-3.29754800	1.84168800
C	2.83767400	-3.21004700	2.17597400
N	3.25854800	-1.96645900	1.75589200
H	4.19292400	-1.59275200	1.85790900
H	2.28106400	-0.31712400	0.76276500
H	0.80747300	-4.09154800	1.98668200
H	3.49904000	-3.90584500	2.66535600
H	0.25464900	-1.85506700	0.84954700
H	-3.08892100	-4.32430400	0.41191600

$Zn(OAc)_2$ / DMA I1b

C	-2.62444	1.14184	0.29671
C	-3.56379	1.41544	1.28568
C	-4.71621	0.63660	1.39189
C	-4.93024	-0.42334	0.50952
C	-2.84080	0.08124	-0.58812
C	-3.99385	-0.70488	-0.47945
C	-1.83067	-0.19397	-1.62925
H	-1.71857	1.73754	0.23424
H	-3.39294	2.23525	1.97672
H	-4.15445	-1.53011	-1.16459
H	-5.44800	0.85313	2.16474
H	-5.82568	-1.03134	0.59352
O	-2.09954	-1.22941	-2.39195
O	-0.83999	0.51369	-1.83980
C	-1.10799	-1.59832	-3.36561
H	-1.51511	-2.47349	-3.86780
H	-0.17273	-1.84160	-2.85671
H	-0.95222	-0.78190	-4.07259
Zn	0.98364	1.05745	-1.07390
O	-0.45909	-1.86365	0.15202
C	-1.06383	-3.14044	0.03173
C	-0.40390	-4.18734	0.91888
H	-1.04745	-3.47124	-1.01718
H	-2.11357	-3.00710	0.31437
H	-0.44292	-3.88160	1.97004
H	0.64628	-4.32665	0.63794
O	1.70257	1.24763	0.71243
C	1.16707	2.13720	1.48408
O	2.21077	0.01878	-2.18828
C	2.49304	-1.22540	-2.03181
C	3.57162	-1.75468	-2.95403
C	1.94511	2.43632	2.74776

H	4.46488	-1.12704	-2.88297
H	3.21725	-1.70290	-3.98900
H	3.82422	-2.78780	-2.71096
H	1.34114	3.01127	3.45167
H	2.83127	3.02304	2.47951
H	2.29151	1.51172	3.21711
O	1.94130	-1.98178	-1.21179
O	0.11486	2.73529	1.22003
H	0.42074	-1.88903	-0.27915
H	-0.91496	-5.15212	0.81887
N	1.04082	2.94871	-2.07074
C	-0.25035	3.63879	-1.86910
H	-1.03597	3.01222	-2.29406
H	-0.43960	3.75840	-0.80223
H	-0.26008	4.61224	-2.37552
C	1.21965	2.70560	-3.52540
H	2.13246	2.14254	-3.71064
H	0.37212	2.11750	-3.88412
H	1.25770	3.66016	-4.06452
C	2.18308	3.65164	-1.50338
C	3.44864	3.05968	-1.60513
C	2.05300	4.86311	-0.82491
C	4.56065	3.67533	-1.04384
H	3.56266	2.09833	-2.09781
C	3.17432	5.47265	-0.25795
H	1.08953	5.34444	-0.71486
C	4.43105	4.88786	-0.36522
H	5.53202	3.19694	-1.12868
H	3.05205	6.41357	0.27061
H	5.29974	5.36512	0.07811

$Zn(OAc)_2$ / DMA l1u

C	-2.41427	1.11212	1.02774
C	-3.32210	2.10124	1.39510
C	-4.19685	2.63293	0.44664
C	-4.15417	2.16521	-0.86527
C	-2.36732	0.63741	-0.28413
C	-3.24559	1.16987	-1.22782
C	-1.36992	-0.47922	-0.61610
H	-1.72638	0.70895	1.76390
H	-3.34234	2.46251	2.41961
H	-3.21554	0.80735	-2.24931
H	-4.90321	3.40882	0.72859
H	-4.82888	2.57507	-1.61198
O	-1.36301	-0.60093	-2.02125
O	-0.13623	-0.26146	-0.09714
C	-0.46114	-1.55747	-2.54872
H	-0.69252	-1.63769	-3.61263
H	-0.59676	-2.53726	-2.07529
H	0.57844	-1.23169	-2.43047

Zn	1.00064	1.22456	-0.59089
O	-1.78101	-1.70693	-0.02144
C	-3.05463	-2.21403	-0.39784
C	-3.23286	-3.56158	0.27358
H	-3.10814	-2.31248	-1.48934
H	-3.84271	-1.51693	-0.08261
H	-3.19656	-3.46204	1.36338
H	-2.44712	-4.25738	-0.03954
O	0.33614	3.02607	0.42069
C	-0.13069	3.39963	-0.69269
O	2.70401	0.43853	-1.62876
C	3.31429	0.34808	-0.52179
C	4.69893	-0.23679	-0.44755
C	-1.00115	4.62254	-0.78851
H	5.41920	0.57442	-0.29533
H	4.95180	-0.77005	-1.36490
H	4.76989	-0.91292	0.40872
H	-0.92287	5.08421	-1.77471
H	-0.74929	5.34342	-0.00845
H	-2.03958	4.30298	-0.63976
O	2.75423	0.76600	0.53844
O	0.09812	2.70459	-1.73568
H	0.36218	-1.24905	1.08181
H	-4.20236	-3.99043	-0.00041
N	0.80352	-1.75241	1.91162
C	1.13971	-0.67389	2.88475
H	1.90884	-0.04417	2.43843
H	0.23362	-0.09427	3.06331
H	1.48079	-1.11184	3.82308
C	-0.21703	-2.68976	2.46273
H	-1.10221	-2.11411	2.73262
H	-0.47308	-3.41347	1.69074
H	0.19854	-3.18988	3.33908
C	1.97740	-2.47947	1.40451
C	2.06310	-2.69711	0.03519
C	2.94405	-2.96636	2.27704
C	3.14061	-3.41757	-0.47351
H	1.30144	-2.29279	-0.62151
C	4.02055	-3.68282	1.75751
H	2.87372	-2.80093	3.34707
C	4.12000	-3.91104	0.38562
H	3.21507	-3.58228	-1.54387
H	4.78160	-4.06350	2.43130
H	4.96254	-4.46829	-0.01198

$Zn(OAc)_2$ / DMA TSb

C	-1.72227100	-0.28387200	1.20958900
C	-2.40147000	0.16942900	2.33755200
C	-3.68006500	0.71216200	2.21562000
C	-4.27682200	0.79586500	0.95843900

C	-2.31781900	-0.20242500	-0.05109400
C	-3.59931900	0.33859400	-0.17079500
C	-1.55008100	-0.57873200	-1.31109800
H	-0.72318500	-0.69479000	1.30856200
H	-1.92924200	0.09851200	3.31330800
H	-4.06590800	0.40468300	-1.14843100
H	-4.20871400	1.06705100	3.09571400
H	-5.27279100	1.21682500	0.85438300
O	-2.42233000	-1.10679500	-2.23087700
O	-0.71359500	0.30240100	-1.78012000
C	-1.90517700	-1.27341800	-3.54895400
H	-2.69341700	-1.77514900	-4.11063400
H	-1.00357500	-1.89571800	-3.54163000
H	-1.67429200	-0.30667800	-4.00228200
Zn	0.82816100	1.06517600	-0.87730000
O	-0.61938500	-1.80905800	-0.84932700
C	-1.22822300	-3.09719500	-0.63500800
C	-0.34964600	-3.91245700	0.29188000
H	-1.37014300	-3.58672100	-1.60348500
H	-2.20873200	-2.90980100	-0.19172100
H	-0.23467300	-3.40894500	1.25655400
H	0.64162300	-4.07174300	-0.14341300
O	1.16017700	1.45602900	1.00124200
C	0.41504200	2.44244700	1.37804300
O	2.34756900	-0.21040200	-1.28703400
C	2.40537100	-1.28719500	-1.94537100
C	3.72148900	-1.64305700	-2.59014100
C	0.52850000	2.82860300	2.83544800
H	4.55433800	-1.26282900	-1.99552700
H	3.76161800	-1.16210600	-3.57454800
H	3.81195500	-2.72128400	-2.73201400
H	-0.04723600	3.73067600	3.04787900
H	1.57760900	2.98579600	3.10303900
H	0.15156800	2.00685100	3.45379000
O	1.43134800	-2.07903000	-2.12400100
O	-0.35534600	3.03388300	0.60501000
H	0.31579000	-1.86492400	-1.45478700
H	-0.81031300	-4.89076300	0.46233000
N	1.32463600	2.61544800	-2.25446800
C	0.05082600	3.26254900	-2.63095000
H	-0.60500500	2.49484400	-3.04416300
H	-0.42041200	3.68428300	-1.74278500
H	0.20995700	4.04082000	-3.38788700
C	1.91543000	2.00044000	-3.47017900
H	2.84650000	1.49234900	-3.22417400
H	1.20909800	1.26870600	-3.86977800
H	2.10990700	2.77171800	-4.22584100
C	2.27617800	3.50505100	-1.60525900
C	3.45424100	2.94967700	-1.09129800
C	2.04794000	4.87287200	-1.46057300
C	4.38907800	3.75321200	-0.45010200

H	3.62977800	1.88049000	-1.17437000
C	2.98882100	5.67339300	-0.80889000
H	1.14313400	5.33377100	-1.83721200
C	4.16170000	5.12260400	-0.30415300
H	5.29466700	3.30362400	-0.05328400
H	2.79313200	6.73623500	-0.70037700
H	4.88982700	5.74914100	0.20215400

$Zn(OAc)_2$ / DMA TSu

C	-1.97589000	1.14283900	0.57902100
C	-3.09919700	1.83148900	1.02556300
C	-4.26700900	1.82956000	0.26199300
C	-4.30115400	1.13582000	-0.94624400
C	-2.00778700	0.44165000	-0.62721600
C	-3.17660600	0.43994100	-1.38907700
C	-0.76867300	-0.31885400	-1.05714200
H	-1.05921700	1.16710900	1.15889300
H	-3.06159400	2.37252300	1.96676800
H	-3.20667500	-0.09985700	-2.32932600
H	-5.14453400	2.36913100	0.60626700
H	-5.20541200	1.13366200	-1.54791300
O	-0.91873900	-0.76487100	-2.33969500
O	0.38857700	0.12531700	-0.69465000
C	0.22936700	-1.38392000	-2.91810100
H	-0.09330200	-1.74055200	-3.89653300
H	0.55853300	-2.22739400	-2.30370500
H	1.04187700	-0.66216500	-3.03026200
Zn	1.18236100	1.87689900	-0.96620100
O	-0.83475900	-1.73531600	-0.18453200
C	-2.04563300	-2.50303100	-0.16112700
C	-1.73054400	-3.95876100	0.12665100
H	-2.49697300	-2.39519900	-1.15052300
H	-2.73104700	-2.07755500	0.58118500
H	-1.28375000	-4.09084400	1.11713200
H	-1.03550700	-4.35532200	-0.61960400
O	0.97612600	2.93687100	0.92227300
C	0.19590700	3.72998700	0.32134000
O	2.02626100	1.83369300	-2.95575000
C	3.14400500	1.57920000	-2.41941500
C	4.35718600	1.30718600	-3.26836400
C	-0.50321400	4.83881900	1.05988100
H	5.26472800	1.64755900	-2.76568300
H	4.26303300	1.78320900	-4.24586900
H	4.43884500	0.22473300	-3.41835500
H	-0.49097200	5.75713400	0.46781100
H	-0.04691500	5.01214900	2.03536800
H	-1.55059100	4.55074800	1.20367400
O	3.23392300	1.51994400	-1.15149100
O	-0.03092700	3.56737600	-0.92114400
H	-0.32353100	-1.62114900	0.81292400

H	-2.65521200	-4.54380400	0.09085100
N	0.32505800	-1.63702200	2.05898500
C	1.25073500	-0.48805900	2.18716300
H	1.97543200	-0.50590200	1.37450000
H	0.68523700	0.44152700	2.11707300
H	1.76876900	-0.53221700	3.15259100
C	-0.75427400	-1.53819900	3.05482500
H	-1.33034800	-0.63515800	2.84062400
H	-1.41581100	-2.40341100	2.97252100
H	-0.36480100	-1.47163100	4.07701700
C	1.05089500	-2.89358800	2.05745800
C	1.82345800	-3.18569700	0.92923900
C	0.98088600	-3.80810700	3.10577600
C	2.52374800	-4.38379400	0.85475900
H	1.85900100	-2.47921100	0.10466200
C	1.68122200	-5.01336100	3.02110000
H	0.38669100	-3.60306500	3.98924000
C	2.45346900	-5.30537700	1.90107700
H	3.11734100	-4.60275800	-0.02781400
H	1.61815700	-5.72235200	3.84125600
H	2.99521300	-6.24434700	1.83985600

$Zn(OAc)_2$ / DMA I2b

C	-1.72882	-0.37028	1.24806
C	-2.35209	0.17977	2.36670
C	-3.53128	0.90909	2.22304
C	-4.08401	1.08076	0.95359
C	-2.27718	-0.20070	-0.02467
C	-3.46017	0.52804	-0.16343
C	-1.53060	-0.69310	-1.26911
H	-0.80466	-0.92845	1.36277
H	-1.91371	0.03879	3.35091
H	-3.89078	0.66401	-1.15056
H	-4.01742	1.34002	3.09384
H	-5.00345	1.64698	0.83225
O	-2.50468	-1.12147	-2.18767
O	-0.71351	0.22884	-1.79365
C	-2.01448	-1.41620	-3.48634
H	-2.86415	-1.81270	-4.04511
H	-1.22058	-2.17261	-3.45310
H	-1.63230	-0.51755	-3.97895
Zn	0.72693	1.06247	-0.87206
O	-0.69644	-1.83129	-0.91755
C	-1.35439	-3.05346	-0.57241
C	-0.36601	-3.93244	0.16826
H	-1.71477	-3.54276	-1.48463
H	-2.22216	-2.82859	0.05718
H	-0.02550	-3.44465	1.08739
H	0.50779	-4.15357	-0.45331
O	1.23156	1.35922	1.00430

C	0.48028	2.35055	1.34168
O	2.36201	-0.24588	-1.28777
C	2.51450	-1.25603	-1.98204
C	3.82279	-1.58254	-2.63264
C	0.57327	2.82075	2.77215
H	4.61337	-0.95541	-2.22138
H	3.73367	-1.39090	-3.70757
H	4.06341	-2.63996	-2.50193
H	0.01631	3.74765	2.91602
H	1.61974	2.96568	3.05511
H	0.15790	2.04744	3.42739
O	1.56032	-2.11497	-2.23281
O	-0.29461	2.88388	0.52407
H	0.70001	-1.89381	-1.75599
H	-0.84289	-4.88100	0.43561
N	1.31796	2.57835	-2.25986
C	0.04911	3.19717	-2.69773
H	-0.58112	2.40967	-3.11388
H	-0.45957	3.63630	-1.83895
H	0.22352	3.95927	-3.46754
C	1.96748	1.95979	-3.44273
H	2.90671	1.48877	-3.15673
H	1.29762	1.19995	-3.85291
H	2.16450	2.72267	-4.20624
C	2.22756	3.49577	-1.58949
C	3.37892	2.96530	-0.99635
C	1.98638	4.86635	-1.50392
C	4.27521	3.79509	-0.33384
H	3.56407	1.89560	-1.03556
C	2.88745	5.69384	-0.83022
H	1.10125	5.30932	-1.94367
C	4.03405	5.16698	-0.24563
H	5.16045	3.36444	0.12499
H	2.68181	6.75851	-0.76798
H	4.73120	5.81434	0.27779

$Zn(OAc)_2$ / DMA I2u

C	-1.97463	1.17420	0.36876
C	-3.14592	1.46325	1.05913
C	-4.38283	1.22880	0.45754
C	-4.44665	0.70589	-0.83445
C	-2.03724	0.64480	-0.92293
C	-3.27649	0.41021	-1.52617
C	-0.77188	0.31385	-1.60961
H	-1.00812	1.35182	0.82942
H	-3.09447	1.86753	2.06548
H	-3.32319	-0.00598	-2.52653
H	-5.29844	1.45360	0.99642
H	-5.40952	0.52438	-1.30168
O	-0.91332	-0.23666	-2.78994

O	0.34436	0.55458	-1.12989
C	0.28915	-0.62702	-3.47714
H	-0.04852	-1.04762	-4.42208
H	0.81400	-1.37684	-2.88272
H	0.92561	0.24431	-3.64192
Zn	1.43976	2.26783	-0.98086
O	-0.78971	-2.18679	-0.52942
C	-2.08795	-2.62493	-0.16071
C	-2.08294	-4.01565	0.45955
H	-2.68396	-2.62065	-1.07924
H	-2.54866	-1.90012	0.52778
H	-1.48345	-4.03528	1.37725
H	-1.65937	-4.74632	-0.23809
O	0.99197	2.98414	0.96113
C	0.20361	3.82773	0.43309
O	2.26685	2.35321	-2.93796
C	3.32802	1.84313	-2.46729
C	4.47960	1.50746	-3.37310
C	-0.62089	4.74699	1.28868
H	5.41777	1.47797	-2.81678
H	4.54500	2.22494	-4.19324
H	4.30135	0.51566	-3.80356
H	-0.71633	5.72696	0.81651
H	-0.19139	4.84450	2.28657
H	-1.62596	4.31941	1.37986
O	3.39466	1.58563	-1.22339
O	0.08674	3.85641	-0.83131
H	-0.28759	-2.00691	0.29718
H	-3.10352	-4.32648	0.71166
N	0.55837	-1.75046	1.95908
C	1.54335	-0.68275	1.75355
H	2.25985	-0.95760	0.97926
H	1.02565	0.21902	1.42015
H	2.09009	-0.45902	2.68260
C	-0.49419	-1.32449	2.87371
H	-0.92956	-0.39852	2.49147
H	-1.28651	-2.07645	2.91635
H	-0.12305	-1.13659	3.89369
C	1.11567	-3.03742	2.20125
C	1.99739	-3.58583	1.25475
C	0.77148	-3.81093	3.31634
C	2.52036	-4.86144	1.42553
H	2.25469	-3.02099	0.36374
C	1.29256	-5.09700	3.47537
H	0.09652	-3.42522	4.07178
C	2.17054	-5.63034	2.53806
H	3.19569	-5.26353	0.67538
H	1.00655	-5.67798	4.34788
H	2.57448	-6.63016	2.66567

4.4.4. Energies of Optimised Structures

Supporting Table S4.1. Double-Zeta and Triple-Zeta Energies for calculated structures.

Structure	**6-31+G(d) (Double-Zeta) Energy / Hartree**	**6-311+G(d) (Triple-Zeta) Energy / Hartree**
$Zn(OAc)_2$ / ABCO I1b	-3180.022956	-
$Zn(OAc)_2$ / ABCO I1u	-3180.017455	-
$Zn(OAc)_2$ / ABCO TSb	-3179.997370	-
$Zn(OAc)_2$ / ABCO TSu	-3179.992781	-
$Zn(OAc)_2$ / ABCO I2b	-3180.003178	-
$Zn(OAc)_2$ / ABCO I2u	-3180.016207	-
$Zn(OAc)_2$ / Im I1b	-3077.073222	-3077.513176
$Zn(OAc)_2$ / Im I1u	-3077.057387	-3077.499292
$Zn(OAc)_2$ / Im TSb	-3077.042957	-3077.482120
$Zn(OAc)_2$ / Im TSu	-3077.030221	-3077.469812
$Zn(OAc)_2$ / Im I2b	-3077.046154	-3077.486211
$Zn(OAc)_2$ / Im I2u	-3077.045613	-3077.485828
$Zn(OAc)_2$ / DMA I1b	-3216.918131	-
$Zn(OAc)_2$ / DMA I1u	-3216.899562	-
$Zn(OAc)_2$ / DMA TSb	-3216.890126	-
$Zn(OAc)_2$ / DMA TSu	-3216.883237	-
$Zn(OAc)_2$ / DMA I2b	-3216.893323	-
$Zn(OAc)_2$ / DMA I2u	-3216.914984	-

4.4.5. Imaginary Frequencies of Transition States

Supporting Table S4.2. Double-Zeta and Triple-Zeta Frequencies for calculated TSs.

Structure	**6-31+G(d) (Double-Zeta) Frequency / cm^{-1}**	**6-311+G(d) (Triple-Zeta) Frequency / cm^{-1}**
$Zn(OAc)_2$ / ABCO TSb	-412.52	-
$Zn(OAc)_2$ / ABCO TSu	-1056.05	-
$Zn(OAc)_2$ / Im TSb	-764.58	-903.63
$Zn(OAc)_2$ / Im TSu	-446.05	-521.75
$Zn(OAc)_2$ / DMA TSb	-408.09	-
$Zn(OAc)_2$ / DMA TSu	-632.40	-

4.5. References

1. G. R. Lima, W. F. Monteiro, R. Ligabue and R. M. C. Santana, *Materials Research*, 2017, **20**, 588-595.
2. U. R. Vaidya and V. M. Nadkarni, *Journal of Applied Polymer Science*, 1988, **35**, 775-785.
3. D. Paszun and T. Spychaj, *Industrial & Engineering Chemistry Research*, 1997, **36**, 1373-1383.
4. G. Xi, M. Lu and C. Sun, *Polymer Degradation and Stability*, 2005, **87**, 117-120.
5. K. Fukushima, O. Coulembier, J. M. Lecuyer, H. A. Almegren, A. M. Alabdulrahman, F. D. Alsewailem, M. A. McNeil, P. Dubois, R. M. Waymouth, H. W. Horn, J. E. Rice and J. L. Hedrick, *Journal of Polymer Science Part A: Polymer Chemistry*, 2011, **49**, 1273-1281.
6. H. W. Horn, G. O. Jones, D. S. Wei, K. Fukushima, J. M. Lecuyer, D. J. Coady, J. L. Hedrick and J. E. Rice, *The Journal of Physical Chemistry A*, 2012, **116**, 12389-12398.
7. Q. Wang, X. Yao, Y. Geng, Q. Zhou, X. Lu and S. Zhang, *Green Chemistry*, 2015, **17**, 2473-2479.
8. Y. Liu, X. Yao, H. Yao, Q. Zhou, J. Xin, X. Lu and S. Zhang, *Green Chemistry*, 2020, **x**, xx.
9. C. Jehanno, J. Demarteau, D. Mantione, M. C. Arno, F. Ruipérez, J. L. Hedrick, A. P. Dove and H. Sardon, *Angewandte Chemie International Edition*, 2021, **60**, 6710-6717.
10. J.-D. Chai and M. Head-Gordon, *Physical Chemistry Chemical Physics*, 2008, **10**, 6615.
11. A. D. Becke, *The Journal of Chemical Physics*, 1997, **107**, 8554-8560.
12. S. Grimme, *Journal of Computational Chemistry*, 2006, **27**, 1787-1799.
13. Y. Minenkov, Å. Singstad, G. Occhipinti and V. R. Jensen, *Dalton Transactions*, 2012, **41**, 5526-5541.
14. S. E. Wheeler and K. N. Houk, *Journal of Chemical Theory and Computation*, 2010, **6**, 395-404.
15. V. A. Rassolov, M. A. Ratner, J. A. Pople, P. C. Redfern and L. A. Curtiss, *Journal of Computational Chemistry*, 2001, **22**, 976-984.
16. V. A. Rassolov, J. A. Pople, M. A. Ratner and T. L. Windus, *The Journal of Chemical Physics*, 1998, **109**, 1223-1229.
17. T. Clark, J. Chandrasekhar, G. W. Spitznagel and P. V. R. Schleyer, *Journal of Computational Chemistry*, 1983, **4**, 294-301.
18. M. Cossi, N. Rega, G. Scalmani and V. Barone, *Journal of Computational Chemistry*, 2003, **24**, 669-681.
19. P. Jaramillo, P. Pérez and P. Fuentealba, *Journal of Physical Organic Chemistry*, 2007, **20**, 1050-1057.
20. W. Kohn and L. J. Sham, *Physical Review*, 1965, **140**, A1133-A1138.

5. Effect of Impurities in PET Glycolysis

5.1. Introduction

Investigation into the effect of impurities in PET glycolysis processes are as old as the field itself. Such examples began with Baliga and Wong's study into glycolysis of green PET flakes, which reportedly had no notable difference from undyed PET flakes.[2] Lopez-Fonseca *et al.*[3] extended the concept to amber, silver, blue, white and multi-layered PET sources. Amber and silver appeared to have had little effect on the BHET yield, whereas blue and white had only a small effect (*ca.* 5% drop in BHET yield), although the authors report the use of coloured PET discoloured the glycolysed product (*i.e.* monomer). Multilayer PET reduced the BHET yield by almost 10%, which is unsurprising as the fused layers are more difficult for the reaction solution to access. A later study into the feasibility of glycolysis of coloured and mixed-material PET sources indicates BHET yield drops by around 5-15% for both compounding factors (Figure 5.1.),[4] confirming these results.

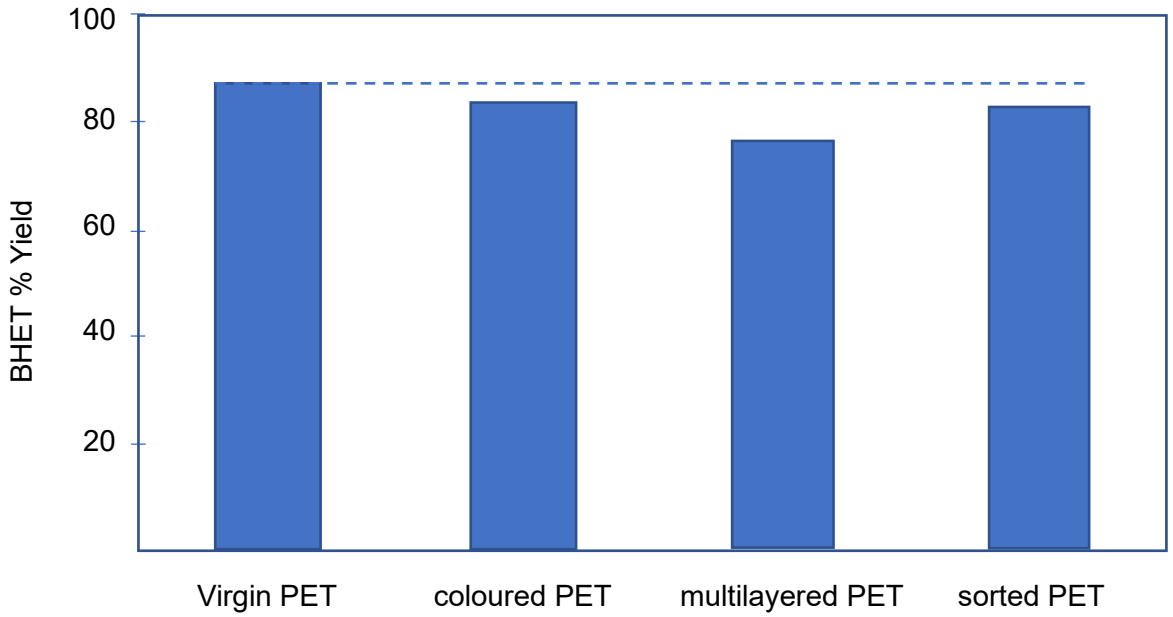


Figure 5.1. BHET yields of $Zn(OAc)_2$-catalysed glycolysis for various PET sources. Adapted with permission from Aguado *et al.*[6, 7]

In 2023, Li *et al*.[5] displayed a study comparing zinc acetate ($Zn(OAc)_2$) and Zn-doped magnetic nanoparticles (MNPs) as combination glycolysis catalysts and decolourants for PET textile waste. It was shown that the MNPs provided significantly higher decolourising properties and slightly lower glycolysis times than $Zn(OAc)_2$ alone. However, this study coloured the textiles using known anthraquinone and azo dyes, rather than using postconsumer pre-dyed material, and also provided increased decolourant activity by an electro-Fenton oxidation process. One advantage of this colouration method is the authors knew the composition of the dyestuffs before and after depolymerisation.

Liu *et al.* reported a selective and mild method of undyed polyester/cotton blend (PCB) glycolysis using betaine-based deep eutectic solvents, selectively degrading PET out of the blend and leaving cotton nearly unaffected.[6] There was approx. 5% mass loss of cotton, and no visible cracking under scanning electron microscopy; the BHET yield was 85%.

In this study the glycolysis of PET will be extended into postconsumer mixed-fibre materials, both undyed and pre-dyed, using a screen of industrially relevant catalysts. A purely chemical method of isolating white BHET from dyed PCBs was also developed. The effect of common flame retardant tris(1,3-dichloro-2-propyl)phosphate[7] (TDCPP) on PET glycolysis was investigated. It is hypothesised based on the literature that dyes and flame retardants will both have small negative effects on the catalyst activity, in the realm of 5-15%.

5.2. Results and Discussion

5.2.1. Undyed PCB Glycolysis

Undyed PCB fabric (in a 65:35 polyester:cotton ratio by weight) was sourced from Navato Textiles. The undyed PCB was depolymerised using a variety of industrial- and research-relevant catalysts, and compared with the most efficient catalysts derived from Chapter 3. The

catalysts used were $Zn(OAc)_2$ (a staple research catalyst); $Zn(OAc)_2$ / urea (in a 1:4 molar ratio), developed by Wang *et al.*[8] and included as the most rapid catalyst developed at the time of this work; 1-butyl-3-methylimidazole·$FeCl_4$ (bmim·$FeCl_4$) developed and employed industrially by Ioniqa technologies;[9, 10] $Zn(OAc)_2$ / DMAP, which was shown by Delle Chiaie *et al*. to be the most effective of the metal salt / base combinations they tried;[11] and finally, $Zn(OAc)_2$ / Im and $Mg(OAc)_2$ / MTBD from the study in Chapter 3 (the most efficient catalysts for $Zn(OAc)_2$ and $Mg(OAc)_2$ respectively). Each study was conducted using 10 mol% of catalyst.

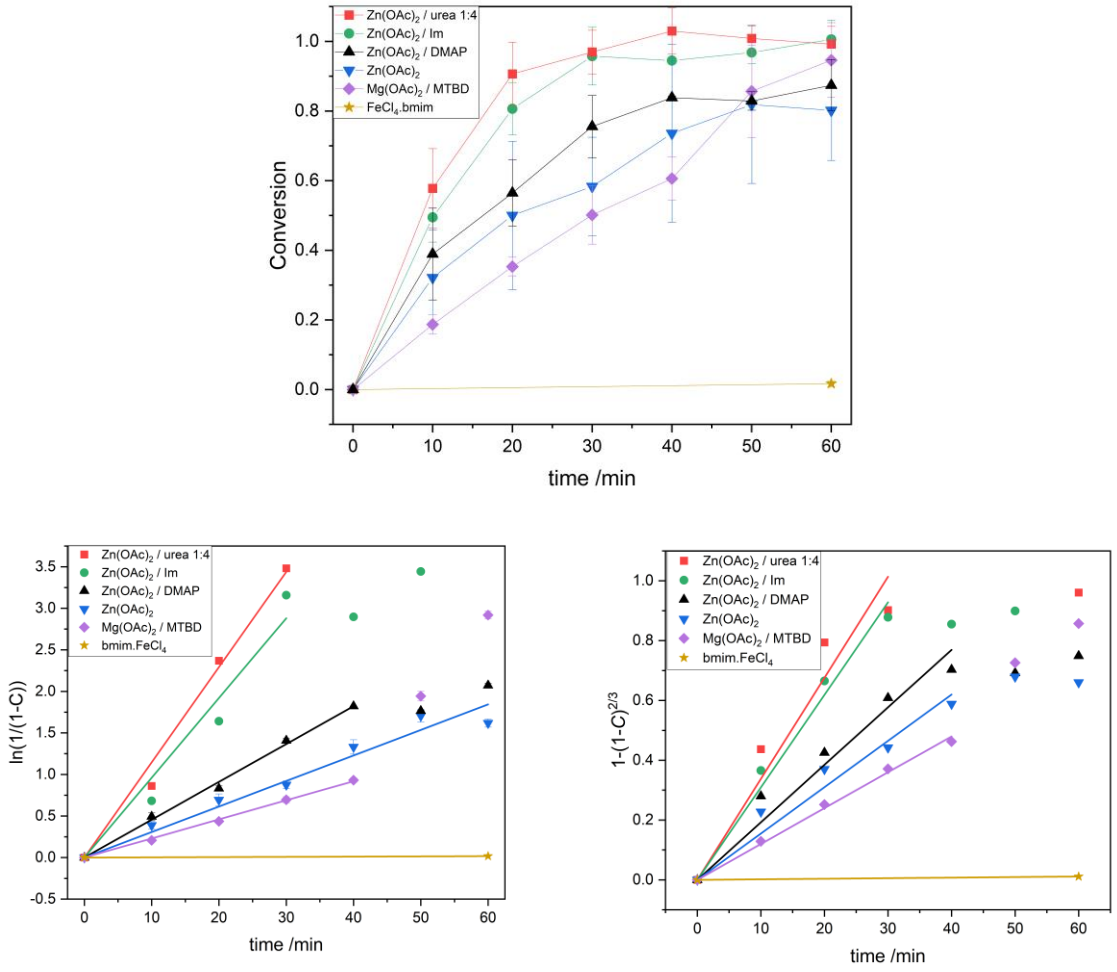


Figure 5.2. Depolymerisation kinetics of undyed PCB with various catalysts (10 mol% loading); a) conversion-time plot; b) Model 1 semi-log plot; c) Model 2 plot.

It was found that the most active catalysts were $Zn(OAc)_2$ / urea and $Zn(OAc)_2$ / Im (Figure 5.2); the values of *k*' and *k*'' have been given below (Table 5.1) (using Models 1 and 2 from Chapter 3). $Mg(OAc)_2$ / MTBD was surprisingly inefficient in comparison with its apparent efficiency towards PET powder, not even competitive with $Zn(OAc)_2$ alone, which strongly indicates PET fabrics have differing kinetic profiles to powder. This is likely a product of a combination of effects, including the increased stirring required to agitate this mixture and the increased ratio of solvent required to properly wet the higher volume of substrate in addition to the change in substrate morphology. Mass loss of cotton from the depolymerisation of PCB was measured as less than 1%.

Additionally, bmim·$FeCl_4$ had effectively no activity towards PCB fabric, an unusual result given Ioniqa's implementation of this catalyst commercially. It is theorised that, given the proprietary nature of the catalyst used by Ioniqa, the catalyst used in this study was incomplete.

Table 5.1. Undyed PCB glycolysis catalyst activities (*k*' and *k*'') using Model 1 and Model 2.

Catalyst	***k*' / min^{-1}**	**Adj. R^2**	***k*'' / min^{-1}**	**Adj. R^2**
$Zn(OAc)_2$ / urea	0.115±0.005	0.994	0.034±0.003	0.970
$Zn(OAc)_2$ / Im	0.096±0.007	0.976	0.0309±0.0014	0.992
$Zn(OAc)_2$ / DMAP	0.0455±0.0009	0.998	0.0192±0.0011	0.984
$Zn(OAc)_2$	0.0307±0.0014	0.986	0.0155±0.0009	0.982
$Mg(OAc)_2$ / MTBD	0.0230±0.0003	0.999	0.0120±0.0002	0.998
bmim.$FeCl_4$	0.00028	n/a	0.00019	n/a

5.2.2. Dyed PCB Glycolysis

The most effective four catalysts from the undyed study ($Zn(OAc)_2$, $Zn(OAc)_2$ / DMAP, $Zn(OAc)_2$ / Im and $Zn(OAc)_2$ / urea (1:4)) were selected to be taken further into a study of the black dyed PCB. The $Zn(OAc)_2$ / urea catalyst was found to be more resilient towards dye impurities than $Zn(OAc)_2$ or $Zn(OAc)_2$ / Im (Figure 5.3). $Zn(OAc)_2$ / DMAP was found to be *more* effective towards black PCB than undyed PCB.

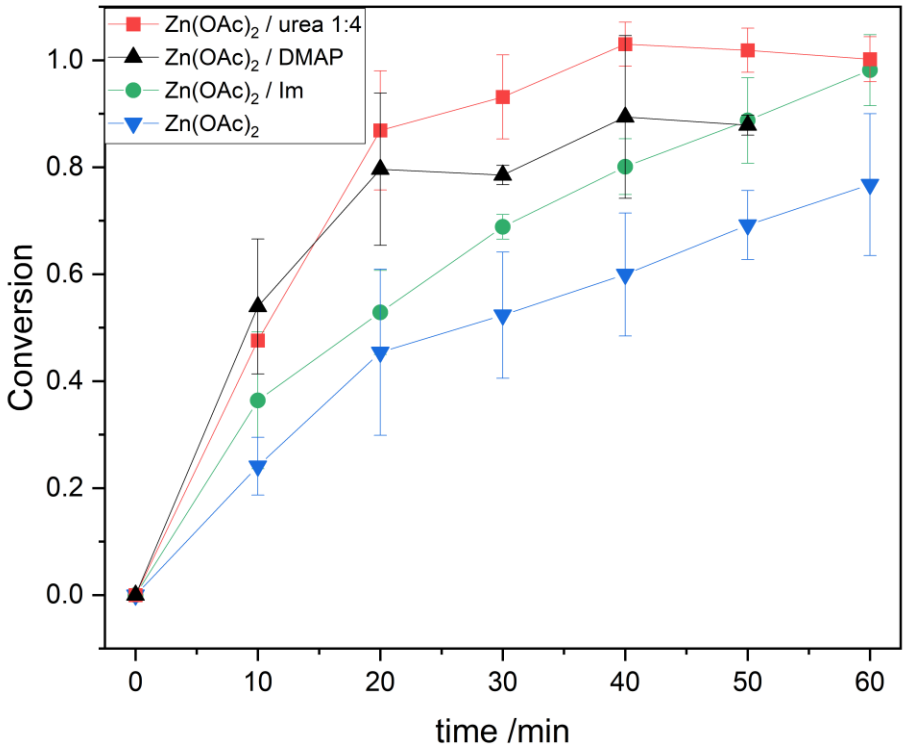


Figure 5.3. Comparison of the three best catalysts from the undyed study using black dyed PCB.

$Zn(OAc)_2$ / Im was most affected by the inclusion of a black dye to the PCB, reducing its pseudo-first-order rate constants *k*' by 0.0351 min^{-1} and *k*'' by 0.0147 min^{-1}, whereas the value of *k*' for $Zn(OAc)_2$ / urea was only reduced *k*' by 0.0205 min^{-1} and *k*'' by 0.0031 min^{-1}. The value for $Zn(OAc)_2$ was also reduced minimally, with a reduction in *k*' of only 0.0066 min^{-1} and in *k*'' of

0.0042 min^{-1}. The value of *k*' and *k*'' for $Zn(OAc)_2$ / DMAP actually increased with black PCB, however, by 0.0128 min^{-1} for *k*' and 0.0068 min^{-1} for *k*''. Because of this, red dyed PCB was depolymerised using $Zn(OAc)_2$ / DMAP also in order to compare the effects of different dyes on the catalyst's activity (Figure 5.4).

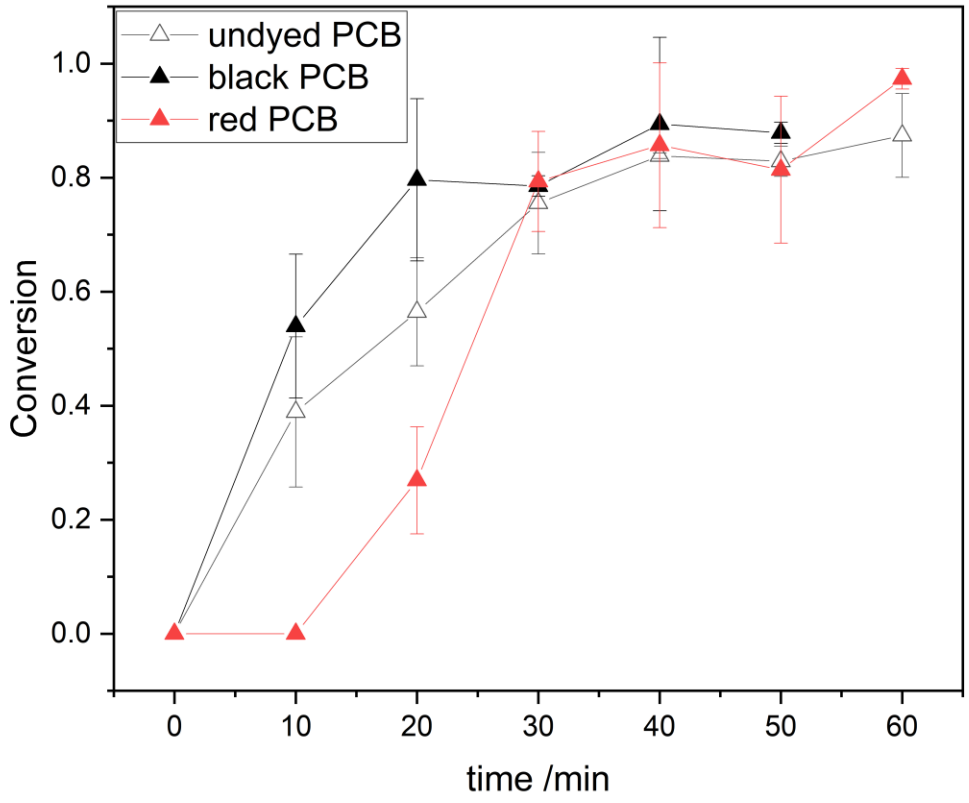


Figure 5.6. Comparison of depolymerisation kinetics of undyed, black and red PCB using 10 mol% $Zn(OAc)_2$ / DMAP as the catalyst.

It is clear from the kinetics that red dyed PCB generates an induction period of around 10 minutes before it begins to depolymerise. This is possibly caused by the red dye initially poisoning the catalyst, then reacting with the catalyst or degrading to a non-poisoning species to produce an active species over the course of the 10 minutes.

The dyed BHET was purified by the method developed in Section 5.5.2 to produce nearly pure white BHET (Figure 5.5.). This was shown to be >98% pure by NMR (Supplementary Figure S5.1).

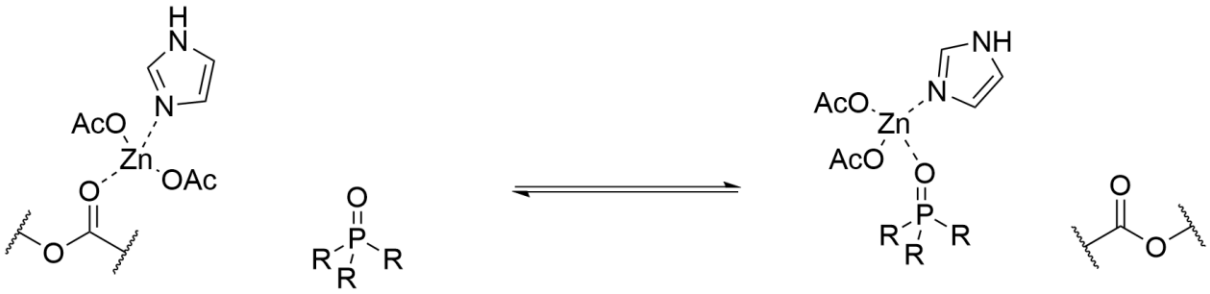


Figure 5.7. BHET from dyed PCB after 0 (left), 1 (middle), and 2 (right) purification steps.

5.2.3. Flame Retardant-Included PET Glycolysis

$Zn(OAc)_2$ / Im appears to be the most sensitive (of the catalysts screened) towards impurities in the PET composition. To this end, PET powder was depolymerised in the same way as described in Chapter 3, using 10 mol% $Zn(OAc)_2$ / Im catalyst, but including TDCPP in the depolymerisation mixture in 0.3 wt% amount. It was hypothesised that the phosphate nature of the flame retardant might bind to the catalyst, poisoning it (*i.e.* reducing its activity by binding to

the catalyst competitively with the substrate), and therefore reducing the catalyst's efficiency (Scheme 5.1).



Scheme 5.1. Possible phosphine oxide poisoning of the catalyst.

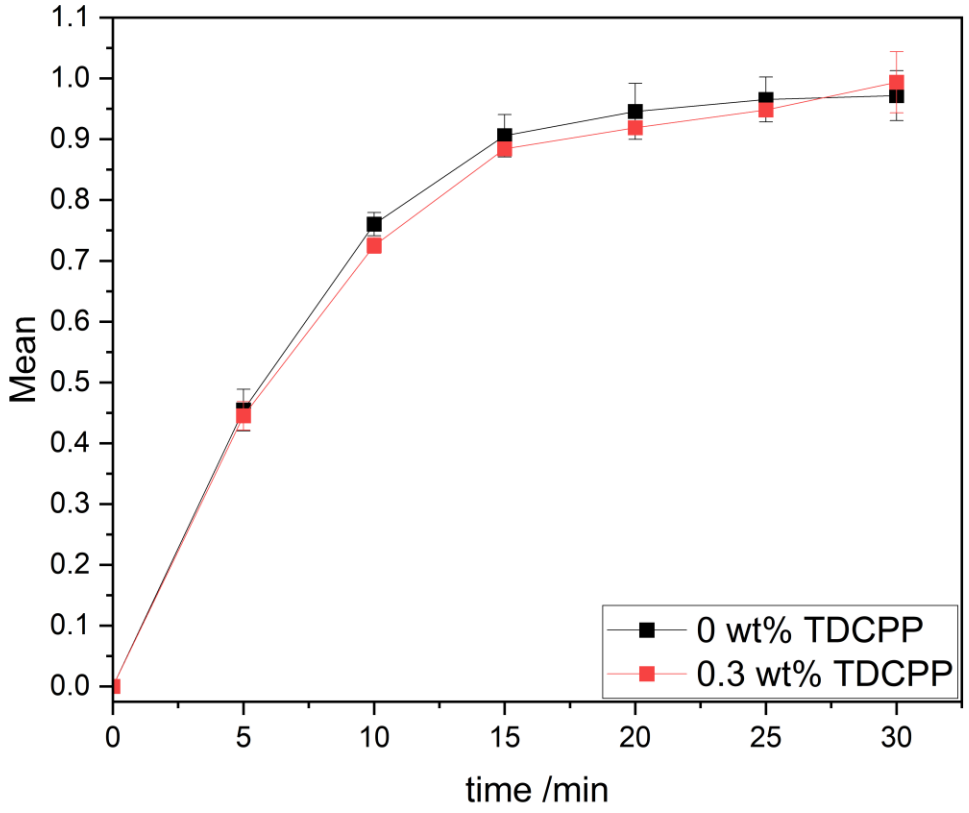


Figure 5.10. Kinetic plot of glycolysis of PET catalysed by $Zn(OAc)_2$ / Im (10 mol%) with and without TDCPP.

The resultant kinetics were compared with the same conditions not including TDCPP (Figure 5.6). It is clear from these results that there is little loss of activity from the inclusion of a typical TDCPP dosage in the PET depolymerisation mixture. The 0.3 wt% values of *k*' and *k*'' were

within 0.017 and 0.003 min^{-1} of the 0 wt% values respectively (approx. 4 standard deviations (S.D.) and 1 S.D. respectively) (all $R^2 > 0.99$).

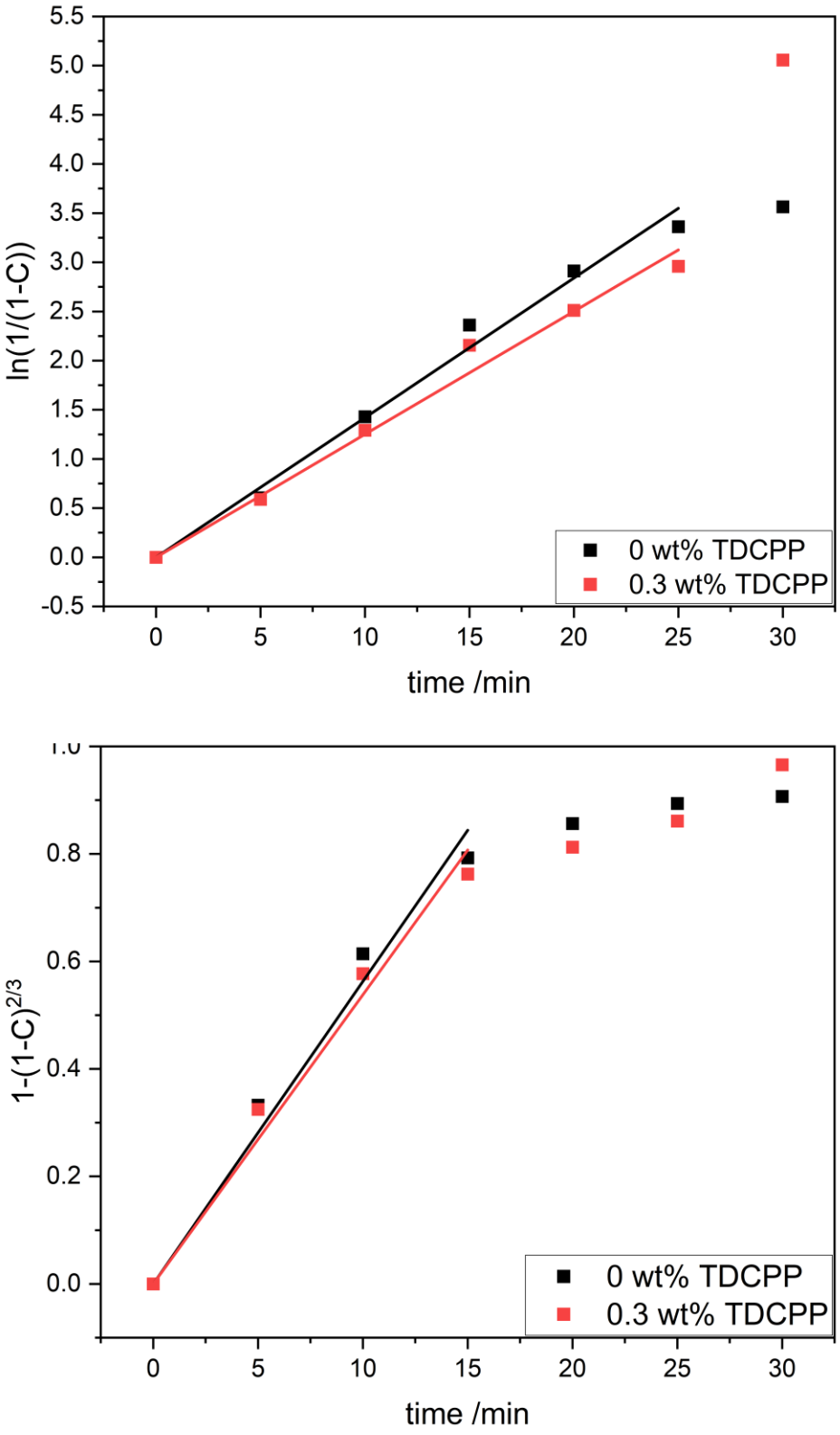


Figure 5.11. Calculation of first-order rate constants using a) Model 1 and b) Model 2.

The difference between contaminated and uncontaminated PET is more pronounced using Model 1 (Figure 5.7). This is hypothesised to be a result of PET powder glycolysis catalysed by $Zn(OAc)_2$ / Im being better modelled by Model 1, therefore its error is lower than Model 2's, and so the lines fall within more S.D.s of each other.

It is clear from these data that the phosphine oxide flame retardant is not poisoning the $Zn(OAc)_2$ / Im catalyst to any significant degree. It is likely that TDCPP does bind at least weakly to the $Zn(OAc)_2$, however, if the results of the Gutmann-Beckett experiment in Chapter 3 are extended. This binding may not be maintained at the reaction's relatively high operating temperature (453 K).

5.3. Conclusions

$Zn(OAc)_2$ / urea (1:4) and $Zn(OAc)_2$ / Im were found to be the most efficient catalysts for undyed PCB glycolysis, whilst $Mg(OAc)_2$ / MTBD was found to be a mediocre catalyst. It is possible this is a result of differing shape of PET particles between the powder and the PCB. Additionally, Ioniqa's ionic liquid catalyst bmim·$FeCl_4$ displayed almost no activity, which is an unusual result given their commercial success. Finally, cotton was recovered in almost quantitative yield.

Dyed PCB was depolymerised in much the same way, and $Zn(OAc)_2$ / urea (1:4) was found to be resilient to the inclusion of dyestuffs. However, rather unusually, $Zn(OAc)_2$ / DMAP increased in *k*' and *k*'' with the inclusion of black dye. It was therefore taken forward into a study of red dye, where a large induction period was measured before once again rapidly depolymerising. Red and black dyed BHET derived from glycolysis of red and black dyed PCB were purified into white BHET, shown to be >98% pure by NMR.

The flame retardant TDCPP was loaded into a glycolysis reaction at 0.3 wt% (a common loading in post-consumer materials) using the most sensitive catalyst. It was found to have a small

negative effect on catalyst activity, suggesting the phosphine oxide does not poison the catalyst to any significant degree.

Further work in this area should likely include additional industrially-relevant catalysts in the screen, and a wider variety of dyes, including PCB dyed by dyestuffs with known structure. The recovered cotton should also be further analysed to check its structural integrity and surface properties have been maintained alongside its mass. Finally, other flame retardants could be screened, although this may prove difficult as most such chemicals are now controlled substances because of their environmental and health impacts.

Depolymerisation of postconsumer PET or PET with impurities included is an important step in making the vision of circular economy a reality. The ability to isolate purified BHET from mixed solutions using chemical methods requires development before it can be implemented industrially, and the catalytic effect needs studying to determine the most efficient method of depolymerisation. However, this study provides inroads into these problems, and shows that they are soluble.

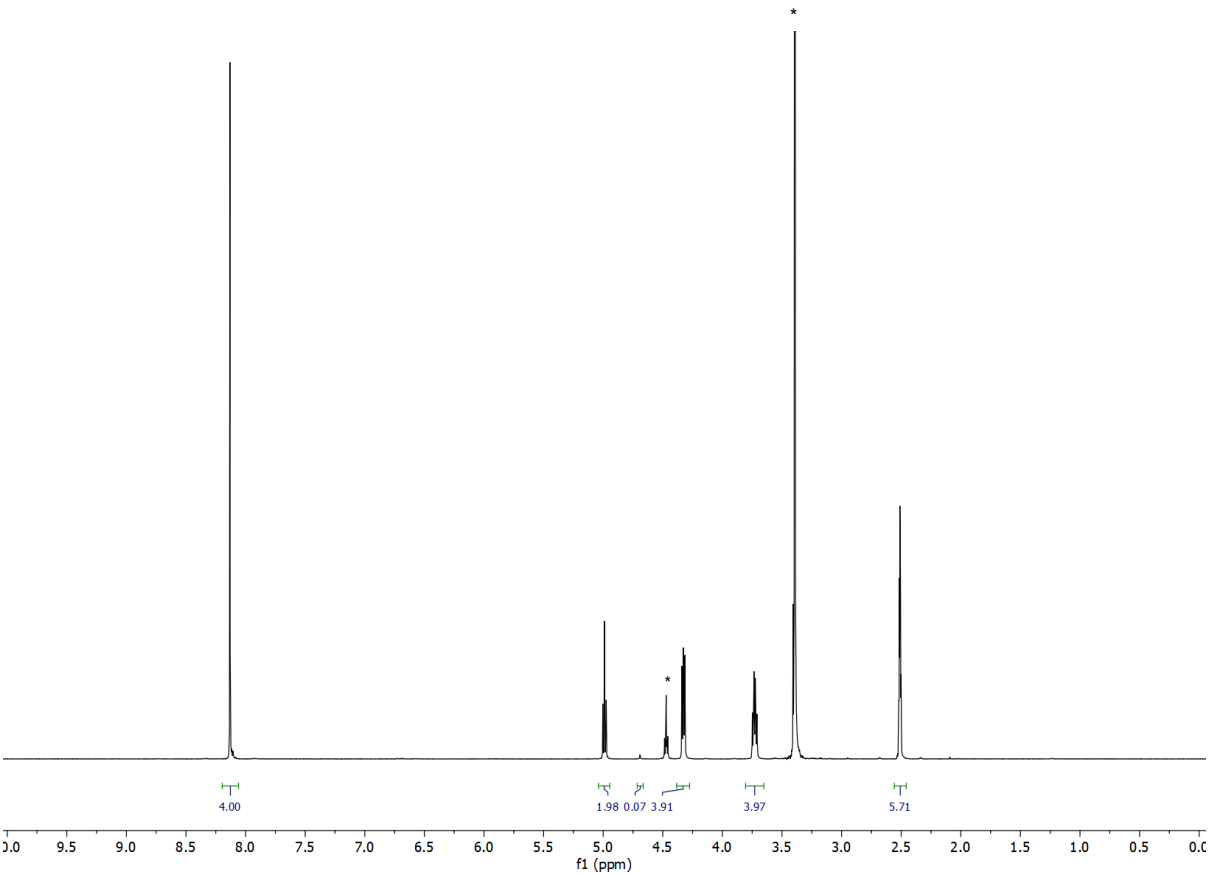
5.4. Supporting Information

5.4.1. PCB Depolymerisation Procedure

A 20 mL scintillation vial was charged with ethylene glycol (14 mL, 15.6 g, 250 mmol, 100 equiv.), metal acetate hydrate ($M(OAc)_2 \cdot xH_2O$) (0.25 mmol, 0.10 equiv.), base (0.25 mmol, 0.10 equiv.) and *N*-methyl-pyrrolidone (0.024 mL, 25 mg, 0.25 mmol, 0.10 equiv.) and sealed with a screw cap. The mixture was brought to 180 °C. PCB (735 mg, 0.25 mmol, 1 equiv.) which had been manually cut into approximately 1 cm^2 pieces, was added to the solution and stirred at this temperature for 1 h. Aliquots of 0.1 mL were taken at regular timepoints, and prepared for ^1H NMR spectroscopy analysis in DMSO-d_6. Once all the PET had been depolymerised, the hot solution was filtered to remove the cotton. Water (45 mL) was added to the solution and cooled to 4 °C for 18 h, and the resulting crystals of bis(2-hydroxyethylene)terephthalate (BHET) (445 mg, 1.9 mmol, 77%) were recovered by vacuum filtration, washing with cold water (5 mL) and drying under reduced pressure.

5.4.2. Dyed PCB Purification Procedure

Red and black dyed PCB fabric (in a 65:35 polyester:cotton ratio by weight) was sourced from Navato Textiles. The dyed PCB was depolymerised in the same way as with undyed PCB. The dye was removed by dissolving the BHET in hot (80 °C) acidified water (0.04 M HCl) (50 mL) and gravity filtered. The filtrate was washed with cold diethyl ether (3 × 50 mL) and the aqueous fraction was neutralized with NaOH (1.0 M) (2 mL). The aqueous solution was cooled to 4 °C for 18 h to precipitate crystals of BHET. This process was repeated twice to yield white BHET (140 mg, 0.6 mmol, 24%).



Supplementary Figure S5.12. ^{1}H NMR Spectrum (400 MHz, 298K, DMSO-d_6) of purified BHET. * = H_2O; X = potential dye

- **References**

1. G. Güçlü, A. Kas¸göz, S. Özbudak, S. Özgümüs¸ and M. Orbay, *Journal of Applied Polymer Science*, 1998, **69**, 2311-2319.
2. S. Baliga and W. T. Wong, *Journal of Polymer Science Part A: Polymer Chemistry*, 1989, **27**, 2071-2082.
3. R. López-Fonseca, I. Duque-Ingunza, B. De Rivas, S. Arnaiz and J. I. Gutiérrez-Ortiz, *Polymer Degradation and Stability*, 2010, **95**, 1022-1028.
4. A. Aguado, L. Martínez, L. Becerra, M. Arieta-araunabeña, S. Arnaiz, A. Asueta and I. Robertson, *Journal of Material Cycles and Waste Management*, 2014, **16**, 201-210.
5. Y. Li, J. Shen, Q. Liu, Y. Zhu, Z. Pang and M. Ge, *Journal of Environmental Chemical Engineering*, 2023, **11**, 109816.
6. L. Liu, H. Yao, Q. Zhou, X. Yao, D. Yan, J. Xu and X. Lu, *Journal of Environmental Chemical Engineering*, 2022, **10**, 107512.
7. I. van der Veen and J. de Boer, *Chemosphere*, 2012, **88**, 1119-1153.
8. Q. Wang, X. Yao, Y. Geng, Q. Zhou, X. Lu and S. Zhang, *Green Chemistry*, 2015, **17**, 2473-2479.
9. E. Barnard, J. J. Rubio Arias and W. Thielemans, *Green Chemistry*, 2021, **23**, 3765-3789.
10. S. E. Lewis, B. E. Wilhelmy and F. A. Leibfarth, *Chemical Science*, 2019, **10**, 6270-6277.
11. K. R. Delle Chiaie, F. R. McMahon, E. J. Williams, M. J. Price and A. P. Dove, *Polymer Chemistry*, 2020, **11**, 1450-1453.

6 Conclusions & Perspectives

In this work, methods of upcycling and recycling poly(ethylene) terephthalate (PET) were explored and expanded.

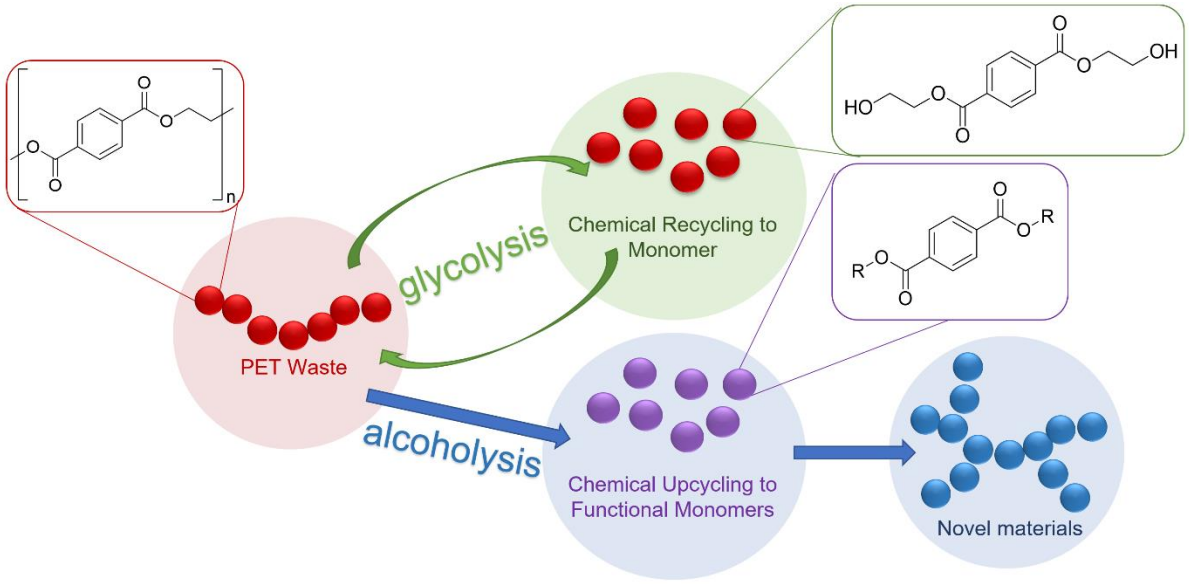


Figure 6.1. The routes explored in this work for PET upcycling and recycling.

PET degradation using glycolysis was made more efficient by use of decreased particle size and highly active dual catalyst ‘ZnAc / DMAP’, allowing access to lower-boiling nucleophiles. The ability to degrade PET directly into value-added products using alcoholysis was then developed, and novel materials were synthesized from these monomers. These materials’ properties can be tuned based on composition or ratio of monomer. One such monomer, bis(perillyl)terephthalate, was able to be 3D-printed using a DLP methodology in conjunction with thiol-ene ‘click’ chemistry. A Hart cube, a structure not able to be traditionally manufactured, was printed with very good resolution as a display of the monomer’s capabilities.

The state of the art in PET glycolysis catalysis was reviewed, and there was found to be a distinct lack of dual catalyst research. Therefore a screen of dual catalysts was commenced, initially based on ZnAc as this is the most well-used PET glycolysis catalyst, as well as a range

of amine bases. Two degradation models were used to evaluate the kinetic profiles of these catalysts. PET was found to glycolyse rapidly using ZnAc / Imidazole, reaching >95% conversion in under 15 minutes and achieving a *k*' first-order rate constant of 0.126 ± 0.003 min^{-1} – a significant improvement over its predecessor, ZnAc / DMAP, which has a *k*' of only 0.074 ± 0.004 min^{-1}. It was also possible to train a predictive model of ZnAc / base *k*' using an equation-building tool, based on the basicity of the base and the calculated bond length between ZnAc and the nitrogen in the base (R^2 = 0.941). In fact, ZnAc / DMAP was the only major outlier, with lower activity than predicted.

Subsequently, a screen of metal acetates which were known to be active towards PET glycolysis was initiated to develop a wider breadth of highly active catalysts for PET glycolysis. A predictive model was developed for these 4 also, but found lacking when new acetates were introduced. The 8 metal acetates were used to train a new model, which has good agreement between prediction and *k*' (R^2 = 0.975) and was able to predict a ninth metal acetate's activity with moderate confidence.

Next, the remaining 3 initial metal acetates were trialled in combination with the same bases. The predictive equations derived for these combinations were more prone to high error than for $Zn(OAc)_2$. A suitable predictive model for all four datasets was unfortunately unable to be drawn up.

Density Functional Theory was utilised to calculate the bond dissociation energies, lengths, angles and geometries of the $Zn(OAc)_2$ / base and $Mg(OAc)_2$ / base combinations. The same methodology was then used to calculate energies and geometries of the intermediates and transition states of the lowest energy pathway of both 'associated' and 'disassociated' catalyst states for three $Zn(OAc)_2$ / base combinations ($Zn(OAc)_2$ / DMA, Im and ABCO). These energies and geometries were used to determine possible mechanistic details of the reaction, and to determine that the 'associated' catalyst state was the lower energy pathway for all three trialled

combinations. It is hypothesized that the bonding between base and metal affects the acetate ligand's hydrogen bonding with the alcohol, therefore changing the shape of the transition state, and thus the activity.

Finally, PET was glycolysed in the presence of impurities including cotton, dyes and flame retardants. Undyed PCB was shown to glycolyse more slowly but this is likely caused by particle shape and size rather than the cotton impurity. Dyes were shown to have a non-negligible effect on activity for all catalysts trialled, and the flame retardant was found to have negligible effect.

Future work in these areas is severalfold.

1. Upcycling of PET has until now been performed *via* aminolysis and hydrogenolysis, so further alcoholysis using other alcohols, both bioderived and not, would greatly expand the literature. Novel materials from renewable resources such as waste polymer as well as the burgeoning industry of additive manufacturing are both ever-expanding areas which can be leveraged by this method.
2. Predictive tools for organometallic dual catalyst development have been developed and implemented, but these tools can be further tested and improved by further screening and testing. In particular, a screen of $Zn(OAc)_2$ with various substituted imidazoles would be useful future work to fine-tune the models of activity.
3. A machine learning model using the work presented here as training data could be a useful avenue, however the training data set would be on the small side. Such a model, in combination with the predictive model presented here, could be extremely useful in dual PET glycolysis catalyst design going forward.
4. DFT modelling of the metal acetate / base combinations not detailed herein is likely a necessary next step for validation and expansion of the predictive models. Similarly, energy level and geometry calculations for the minimum energy pathways of more

$Zn(OAc)_2$ / base combinations, as well as of metal acetate / base combinations using metals other than zinc, will be necessary.

5. Further study into the effects of various impurities on PET glycolysis catalysts is needed, as this work provides only the initial steps into such a study. Colourimetric and mass spectrometry analysis of dyed PET fabrics and the resultant BHET would provide a more quantitative approach to analysing the depolymerisation of dyed fabrics. Additionally, a more expanded screen of fibre, dye and flame retardant impurities could prove useful, especially for mixed fibres such as PET-nylon or PET-wool.

It follows therefore that this work both provides valuable inroads into the various fields covered, and sets up important experiments to follow.



Figure 6.2. Magazine covers representing the prevailing opinion on plastics then and now.

In the modern era humanity faces a variety of environmental and resource challenges; several of these centre around the use of oil and plastic. Plastic chokes our rivers and oceans, kills and mutilates the wildlife that live there, leaches toxic chemicals – the issues are near-endless. Additionally, the extraction of oil continues to feed the fossil fuel industries. Improving our recycling capabilities allows us to use this waste as a raw resource, not only reducing the waste that finds its way into the environment, but also our reliance on fossil fuels as an unsustainable resource from which all our plastics are derived and a fuel source which pollutes our environment.

All things considered, the plastics industry is a runaway train of consumption, and a recycling revolution is the one of the few aspects which can truly put the brakes on it. However, people are beginning to wake up to this reality: single-use plastic bans are proliferating across the western world, and the everyday person is more aware than ever of issues surrounding plastic use. And yet, every year more and more plastic is produced, and thus more and more waste. Production is projected to grow exponentially, reaching nearly 600 million tonnes per year in 2050, and, based on the current rate, recycling rates are projected to reach only 44%; therefore development of these techniques of recycling in tandem with strong public messaging will only grow in importance as long as this scaling-up of plastic industry runs free.